Chemical Weathering and Erosional Transport in an Ancient Shield Terrain

Thesis

Chemical Weathering and Erosional Transport in an Ancient Shield Terrain

Thesis presented for the degree of
Doctor of Philosophy

Josh Wimpenny M.E.Sci

November 2008

Department of Earth and Environmental Sciences, Centre for Earth, Planetary, Space and Astronomical Research, The Open University, Walton Hall, Milton Keynes, UK.

Abstract

This project investigates how isotope systems respond to changes in continental weathering processes and the consequences for the chemical composition of the oceans. Both experimental and natural data indicate that Li and Mg stable isotope systems preserve information on the mineral reactions controlling water chemistry. Dissolution experiments indicate that primary mineral dissolution has little effect on Li, but does fractionate the isotopes of Mg, whereas secondary mineral formation involves preferential uptake of the lighter isotopes of both Li and Mg. Glacial regions have low chemical weathering rates so their rivers should, in principal, have Li isotope compositions (δ^7Li) that are similar to those of the underlying rock. In practise, glacial rivers in Greenland have δ^7Li values that differ significantly from the source rock. Subglacial uptake of ^{6}Li by iron oxyhydroxides appears to influence the riverine Li isotope composition. In contrast, the principal control on Mg isotopes in glacial rivers appears to be primary mineral weathering. Carbonate dissolution dominates the chemistry of glacial rivers, and this phase possesses a light Mg isotope composition imparting this signature to the Greenland rivers. Both the Li and Mg isotope compositions of glacial rivers are similar to their respective global riverine averages, suggesting that the impact of glaciation on the Li and Mg composition of seawater may be small. The Re-Os radiogenic isotope system is also a useful tracer of continental weathering, its composition in the oceans being sensitive to changes in the flux and composition of continental weathering. Laterites are widespread in tropical regions and are shown to contain high concentrations of highly unradiogenic Os. Consequently, their subsequent weathering and erosion has potential to significantly affect the Os isotope composition delivered to the oceans.

Acknowledgements

I would first like to thank my supervisors Kevin Burton, Rachael James, Sigurdur Gislason and Mouhcine Gannoun. I have had a great deal of encouragement and guidance from them over the last few years and they have dedicated a lot of time to my research, both with the analytical and interpretative sides of my PhD. I would also like to thank Ian Parkinson for agreeing to supervise me over the last few months!

A significant portion of my time was spent processing and analysing samples in the laboratory here at the Open University. ICP-MS analyses could not have been possible without the help of Nick, Fatima and especially Sam who always found time to run samples even when it really wasn't her job to do so! Analyses by MC-ICP-MS were always a struggle but made easier with the help of Peter, Louise, Ian and Manuela. The preparation of glass discs for XRF analyses were carried out by John W. I would like also like to thank Mike Widdowson for providing the laterite samples and for all the help with the laterite project. Experimental work was performed in Reykjavik at the Institute of Earth Science; particular thanks go to Bergur, Eydis, Therese, Helgi, Saemi, Andre, Gabriel and to Ingvi who ran the samples on ICP-AES. Everybody was very friendly and welcoming to me which made my time in Iceland so enjoyable.

Life in Milton Keynes takes a little getting used to but it was made a lot easier (and more fun) by all the people I have lived and worked with. I would like to thank all of my office mates over the years; Chris (the monkey), Jen, Bryony, Amy and Trish for putting up with me over the last few years. Thanks also to my housemates Martin, Steve, Sam, Wes, Joe (the Chief), and Pierre as well as all the guys from Iceland

including Magda, Ducca, Anu, Andrea, Jan, Morgan and Heike. Other thanks go to Carl, Alison (1), Ian O, Alison (2), James, Will, Clare, Matt, Anne, Dave, Jason, Jess, Mark and a special mention to Phil Pogge for helping me sample the rivers in Greenland.

I also need to mention some people from my Liverpool days and from back in Wales; thanks go to Simon, Paddy, Ste, Dave B, Chris, Rob, Seyon, Shaun, Max, Tom and Lisa. Maybe now I've finished I can actually go and visit some of you guys!

Finally, I couldn't have done this without the love and support of my family; it's always great to go home even if we don't live in Wales anymore! So special thanks to my Mum and Dad, my brother Ross and his family, Nan, and last but not least to my sister Anna (I nearly submitted my thesis before you) for putting up with my teasing over all these years...!

Contents

Appendices

Appendix A - Analytical techniques and experimental methods

Appendix B – Data from the analysis of Greenland rivers

Appendix C – Experimental data

Appendix D – Laterite data

Appendix E – Laterite paper

Figures

Chapter 1 - Introduction

Chapter 2 – Methods

Chapter 3 – The behaviour of lithium and lithium isotopes during glacial weathering

Chapter 4 – The behaviour of magnesium and magnesium isotopes during glacial weathering

Chapter 5 – Isotopic changes accompanying the experimental dissolution of basalt glass and forsterite

Chapter 6 – The dissolution of basalt glass and forsterite in seawater

Chapter 7 - Rhenium and osmium isotope and elemental behaviour accompanying laterite formation in the Deccan region of India

Chapter 1

Introduction

The aim of this thesis is to investigate how changes in climate and lithology affect silicate weathering processes and in turn how this influences the continental weathering signal delivered to the oceans. This investigation is divided between the study of natural systems such as rivers and weathering profiles, and experimental systems where external variables such as temperature and pH can be controlled. Primary mineral dissolution and secondary mineral precipitation are two of the most important processes that control aqueous geochemistry. By investigating how these weathering processes affect isotope systems in controlled experimental environments it is hoped that such information can shed light on their behaviour in natural systems.

1.1. Silicate weathering

1.1.1. Silicate weathering reaction

Silicates constitute around 90% of the rocks exposed at the Earth's land surface (GARRELS and MACKENZIE, 1971). The weathering of calcium and magnesium-silicate rocks can cause long term changes in the Earth's climate by altering the CO_2 concentration of the atmosphere. Silicate weathering involves hydrolysis reactions that consume the reactant species to form weathering products (WHITE, 2003):

$$CaSiO_3 + 2H_2CO_3 = Ca^{2+} + 2HCO_3^- + SiO_2 + H_2O \qquad \textit{Equation 1.1}$$

The dissolution of silicates produces dissolved species such as Ca^{2+}, Mg^{2+} and bicarbonate (HCO_3^-) ions, which are subsequently transported to the oceans via rivers. The bicarbonate ion is part of the carbonic acid system (along with H_2CO_3 and CO_3^{2-},

Equations 1.2-1.4) which buffers the pH of seawater over short timescales. The activities of these species in solution are dependent on the solution pH (APPELO and POSTMA, 2005). At the pH of seawater (~pH 8) the dominant species is HCO_3^-, which is free to combine with Ca^{2+} to form calcite (Equation 1.5) or Mg^{2+} to form dolomite. The result of the continental weathering of Ca and Mg-silicate rocks is that 2 moles of CO_2 are drawn down; one mole is released back to the atmosphere while one mole is stored over a long time period as carbonates (BERNER et al., 1983; WALKER et al., 1981). Thus, the weathering of Ca and Mg silicates causes a net drawdown of CO_2 from the atmosphere in a process that operates on a timescale of millions of years (WALKER et al., 1981). For this reason silicate weathering can only affect the Earth's climate over geological time scales.

$$CO_{2(g)} + H_2O \Leftrightarrow H_2CO_3 \quad \text{(dominant at pH<6.3)} \qquad \textit{Equation 1.2}$$

$$H_2CO_3 \Leftrightarrow H^+ + HCO_3^- \quad \text{(dominant at pH>6.3, <10.3)} \qquad \textit{Equation 1.3}$$

$$HCO_3^- \Leftrightarrow H^+ + CO_3^{2-} \quad \text{(dominant at pH>10.3)} \qquad \textit{Equation 1.4}$$

$$Ca^{2+} + 2HCO_3^- = CaCO_3 + H_2O + CO_2 \qquad \textit{Equation 1.5}$$

The whole process of calcium-silicate dissolution and the associated drawdown of CO_2 can be summarised by the following equation (UREY, 1952):

$$CaSiO_3 + CO_2 \Leftrightarrow CaCO_3 + SiO_2 \qquad \textit{Equation 1.6}$$

Although the combination of magnesium with bicarbonate to form dolomite (Equation 1.7) does in theory cause CO_2 drawdown and may have been important in the ancient

oceans, recent studies have shown that this process is not important today (HARDIE, 1996; HOLLAND, 2005)

$$Ca^{2+} + Mg^{2+} + 2CO_2 + 2H_2O = MgCa(CO_3)_2 + 4H^+$$ *Equation 1.7*

Instead most of the removal of dissolved Mg^{2+} from the oceans occurs during exchange with Ca^{2+} in mid-ocean-ridge basalts or by precipitation as magnesium silicates e.g. the precipitation of Mg-saponites (GISLASON et al., 2006), as in Equation 1.8.

$$3.165Mg^{2+} + 0.33Al^{3+} + 3.67SiO_2 + 4.66H_2O = Mg_{3.165}Al_{0.33}Si_{3.67}O_{10}(OH)_2 + 7.32H^+$$

Equation 1.8

This exchange at mid ocean ridges (MOR) can be simplified to:

$$Mg^{2+} + \text{Ca-basalt} \rightarrow Ca^{2+} + \text{Mg-basalt}$$ *Equation 1.9*

This exchange between magnesium and calcium is so efficient that it has been proposed that Mg indirectly causes the drawdown of CO_2 by liberating Ca^{2+} into solution which can then react as in Equation 1.5 (STANLEY and HARDIE, 1999).

The weathering of carbonates is generally faster than that of silicate rocks (MEYBECK, 1987), but carbonate dissolution has no long term effect on the composition of the Earth's atmosphere. This is because the carbonate weathering reaction and formation of carbonates in the oceans consumes and releases one mole of CO_2 (Equation 1.10), thus unlike the silicate weathering process there is no net change in atmospheric CO_2.

$$Ca^{2+} + CO_2 + H_2O = CaCO_3 + 2H^+$$ *Equation 1.10*

1.1.2. Silicate weathering rate

There are many different silicate minerals and they have different weathering susceptibilities depending on their chemical composition (intrinsic properties). Also, a mineral will weather more or less rapidly depending on the climate that it is subjected to (extrinsic properties) (WHITE, 2003). Knowing the weathering rate of these minerals is important; Ca or Mg-silicate minerals that weather more easily will consume CO_2 more rapidly than those minerals that weather slowly. Quartz is considered to be the least reactive mineral, at the other end of the scale minerals such as forsterite and anorthite are less stable at Earth surface conditions and hence will weather far more easily (BRANTLEY, 2003).

Extrinsic factors such as climate have an important influence over the chemical weathering rate, changes in temperature cause changes in the reaction rate of most chemical reactions including silicate hydrolysis. Surface runoff is also important (GAILLARDET et al., 1999b); minerals will chemically weather only in the presence of water so increased precipitation will increase the timescales of mineral-water contact. Higher runoff also has the effect of flushing reactants such as HCO_3^- and organic acids through the system faster, and diluting solutions so systems are further away from equilibrium (WHITE, 2003). Results of a study by Gaillardet et al. (1999b) demonstrate a linear correlation between runoff and weathering rate, and the same study also shows a general increase in weathering rate with temperature. Consequently, it seems likely that if both temperature and runoff are increased then the silicate weathering rate will also increase, causing more CO_2 to be drawn down and deposited as carbonates. This

will, in turn, lower the CO_2 concentration in the atmosphere and so decrease temperature and runoff, leading to a reduction in silicate weathering rate. In practise this negative feedback loop is thought to occur over millions of years and helps to keep the Earth's climate relatively constant (WALKER et al., 1981).

Another factor that affects the chemical weathering rate is the rate of physical weathering. In regions where physical weathering is high there is a high production rate of detrital sediment. This creation of new unaltered surfaces increases the potential for chemical weathering. Studies have shown that in mountainous regions with high runoff the chemical weathering intensity is enhanced simply because the yield of sediment in these regions is high (GAILLARDET et al., 1999a; WEST et al., 2005).

1.1.3. Riverine systems

Much of the continental material produced by weathering is transported to the oceans by rivers, thus their study is crucial in providing information on the continental weathering signal that is transferred to the oceans. Lithology plays a key role in controlling the chemistry of rivers, particularly with regards to major element compositions. The ionic composition of rivers is generally dominated by Ca^{2+} and HCO_3^-, and they can also have substantial concentrations of Mg^{2+}, Na^+, K^+, Cl^- and SO_4^{2-} (MEYBECK, 2003). The production of HCO_3^- occurs during the weathering of silicate minerals by carbonic acid and during the dissolution of carbonate minerals (Section 1.2.1.). This carbon can only be removed from the atmosphere over long timescales by combination with calcium or magnesium in the oceans and deposition and burial as carbonates. The lithological control over riverine systems is highlighted by the difference in chemistry between rivers that drain monolithological catchments (MEYBECK, 2003). For example rivers that drain carbonate rocks will have high concentrations of Ca^{2+}, rivers draining

evaporitic rock will have high Cl^- and SO_4^{2-}, those draining alkaline igneous rocks may have high Na^+ concentrations. Large rivers generally flow over mixed lithologies so that the lithological influence is less obvious. The compositions of these rivers will be dominated by the most easily weatherable lithologies; for example evaporite rocks and carbonates have been shown to dissolve between 10 and 100 times faster than silicates (DUPRE et al., 2003; MEYBECK, 1987). Glacial rivers are an example of where this preferential dissolution can be important; Ca^{2+} dominates the cation content in these rivers even if the underlying bedrock is silicate (ANDERSON et al., 1997; TRANTER, 2003). Estimating the relative proportions of silicate to carbonate weathering is important; only silicate weathering causes drawdown of CO_2 over geological timescales. This is usually performed by calculating element ratios such as Ca/Na and Mg/Na (GAILLARDET et al., 1999b). The benefit of using element ratios is that it allows direct comparison between rivers from different climatic regimes.

As described above, easily weathered minerals, such as carbonates, can have a disproportionate influence on river chemistry. The same can be said of easily weathered silicates; the result is that the dissolved load of a river does not always reflect the chemistry of the bedrock. This effect is termed incongruent weathering; that is, those minerals that are least stable at Earth surface temperatures and pressures will react more readily and their composition will dominate river chemistry. Moreover, individual minerals themselves may not always dissolve congruently; for example the calcium rich cores of plagioclase may weather more rapidly than the more sodic rims leaving plagioclase rich watersheds with a higher Ca:Na ratio than predicted from the bedrock (WHITE, 2003). Also, there is a range of element mobilities during weathering, and elements such as sodium, calcium and magnesium are more mobile than elements like iron and aluminium (GISLASON et al., 1996). As a consequence the dissolved load will

always carry a proportionally higher amount of mobile elements than the weathered bedload, which will contain a higher proportion of immobile elements such as iron, titanium and zirconium (GAILLARDET et al., 2003). The suspended sediment is generally more weathered than the bedrock and has developed a higher proportion of secondary minerals such as clays. Due to the high sorption capacity and relative large surface area of the clays, the suspended sediment also often has high concentrations of mono and divalent cations, including transition metal ions such as copper, vanadium and cadmium (PEACOCK and SHERMAN, 2004; PEACOCK and SHERMAN, 2005; SHERMAN and PEACOCK, 2004). While incongruent weathering is illustrated by the difference in the chemistry of the bulk rock and solution, it is also shown by differences in isotope ratios between riverine phases. An example of this behaviour is provided by the lithium isotope system; during secondary mineral formation the light isotope ^{6}Li is retained in secondary phases leaving the dissolved phase isotopically heavy (HUH et al., 1998). As a result the lithium composition of the dissolved load is always isotopically heavy relative to the bedrock composition. This incongruent weathering is common where the dominant weathering regime is chemical. The weathering congruence increases where the physical weathering intensity rises and intrinsic properties have less control over the weathering susceptibilities. Glacial regions are an example of areas where physical weathering dominates.

1.2. Cenozoic climate

1.2.1. Climate change

The climate of the Earth is not static and is controlled by many different processes that operate over different timescales. Changes to the Earth's climate have been inferred

from observations in the rock record, both marine and terrestrial. The Cenozoic climate record has been reconstructed using variations in the isotopic composition of marine sediments and organisms, one such proxy is the oxygen isotope record ($\delta^{18}O$) (ZACHOS et al., 2001). Records of oxygen isotopes have shown that over the last 50 million years the $\delta^{18}O$ ratio of the oceans (inferred from benthic foraminifera) has risen, representing global cooling over this time period (see Fig. 1.1).

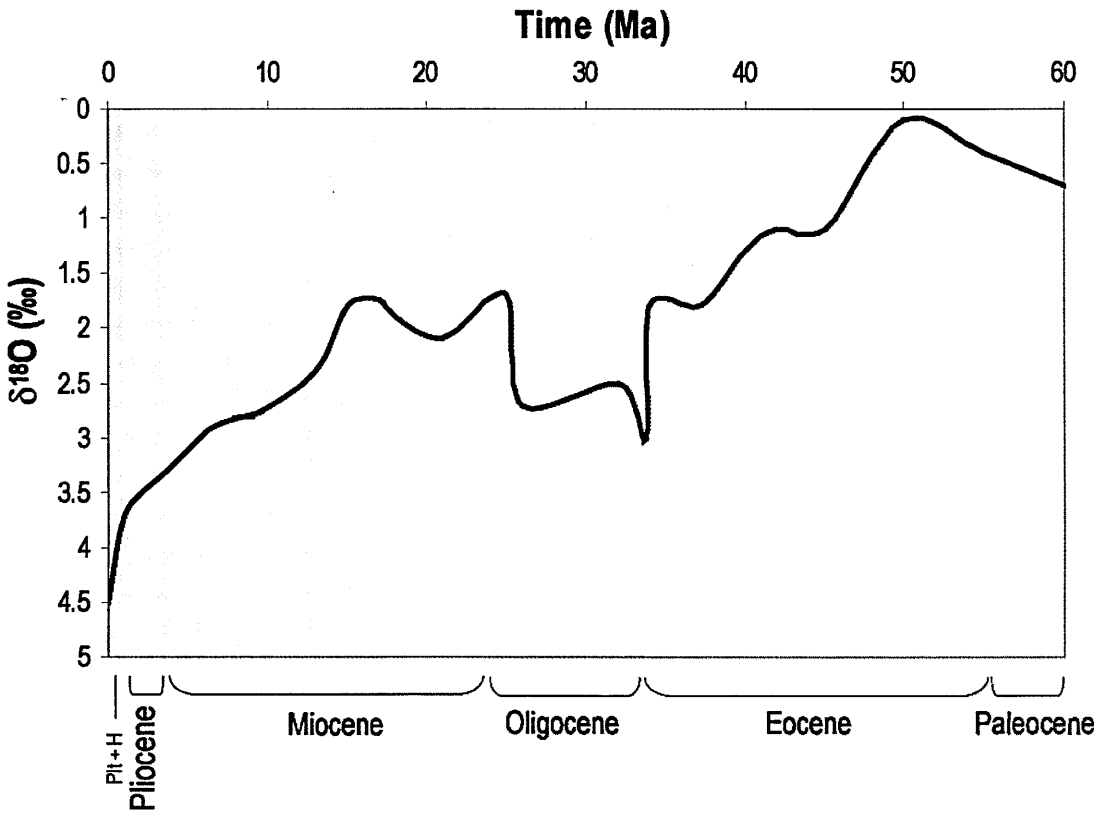

Fig. 1.1 Oxygen isotope composition of seawater over the last 60Ma. Data taken from compilations by Zachos et al. (2007) and Molnar (2004).

As can be seen from Fig. 1.1 the rise in the $\delta^{18}O$ ratio is not consistent, it increases throughout the Eocene (56-33Ma) and then rises sharply at the Eocene-Oligocene boundary (33Ma). There is then a decrease in the oxygen isotope value due to a warming period in the Miocene (23-15Ma) before the isotope ratio increases again at around 15 million years ago, and increases rapidly between 4 and 2 million years ago.

This cooling trend through the Cenozoic has continued on until the present day (anthropogenic global warming excluded).

1.2.2. Causes of climate change

Changes in climate over the Cenozoic have occurred on both long and short timescales. Short timescale changes such as the waxing and waning of the ice sheets during the last 2-3 million years are caused by changes in the Earth's orbital shape (eccentricity), axial tilt (obliquity) and the wobble of the Earth as it spins on its axis (precession); these effects are known as Milankovitch cycles (BERGER, 1988). Over longer timescales changes in the atmospheric levels of CO_2 have widely been recognised as a potential cause of this decrease in temperature.

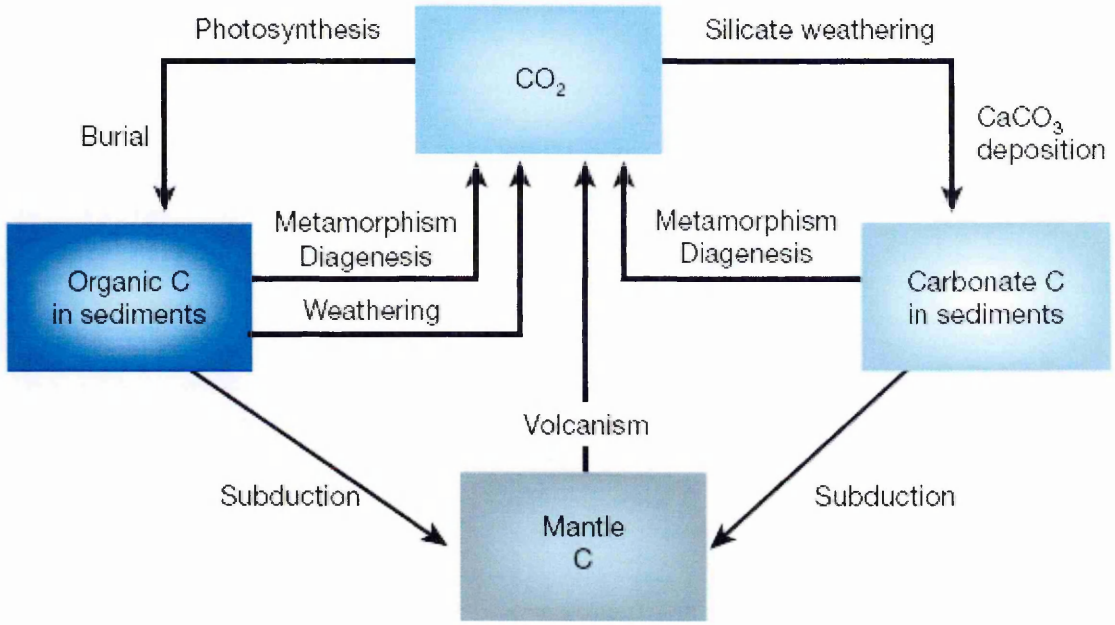

Fig. 1.2. - The long term carbon cycle (Berner 2003)

Atmospheric CO_2 concentrations are controlled by the long term carbon cycle which can be divided into two sub cycles. On the one hand carbon cycles biologically via the formation of organic matter during photosynthesis and its burial as organic rich

sediments, and on the other hand carbon cycles chemically during silicate weathering and the precipitation of carbonates; these processes are illustrated in Fig. 1.2. (BERNER, 2003). Carbon dioxide is a greenhouse gas; it helps to trap solar radiation in the Earth's atmosphere thus keeping the atmosphere warm. By decreasing the concentration of CO_2 in the atmosphere more solar radiation can escape and so the atmosphere will cool. Records from boron isotopes suggest that the CO_2 concentration in the atmosphere has decreased over the Cenozoic (PEARSON and PALMER, 2000) and that decreases in the CO_2 concentration at ~15Ma and 3Ma coincide with intensification of the Antarctic and Northern hemisphere glaciations (Fig. 1.3.).

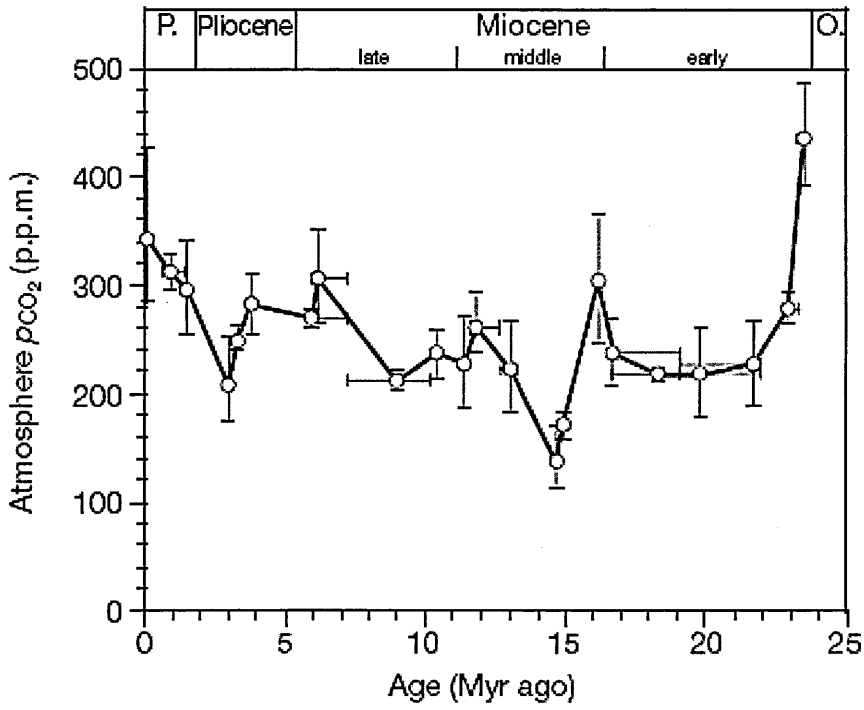

Fig. 1.3 - The record of carbon dioxide concentration in the atmosphere over the last 25 million years (Pearson & Palmer 2000)

Changes in the cycle of carbon can result from factors such as changes in mantle activity and volcanism (volcanism will cause outgassing of CO_2) and changes in primary productivity (enhanced primary productivity causes more CO_2 drawdown). During the late Cretaceous mantle activity was greater, and large amounts of oceanic

plateau basalt were produced so a high atmospheric CO_2 concentration is thought to have been maintained (TAJIKA, 1998). In the Cenozoic mantle activity decreased so less CO_2 was outgassed. This is thought to be one reason why CO_2 levels dropped, particularly in the early stages of the Cenozoic. Primary producers utilise CO_2 during photosynthesis to create organic compounds and oxygen, thus periods of high primary production will cause large quantities of CO_2 to be drawdown. Such periods are inferred from sharp decreases in atmospheric CO_2 at 15Ma and 4-2Ma (PEARSON and PALMER, 2000) and were probably caused by enhanced deep water formation. Section 1.1 described silicate weathering and the associated drawdown of CO_2; enhancement of the silicate weathering rate is another possible cause of the decrease in CO_2 concentrations and climate change during the Cenozoic.

1.2.3. Weathering and climate change

It has been proposed that the change in the concentration of atmospheric CO_2 and associated change in climate that occurred during the Cenozoic may be related to an increase in the rate of silicate weathering in response to the uplift of mountainous regions such as the Himalayas and the Andes (BLUM et al., 1998; RUDDIMAN and PRELL, 1997). These uplifted terrains erode relatively rapidly due to steep slopes, lack of vegetation, possible glaciation and active faulting. Coupling the exposure of unaltered rock with greater monsoonal circulation enhances chemical weathering, as does the production of fine grained little altered sediment (RUDDIMAN and PRELL, 1997). In theory such orogenically enhanced weathering could cause an increase in the net drawdown of CO_2 from the atmosphere, as has been inferred in the study of Pearson and Palmer (2000).

This hypothesis linking Cenozoic climate to enhanced silicate weathering is supported by the isotope records of strontium and osmium in seawater. The strontium and osmium isotope systems have a number of similarities; for example, they are isotopically homogeneous in seawater (LEVASSEUR et al., 1998; SHARMA et al., 1997) and they have a radiogenic end member that is sourced from continental weathering (RAVIZZA and ZACHOS, 2003). The oceanic record of strontium isotopes during the Cenozoic is well established with a rapid rise of the $^{87}Sr/^{86}Sr$ ratio over the past 40Ma (Fig. 1.4, (DEPAOLO and INGRAM, 1985; HESS et al., 1986; RICHTER and DEPAOLO, 1988)). The osmium isotope record also shows that seawater has become increasingly radiogenic during this time (PEGRAM and TUREKIAN, 1999). As both isotope systems become increasingly radiogenic it must signify a change in the continental weathering input, either with respect to the flux of material or to the composition of that material. This change in the weathering signal is commonly explained by increasing amounts of uplift such as that caused by the Himalayas (RAYMO et al., 1988) and the onset of glaciation (ARMSTRONG, 1971). Both mechanisms can cause higher continental weathering rates; this change in flux would change the balance between continental and hydrothermal strontium (or osmium), leading to an increase in the $^{87}Sr/^{86}Sr$ (or $^{187}Os/^{188}Os$) ratio. Unfortunately there are problems with using the strontium and osmium isotope systems to infer changes in weathering rate of silicates. As already stated a change in the oceanic composition can be caused by a change in the flux or a change in the composition of continental material, not all rocks have the same isotopic composition (ESSER and TUREKIAN, 1993; PALMER and EDMOND, 1992). High levels of strontium are associated with carbonate rocks and high levels of osmium with organic rich sediments (PALMER and EDMOND, 1992; PIERSON-WICKMANN et al., 2002). A study of Himalayan rivers by Blum et al. (1998) shows that the relative contributions of

silicate weathering to the riverine flux of HCO_3^- is just 18%, the remainder originates from carbonate weathering. Similar studies also show the importance of carbonate dissolution in controlling the composition of strontium derived from Himalayan weathering (HARRIS et al., 1998). This shows that while the increased $^{87}Sr/^{86}Sr$ ratio may be related to Himalayan uplift it relates less to changes in the Earth's climate because carbonate dissolution does not affect the atmospheric CO_2 composition over long time periods. Thus the preferential weathering of certain lithologies such as carbonates or organic rich sediments can obscure the seawater record for a specific isotope system; changes in the isotopic composition may represent changes in the dominant weathering lithology not changes in the silicate weathering rate. For this reason other isotope proxies have been investigated such as lithium and magnesium, the compositions of which are less dependent on the underlying lithology.

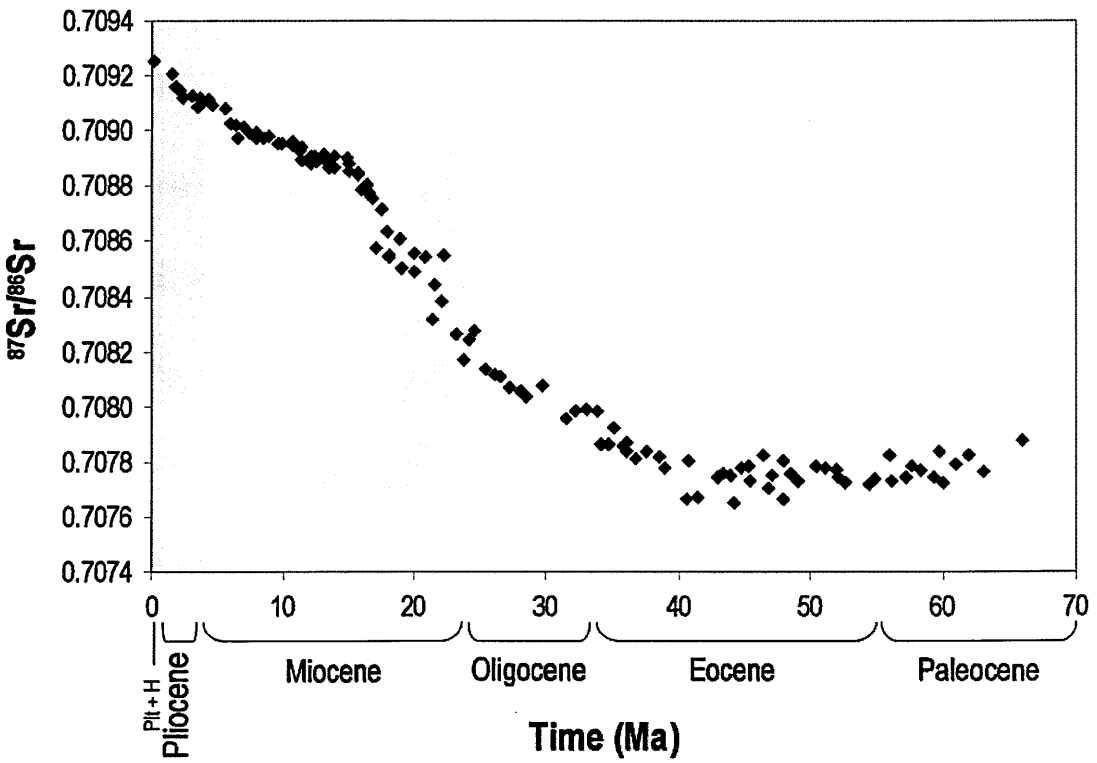

Fig. 1.4 - Variations in the $^{87}Sr/^{86}Sr$ of seawater over the past 70 million years. Data taken from DePaolo & Ingram, (1985), Hess et al. (1986), and Richter et al. (1988).

1.2.4. Modern glacial regions

Global cooling during the Cenozoic led to the formation of permanent ice sheets in the Southern and Northern hemispheres. The formation of this ice has a global impact on the intensity of weathering and the erosional flux delivered to the oceans. Firstly the formation of large volumes of ice reduces the volume of liquid water in the oceans and consequently causes a drop in sea level. Falling sea levels expose more continental crust to be weathered and eroded; over the past 5Ma twice as much terrigenous sediment has accumulated on the ocean floor than over any other similar time period (HAY et al., 1988; MOLNAR, 2004). The highest increase in sedimentation rates occur between 4 and 2Ma, at the same time as the intensification of Northern Hemisphere Glaciation (NHG). There is also a less obvious increase in sedimentation rates at ~15Ma which coincides with oxygen isotope data that imply global cooling (MOLNAR, 2004) and a fall in atmospheric CO_2 (PEARSON and PALMER, 2000); this is coincident with the expansion of the Antarctic ice sheet. In addition to the formation of ice sheets, glaciers also occur in high mountains such as the Himalaya and Andes; the presence of these glaciers enhances the physical weathering rate to much greater levels than would be caused by mountain rivers (ANDERSON et al., 1997). Today, glaciers are found on every continent and in 47 different countries. Major glaciers occur in Antarctica, Greenland, Iceland, Canada and Patagonia.

The majority of this ice is in Antarctica (~90% of the total ice on Earth) with the next largest ice sheet being on Greenland. The high physical weathering potential of glaciers is caused by the fact that when ice builds up to a sufficient thickness it will move downhill (or flow) due to the force of gravity overcoming the resistance to movement of the ice (LEEDER, 1999). As the glacier moves downhill its base and sides exert great forces causing the rock beneath it to be ground to fine silt and clay sized

particles (or rock flour). This sediment is carried within the ice until it reaches the front of the glacier and is deposited during melting. Glaciers produce huge quantities of this fine grained sediment which may then be deposited as wind blown loess, or carried as outwash within the proglacial rivers. While chemical weathering in glacial regions is less intense, this relatively fresh sediment has a high chemical weathering potential due to its high surface area and strain experienced (PETROVICH, 1981). Chemical weathering can also occur in subglacial regions, this is dependent on whether there is liquid water at the base of the glacier. The source of this water is either from surface melting and transfer englacially (within the glacier) to the ice-rock interface along crevasses and moulins (Fig. 1.5. (ZWALLY et al., 2002)) or by melting at the ice-rock interface due to the fact that water is more dense than ice. This subglacial water creates pressure and can buoyantly support the glacier, if this pressure is close to the ice flotation pressure then the glacier will flow at relatively fast rates (~1km/year) (CLARKE, 2005). A number of studies have shown that there is a correlation between surface melting and ice sheet acceleration due to penetration of water to the ice-rock interface (MCMILLAN et al., 2007; ZWALLY et al., 2002). The presence of subglacial water is important because it will have had a longer water-rock contact time than water that has formed on top of the glacier itself (supraglacial water) so will have experienced more chemical weathering. Though still dilute, the high volume of water and higher than expected water-rock contact time means that the chemical denudation rates in glacial catchments can be similar to denudation rates in non-glacial catchments with similar discharge (ANDERSON et al., 1997). Silicate denudation rates are generally much lower however due to the low chemical weathering intensity (ANDERSON et al., 1997). These properties are reflected in the chemical compositions of glacial rivers; they are generally dilute, high in Ca^{2+}, K^{+} and SO_4^{2-} (which originate from easily weathered

trace phases and the oxidation of sulphides) and low in silicon relative to non-glacial rivers (TRANTER, 2003), they also carry a relatively high amount of suspended sediment. This difference in chemistry combined with similar denudation rates to non glacial regions suggests that the intensification of glaciation in the Cenozoic had the potential to alter the composition of continentally derived runoff. Chapters 3 and 4 of this project investigate the composition of rivers with respect to lithium and magnesium isotopes and compare their behaviour to that from non-glacial rivers. The aim is to assess whether global glaciation could have affected the composition of continental runoff.

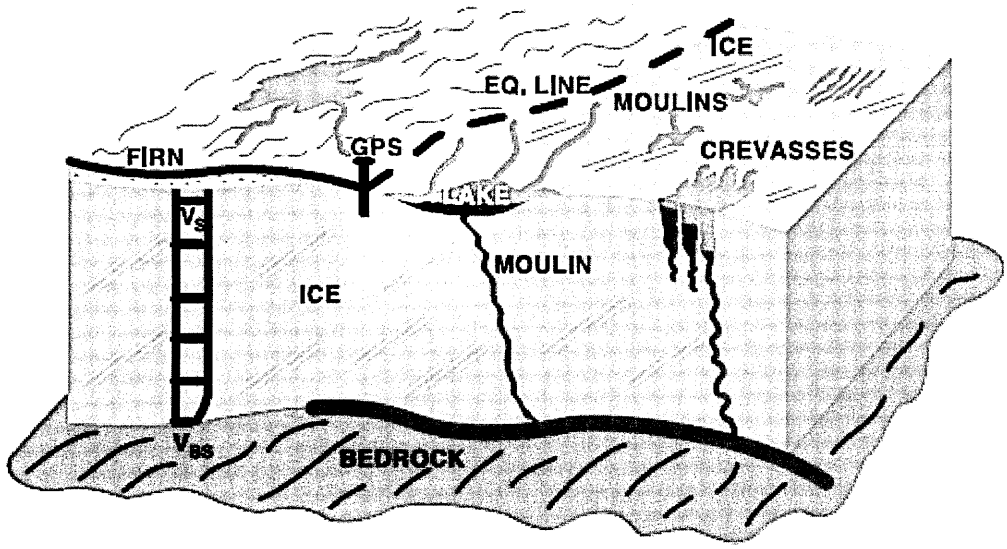

Fig. 1.5 - Schematic of glaciological features including surface lakes, moulins and crevasses (Zwally et al. 2002)

1.3. Weathering processes in experimental systems

1.3.1. Experimental systems

Understanding how isotope systems behave in the natural environment can be complicated by the number of factors that can influence their behaviour. For example the magnesium composition of river waters is dependent on the underlying lithology,

weathering processes such as the formation of secondary minerals (GALY et al., 2002; TIPPER et al., 2006) and biological factors such as the uptake of magnesium by plants (BI et al., 2008; BLACK et al., 2006). For this reason isolating how one factor such as secondary mineral formation affects the magnesium system is difficult; the same is true for all isotope systems in the natural environment that are controlled by multiple factors. A way to counter this problem is to set up experimental systems that can be controlled yet still mimic certain natural conditions.

Such experimental systems can be either open or closed; closed system experiments take place in batch reactors, a self contained setup where nothing is input or output from the system unless specifically changed by the user. Open system experiments take place in through-flow reactors, where there is continual input and output of solution to and from the reactor. There are advantages and disadvantages to each approach. For example, over time closed system experiments lead to a build up of high elemental concentrations in solution and so promote the precipitation of secondary minerals. They are also far simpler to set-up and run, and depending on the apparatus used can be much less expensive. Open system experiments can maintain far lower concentrations in solution (depending on the flow rate used) so are ideal for experiments carried out far from equilibrium such as those designed to determine dissolution rate. When taken together with the benefits of being able to control the flow rate of solution, this means that most experimental work today is carried out using through flow reactors.

Studies involving the determination of dissolution rates of minerals and rocks are extensive, and include many of the major rock forming minerals, including feldspars (ANBEEK et al., 1994; BLAKE and WALTER, 1999; BRANTLEY and STILLINGS, 1996; CHARDON et al., 2006; HOLDREN and SPEYER, 1986; KOBAYASHI et al., 2001; OELKERS and SCHOTT, 1995; OELKERS and SCHOTT, 1998; PETROVIC, 1976; PETROVIC et al.,

1976; SHOTYK and NESBITT, 1992; STILLINGS and BRANTLEY, 1995; STILLINGS et al., 1996; WELCH and ULLMAN, 1996), forsterite (AWAD et al., 2000; CHEN and BRANTLEY, 2000; GIAMMAR et al., 2005; GRANDSTAFF, 1978; KOBAYASHI et al., 2001; LIU et al., 2006; OELKERS, 2001; POKROVSKY and SCHOTT, 2000; ROSSO and RIMSTIDT, 2000; VANHERK et al., 1989; WOGELIUS and WALTHER, 1991; WOGELIUS and WALTHER, 1992), basalt glass (BERGER et al., 1994; BERGER et al., 1988; CROVISIER et al., 1987; CROVISIER et al., 1983; DAUX et al., 1997; GISLASON and OELKERS, 2003; OELKERS and GISLASON, 2001; TECHER et al., 2001; WOLFF-BOENISCH et al., 2006; WOLFF-BOENISCH et al., 2004) and quartz (ANBEEK et al., 1994; BLAKE and WALTER, 1999; MURPHY and HELGESON, 1989; POULSON et al., 1997). Consequently, today there is a great deal of information concerning the dissolution rates of rock forming minerals and natural glasses under different pH and temperature conditions and different solution compositions.

1.3.2. Investigation of isotopic changes in laboratory experiments

While there are abundant dissolution rate data from laboratory experiments, there has so far been very little work that has investigated how isotope systems behave during water-mineral interactions in a controlled environment. There are two scenarios that will be investigated in the current project; the behaviour of isotope systems in far from equilibrium conditions where dissolution of the primary mineral is the only process occurring, and the behaviour at near to equilibrium conditions where secondary mineral formation may take place.

The question of whether isotopes fractionate during mineral dissolution is as yet unanswered. In the case of far from equilibrium mineral dissolution, fractionation appears unlikely as demonstrated for lithium isotopes during the dissolution of basalt

(PISTINER and HENDERSON, 2003). However, slight preferential release of one isotope during dissolution has been observed for iron isotopes during the dissolution of hornblende in the presence of organic ligands (BRANTLEY et al., 2004) and remains a possibility. There is, in theory, more potential for the precipitation of secondary minerals to cause isotopic fractionation, particularly for the lithium and magnesium systems which have been shown to fractionate during the formation of secondary minerals in rivers (HUH et al., 1998; TIPPER et al., 2006). Silicate minerals have different chemical compositions and are stable at different conditions, and different silicate minerals have different isotopic compositions. For example analyses of ultramafic mineral separates show that olivine always has a higher δ^7Li value than pyroxene (SEITZ et al., 2004), while biotite often has a far more radiogenic osmium composition than minerals such as quartz and feldspar (PEUCKER-EHRENBRINK and BLUM, 1998). The dissolution of one mineral and formation of a secondary phase should cause an uptake of (for example) lithium that has a different isotopic composition to that of the dissolving mineral, thus changing isotopic composition of the solution. There have, as yet, been very few attempts to investigate the isotopic shift associated with the formation of secondary minerals. A study of the behaviour of lithium isotopes during smectite formation (VIGIER et al., 2008) and iron isotopes during haematite formation (SKULAN et al., 2002) give mixed results; lithium being fractionated while iron is not. It is hoped that this investigation will shed new light on the question of how primary mineral dissolution and secondary mineral formation will potentially affect the behaviour of isotopic tracers of weathering processes such as Li and Mg. Ultimately this information can be used to assess how these isotope systems behave in the natural environment such as the glacial river catchments in Greenland.

1.3.3. The dissolution of minerals in seawater

The continental weathering flux is comprised of both the dissolved load and suspended sediment; much of the previous work investigating continental weathering has focussed on the dissolved load of rivers as this dissolved material can directly influence seawater composition (DUPRE et al., 2003; GAILLARDET et al., 1999b; MEYBECK, 1987). However the total suspended sediment flux is not trivial; an estimated 20 billion tonnes of sediment is transported by rivers every year (MILLIMAN and SYVITSKI, 1992). Much of this sediment is buried but some is also reworked and subjected to further weathering thus can continue to influence seawater chemistry. High relief and tectonically active islands contribute >45% of river suspended material that is carried to the oceans via rivers (MILLIMAN and SYVITSKI, 1992), much of this material is basaltic in origin. For example detrital sediment from Icelandic glacial rivers has been shown to have a high basaltic glass content (STEFANSDOTTIR and GISLASON, 2005) and though this glass may already be weathered it still readily dissolves on contact with seawater (GISLASON et al., 2006). The ubiquity of basalt glass at mid ocean ridges and on the sea floor as well as that which is continentally derived, together with its high reactivity means that the interaction between basalt glass and seawater is globally important. Unfortunately experimental studies of the dissolution of basalt glass in seawater at low temperature are limited (CROVISIER et al., 1987; STAUDIGEL et al., 1998; STEFÁNSDÓTTIR and GÍSLASON, 2006). Consequently, part of this thesis work also involved an experimental investigation of the dissolution of basalt glass in seawater in order to determine dissolution rates and to assess the behaviour of the lithium and magnesium isotope systems during this interaction.

1.4. Isotope systems as a tracer of continental weathering

Many natural isotopes (both radiogenic and stable) have been used to study processes that range from solar system formation, to mantle differentiation, to weathering and climate change yielding information on both mechanisms and timescales. However, each isotope system responds in a different way, and for radiogenic systems on different timescales. Thus it is crucial to use a system that is appropriate to the application. The focus of this thesis is to study the effects of weathering on key isotope systems used as proxies of climate change in marine sedimentary archives. Amongst those isotope systems that have been used in the study of weathering are the radiogenic systems Rb-Sr (GALY et al., 1999; MCARTHUR et al., 2001; PALMER and EDMOND, 1989; VIERS et al., 2000), Sm-Nd (BURTON et al., 1999b; VANCE and BURTON, 1999), Lu-Hf (BAYON et al., 2006; VAN DE FLIERDT et al., 2002), Re-Os (BURTON et al., 1999a; ESSER and TUREKIAN, 1993; LEVASSEUR et al., 1999; PEUCKER-EHRENBRINK and BLUM, 1998; RAVIZZA and TUREKIAN, 1992; SHARMA et al., 1999) and U-series (POGGE VON STRANDMANN et al., 2006; RIOTTE et al., 2003) and the stable isotope systems of Li (CHAN et al., 1992; HUH et al., 1998; PISTINER and HENDERSON, 2003; TENG et al., 2004), Ca , Mg (TIPPER et al., 2006; YOUNG and GALY, 2004) and more recently Si (DE LA ROCHA et al., 2000; GEORG et al., 2007).

1.4.1. Stable isotope systems

The benefits of using a stable isotope system, such as those of lithium and magnesium, is that the isotope compositions are dependent on both the composition of the underlying bedrock as well as the processes of weathering. These systems show significant fractionation due to the large relative mass differences between isotopes.

1.4.1.1 Lithium

Lithium has two stable isotopes in approximate abundances of $^{6}Li \sim 7.5\%$ and $^{7}Li \sim 92.5\%$. Because of its relatively large mass difference it has the potential to fractionate in nature and hence to be a good tracer of weathering processes. Lithium isotope ratios are reported relative to the NIST LSVEC standard:

$$\delta^{7}Li = \left[\left(\frac{\left(\frac{^{7}Li}{^{6}Li} \right)_{sample}}{\left(\frac{^{7}Li}{^{6}Li} \right)_{LSVEC}} \right) - 1 \right] \times 1000 \qquad \textit{Equation 1.10}$$

Due to this large relative mass difference there is a significant range of $\delta^{7}Li$ values in the natural environment, from saprolites with an extremely light isotope ratio of -20‰ (RUDNICK et al., 2004) to seawater with a uniform composition of 31‰, up to the dissolved load in rivers which can exceed 40‰ (POGGE VON STRANDMANN et al., 2006). Lithium behaves conservatively in the oceans with a residence time of around 1 million years, and the isotope composition is globally uniform in the oceans with an average $\delta^{7}Li$ ratio of 31‰ and Li concentration of 0.17ppm (HATHORNE and JAMES, 2006). These values are maintained by the balance of the Li inputs and outputs to and from the ocean. Lithium is added to the oceans by both rivers ($\delta^{7}Li \sim 23‰$, (HUH et al., 1998)) and high temperature hydrothermal fluids at mid ocean ridges ($\delta^{7}Li \sim 6.7‰$, (BRAY et al., 2001)). Both of these Li sources are isotopically lighter than seawater itself, which suggests that within the oceans some process must be occurring that preferentially removes the light isotope of lithium (^{6}Li), leaving the dissolved phase to be isotopically heavy. Studies of oceanic basalts suggest that during weathering processes the

formation of secondary minerals such as clays preferentially take up ^{6}Li (CHAN et al., 1992). This process has been shown to occur both naturally in rivers and experimentally through mineral sorption and precipitation experiments (CHAN and HEIN, 2007; HUH et al., 1998; KISAKUREK et al., 2005; KISAKUREK et al., 2004; PISTINER and HENDERSON, 2003; VIGIER et al., 2008). Lithium can be adsorbed into loosely bound outer sphere sites caused by electrostatic attraction (physisorption), or more tightly bound by chemical bonds (chemisorption) (CHAN and HEIN, 2007). Physical adsorption is the result of electrostatic attractions between the mineral surface and ions in solution. These attractions form outer sphere complexes on the mineral surface and neither Li isotope is preferentially adsorbed so for example there is no isotopic fractionation when Li is adsorbed onto the negatively charged surface of smectite (PISTINER and HENDERSON, 2003). This was also shown by Chan & Hein (2007) during leaching experiments on Fe-Mn crusts. The second mechanism is chemisorption; this involves the formation of chemical bonds in the inner sphere of the mineral surface. Chemisorption occurs even when the charges on the mineral surface and adsorbing species are the same. It has been shown to preferentially incorporate certain elements and isotopes. Results of Li adsorption experiments on ferromanganese minerals (CHAN and HEIN, 2007) show that amorphous goethite preferentially sorbs ^{6}Li into inner sphere surface complexes, thus causing Li isotope fractionation. This incorporation of ^{6}Li into inner sphere bonds also occurs during sorption onto illite (WILLIAMS and HERVIG, 2005) and smectite (VIGIER et al., 2008). Within the oceans the preferential removal of ^{6}Li occurs in a number of ways. A major mechanism of removal is the alteration of sea floor basalt and the incorporation of Li into alteration products such as smectite (CHAN et al., 1992). The formation of altered minerals by hydrothermal processes is also important; hydrothermally altered rock having a lighter

lithium composition than unaltered rock (CHAN et al., 1994). The last major mechanism of removal is the alteration of continental sediments that are input by rivers and associated uptake of lithium. For example a recent study of an Icelandic estuary shows that the Li concentration and composition of basaltic sediment alters with salinity, suggesting that the further weathering of continental sediment in seawater could be significant for the oceanic lithium budget (POGGE VON STRANDMANN et al., 2008).

1.4.1.2. Magnesium

Magnesium has 3 stable isotopes, ^{24}Mg (79% abundance), ^{25}Mg (10%) and ^{26}Mg (11%). During processes such as evaporation these isotopes partition according to mass causing isotope fractionation that is large enough to be measurable.

Like lithium, magnesium isotopes ratios are normalised to a standard; in this study the standard used is Dead Sea magnesium (DSM3):

$$\delta^{26}Mg = \left[\left(\frac{\left(\frac{^{26}Mg}{^{24}Mg} \right)_{sample}}{\left(\frac{^{26}Mg}{^{24}Mg} \right)_{DSM-3}} \right) - 1 \right] \times 1000 \qquad \textit{Equation 1.11}$$

The concentration and isotopic composition of seawater are uniform at 53mmol/l and 0.82 ‰ (TIPPER et al., 2006). The major source of magnesium to the oceans is from continental waters via the dissolution of both Mg- carbonates and silicates. The major sinks are via mole-for-mole exchange with Ca on basalts at mid ocean ridges (BERNER, 2004), and via dolomite precipitation (HOLLAND and ZIMMERMAN, 2000). There is also exchange with Ca in detrital sediments derived from continental weathering, particularly clays and volcanic glasses (GISLASON et al., 2006). Recent studies have

shown that the dissolution of this suspended sediment in deltas and estuaries can be a major source of dissolved solids in seawater (GISLASON et al., 2006).

Table 1.1

The magnesium isotope composition of some common rocks, and rock averages

Sample	**δ^{26}Mg** (relative to DSM-3)	**Reference**
Basalt	-0.09 to -0.18	Wiechert et al. 2007
Basalt Glass	-0.2 to -0.26	Wiechert et al. 2007
Olivine	-0.06 to -0.08	Wiechert et al. 2007
Clinopyroxene	0.04 to 0.06	Wiechert et al. 2007
Chondritic meteorites	-0.24 to -0.49	Wiechert et al. 2007
Limestone	-2.5	Tipper et al. 2006
Silicate rock average	-0.5	Tipper et al. 2006
Silicate soil average	-0.03	Tipper et al. 2006
Riverine average	-1.09	Tipper et al. 2006

Work by Galy et al. (2002) and Tipper et al. (2006) has shown that magnesium will readily fractionate in the weathering environment, although not to the same extent as lithium because the relative mass difference between magnesium isotopes is far smaller. Results of carbonate studies (BUHL et al., 2007; GALY et al., 2002) show that the magnesium isotope composition of speleothems is isotopically lighter than the drip water, suggesting that the light isotope is preferentially incorporated into the solid phase leaving the resultant solution isotopically heavy. However, later studies of silicate weathering (TIPPER et al., 2006) suggest that soils are isotopically heavier than the silicate bedrock and the corresponding water is isotopically light. These studies show that the magnesium system is more complicated than that of lithium; magnesium isotopes are controlled by both lithology and more importantly by weathering processes. Because the composition of seawater (-0.82‰) is isotopically heavier than that of the riverine average (-1.09‰, Tipper et al. 2006) (the major source of magnesium to the

oceans) it means that one of two processes must be occurring within the oceans. Either the oceans are not at a steady state with respect to magnesium and/or magnesium isotope ratios must be fractionated in the ocean (TIPPER et al., 2006). In order to get an ocean that is isotopically heavier than its source, removal of magnesium must preferentially take out light magnesium, suggesting that carbonate formation is the main cause.

A further complication to the magnesium system is the impact of biology and fractionation caused by biological processes. Magnesium is the central metal atom in the chlorophyll molecule so is crucial for photosynthesis and the formation of life on Earth. A study investigating isotopic changes (BLACK et al., 2006) shows that chlorophyll preferentially takes up the light magnesium isotopes relative to the growth medium. Conversely, a study by Ra & Kitagawa (2007) shows that chlorophyll in marine phytoplankton is isotopically heavy relative to seawater. Magnesium is also present in plant proteins and stored as free Mg^{2+} in the vacuoles of plant cells (SHAUL, 2002). A study by Bolou Bi (2008) shows that during higher plant growth the bulk plant is isotopically heavy relative to the magnesium source. This preferential uptake of heavy magnesium is highlighted by an experiment using a living root; after 60 minutes in a magnesium solution the solution became between 2.4 and 3.1 ‰ lighter than the source magnesium.

Evidence from chemical and biological studies shows that the magnesium system is very complicated with no controlling factors being fully resolved. This leaves the determination of its behaviour in natural systems very difficult. For this reason more work investigating this potentially useful weathering tracer is needed.

1.4.2. Radiogenic isotope systems

Radiogenic isotope systems are those where a radioactive parent isotope decays to the radiogenic daughter isotope. These systems are useful because lithology plays an important part in determining the isotopic composition of the signal derived from continental weathering (BLUM and EREL, 2003). Age of the rock is also important; an older rock should in theory have a more radiogenic isotope composition (DICKIN, 1995). If the half life of parent-daughter decay is known then ages of the rock can be estimated.

1.4.2.1. Rhenium-Osmium (Re-Os) system

Osmium is a platinum group element with seven naturally occurring isotopes. One of these, ^{187}Os, forms from the beta decay of ^{187}Re and the ratio of parent to daughter has been used for many years as a geochemical tracer and dating tool. Rhenium and osmium have different compatibilities during partial melting; osmium is a compatible element and stays in the mantle while rhenium is mildly incompatible and enters the melt. For this reason rocks in the crust (both continental and oceanic) have high Re/Os ratios. Over time the rhenium will decay to ^{187}Os so older rocks will have much higher concentrations of ^{187}Os and higher $^{187}Os/^{188}Os$ ratios.

The major control over the osmium composition of the continental crust is rock type and age. Different rock types have different $^{187}Re/^{187}Os$ ratios and so will produce different amounts of ^{187}Os over time. River studies have shown that the dissolved load is not always compositionally similar to the suspended or bedloads, and this is attributed to incongruent dissolution of mineral phases (GANNOUN et al., 2006). Examples of minerals that dissolve incongruently and have an impact on riverine chemistry are biotite which contains relatively radiogenic osmium (PEUCKER-EHRENBRINK and BLUM, 1998) and olivine and pyroxenes which have extremely high $^{187}Re/^{187}Os$ ratios and so

develop high levels of radiogenic osmium on relatively short timescales (GANNOUN et al., 2004). Incongruent weathering of these phases can therefore have a significant impact on the riverine osmium composition and potentially affect the composition of seawater.

The oceanic composition of rhenium and osmium reflects a balance of inputs from continental weathering, exchange at mid oceanic ridges and micrometeoritic dust. When this balance shifts the oceanic composition will change and this is reflected in the sediment record. Over the last 50 million years the oceanic $^{187}Os/^{188}Os$ ratio has increased from ~0.2 at the K-T boundary to ~1.06 at the present day (Fig. 1.6). The composition of the continental weathering input is estimated to be 1.5 compared to the $^{187}Os/^{188}Os$ composition of micrometeoritic material and basaltic crust (~0.13), with the latter sources varying only very slightly over the Cenozoic. This means the change to a more radiogenic osmium composition can be attributed to variations in the continental weathering signal input to the oceans.

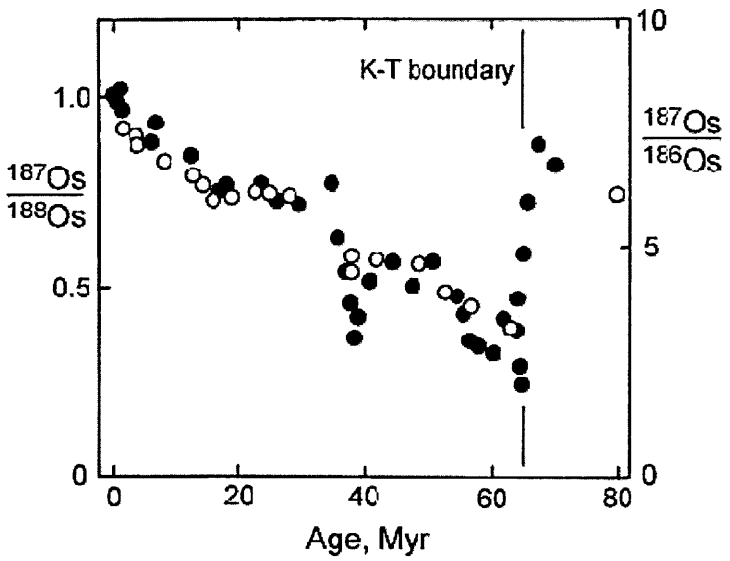

Fig. 1.6 - Plot of Os isotope ratio of sediment leachates against age during the last 80 million years (Dickin 1997)

Rhenium and osmium are not distributed evenly in the continental crust, instead they are concentrated in accessory phases such as PGE alloys and sulphides, as well as having high concentrations in organic rich rocks such as black shales. For this reason the composition of bedrock and the rivers that drain them depend on the weathering of these PGE rich phases. Studies have shown that intensely weathered soils called laterites can be enriched in PGE-rich alloys (BOWLES, 1986), so could potentially have high rhenium and osmium concentrations. Laterites are estimated to cover ~30% of the exposed continental crust (TARDY, 1997) and commonly have thicknesses of between 20 and 100m (BRIMHALL et al., 1991). An initial study of the Re-Os system in lateritic soils (SHARMA et al., 1998) shows that there is a substantial enrichment of osmium in the topsoil. The last part of this thesis will involve the study of two laterite profiles in India and investigate the behaviour of the Re-Os system during intense tropical weathering.

1.5. Project Aims

The overall objective of this project iss to investigate continental weathering processes; more specifically to determine how changes in climate, weathering intensity and lithology can affect the behaviour of different isotope systems as well as the continental weathering flux to the oceans. To this end the first aim of this project has been to investigate recently glaciated river catchments in Greenland to study the water chemistry and how the lithium and magnesium isotope systems behave in this environment. The lithium and magnesium isotope systems are relevant in this case because they respond to changes in weathering processes; both elements fractionate during the formation of secondary minerals. In theory their behaviour in glacial rivers

where secondary mineral formation will be less important, should be different to their behaviour in non-glacial rivers. This is investigated in Chapters 3 and 4.

Gaining a full understanding of the behaviour of such isotope systems in natural systems is complicated by factors such as lithology and (for magnesium) biology. For this reason the second aim of the project has been to investigate the behaviour of these isotope systems during experimental weathering reactions (Chapters 5 and 6). It is hoped that the results of these experiments will enable better understanding of the behaviour of these isotope systems in natural systems such as the Greenland rivers.

The final part of this project is an investigation of extreme tropical weathering of continental sediments and the associated formation of laterite profiles. These weathering profiles are known to concentrate elements such as iron and aluminium, but also the platinum group elements such as osmium. For this reason two Indian laterite profiles have been analysed (Chapter 7) with the aim of understanding how their formation will affect the global cycle of rhenium and osmium.

Chapter 2

Analytical techniques and experimental methods

This chapter describes the various methods used for sample collection, processing and analysis. This includes detailed descriptions of dissolution techniques for ICP-MS analyses, Re-Os sample extraction and cation column chemistry for separation of lithium and magnesium. The chapter also details the methods for analyses of Re-Os by TIMS, and Li and Mg isotopes by MC-ICP-MS. Finally, the techniques used for the setup and running of dissolution and precipitation experiments are described.

2.1 Sample Collection

2.1.1. Greenland rivers – July 2006

A total of 15 river samples were collected from the Kangerlussuaq region of western Greenland (Chapters 3 and 4). At each sample location a total of 25 l of water was collected and stored in pre-cleaned (acid washed) containers. Between 100 and 200 g of the bedload sediment was also taken at each locality and stored in clean plastic bags. Approximately 100 ml of the river water was filtered (0.2 μm) in the field using a hand pump. The difference in mass of the filter before and after filtration was used to calculate the concentration of suspended sediment in each river sample. A series of in situ measurements were also made; pH (using a Hanna Instruments pH sensor), temperature and TDS (using a Hanna Instruments TDS meter) were all recorded at each sample location. Within 12 hours of sampling the water samples were filtered (<0.2 μm) using a Sartorius frontal filtration unit; the suspended particulates were collected from each filter and stored while filtered water was either collected for later analysis or further filtration. Ten litres of filtered water was retained for co precipitation with iron solution and concentrated purified ammonia in order to collect sufficient quantities of

low abundance metal cations such as uranium and thorium. The last 5-10 l of the filtered water from each sample was filtered again (10 kD) using a Sartorius tangential filtration system. The result of this process is that any molecules larger than 10 kD are prevented from passing through the filter membrane, such that the residual solution is a mixture of colloids and the initial filtrate (<0.2 μm, >10 kD), while the filtrate contains only truly dissolved material (<10 kD). The ultrafiltration process continued until around 250 ml of residual solution was left. The total filtration process is illustrated below in Fig. 2.1.

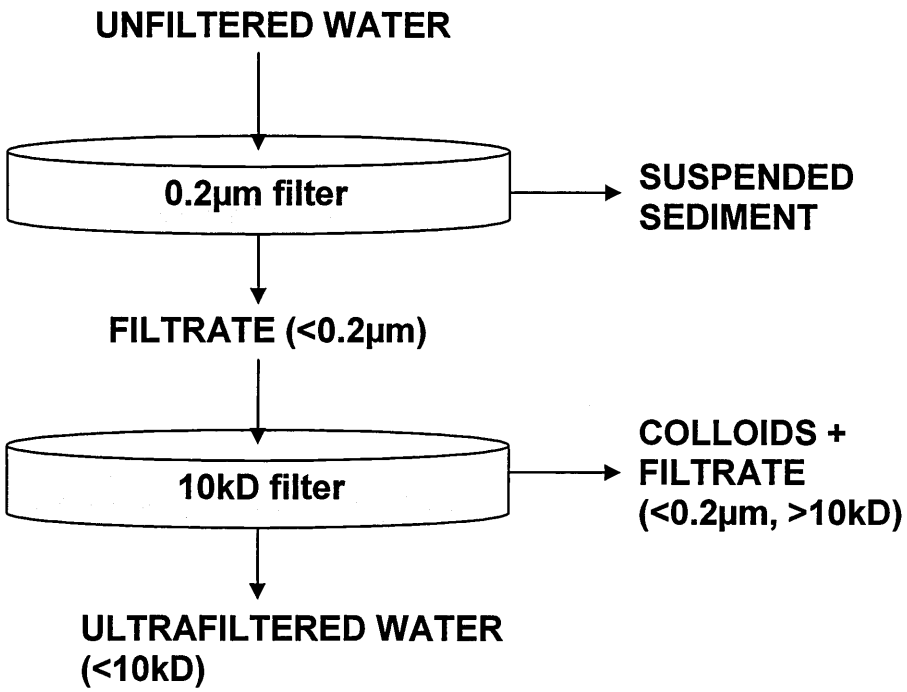

Fig. 2.1 – A diagram showing the filtering steps used in this study.

Alkalinity measurements were performed subsequent to filtration in order to keep the volume of CO_2 that could dissolve into solution to a minimum. The alkalinity of each river sample was measured by titrating against 0.01M HCl. A 40 ml sample of river water was taken, to which between 50 and 200μl of 0.01M HCl was added at each step and the pH change recorded until the concentration of H^+ starts to rise linearly with

the amount of H^+ added (APPELO and POSTMA, 2005). The volume of acid used is then plotted against the Gran function (G) (Equation 2.1). A typical plot is given in Fig. 2.2.

$$G = (V + V_o) \cdot 10^{-pH} \qquad \textit{Equation 2.1}$$

Where V = the volume of acid added and V_0 = the initial volume of solution

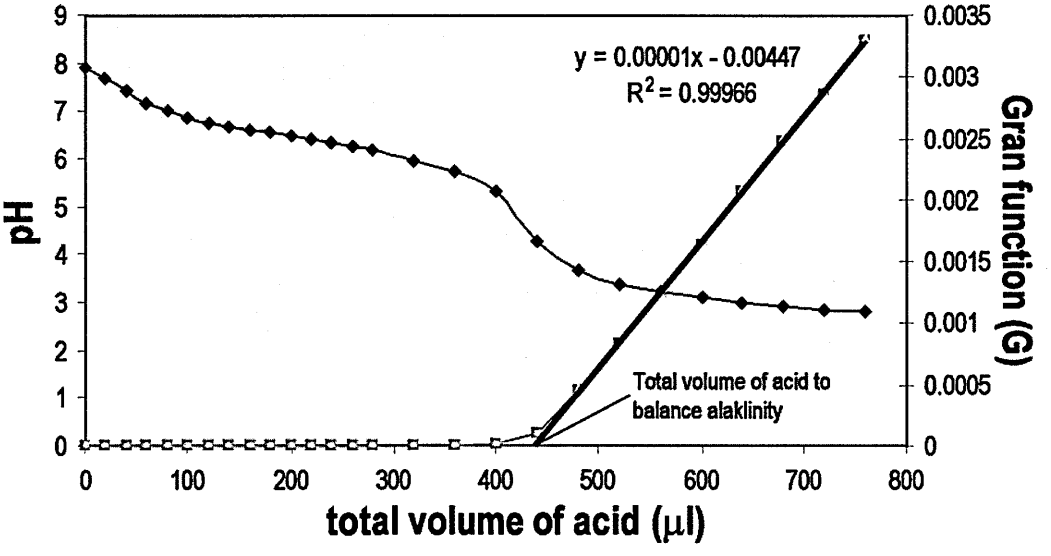

Fig. 2.2 - A graph showing the calculation of alkalinity in a seawater sample. The blue line shows the change in pH with volume of acid that is added. The pink line shows the Gran function. The intersect between the straight line and the x-axis gives the volume of acid needed to neutralise the alkalinity of the solution.

The equivalence point is found by extrapolating the linear part of the graph to the x-axis, this being the volume of acid needed to neutralise the alkalinity. All alkalinity measurements were performed in this way throughout the course of the study, although measurements of seawater alkalinity were performed with a sample size of 20ml and titrated with 0.1M HCl.

2.1.2. Laterite weathering profiles

A study of two Indian laterite profiles is presented in Chapter 7. All samples were collected prior to this study; the Bidar laterite succession being previously analysed for lithium (KISAKUREK et al., 2004) and Sr and Nd isotopes (MASON, 2000).

Samples from both laterite profiles were taken at key textural horizons, or else taken immediately above or below (i.e. bracketing) levels where distinct textural changes are observed. Because the weathering profiles are highly heterogeneous, both vertically and horizontally, large samples (between 1 and 3 kg) were taken from 2-3 sample sites in the same horizon and these samples were then homogenised by milling with agate.

2.2 Sample Processing

2.2.1. XRF major elements

Major element analyses of rock and sand samples were performed by XRF (X-Ray Fluorescence). Rock samples were crushed using a jaw crusher, crushed rock and sand was then ground to a powder of around 200 μm using an agate tema. Fused glass discs were made using a combination of dried rock powder and lithium metaborate flux in a ratio of 5:1. This was heated at 1100°C in Pt-5%Au crucibles, with the molten liquid moulded into a fused glass disc. Once cool this glass disc could then be analysed by XRF (Section 2.5.1.1). The percentage loss on ignition (LOI) of volatile components such as CO_2 and H_2O was calculated separately. This was carried out by measuring the change in mass of rock powder before and after igniting at 1000°C for one hour.

2.2.2. ICP-MS chemistry

Major and trace elements in the suspended sediment and in solution, as well as trace elements in rocks and sands were all analysed by ICP-MS. Solid material was ground to a powder using an agate mill (as for XRF analyses) and a 0.1g aliquot then dissolved using 1ml of 15M Teflon distilled (TD) HNO_3 and 2 ml of Aristar HF at 120°C for 24 hours. The full ICP-MS dissolution procedure is presented below:

- Weigh out ~0.1g of sample powder as precisely as possible into a 15ml Savillex vial.
- Add 1ml of 15M TD HNO_3 and 2ml of Aristar HF
- Cap and heat on a hotplate at 120°C for 24 hours
- During this period, remove the vial from the hotplate and sonicate the solution twice
- Evaporate the sample to incipient dryness
- Add 2ml of TD 6M HCl
- Heat the sample on a hotplate at 120°C for 24 hours
- Remove the cap and evaporate the sample to incipient dryness
- Add 2ml of 15M TD HNO_3 and 4ml of MilliQ (MQ) H_2O
- Cap and heat on a hotplate at 120°C for 24 hours
- During this period, remove the vial from the hotplate and sonicate the solution twice
- Remove the cap and evaporate the sample to incipient dryness
- Add 3ml of 15M TD HNO_3 and 6ml of MilliQ (MQ) H_2O
- Cap and heat on a hotplate for at least 4 hours

- Add the sample to a 125ml bottle that has been weighed and acid cleaned. Rinse the sample vial out 3 times with MQ.
- Add enough MQ water for a 1000 times dilution.

Processing the dissolved samples was far more straightforward; this simply involved all solutions being acidified to 2% HNO_3 using 15M TD HNO_3.

2.3 Leaching experiments

Three suspended sediment samples were subjected to a two stage acid leaching process similar to that used in Chan & Hein (2007). A gentle leach involving buffered acetic acid, designed to remove freely exchangeable cations, was followed by a more vigorous leaching procedure involving 2N TD HCl, designed to remove cations bound to iron and manganese oxyhydroxides. The leachates were then analysed using ICP-MS and further analysis was carried out for lithium isotopes by MC-ICP-MS (multi-collector inductively coupled plasma mass spectrometer). Details of the mass spectrometry are presented in Sections 2.3 and 2.4.

The two stages of the leaching process are described below:

Stage 1 – Acetic acid leach

- Add ~0.2g of suspended sediment to an acid cleaned 14ml centrifuge tube.
- Add 8 ml of sodium acetate buffer solution (pH 4.6, Riedel de Haan). Cap and agitate in an ultrasonic bath for 45 minutes.
- Centrifuge for ~10 minutes at 4500 rpm. Remove the supernatant and store in a cleaned 30 ml Savillex vial.

- Add another 8ml of buffer solution to the residue. Cap and shake vigorously to make sure the sediment returns to solution. Agitate in the ultrasonic bath for 45 minutes.
- Remove the supernatant and add to the same Savillex vial.
- Add another 8ml of buffer solution, repeat as above.
- Add 8ml of Milli-Q water, repeat as above.
- Dry down the combined solutions and make up to 10ml of 2% TD HNO_3.

Stage 2 – HCl leach

- Transfer the residue from stage 1 to a clean 30ml Savillex vial.
- Add 8ml of 2N TD HCl and heat on a hotplate (at ~120°C) overnight.
- Transfer the contents of the Savillex vial to a clean centrifuge tube, centrifuge add the supernatant solution to a clean 30ml Savillex vial.
- Add 8ml of Milli-Q to the residue, cap and agitate in an ultrasonic bath for 45 minutes. Centrifuge and add the supernatant solution to the solution in the Savillex vial.
- Dry down the solution and redissolve in 10ml of 2%TD HNO_3.

2.4 Isotope Chemistry

2.4.1. Rhenium and osmium: sample preparation and chemistry

The laterite samples were measured for changes in the $^{187}Os/^{188}Os$ and $^{187}Re/^{188}Os$ isotope ratios. They were processed using the isotope dilution technique developed by (BIRCK et al., 1997). Samples were ground to a fine powder using an agate tema. Sample powders were spiked with a mixed ^{185}Re-^{190}Os spike solution and dissolved

using a mixture of HF and TD HBr at 140°C for 72 hours. This technique requires that the spike equilibrates with the osmium in the sample so that after dissolution they must be in the same oxidation state. The separation is achieved by using CrO_3 (in HNO_3) to convert all the Os from the sample and spike into OsO_4. Because OsO_4 penetrates readily into the plastic walls of Teflon beakers the yield of osmium can become severely reduced. In order to counter this process the OsO_4 is extracted into liquid bromine, dried down and the residue purified by microdistillation. Separation of Re is much more straightforward, it generally exists in one oxidation state, does not penetrate into Teflon and does not evaporate at temperatures below 200°C. An aliquot for rhenium analysis is dissolved in 2% HNO_3 and extracted using iso-amylol.

There is a possibility that low temperature acid digestion may not recover all the Re and Os present in the samples, particularly when PGE-rich phases are present (MEISEL et al., 2003). Thus, in order to ensure that both Re and Os are fully recovered from the samples studied here, high pressure and high temperature microwave sample decomposition (Multiwave 3000, Anton Paar®) was also used. The duplicated samples were chosen so as to be representative of the entire range observed for both profiles. Approximately 0.2 g of sample material was spiked and digested using HF+HCl (3:3 ml) acid mixture in a fluoropolymer vessel at 240 °C and 60 bar for 2 h. The solutions were then transferred into a PFA pressure vial, evaporated to dryness and redissolved with HF-HBr (2:2 ml) at 150°C for 48 h. The subsequent sample oxidation and Os extraction step was similar to that used in the technique described above.

2.4.2. Lithium isotope chemistry

Samples were dissolved using the ICP-MS dissolution technique previously described in Section 2.2.2, or are experimental/natural solutions. When analysing solutions by

MC-ICP-MS the mass spectrometer uses up ~0.5 ml per sample run and a concentration of ~10ppb is needed to measure the Li isotope ratio effectively. For this reason at least 5ng of Li is needed to run each sample once. It is beneficial to be able to run repeat measurements where possible so typically between 10 and 20 ng of each sample was processed. In order to prepare adequate amounts of each sample for lithium analysis the Li concentration of all samples was determined by ICP-MS prior to isotopic characterisation. Once sufficient solution is dried down the sample can be loaded on to the cation columns and the lithium can be isolated by cation exchange chromatography.

The technique for purification of lithium is similar to that documented by James and Palmer (2000). The cation columns used in this study are Teflon with an internal diameter of 6mm. They are loaded with 2.4ml of Bio-Rad AG50W-X12 200-400 mesh cation exchange resin to a resin height of 8.5cm. Prior to loading the columns are pretreated with MQ water in order to wet the resin and to remove any air bubbles. Next, 8ml of TD 0.2N HCl is added, after this stage the column height is measured to make sure the resin height it is 8.5cm, if this is not the case resin needs to be removed/added and 4ml more TD 0.2N HCl is added.

After pre-treatment the following method is performed:

- Add ~ 0.1ml of 0.2N TD HCl to each sample and make sure sample is fully dissolved. If not add more 0.2N TD HCl to a maximum of ~0.5ml.
- Once the sample has been dissolved carefully add it to the top of column.
- Once the sample has eluted add 0.5ml 0.2N TD HCl to the column and repeat this step once more.
- Elute 20ml of 0.2N TD HCl through the column and discard the flushed acid.
- Elute 21ml of 0.2N TD HCL and collect all the acid in precleaned Savillex vials.
- Dry down the sample.

- Prior to analysis by MC-ICP-MS the sample can be dissolved in 3% TD HNO_3. The volume of nitric acid used is dependent on the mass of lithium that has been processed. Enough acid should be used so that the resultant solution has a lithium concentration of 10ppb.
- After the sample has eluted clean the columns by flushing through ~25ml of 6M TD HCl.
- Subsequently elute 8ml of MQ H_2O through the column and store each cleaned column in MQ water to keep the resin moist.

2.4.3. Magnesium isotope chemistry

The separation of magnesium also uses cation exchange chromatography similar to that for lithium. The major difference between these techniques is the use of an anion column for all rock samples to remove any potential interference from iron, as used by (WIECHERT and HALLIDAY, 2007).

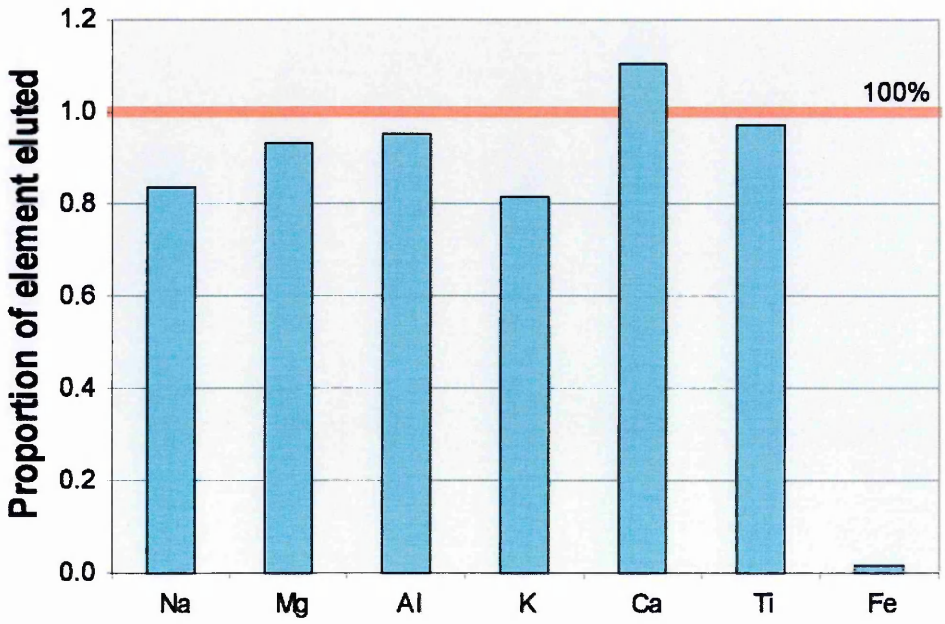

Fig. 2.3. - A plot showing the proportion of elements that are eluted through the anion column using the rock standard AGV-1

Fig. 2.3 shows the yield of cations that are eluted through the anion column (where 1 = 100%). Most major cations are unaffected (including magnesium) while the yield of iron that is recovered is very low (~2%) indicating that most of the iron is retained on the column. The anion stage is not needed for river or seawater samples as the concentration of Fe is low. Once the magnesium has been separated the samples are analysed by MC-ICP-MS; because Mg has a high natural abundance the samples can be run under wet plasma conditions and the typical sample size is between 500 and 2000 ng of Mg.

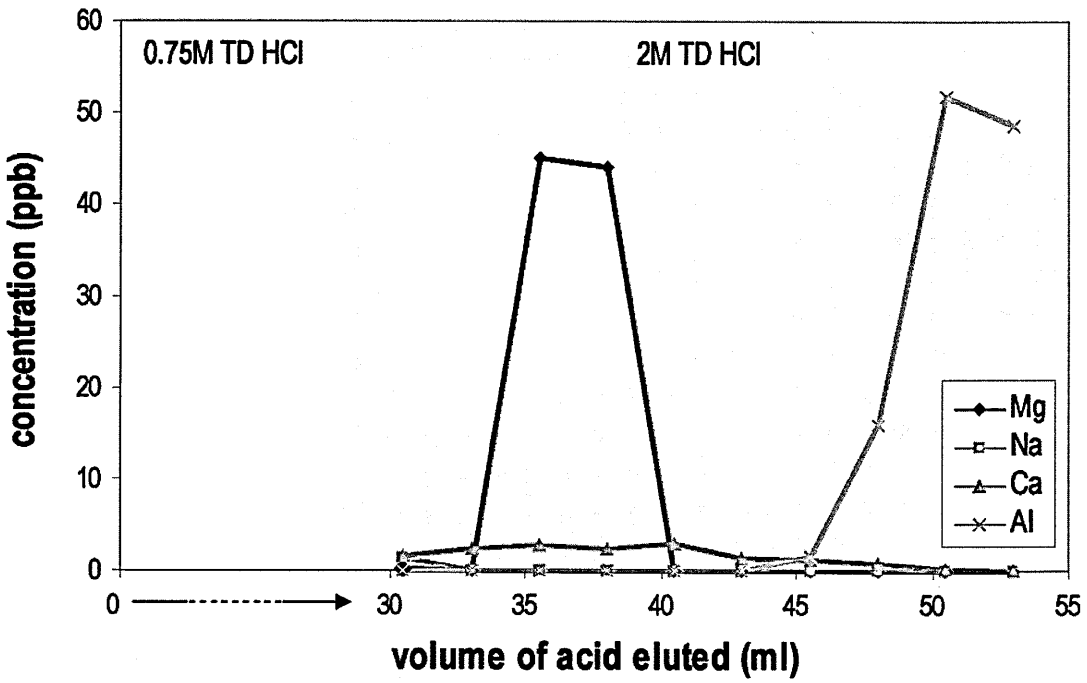

Fig. 2.4 - A cation column calibration showing the separation of Mg from Ca, Na and Al.

The cation columns used are identical to those used for the processing of lithium, together with the Bio-Rad AG50W-X12 resin. The addition of certain elements (Ca, Na and Al) to a magnesium solution has been shown to cause a mass bias, affecting the δ^{26}Mg ratio by between 0.2 and 1‰ (GALY et al., 2001). It is therefore important to

demonstrate that these elements have been removed from solution during the chemical separation. As can be seen from Fig. 2.4 during the first 14ml of eluted 2N TD HCl all of the magnesium is collected but there is little Na, Ca or Al (see Appendices A1 and A2 for data from the anion and cation column calibrations). Na is removed earlier on during the elution of 0.75N HCl, and the Ca and Al are removed later. Anion columns are also Teflon and have a total volume of 2.1ml and column diameter of 6mm. The anion resin used in these columns is Bio-Rad AG1-X8 (200-400 mesh).

Anion Column

- Preclean columns with MQ water and 8 ml of 6M HCl.
- Check resin height. If it is not 7 cm add or remove resin and elute a further 4 ml of 6M HCl.
- Dry down the sample aliquot (containing 500-2000 ng of Mg) and re-dissolve in ~0.5 ml of 6M HCl.
- Load sample into the top of the anion column
- Elute Mg with 7 ml of 6N TD HCl
- Dry down the sample to incipient dryness; pass through the cation column (see below).

Cation Column

- Precondition the resin with 4 ml of 6N TD HCl followed by 8ml of 0.75N TD HCl.
- Check resin height. If it is not 8.5 cm then add/remove resin and elute a further 4 ml of 0.75N TD HCl.
- Re-dissolve the sample in ~0.1 ml of 0.75N TD HCl.

- Wash in sample with 2 × 0.5 ml of 0.75N TD HCl.
- Elute light cations with 28 ml of 0.75N TD HCl.
- Collect Mg in14 ml of 2N TD HCl.
- Dry to incipient dryness.
- Clean the columns using 25 ml of 6M TD HCl, followed by 8ml of MQ water, then 8 ml of 6N TD HCl and finally 8 ml of MQ water.

2.5 Mass spectrometry

2.5.1. Major and trace element analyses

2.5.1.1. Rock, sand and suspended particulates

Major element analyses were carried out by X-ray fluorescence (XRF) for all Greenland rock and sand samples. Analyses were performed using an ARL 8420+ dual goniometer wavelength-dispersive XRF spectrometer employing routine XRF procedures and analytical packages. Elemental intensities were corrected for background and known peak overlap interferences and medium-term instrumental intensity drift was taken into account using a drift normalisation monitor. The accuracy of the XRF measurements is determined by running reference samples of a known composition and comparing the measured value with the literature value. The standards used were WS-E (Whin-Sill dolerite) and an in house standard OUG94; measured values are typically within 1% of the certified values (Appendix A3).

Trace and minor element analyses for rock samples and major element analyses for suspended particles and experimental minerals and glass were performed using an Agilent 7500a ICP-MS. All samples were dissolved and diluted to a factor of 1000 and were run with sample-specific standards. All measurements were calibrated using a

series of rock standard reference materials and an internal standard consisting of Be, Rh, In, Tm, Re and Bi. The rock standards used were JB-2 (JGS basalt), BIR-1 (USGS basalt), BHVO-1 (USGS basalt), BCR-2 (USGS basalt), AGV-1 (USGS andesite), W-2 (USGS diabase), G-2 (USGS granite), SDC-1 (USGS mica-schist) and JG-2 (JGS granite). During each sample run one sample or standard was measured every 5-7 samples to monitor machine drift during the sample run. During analysis of rocks, two standards (JB-2 and BIR-1) were routinely measured to assess external reproducibility; the external reproducibility of major element analyses (2σ) is presented in Appendix A4 and the external reproducibility of minor element analyses is presented in Appendix A5. The 2σ external error is <6% for all major (JB-2) and minor (BIR-1) element analyses.

2.5.1.2. Solutions

Major and trace element concentrations in aqueous samples were also measured by ICP-MS. Multi element standards were made up using single element standard solutions that had a concentration of 1000ppm; these were diluted to the required standard concentration using 2% HNO_3 (TD). Analyses of 5 standard solutions of varying known concentrations enabled the construction of a calibration curve which in turn meant results could be converted from cps (counts per second) to ppm. These standard solutions included the following elements: Si, Al, Mg, Ca, Na, K, Ti (major elements), Li, Fe, Cr, Zn, Cu, Rb, Sr, Ba (minor elements) as well as the rare earth elements (REE). The in house standard Sco2/15 (Scottish river water) and the riverine standard SLRS-4 (Ottawa river water, NRCC) were used to monitor and correct for any machine drift (see Appendices A6 and A7). External reproducibility as determined from repeat measurements of SLRS-4 is better than 8% (2σ). A comparison of measured SLRS-4 values with the certified values is presented in Appendix A8.

Cation concentrations in the experimental solutions (Chapter 5) were initially measured by ICP-AES at the University of Iceland. This technique works well for major elements but trace elements such as lithium cannot be so easily measured. For this reason most solutions were also measured by ICP-MS at the Open University following the method described above. For ICP-AES measurements all solutions were acidified with suprapure HNO_3 to an acid concentration of 0.5%. Experimental solutions were run alongside an in house standard; a natural water sample from the Selsund area of Iceland which was calibrated against SPEX CertiPrep single element standards. Duplicate measurements of the experimental solutions yielded relative errors of less than 5%.

Seawater experimental solutions were also run using a combination of the ICP-AES in Iceland and ICP-MS at the Open University. ICP-AES measurements were run alongside an in house standard which comprises a mix of Selsund water and N. Atlantic seawater. A dissolved solid content of 1% is usually regarded as the maximum for the sample introduction system (in order to avoid nebuliser degradation). Seawater has a TDS of 3.5% so all seawater samples were diluted by at least 10 times before introduction to the ICP-AES. For ICP-MS analyses, an artificial seawater solution was prepared using pure salts partly following the method of Kester et al. (1978). The major constituents of this standard were NaCl, KCl and Na_2SO_4. Other elements were added to this in the form of ICP standard solutions (1000ppm). The final TDS of this standard was ~2.9%.

Dissolved anion concentrations were determined using a Dionex ion chromatograph. Anions measured were fluoride, formate, acetate, chlorite, chloride, sulphate, nitrate and phosphate. Two separate runs were performed and the

measurements were calibrated using standard solutions. Detection limits are 0.1ppm and the external reproducibility is better than 10% (2σ), as shown in Appendix A9.

2.5.2. Isotopic analyses

2.5.2.1. Re and Os mass spectrometry

Samples were loaded onto high purity (99.999%) platinum ribbon. Firstly the ribbon is cut into 2 cm lengths and constructed into a filament and ultrasonically cleaned for ~1min, before rinsing with MQ water and rinsing again with acetone. When dry the filament is degassed by passing current through it until it glows red (at around 2.5A) for 2 minutes and then repeating this procedure. Once the filament is degassed the sample can be loaded, using a current of 0.5A for Re and 0.6A for Os. Osmium is loaded slowly and then covered with a mixture of NaOH and $Ba(OH)_2$. When this is dry the filament is carefully heated until the sample starts to melt, then immediately cooled. The purpose of applying NaOH/$Ba(OH)_2$ is to suppress any organic interferences at masses 233-235. When analysing Re the sample is loaded onto the Pt filament at 0.5A and again covered with NaOH and $Ba(OH)_2$ but the sample is not subsequently melted.

The Re and Os samples were analysed at the Open University using a Thermo-Finnegan Triton (TIMS). During analysis the filament is slowly heated to around 800°C. The first species to be emitted is Br_2 which can be used to focus the beam. With further heating up to around 950°C the Os species (in particular OsO_3^-) are emitted and with further focussing on the most abundant isotope (^{192}Os) the osmium signal can be measured. Isotope ratios are all measured relative to ^{188}Os, with the instrumental mass fractionation corrected by normalising to the $^{192}Os/^{188}Os$ ratio of 3.08271. Rhenium samples were run in a similar way to those of Os, although Re is emitted at

lower temperature than Os as ReO_4^- ions, so the filament did not need to be heated as high.

The average total procedural blank for the Bidar samples was 0.41 pg for Os and 4.75 pg for Re; the Os isotopic composition of the blank ($^{187}Os/^{188}Os$) was 0.179±0.005. Corresponding blanks for Goa were 0.22 pg for Os and 4.42 pg for Re; the Os isotopic composition of the blank was 0.186±0.007. The average procedural blanks for the microwave digestion technique are 0.083 pg for Os with $^{187}Os/^{188}Os$ of 0.250±0.021 and 3.6 pg for Re.

2.5.2.2. Lithium isotope analyses

Lithium isotope ratios were measured on two different multi collector inductively coupled plasma mass spectrometers (MC-ICP-MS); a Thermo-Finnegan Neptune MC-ICP-MS and a Nu-Plasma MC-ICP-MS. The reason for this split was because a new MC-ICP-MS (Thermo-Finnegan Neptune) was installed at the Open University and initially was used for isotope measurements because it can achieve greater precision. However, due to issues of stability associated with the Aridus II desolvating nebuliser it was a challenge to obtain reproducible data. For this reason the majority of analyses were subsequently performed on the Nu-Plasma.

a) Li measurements: Neptune

Measurements on the Neptune were carried out in conjunction with an Aridus II desolvating nebuliser. All samples were diluted with 3% TD HNO_3 to a Li concentration of 10ppb. The beam signal for ^7Li varied from around 3.5 to 5V with a 10ppb solution, corresponding blanks (3% HNO3) had a ^7Li beam signal of 70-100mV or ~2% of the total sample beam. The two Li isotopes were measured using Faraday

cups, with ^{6}Li collected in the L4 cup and ^{7}Li collected in the H4 cup. Each sample measurement consisted of 1 block of 20 measurements; prior to each measurement the program ran a baseline measurement by defocusing the beam and then peak-centering the Li species.

b) Li measurement: Nu-Plasma

Isotope measurements on the Nu-Plasma were carried out in conjunction with a Nu-DSN desolvating nebuliser. Samples were prepared exactly as they were for use with the Neptune with all solution concentrations at 10ppb. The intensity of the signal (^{7}Li) on the Nu-Plasma was ~1V with a background of ~6mV or 0.6% of the total sample beam. The isotopes were measured simultaneously on Faraday cups with ^{6}Li collected in Far0 and ^{7}Li collected in Far11. Each sample run consisted of 1 block of 20 measurements and was preceded by measuring zeros. The composition of this blank was then subtracted from the sample measurement online.

The standard sample bracketing technique was used to calculate isotope ratios for both Li and Mg isotopes. This involved the measurement of standards before and after each sample measurement, the isotope ratio of the sample being expressed as a ‰ difference from the average isotope ratio of the two bracketing standards. During the measurement of Li isotope ratios all samples were measured relative to the NIST LSVEC standard as shown below:

$$\delta^{7}Li = \left\{ \frac{\left(\frac{^{7}Li}{^{6}Li}\right)_{Sample}}{\left(\frac{^{7}Li}{^{6}Li}\right)_{LSVEC}} - 1 \right\} \times 1000 \qquad \textit{Equation 2.2}$$

The standard error associated with each sample measurement is also calculated using the standard-sample bracketing technique. Details of how this error has been propagated are given in Appendix A10. Typically the internal precision (2σ) attained with the Nu-Plasma was better than 0.2‰, and internal precision on the Neptune was better than 0.1‰.

The external reproducibility of the lithium isotope ratios was monitored by routine measurement of IAPSO seawater during an analytical session (see Appendix A11). Over a total of 40 seawater standards were measured during the course of this project, the average δ^7Li value was 31.08 ±0.82‰ (2σ). This compares favourably with literature values for the composition of seawater (~31‰) (CHAN and EDMOND, 1988; JAMES and PALMER, 2000).

2.5.2.3. Magnesium isotope analyses

Magnesium isotope ratios were measured on a Thermo-Finnegan Neptune MC-ICP-MS. All samples were run at medium resolution using a wet plasma, and diluted using 3% HNO_3 to give a final concentration of 500ppb of Mg in solution. A typical ^{26}Mg signal with 500ppb DSM3 was between 10-12V; the blank (3% HNO_3 solution) typically gave <0.01V of ^{26}Mg, this blank was subtracted offline during data processing. The three magnesium isotopes (24, 25 and 26) were collected and measured on Faraday cups (L3, centre and H3 respectively). Each sample run consisted of 1 block of 20 isotope measurements, with average isotope ratios and concentrations taken from these 20 measurements.

All measurements are reported as δ^{26}Mg relative to the DSM-3 standard, which is measured before and after each sample:

$$\delta^{26}Mg = \left(\frac{\left(\frac{^{26}Mg}{^{24}Mg}\right)_{Sample}}{\left(\frac{^{26}Mg}{^{24}Mg}\right)_{DSM-3}} - 1 \right) \times 1000 \qquad \textit{Equation 2.3}$$

The internal precision of the Mg isotope measurements was calculated using the technique in Appendix A10. Typically the internal precision of δ^{26}Mg measurements was better than 0.05‰, and the internal precision of δ^{25}Mg measurements was better than 0.03‰.

The use of DSM-3 and CAM-1 as standard reference materials for the magnesium system was proposed by Galy et al. (2003) and both are now widely used in the study of magnesium isotopes. Relative to DSM-3, CAM-1 has a δ^{26}Mg composition of -2.58‰ ±0.14 (GALY et al., 2003), while seawater has a δ^{26}Mg composition of -0.82‰ (CARDER et al., 2004; DE VILLIERS et al., 2005). In order to monitor the external reproducibility of the magnesium isotope measurements the standard CAM-1 was routinely measured at least 2-3 times during an analytical session (Appendix A12). The average δ^{26}Mg composition of CAM-1 measured over the course of this study (n=24) is -2.62 ±0.13‰ (2σ) while the average δ^{25}Mg composition is -1.35 ±0.06‰ (2σ).

2.6. Dissolution and Precipitation Experiments

2.6.1. Minerals

2.6.1.1. Basalt glass

The basaltic glass used in these experiments is from the Stapafell Mountain in south west Iceland. It is the same as that used in previous studies of the dissolution of basalt glass by Oelkers and Gislason (2001) and Gislason and Oelkers (2003). The sample preparation and composition are described in detail in these publications. In brief, the chemical composition is $Na_{0.08}Ca_{0.263}Mg_{0.281}Fe_{0.188}Al_{0.358}SiO_{3.32}$, which is close to the mean composition of oceanic crust and MORB. Basalt glass samples were crushed and sieved to collect grains between 40 and 120μm and ultrasonically cleaned with acetone to remove any fine particles. The surface area of the basalt glass was measured using the three point Brunauer-Emmett-Teller (B.E.T.) method (BRUNAUER et al., 1938). This approach involves the measurement of surface area calculated from the volume of gas (usually Kr or N_2) that can be adsorbed onto the mineral surface, thus taking into account the surface roughness of a mineral. For this reason B.E.T. surface area is always greater than the geometric surface area which assumes all grains are spherical. The surface area of the unreacted basalt glass powder has a B.E.T. surface area of 23,000cm^2/g and a geometric surface area of 250cm^2/g.

2.6.1.2. Forsterite

The olivine used was San Carlos forsterite and was obtained from Wards Natural Science. San Carlos olivine has been extensively used in the past, both in experimental work (OELKERS, 2001; POKROVSKY and SCHOTT, 2000) and for isotopic analyses (PEARSON et al., 2006; WIECHERT and HALLIDAY, 2007) and has an approximate composition of $Mg_{1.82}Fe_{0.18}SiO_4$ (Fo91). Crystals were first handpicked and then

crushed using an agate mortar. These were subsequently milled and sieved to collect grains between 40 and 120μm. Forsterite powder was then ultrasonically cleaned in acetone; this cleaning step was repeated until all fines were removed before drying overnight at 60°C. The surface area of forsterite powder has been estimated previously (OELKERS, 2001; POKROVSKY and SCHOTT, 2000) using similar forsterite ground to the same size fraction. The estimated BET surface area is 800cm^2/g. The forsterite was used in dissolution, precipitation and seawater experiments (Chapters 5 and 6)

2.6.2. Experimental setup

2.6.2.1. Dissolution experiments

All dissolution experiments were performed using Parr titanium through flow reactors. The reactors were heated in a furnace for 24 hours prior to experimentation in order for a titanium oxide layer to form inside – titanium oxide being less reactive than titanium. The reactor set up is shown in Fig. 2.5.

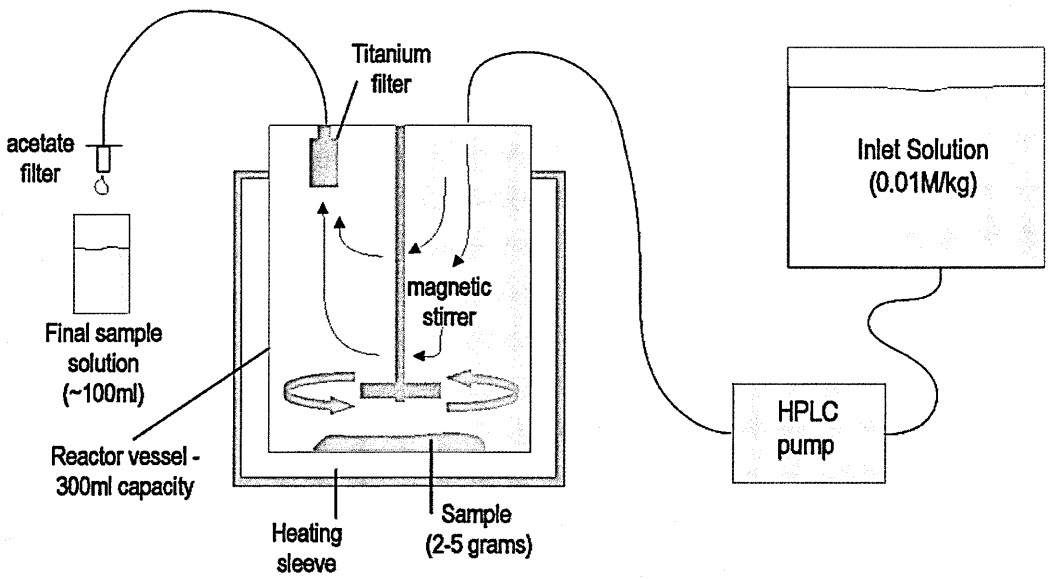

Fig. 2.5 - The experimental setup for the dissolution experiments

The dissolution apparatus consisted of the reactor vessel (volume of 300ml), a motor driven stirring device, and a pressure regulator. The temperature of the reactor was controlled using a Parr heating sleeve capable of maintaining temperatures up to 300°C. Low temperatures could be achieved by the use of an internal cooling loop connected to either tap water or a refrigerated coolant; by this method temperatures down to ~7°C could be maintained. The motorised stirrer kept the reacting mineral in suspension thus aiding the dissolution process by keeping the reacting surfaces exposed. Stirring also prevents the dissolution becoming dependent on the rate of diffusive transport away from mineral surfaces. Gislason & Oelkers (2003) show that at pH 2-3 stir rates should be kept above 550rpm and 350rpm respectively, to ensure that dissolution rates are surface reaction controlled.

All reacting solutions were prepared to a molar strength of 0.01mol/kg. They were prepared using deionised water and sufficient quantities of suprapure HCl and NH_4Cl to attain the desired pH. Solution was introduced to the vessel via the input valve in the lid and removed via a titanium filter that collected any solid particles from the output solution. After precleaning the apparatus with dilute acid, solutions were introduced to the reactor firstly via PTFE tubing connected to a high precision High Pressure Liquid Chromatography (HPLC) pump capable of maintaining flow rate between 0.1 and 10 g/min with a maximum flow rate error of +/-10%. This solution was then introduced to the reactor via 0.1mm titanium tubing. On leaving the reactor solution passed through PTFE tubing to an acetate 0.2 μm filter directly before sampling. Sample containers were 125ml PTFE sample tubes; they were rinsed with deionised water and cleaned using dilute reagent grade HCl, before further thorough rinsing with deionised water. All samples were acidified using suprapure grade HNO_3 to 0.5% in order to be later run on the ICP-AES (2.5.1.2.). Prior to acidification the

sample solution was analysed for pH. This was done immediately after sampling to allow the pH to remain unaffected by the dissolution of CO_2.

On commencement of each experiment 3 residence times were left before the first sampling, and then another 3 residence times in between each sample. If during the experiment any changes were made to the setup, such as changing flow rate or pH, then a 3 residence time gap was left before sampling began again. The residence time is defined as the time to fill up the reactor once. On sampling all solutions had their pH measured and were weighed in order to determine the actual flow rate. The sample size was around 100ml.

2.6.2.2. Precipitation experiments

The precipitation experiments were performed in three polypropylene through flow reactors immersed in a water bath as shown in Fig. 2.6.

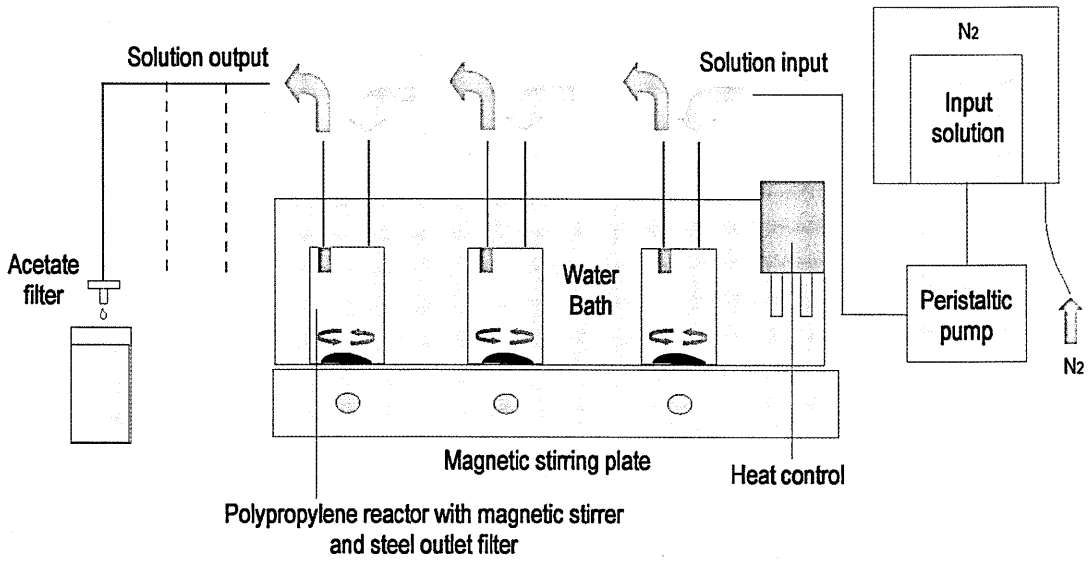

Fig. 2.6 - The experimental setup for the precipitation experiments

All the reactors were precleaned with reagent grade and suprapure HNO_3 before rinsing with deionised water. The experimental setup was very similar to that used in the dissolution experiments. Polypropylene reactors were used in order to prevent the titanium reactors from becoming contaminated with secondary minerals. There is no in built stirring mechanism within the polypropylene reactors so Teflon coated magnetic stirrers were used to stir the solution throughout the experiment. Floating stir bars were used in order to prevent the possibility of grinding the mineral phase and hence increasing its surface area during the experiment. Temperature was maintained using the water bath, and temperatures between 25 and 75°C were used in these experiments.

As for the dissolution experiments, solutions were prepared to a 0.01mol/kg concentration, because high pH values were needed a combination of NH_4Cl and NH_4OH was used in order to obtain pH10 and 11. At these high pH values the precipitation of carbonates is a possibility because the dominant carbonic acid species is CO_3^{2-}. To stop this occurring the input solutions were kept in a mantle of nitrogen gas. Solutions were introduced to the reactors using a Masterflex peristaltic pump that was able to maintain a flow rate of between 0.1 and 10 g/min, depending on the diameter of the Masterflex tubing. The solution was pumped into the reactor through the lid and output via a steel filter. Prior to sampling the solution passed through a sterile acetate 0.2μm filter. On sampling all solutions were immediately acidified using suprapure HNO_3, pH was measured (from an unacidified sample) and the solution was weighed in order to calculate the actual flow rate. All sample sizes were around 100ml.

2.6.3. Experimental Method

The general method for running each experiment is the same for both dissolution and precipitation experiments. The apparatus was always acid cleaned prior to each

experiment and then cleaned in deionised water. Once clean the mineral phase was added to an empty reaction vessel and the vessel filled with the 0.01mol/kg solution. In experiments where the pH was changed (dissolution experiments) the lowest pH was always used last because it caused the most alteration of the sample and largest change in the mineral surface area. At the beginning of each experiment, and after any change in the experimental parameters such as flow rate, temperature and pH, sampling began only after three residence times. During the experiment solution is constantly output from the reactor, thus sampling was simply a case of collecting liquid at a given time. All outlet solution was filtered twice; once through a titanium/steel filter and once through a 0.2μm polypropylene (PPE) filter.

At the end of each experiment deionised water was flushed through the system and the rock powder was collected and dried down ready for future analysis. In the event of secondary mineral precipitation reagent grade HCl was pumped through the reactor for 24 hours before cleaning with suprapure HCl for a further 24 hours and a final clean with deionised water. Solution and total procedural blanks for both dissolution and precipitation experiments are presented in Appendix A14.

2.6.4. Seawater experiments

The seawater experiments were performed on basaltic glass and forsterite. The basalt glass used was identical to that used by Gislason & Oelkers (2003) while the forsterite was similar to that used by Pokrovsky & Schott (2000). More details on the composition and preparation of both mineral phases are presented in 2.6.1. The seawater experiments were carried out using one litre polypropylene batch reactors. Each reactor vessel was cleaned using 2% HNO_3 acid and deionised water prior to the start of the experiment. Most experiments were performed at room temperature (~25°C)

and the reactors were kept on rollers that continuously rotated so that some of the mineral sample always remained in suspension. One experiment (BGSW5) was performed at lower temperature (~4°C) and so could not be carried out in the same way; this reactor was refrigerated and continuously stirred by a Teflon coated magnetic stir bar. The seawater was taken from the North Atlantic (STEFANSDOTTIR and GISLASON, 2005) and from the Southern Ocean (JONES and GISLASON, IN PRESS). All seawater was filtered and then irradiated using UV radiation prior to experimentation. The basalt glass and forsterite sample sizes varied from between 10 and 30g in each reactor, and temperature was regularly monitored with fluctuations of ±0.2°C. Samples were taken by pumping solution out of the reactors using a Masterflex peristaltic pump. Each sample was filtered using sterile 0.2μm filters and pH was measured immediately after sampling. No attempt was made to limit the CO_2 flux into the system and no seawater was replaced in the reactors after samples were taken. For this reason the sample size was only ~40ml in order to prevent the total volume of solution falling too rapidly after each sample. At the end of the experiments the final solution was used to measure the alkalinity, and can be compared with the alkalinity of the unaltered seawater. The minerals were drained of as much seawater as possible and then centrifuged and drained again. No washing with deionised water was performed prior to drying because it may dissolve any secondary minerals that may have formed. For this reason a small amount of evaporitic mineral may have formed on drying at 60°C.

Chapter 3

The behaviour of lithium and lithium isotopes during glacial weathering

3.1. Introduction

Northern Hemisphere glaciation (NHG) is thought to be relatively recent in the geological timescale, the onset perhaps occurring as early as ~10-12Ma (MASLIN et al., 1998). Intensification of this glaciation (~2.7Ma) and the formation of ice in the Arctic, Greenland and Alaska is thought to have been caused by a combination of higher frequency changes in the Earth's obliquity and summer warming in the Pacific that provided an increase in the moisture transported to high northern latitudes (HAUG et al., 2005). Glaciation affects the intensity of weathering that silicate rocks are subjected to. This is important because over geological timescales the weathering of Ca-Mg silicates causes a net drawdown in CO_2 and so can cause atmospheric cooling. Thus the formation of glaciers and long term glaciation are closely linked to changes in the Earth's climate. Results from seawater analyses of isotope systems such as Os (BURTON, 2006), Sr (MCARTHUR et al., 2001) and Li (HATHORNE and JAMES, 2006) suggest that over the last 8Ma silicate weathering intensity has increased despite global cooling and the onset of NHG. A possible reason for this discrepancy is a shift to a more physical weathering regime because of the intensification of global glaciation.

Glaciers create highly physical weathering regimes; grinding and mechanical erosion produce high volumes of fine grained sediment (LEEDER, 1999). In theory, the rate of chemical weathering caused by glaciation should be relatively low; glacial regions are frozen for long periods, water-rock contact time is short, and the formation

of soils and vegetation is minimal or absent. However, increased physical weathering is often accompanied by enhanced chemical weathering (GAILLARDET et al., 1999b; GISLASON et al., 1996) and consequently chemical denudation rates in glacial environments can be comparable with rates of weathering in temperate catchments with comparable runoff (ANDERSON et al., 1997; SHARP et al., 1995; TRANTER et al., 2002). These high chemical denudation rates are a result of high water flux and the production of fine grained sediment with high surface areas that are highly weatherable (ANDERSON et al., 1997). This sediment is eventually transported to the oceans; sediment supply from Greenland has a significant influence on the chemistry of waters in the North Atlantic and waters west of Greenland (HASHOLT, 1996). Furthermore, recent work has shown that deltas can act like fluidised bed reactors, because the suspended sediment that has been transported and deposited by riverine processes is subsequently reworked and chemically altered (GISLASON et al., 2006). This alteration of this suspended sediment can provide a chemical flux to the oceans that, for some elements, is at least as great as that provided by the dissolved load.

As well as carrying high volumes of suspended sediment the chemical composition of the runoff derived by glacial weathering is different from that of non-glacial rivers. Glacial runoff is dominated by Ca^{2+}, SO_4^{2-} and HCO_3^-, and usually contains relatively high amounts of K^+ and relatively low amounts of Si compared to non-glacial rivers (ANDERSON et al., 1997; TRANTER, 2003). The high concentrations of K^+, SO_4^{2-} and particularly Ca^{2+} in glacial waters occur irrespective of the bedrock lithology (ANDERSON et al., 2000; ANDERSON et al., 1997; RAISWELL and THOMAS, 1984). High levels of Ca^{2+} in solution result from preferential weathering of carbonates and aluminosilicates; this occurs even in regions dominated by igneous and high grade metamorphic rocks because the dissolution kinetics of divalent cations are more rapid

than those of monovalent cations (WHITE et al., 2001). In contrast to glacial rivers, those from non glacial settings are dominated by chemical weathering and so generally have higher total dissolved solids (TDS) as well as higher silica concentrations reflecting the higher silicate weathering intensity. Their composition more accurately reflects that of the underlying lithologies as well as climatic influences such as rainfall and runoff (MEYBECK, 2003).

Thus, glacial and non glacial rivers have major physical and chemical differences. The aim of this study is to investigate how Li behaves in rivers from a recently glaciated area in south-west Greenland. Lithium isotopes readily fractionate during weathering because of their large relative mass difference (HUH et al., 1998). The Li composition is controlled by weathering processes; in particular by the formation of secondary minerals and adsorption onto secondary minerals such as clays and iron oxides (CHAN and HEIN, 2007; HUH et al., 1998). The light isotope, ^{6}Li, is preferentially retained in the solid phase leaving the fluid phase to be isotopically heavy (CHAN et al., 1992). By studying river waters that have experienced different weathering regimes (chemical vs physical) the aim is to achieve a better understanding of the processes that regulate both the flux of Li to the oceans and the isotopic composition of that Li.

Greenland has an area of 2,166,086 km² (836,109 sq mi), of which the Greenland ice sheet covers 1,755,637 km² (677,676 sq mi) or 81% of its land area. The Greenland ice sheet is the second largest ice sheet in the world after Antarctica with around 2.5 million km^3 of ice (or around 10% of the total global ice mass). The weight of this ice sheet has depressed the central land area to form a basin lying more than 300 m (1,000 ft) below sea level. Recent changing climate conditions have led to increased ice sheet melting. Laser altimetry shows that between 1997 and 2003

Greenland lost ice at a rate of ~80 +/- 12km^3/yr (KRABILL et al., 2004). More recent gravity measurements have shown that between 2002 and 2005 an estimated 239 +/- 23 km^3/yr has been lost, suggesting that the melting is accelerating as the climate continues to warm up (CHEN et al., 2006). This melting is concentrated at the ice sheet margins, so the sheet is retreating inland exposing new terrain to chemical weathering.

Estimates of the current global average glacial runoff range from 0.3×10^{12}m^{3}yr^{-1} to 1×10^{12} m^{3}yr^{-1} of which around 0.3×10^{12}m^{3}yr^{-1} comes from Greenland and 0.04-5 $\times10^{10}$m^{3}yr^{-1} comes from Antarctica (TRANTER, 2003). Glacial runoff provides between 0.6-1% of the global average runoff and the flux from Greenland is the dominant source. With increasing global warming the flux from melting glaciers will increase and this will almost certainly affect the chemical composition of seawater.

Despite the importance of the Greenland ice sheet to global runoff there have been very few studies of rivers from this area, in particular their chemical composition and the link that they provide between the weathering of continents and seawater composition. Existing studies have focussed on quantifying discharge and solute fluxes in single catchments, including Disko Island (YDE et al., 2005) and the Imersuaq Glacier (YDE and KNUDSEN, 2004). This investigation is the first to assess the behaviour of isotope systems accompanying weathering in rivers from Greenland. The aim of this study is to investigate the behaviour of Li and Li isotopes in glacial rivers and compare this to results from non-glacial regions. Could changes in the weathering regime, such as those associated with glaciation, change the continental weathering signal? Ultimately, could the changes in the Li concentration and composition of seawater over the past 8Ma be related to the intensification of glaciation in the northern hemisphere?

3.2. Geological setting

The geology of Greenland is characterised by ancient metamorphic rocks dating back billions of years, forming what is known as Precambrian shield. Some of the oldest known rocks on Earth are found in Greenland, at Isua in the south west of the island with an age of around 3800Ma (APPEL, 1998). The geological development of Greenland spans a huge period from the earliest rocks in the Archaean to relatively modern Quaternary geology. Despite this range Greenland is dominated by crystalline rocks of the Precambrian shield, formed during a succession of Archaean and early Proterozoic orogenic events which stabilised as a part of the Laurentian shield about 1600 Ma ago (ESCHER and PULVERTAFT, 1995). The shield area can be divided into three distinct basement provinces: (1) Archaean rocks (3100–2600 Ma old, with local older units), almost unaffected by Proterozoic or later orogenic activity; (2) Archaean terranes reworked during the early Proterozoic around 1850 Ma ago; and (3) terranes mainly composed of juvenile early Proterozoic rocks (2000–1750 Ma old). This Archaean and early Proterozoic basement comprises around half of the ice free area of Greenland (ALLAART, 1982; ESCHER and PULVERTAFT, 1995)

The glacial and non glacial rivers analysed in this project are located in southwest Greenland close to the town of Kangerlussuaq, situated at the head of the fjord of the same name (Fig. 3.1). The area around Kangerlussuaq is dominated by Archaean gneiss metamorphosed to amphibolite and granulite facies as well as intrusive igneous rocks of a similar age (ESCHER and PULVERTAFT, 1995). Swarms of alkaline dykes were intruded between 1200 – 600Ma, including some kimberlite dykes which have been found to contain diamond. For this reason the Kangerlussuaq region has recently experienced a great deal of geological exploration and interest from prospecting companies.

Glaciation dominates the topography and there are numerous signs of recent glaciation including moraines, u-shaped valleys and glacial lakes. Deglaciation in central West Greenland started around 12,300 years BP and most of the inland ice reached its present position between 710 and 6,500 years BP (WILLEMSE et al., 2003) although more recent climate change has accelerated this deglaciation. Russells Glacier (Fig. 3.1) is now around 30km from the town of Kangerlussuaq and is the source of numerous jokulhlaups, the most recent of these occurring in 1987. These have substantially reworked glacial sediments, which in some areas form distinctive moraines and jokulhlaup deltas (RUSSELL, 2007). In recent years the ice sheet has retreated due to global warming but climate is still characterised by extreme cold in winter, as a consequence vegetation is sparse and confined to low lying shrubs and grass. The mean annual temperature is -5 °C, although the annual temperature range is ~30 °C. Kangerlussuaq sits in an area of negative precipitation; the total evaporation exceeds precipitation by ~150mm each year. Precipitation is highest in August with an average of 28mm. Aeolian deposits are common in the region, especially near to the ice sheet and on hills (WILLEMSE et al., 2003) resulting from the combination of arid conditions and high volumes of fine grained sediment. As a result of low average temperatures the study area is underlain by continuous permafrost; the numerous glacial lakes are frozen for over 9 months of the year, while the fjord itself is frozen between the end of November and mid June. The area is sparsely populated (human influence is confined to the area around Kangerlussuaq) and as such the samples have experienced minimal anthropogenic input.

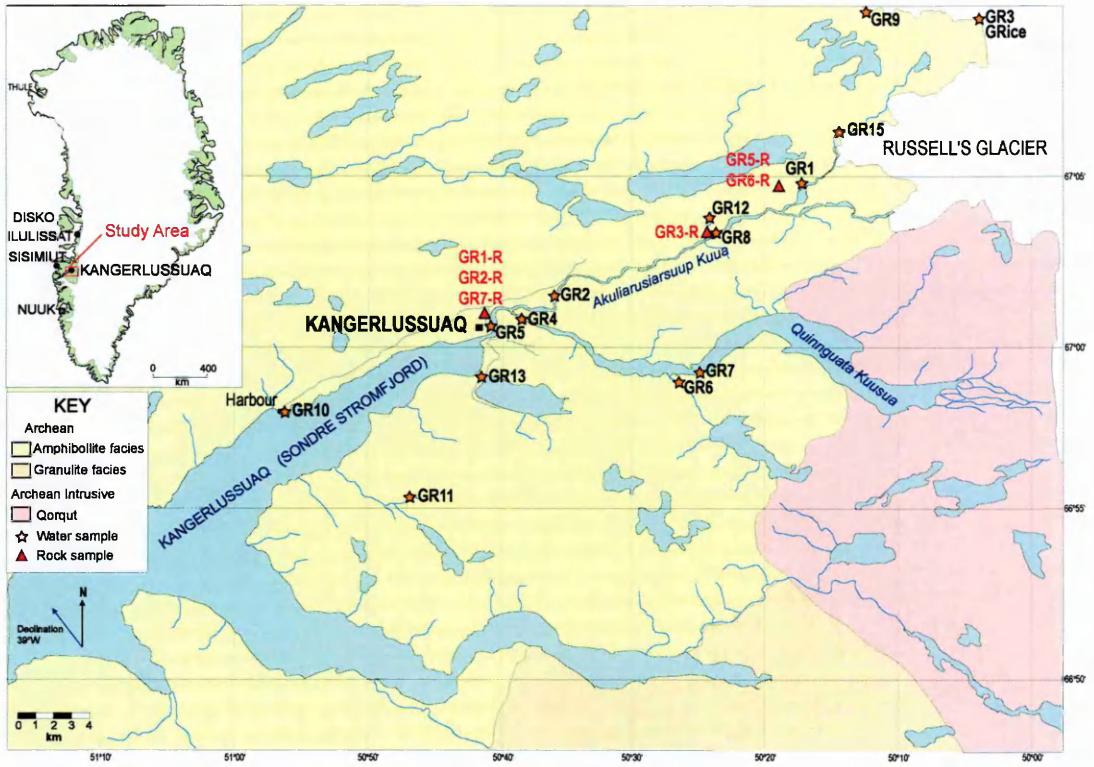

Fig. 3.1 – A map showing the locations of river water and rock samples in this study.

Samples were taken from both 'glacial' and 'non-glacial' rivers. For the purposes of this study glacial rivers refer to rivers that are directly sourced from the glacier via surface run off, and non glacial rivers are those that are not directly sourced from the glacier. The majority of the glacial river samples were taken on Akuliarusiarsuup Kuua (sometimes referred to as the Watson River), which flows to the south-west from Russells Glacier, as it has relatively easy access for sampling. Samples were also taken from the Qinnguata Kuusua river which flows from the ice sheet directly east of Kangerlussuaq. The dominant underlying lithologies of both rivers are amphibolite facies gneiss, although the catchment for Qinnguata Kuusua is also underlain by Archaean intrusives. These rivers supply large volumes of glacial sediment, near to the ice sheet they form braided systems with wide expanses of sand, gravel and quicksand. For this reason access to these rivers is severely restricted, especially Qinnguata Kuusua where there is no access road. Non glacial rivers and

streams were sampled from a number of locations, mostly close to the two main glacial rivers.

3.3. Methods

3.3.1. Sampling procedure

The fifteen river samples were collected in July 2006. Each river sample involved collection of 25l of water and ~100g of bedload sediment. At each sample site the pH, temperature and TDS of the water was also recorded.

Within 12 hours of collection all 25l water samples were filtered (<0.2μm) and either stored for later analysis or filtered again (10kD) to separate the colloids; further details of the sampling procedures, filtering processes and alkalinity titration are given in Section 2.1.1.

3.3.2. Leaching Experiments

Three suspended sediment samples were subjected to a two stage acid leaching process similar to that used in Chan & Hein (2007). A gentle leach involving buffered acetic acid, designed to remove freely exchangeable cations, was followed by a more vigorous leaching procedure involving 2N TD HCl designed to remove cations bound to iron and manganese oxyhydroxides. The leachates were then analysed using ICP-MS and further analysis was carried out for lithium isotopes by MC-ICP-MS (multi-collector inductively coupled mass spectrometer). The leaching process is described in more detail in Section 2.3.

3.3.3. Major and Trace elements

The methods used for sample processing which include rock crushing and preparation for analysis by XRF, and the dissolution of solid samples for analysis by ICP-MS are described in detail in Section 2.2. All major element analyses of rock and sand samples were performed by XRF (Section 2.5.1.1). The accuracy of the XRF measurements is assessed by the reproducibility of known standards; these typically reproduce to within 1% of the certified values.

Major element analyses of the suspended sediment and all trace element analyses for rock and sand were performed using ICP-MS. These measurements were calibrated using a series of rock standard reference materials and an internal standard consisting of Be, Rh, In, Tm, Re and Bi. Details of the sample analysis and reproducibility of standards are given in Section 2.5.1.1. In brief, the concentrations of measured standards are mostly close to certified concentrations. The external error for both major and minor elements is better than 6% (2σ).

River waters were also analysed by ICP-MS; their preparation involved being acidified with 15M TD HNO_3 to a concentration of 2% HNO_3. These waters were calibrated using multi element standards, and the external reproducibility was assessed by repeat measurements of the river water standards SLRS-4 and in house standard Sco2/15. Details of the sample analysis and reproducibility of standards are given in Section 2.5.1.2. External reproducibility (as determined from repeat measurements of SLRS-4) are better than 8% (2σ), a comparison of measured SLRS-4 with the certified values is presented in Appendix A8.

Dissolved anions were measured using a Dionex ion chromatograph. Anions measured were chloride, sulphate, nitrate and phosphate. Two separate runs were performed and the measurements were calibrated using standard solutions (see

Appendix A9). Detection limits are 0.1ppm and the external reproducibility is better than 10% (2σ).

3.3.4. Lithium isotope measurements

Separation of lithium for isotope analysis was carried out by ion chromatography following the method of James & Palmer (2000) (Section 2.4.2). Isotope measurements were performed on both the Thermo-Finnegan Neptune and Nu Instruments MC-ICP-MS at the Open University. Lithium isotope ratios were calculated by the sample-standard bracketing technique with all ratios reported as a ‰ difference relative to the standard LSVEC. More details concerning lithium sample analysis are given in Section 2.5.2.2. The external precision of the analyses was determined by repeat measurements (n=40) of the IAPSO seawater standard measured over the course of this study. The mean and standard deviation (2σ) of these analyses is 31.08‰ ±0.82‰ (see Appendix A11).

3.4. Results

3.4.1. Field measurements

In situ measurements of pH, temperature, TDS and total suspended solids (TSS) are presented in Appendix B1. Glacial river waters are colder (0.3-8°C) than non glacial waters (10-19°C) because they are sourced directly from the glacier. TDS and TSS data also reflect the river type; glacial rivers have relatively high TSS (0.2-0.85 g/l) and low TDS (2-18μS) while non glacial rivers show the opposite with a low TSS (0.001-0.16 g/l) and high TDS (25-2600μS). TDS and TSS both increase downstream in the glacial rivers (Fig. 3.2).

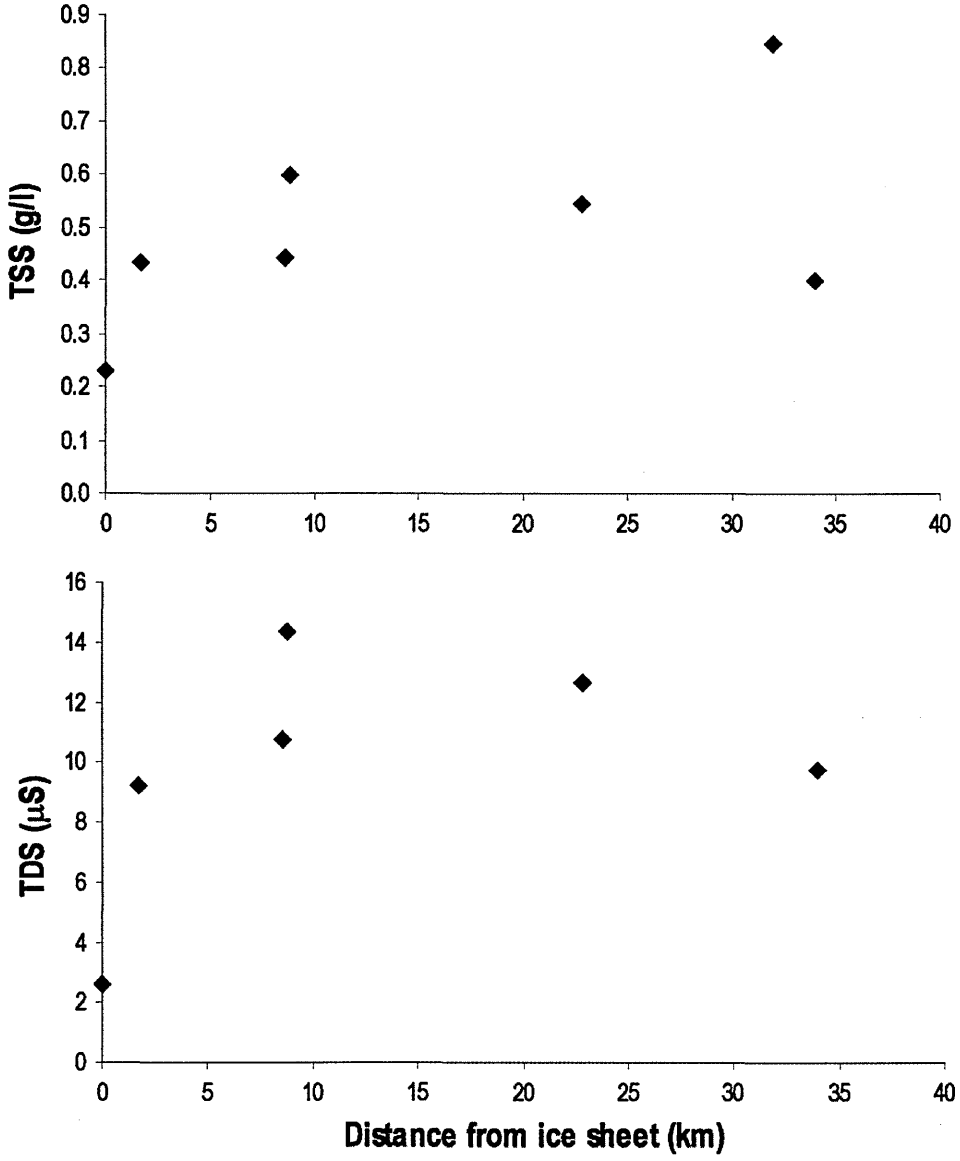

Fig. 3.2 – Variation in TDS and TSS in glacial rivers as a function of the distance downstream from the ice sheet.

The pH of these rivers varies between 6.3 and 8.5 with most glacial rivers having a pH of between 7 and 8. The exception is sample GR3, which was recovered from a stream flowing from on top of the glacier and had no contact with the bedrock (i.e. supraglacial), this sample has a lower pH (6.3). Non glacial rivers have a similar pH range to the glacial rivers although three of the six rivers sampled have a pH of greater than 8. Glacial rivers have a relatively low alkalinity (ranging between 0.02 and

0.15 meq/l) compared to the non glacial rivers (between 0.26 and 1.74 meq/l). Within the glacial rivers the alkalinity increases with distance from the ice sheet in a similar way to the TDS and TSS.

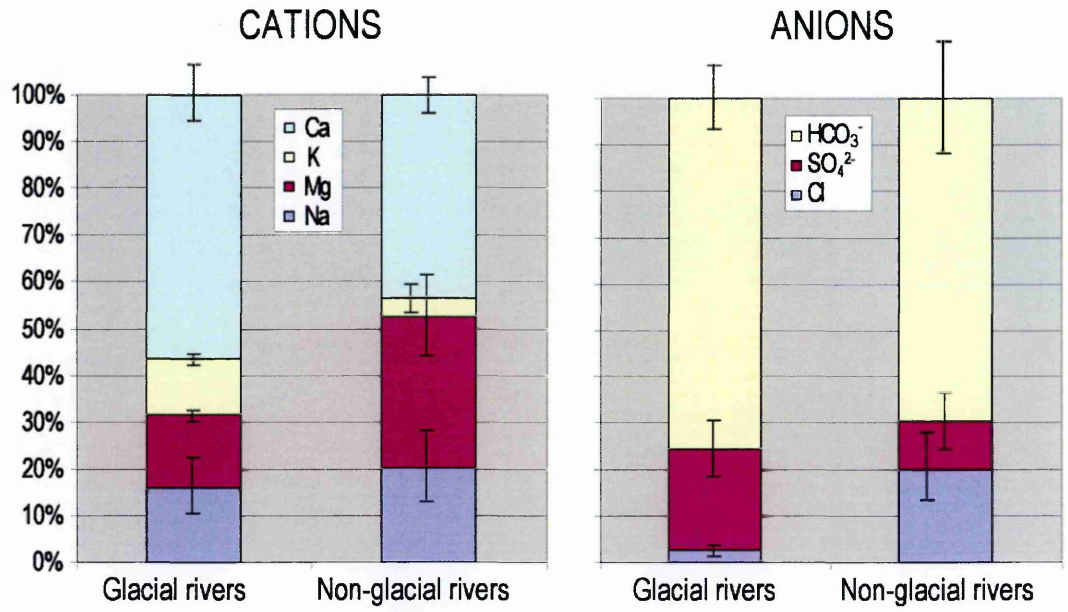

Fig. 3.3 – Average cation and anion compositions of glacial and non glacial rivers. Error bars show 1 standard deviation of the mean value.

3.4.2. Major and trace element data

3.4.2.1. Dissolved load

Cation and anion data for the dissolved load is presented in Appendix B2. The average of the sum of the major cations (Na^+ + Mg^{2+} + Ca^{2+} + K^+) in the glacial rivers is 134µeq/l and 1419µeq/l in non glacial rivers. As a percentage of the cation sum Ca^{2+} dominates in both the glacial and non glacial rivers (on average 57 and 44% respectively, Fig. 3.3). Sodium concentrations are similar between the two sets of rivers, and both glacial and non glacial rivers have ~16% Na^+. The biggest difference between the glacial and non glacial rivers in terms of the major cations is the behaviour of potassium and magnesium. Glacial rivers have a K and Mg concentration of ~12 and

16% respectively compared to K and Mg concentrations of ~5 and 36% in non glacial rivers. These differences in the chemical composition of glacial versus non-glacial rivers are illustrated in a ternary diagram (Fig. 3.4).

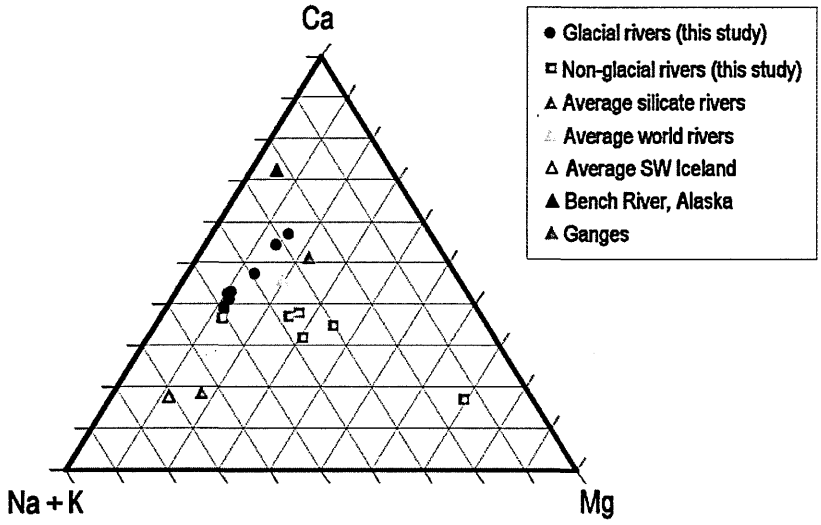

Fig. 3.4 – A ternary diagram showing the major cation compositions of glacial and non glacial rivers in Greenland. Data for a selection of other rivers are shown for comparison. Data for average silicate rivers from Gaillardet et al. (1998), average world rivers from Meybeck (2003), the average composition of rivers from SW Iceland taken from Gislason et al. (1996), Bench River data from Anderson et al. (2000) and data for the Ganges from Galy et al. (1999).

There is a range of silica concentrations in solution; glacial river samples contain from 6.3 to 43 μmol/l while non glacial rivers have a wider range of concentrations from 4 up to 325 μmol/l. The global average for dissolved silica is 130 μmol/l (MILLOT et al., 2002), indicating the glacial rivers have lower than average dissolved silica and some non glacial rivers have greater than average dissolved silica. Iron concentrations in the dissolved load are between 87 and 690 nmol/l in glacial rivers, compared to between 170 and 12700 nmol/l in non glacial rivers. All but two rivers have an iron concentration below the riverine average of 1180 nmol/l (GAILLARDET et al., 2003). The anion content of Greenland rivers is almost entirely comprised of bicarbonate, sulphate and chloride ions. The dominant anion is

bicarbonate in all rivers, but the concentration of sulphate and chloride ions varies between glacial and non glacial rivers; in glacial rivers the sulphate concentration is far greater than that of chloride while the reverse is true in non glacial rivers (Fig. 3.5).

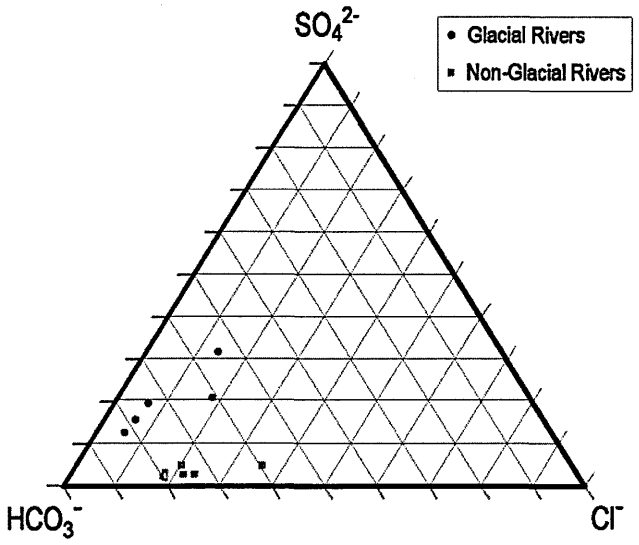

Fig. 3.5 – A ternary diagram illustrating the difference between anion compositions in glacial and non-glacial rivers.

The high organic content of samples GR11 and GR12 is reflected by nitrate concentrations of 0.7 and 5 mg/l; nitrate is below detection limit in all other river samples. The average anion sum in glacial rivers is 137 μeq/l. This balances the cation sum and shows that all of the major ions are accounted for. The average anion sum in non glacial rivers is 1221 μeq/l. This is 14% lower than the corresponding cation sum (Fig. 3.6) probably because of the presence of humic substances that have not been measured.

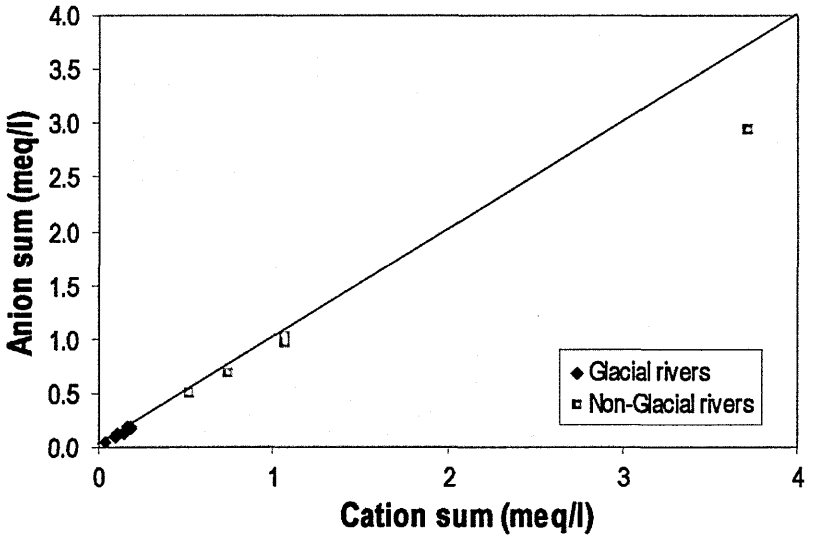

Fig. 3.6 – A graph showing the anion and cation sums for all Greenland river samples.

3.4.2.2. Colloids and ultrafiltered waters

The chemical composition of the dissolved load includes everything in solution that is below 0.2 μm. Today much research has been performed on smaller size fractions within the dissolved load by ultrafiltering the water to separate out colloids (DREVER and STILLINGS, 1997; POKROVSKY and SCHOTT, 2002; RIOTTE et al., 2003). Colloids are inorganic or organic particles that are between 1nm and 0.2μm in size and are carried in suspension (GAILLARDET et al., 2003). The most common mineral colloids are metallic oxyhydroxides (mostly Fe-, Al- and Mn- oxides) and clays while organic colloids are dominated by humic and fulvic acid (DUPRE et al., 1999; GAILLARDET et al., 2003; POKROVSKY et al., 2005; SIVRY et al., 2006).

Major and trace element data for colloids (<0.2μm, >10kD) and the ultrafiltered fraction (below 10kD) are given in Appendix B3. The colloidal fraction has higher concentrations of all elements (Al^{3+}, Na^{+}, Ca^{2+}, Mg^{2+}, K^{+}, Li^{+}, Fe^{2+}) relative to the dissolved and ultrafiltered waters. Concentrations of iron, copper and aluminium are particularly high in the colloidal phase; for example iron is below detection in the

ultrafiltered phase while the colloidal fraction has iron concentrations from 2350 to 352000 nmol/l. The major cation composition of the ultrafiltered waters are shown in Fig. 3.7. In comparison to the dissolved (<0.2 μm) fraction (Fig. 3.3) note that the composition of the non-glacial and glacial waters contain relatively similar Ca^{2+} concentrations. Results show that the major differences between the two sets of river are the relative proportions of K and Mg.

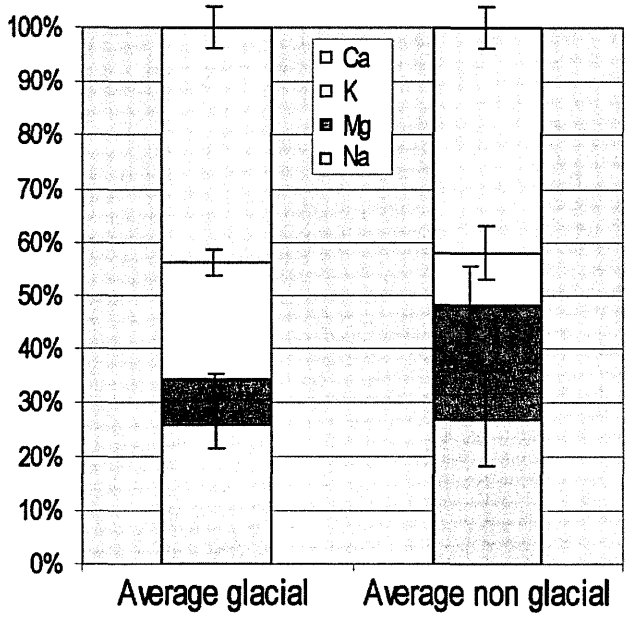

Fig. 3.7 – A graph comparing the major cation composition of ultrafiltered waters for glacial and non glacial rivers. Error bars show 1 standard deviation of the mean value.

The separation of the river waters into colloids, ultrafiltered (<10kD) and dissolved (<0.2μm) is achieved by using tangential ultrafiltration equipment as explained in Section 3.3.1. One drawback to this method is that the filter can retain some elements and possibly cause sample contamination (ANDERSSON et al., 2001; DUPRE et al., 1999; RIOTTE et al., 2003). A way to check whether elements are being affected by the ultrafiltration process is to calculate a mass balance, between the concentration of the water to be filtered and the two ultrafiltered phases (the colloids or retentate and <10kD water or the filtrate). In this study the volumes of water used were

not well constrained and an estimated 10l of water was ultrafiltered until ~250ml of retentate was produced. Using these figures mass balance calculations suggest that some elements are not affected by the ultrafiltration process; Li, Na. Mg, K and Sr all balance to within ±15%. Some calcium is retained during ultrafiltration; calcium balances to within ±25%. Elements which seem to be strongly affected by ultrafiltration are Al, Fe and Si. Aluminium is lost during ultrafiltration in all but one sample, with between 10 and 80% of the aluminium retained by the filter. Iron is also commonly lost during ultrafiltration although there is a gain of up to 23% in three samples. This behaviour of aluminium and iron is consistent with previous work suggesting that colloids such as Fe and Al-oxyhydroxides are fixed to the filtration membrane (RIOTTE et al., 2003). Silicon behaves differently; the ultrafiltered fraction is enriched in silicon in all but one sample by between 6 and 75%. This means that the filtration cassette is contaminating the solutions with silicon suggesting that silicon concentrations in the ultrafiltered fraction are unreliable.

3.4.2.3. Rocks, sands and suspended material

Major and trace element data for the bedrock, bedload and suspended load are presented in Appendix B4, and the major cation compositions are presented in a ternary diagram for each of the three phases (Fig. 3.8).

Analyses of suspended sediments are limited to sediment from glacial rivers; the low TSS in non glacial rivers meant that there was not enough sediment to measure the concentrations. The suspended load has a relatively consistent composition throughout all of the samples. Silicon concentrations have not been measured because the dissolution procedure involves the use of HF. If it is assumed that silicon is the most

abundant cation present then the next most dominant cation is aluminium at ~6.8 Wt%. The suspended sediment also has an iron concentration of ~4.4 Wt%.

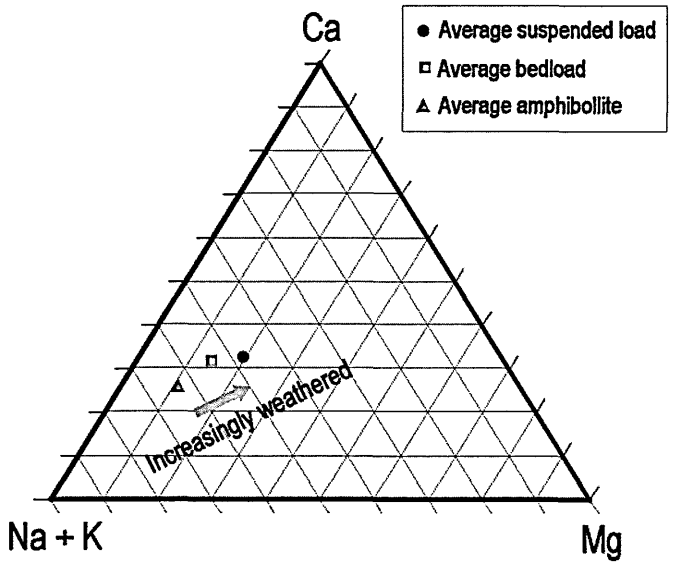

Fig. 3.8 – A comparison of the cation composition of the solid phases of Greenland rivers (bedload and suspended load), showing the change in composition with increasing weathering intensity. Data for average amphibolite are taken from Wells (1978).

The composition of the bedload is similar to that of the suspended sediment in particular the sodium and aluminium concentrations. Other major cations such as magnesium, calcium, potassium and iron have on average higher concentrations in the suspended sediment, for example the average magnesium composition of the suspended sediment is 1.9 Wt% compared to 1.1 Wt% in the bedload. The iron concentration in the bedload is quite variable; from 2.2 Wt% at GR8 to 7.1 Wt% at GR4. In general the chemical composition of the bedload from glacial rivers is very similar to that recovered from non glacial rivers.

A selection of unweathered bedrock was sampled; mostly from adjacent to the Watson River. As a collection they vary widely in chemical composition and are not all representative of the dominant lithology in the Kangerlussuaq region. The area is part

of the Archaean shield and dominated by amphibolite grade gneiss with a mineral assemblage consisting of biotite-garnet-cordierite-sillimanite-quartz. Comparison with the compilation of Wells (1978) suggests that the rock samples GR2R and GR6R are the closest in composition to the average Greenland amphibolite. They are also the closest in composition to the bedload, which is assumed to be the least weathered riverine phase. In particular the silicon concentrations of the bedrock and bedload are almost identical (~31 Wt%), while iron is on average over 1.8 Wt% greater in the bedload relative to the bedrock.

3.4.3. Lithium and lithium isotope data

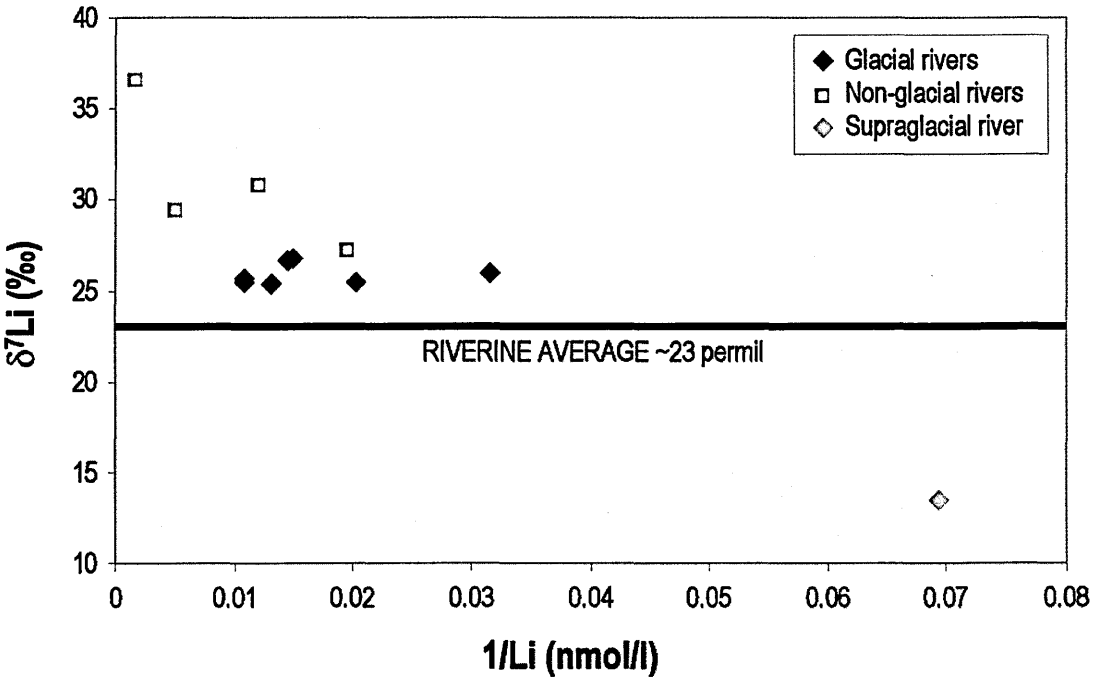

Fig. 3.9 – A graph showing the δ^7Li value and 1/Li for glacial and non glacial rivers. The global average δ^7Li value of river waters (23‰) is taken from Huh et al. (1998).

Lithium and lithium isotope results for the different riverine phases are presented in Appendices B2, B3 and B4. The concentration of lithium in the dissolved load ranges from 14 nmol/l at GR3 to 1810 nmol/l in GR10. Sample GR10 was taken at the harbour

and thus contains a seawater component, for this reason GR10 is excluded from any subsequent discussion. On average the lithium concentration in glacial rivers is 60 nmol/l compared to a higher average of 180 nmol/l in non glacial rivers (Fig. 3.9). The isotope composition of Li varies from 13.5 to 36‰ compared to an average riverine Li composition of 23‰ (HUH et al., 1998). Most glacial rivers have a δ^7Li value close to ~26 ‰; sample GR3 (supraglacial) has a more isotopically light lithium composition (δ^7Li of 13.5‰) while non glacial rivers tend to have higher δ^7Li values, ranging between 27.1 and 36.5‰.

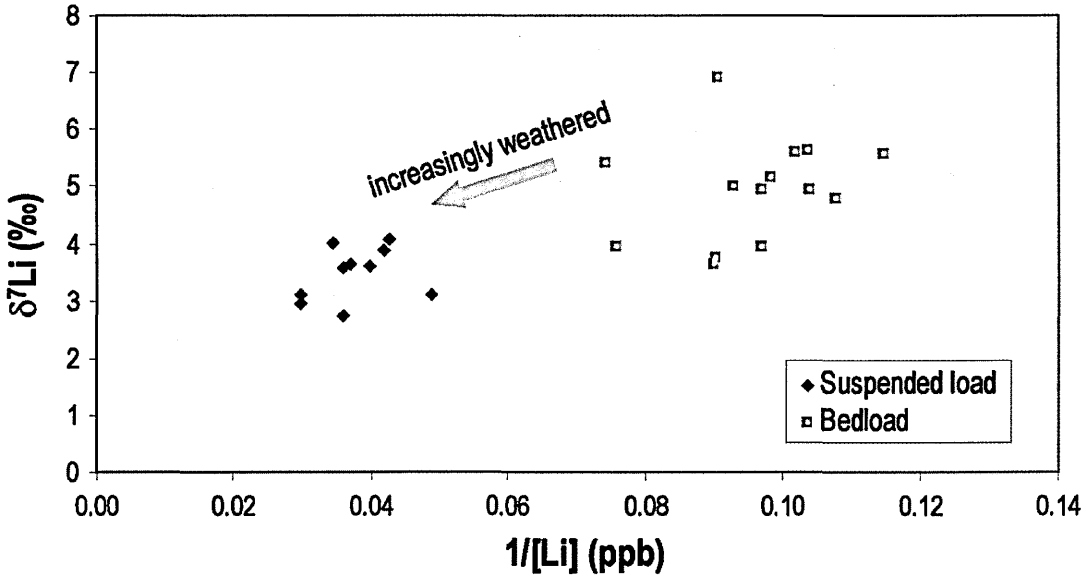

Fig. 3.10 – A graph comparing the δ^7Li composition and Li concentration of suspended sediments and bedload.

Concentrations of lithium in the suspended load are higher than they are in the bedload or bedrock with a range of concentrations between 24.9 and 35.5 ppm and average concentration of 28.8 ppm. The δ^7Li value of the suspended load (between 2.7 and 4.1 ‰) also tends to be lower than that of the bedrock and bedload. In comparison the bedload has the lowest Li concentration with an average of 10.6 ppm and higher δ^7Li (3.64 to 6.91‰, Fig. 3.10). A range of bedrock samples were taken and these have

a far greater range in Li concentration ranging from 11.3 to 26.2 ppm. The average δ^7Li value of the bedrock is 8.8‰ which is higher than the average of the suspended or bedload.

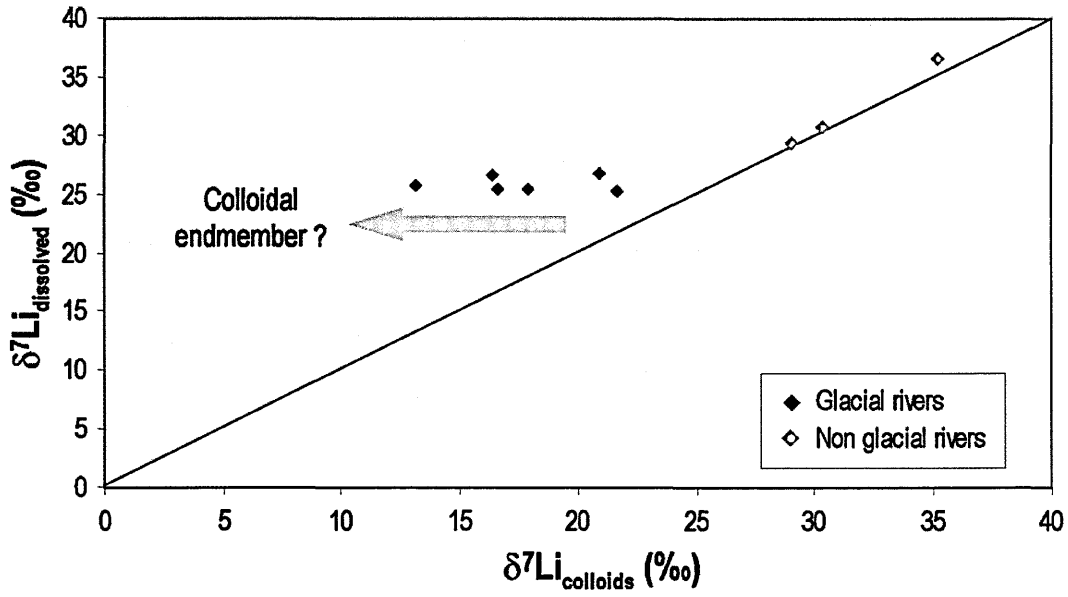

Fig. 3.11 – A graph showing the δ^7Li value of the colloidal fraction relative to the dissolved load.

Lithium concentrations are very similar between the dissolved (>0.2um) and ultrafiltered waters (<10kD); for example in GR1 the dissolved load has a lithium concentration of 49 nmol/l compared to 44 nmol/l in the ultrafiltered phase. The isotopic composition of the colloids in non glacial rivers is the same as that measured for the dissolved load, but the colloids in glacial rivers are isotopically lighter than the corresponding dissolved load (Fig. 3.11). The δ^7Li value of the glacial colloids ranges from 13 to 21‰ while the corresponding dissolved load is between 25.5 and 26.7‰. The δ^7Li values of a selection of ultrafiltered waters have also been measured; results show that the ultafiltered water has an identical lithium composition to the corresponding dissolved phase.

3.4.4. Leaching experiments

The results of the three leaching experiments are presented in Appendix B5 and illustrated in Fig. 3.12.

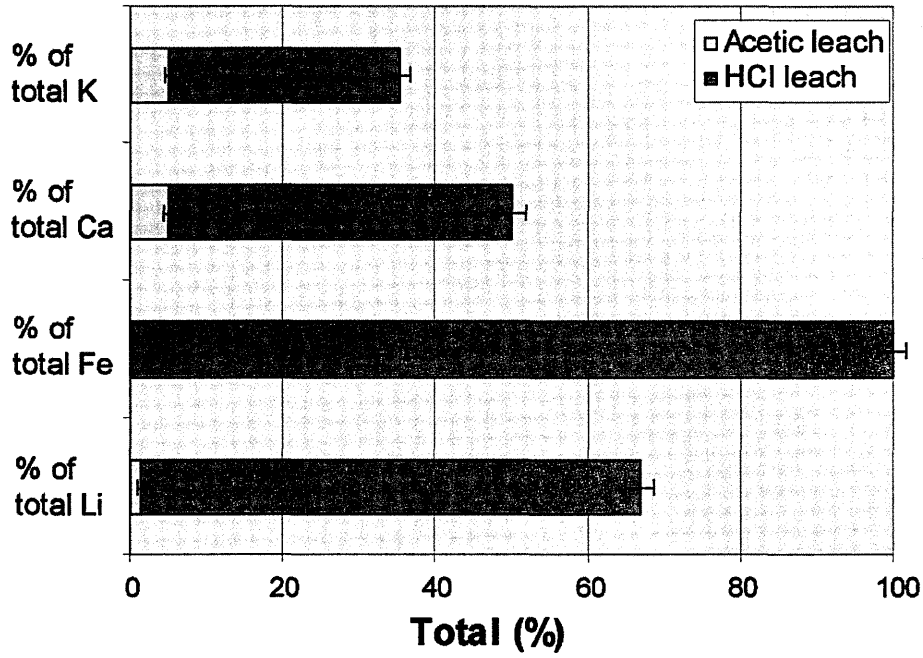

Fig. 3.12 - Results of the two stage leaching procedure showing the average total percentage of each element that is leached by an acetic acid buffer and 2N HCl. The total % of each element is calculated from the mass of each element that is in 0.2g of the suspended sediment sample. Error bars are 1 standard deviation of the mean value.

Three suspended sediment samples were analysed, their chemical similarities are reflected by the results of the leaching experiments which show little variation between the samples. The results presented in Appendix B5 have both the solution compositions in ppm and the total % of each element that the leaching step removes from the sediment. A greater proportion of each element, as expected, is leached by the stronger acid (2M HCl). For example the acetic leach removes around 1.5% of the total available lithium, while the HCl leach removes ~65% of the total lithium. Another element that shows a large contrast in abundance between the acetic and HCl leaches is iron; mass balance shows that only 0.5% of the available iron is leached by acetic acid

while nearly 100% of the iron from the suspended sediment is removed by the strong acid leach. Other elements that have a high concentration in this leach are Ni (~93% of total suspended Ni), Zn (~70%) and Mn (~65%).

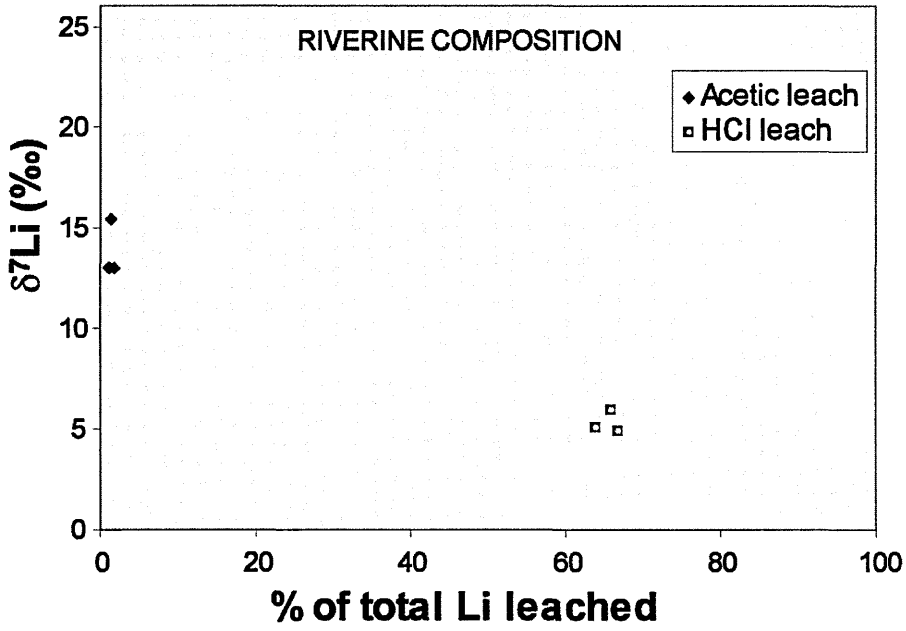

Fig. 3.13 - The δ^7Li composition of fluid derived from the two stage acid leaching process on suspended sediments (GR1, GR5 and GR7).

While the concentration of lithium that is removed by the different leaching stages is dissimilar further analyses of the fractions show that the compositions of the two leaching stages are different with respect to lithium isotopes (Fig. 3.13). The acetate leach has a δ^7Li value of ~15‰ while the HCl leach has lower δ^7Li (~5‰).

3.5. Discussion

3.5.1 Physical characteristics

The source of proglacial river water is a combination of surface and subglacial melting (ANDERSON et al., 2000; DAS et al., 2008; TRANTER, 2003). As a consequence the

glacial rivers contain large volumes of water and are fast flowing; for this reason the water-rock contact time and thus the intensity of chemical weathering is low. This explains the relatively low average temperature (4.6°C) of the glacial rivers relative to the non glacial rivers (12.3°C) and the low TDS (10.5µS) relative to the average TDS of the world rivers (50µS, Gaillardet 1999). Temperature has a direct impact on the rate of chemical reactions as illustrated by the Arrhenius equation:

$$k = A \times \exp\left(\frac{-E_a}{RT}\right) \qquad \textit{Equation 3.2}$$

where A is the pre-exponential factor and E_a is the activation energy, R is the gas constant, and T the temperature in K.

Thus reactions such as the hydrolysis of silicates will increase exponentially with increasing temperature, and so relative to non glacial rivers the rate of reaction will be lower. This is illustrated in Fig. 3.14, which shows a positive relationship between temperature and TDS.

Alkalinity is the capacity of a solution to neutralise acid and is usually dominated by carbon species which at pH values of less than 8.3 are mostly in the form of HCO_3^- (APPELO and POSTMA, 2005). In the glacial rivers the alkalinity increases from the source of the rivers to 30km downstream. Alkalinity is produced during the weathering of silicate rocks and can also be related to the contact time with atmospheric CO_2. The trend in alkalinity generally follows that of TDS, showing that rivers with higher alkalinity have a higher silicate weathering intensity.

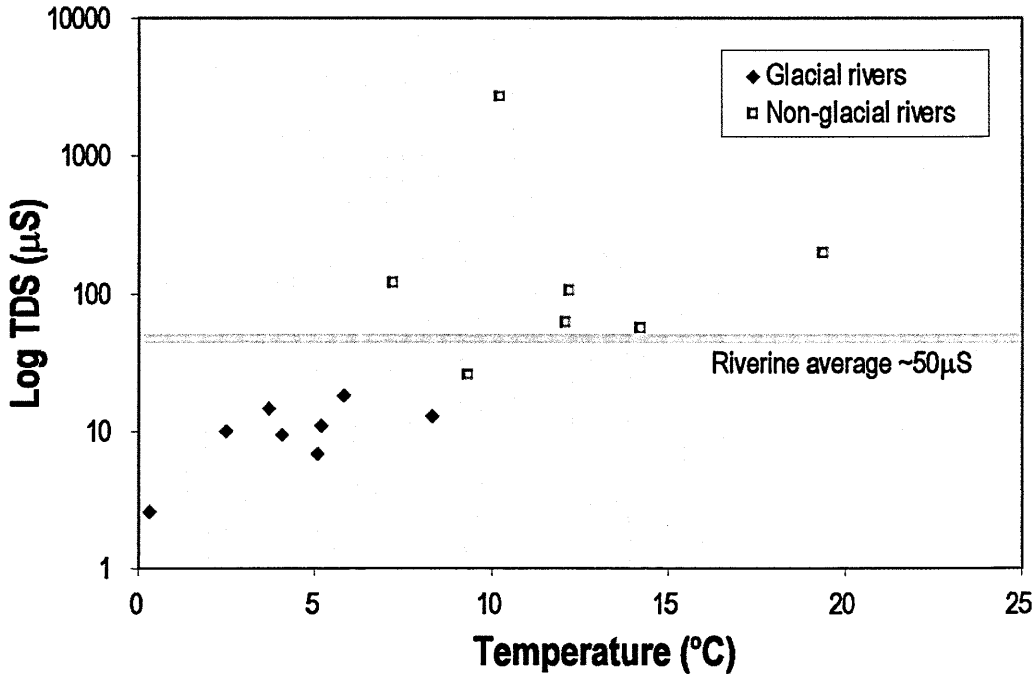

Fig. 3.14 – A graph showing the TDS vs temperature in both glacial and non glacial rivers. The average riverine TDS (50µS) is from Gaillardet et al. (1998).

Glacial rivers also characteristically have high TSS (on average 0.5g/l compared to 0.045g/l in non glacial rivers) due to their direct link to the ice sheet; glaciers produce high amounts of fine grained sediment that can be transported in the meltwater, there is evidence for this fine grained sediment in the glacial sediments and landforms in and around the Kangerlussuaq region (RUSSELL, 2007) and the abundance of wind blown dust. This fine grained sediment can be easily transported by the glacial rivers, in particular because the rivers are fast flowing, and the high flux of water means that the total mass of sediment that is carried is high.

In contrast the non glacial rivers are not directly linked to the glacier so glacial meltwater doesn't directly flow into them. Kangerlussuaq is in an area of negative precipitation and underlain by continuous permafrost (JORGENSEN and ANDREASEN, 2007) so the amount of rainwater and groundwater flow into the non glacial rivers is low. For this reason the volume of water carried in these rivers is small relative to the

glacial rivers, and because they have slower flow rates the contact time between water and rock is far higher and the chemical weathering intensity is greater. The low flow rate and isolation from the glacier means that total sediment that is carried in suspension is also much lower than in glacial rivers. The brown colour of the filtered water (in particular GR11 and GR12) indicates that organics such as humic acid are likely to be present in these rivers (GAILLARDET et al., 2003) while there is no obvious organic presence in the glacial rivers. Despite the rivers being called 'non-glacial' they are not representative of non-glacial rivers worldwide; many rivers draining non glacial regions discharge huge volumes of water such as the Amazon (~6600km^3/yr) and the Congo (~1200km^3/yr). As well as having a far greater discharge these rivers can also carry high amounts of suspended sediment e.g. the Ganges which has an average TSS of 1100mg/l (GAILLARDET et al., 1999a). Though the 'non-glacial' rivers in this study cannot be representative of major rivers worldwide the two sets of river in this study do represent extremes in intensity of chemical weathering and so make an important comparison of how differences in the weathering intensity can affect the behaviour of stable isotope systems.

Variations in pH in natural waters can result from two processes; a) the consumption of protons during the weathering of silicate rocks, b) the generation of protons by atmospheric CO_2 entering solution or oxidation of sulphides. The sample with the lowest pH is the supraglacial sample (GR3, pH 6.3); this low pH suggests that the water has had no contact with the bedrock and so the consumption of protons by silicate weathering is limited. In contrast the proglacial rivers have higher pH's (7.1 to 8.4) indicating that these waters have had a longer contact time with the bedrock thus the level of weathering is greater and more protons are consumed. The proglacial water is sourced either from surface melting or subglacially, in either case it must flow through

the subglacial zone; here the dominant reactions are silicate and carbonate hydrolysis which can raise the pH of the water as high as pH 9 and 10. Another important reaction in the subglacial environment is the oxidation of sulphides as shown in Equation 3.3 (TRANTER, 2003):

$$4Fe_2S + 16Ca_{(1-x)}Mg_xCo_3 + 15O_2 + 14H_2O \Rightarrow$$
$$16(1-x)Ca^{2+} + 16xMg^{2+} + 16HCO_3^- + 8SO_4^{2-} + 4Fe(OH)_3 \qquad \textit{Equation 3.3}$$

Sulphide oxidation produces protons which lowers the pH of the water as well as producing by products such as iron oxyhydroxides. This reaction consumes oxygen where it is available but does not always require atmospheric oxygen to be present; it can be supplied from bubbles in the melting ice and the reaction can also be mediated by sulphur oxidising bacteria that use Fe(III) as an oxidising agent (BOTTRELL and TRANTER, 2002; TRANTER, 2003). As well as lowering the pH the provision of protons enhances the dissolution of carbonates by lowering the saturation state of carbonates in solution (TRANTER, 2003). The resulting solution has a pH that reflects a combination of processes; the supraglacial chemical weathering of silicates consumes protons, but the oxidation of sulphides prevents the pH of the resulting subglacial water rising above ~9. The closest proglacial sample to the ice sheet is GR1, the pH of which is 8.4. Further downstream from GR1 the pH decreases to ~7.2 at the entrance to the fjord at Kangerlussuaq. This shows that outside of the subglacial environment the production of protons by CO_2 entering solution must be greater than the consumption of protons by silicate weathering and indicates that the weathering rate in these glacial rivers must be relatively low.

Non glacial rivers have a similar range in pH to the glacial rivers. Sample GR12 has a high pH (8.25) and also high TDS, which suggests that protons have been consumed by weathering reactions. Conversely sample GR11 has a low pH (6.8) and relatively low TDS (25μS) indicating that the weathering intensity is low and atmospheric CO_2 plays a greater role in controlling pH.

3.5.2. Major and trace elements

3.5.2.1. Dissolved load

Major and trace element analyses show that there are both similarities and differences between chemical compositions of the glacially and non glacially sourced rivers. In both sets of river the most abundant major cation is Ca^{2+} and the most abundant anion is the bicarbonate ion (HCO_3^-), despite the underlying lithology being essentially a monolithological area of amphibolite grade gneiss and ancient volcanics with only trace amounts of carbonate present (WELLS, 1979). These high Ca^{2+} concentrations in glacial rivers are consistent with previous research on glacial processes (ANDERSON et al., 1997; TRANTER, 2003) as explained in Section 3.1.

The greatest difference between the major cation contents of the glacial and non glacial rivers are the relative proportions of K^+ and Mg^{2+} ions. Changes in the relative proportions of cations in rivers are often driven by changes in lithology (MEYBECK, 2003). However, since the source terrain is essentially monolithological (Wells 1978), it is more likely that the differences in cation concentrations are caused by differences in chemical weathering intensities. The variation in potassium concentrations can be illustrated by the K/Na ratio. In most non glacial rivers the molar K/Na ratio is ~0.33 while this ratio tends to be higher (~1) in glacial rivers (ANDERSON et al., 2000); in the Greenlandic rivers the K/Na ratio exceeds 1 in the three river samples that have the

closest proximity to the ice sheet (GR1, GR3 and GR9). This increase in the K^+ concentration is caused by non stoichiometric biotite dissolution and the leaching of interlayer K, a process that is relatively rapid under glaciers and in glacial soils (ANDERSON, 2005; ANDERSON et al., 1997; BLUM et al., 1998; NEWMAN and BROWN, 1969; SHARP and GOMEZ, 1986; STALLARD, 1995). The combination of preferential K^+ release from interlayer biotites, with a relatively small amount of sodium release due to the low intensity of chemical weathering, means that the K/Na ratio is greater than in non glacial rivers. Non-glacial rivers have significantly higher concentrations of magnesium than glacial rivers (16% of major cations in glacial rivers compared to 36% in non glacial rivers). Because the weathering intensity is higher in non glacial rivers the processes that are important in glacial rivers such as the interlayer leaching of biotite and dissolution of trace carbonates are less important. As a consequence the chemistry of the non glacial rivers is dominated by silicate rock dissolution and so the relative proportion of magnesium that is mobilised is higher.

There are also differences with regards to the relative anion composition in the two river types. Glacial rivers have a proportionally higher SO_4^{2-} concentration compared to non glacial rivers (22% compared to 10% in non glacial rivers); this is because the chemical composition of glacial rivers is strongly influenced by subglacial processes (TRANTER, 2003) and one of the most important is the oxidation of sulphides (Equation 3.2). While sulphide oxidation will still occur in non glacial rivers the relatively high chloride concentrations mean that proportionally the levels of sulphate in solution are lower than in glacial rivers.

It is useful to use the Cl/Na ratios of the water in order to assess how much influence seawater has over the chemical compositions of the rivers. The low Cl^- concentrations in the glacial rivers (averaging 0.13 mg/l or ~3% of the total anion

content) and low Cl/Na ratios (~0.2 compared to 1.8 in seawater) suggest that seawater influence is small. The supraglacial sample GR3 has the highest Cl/Na ratio of 0.6 showing that even on the ice itself the influence of aerosols is low, or possibly masked by the weathering of glacial and aeolian sediment which may provide relatively high amounts of sodium. In non glacial rivers the chloride concentration is much higher (averaging 8.7 mg/l or ~20% of the anion content) due to a combination of high levels of evaporation in the Kangerlussuaq region (ANDERSON et al., 2001; JORGENSEN and ANDREASEN, 2007) and the fact that the non-glacial rivers themselves have small water volumes; this leaves the resulting fluid more concentrated. As a result of this high chloride concentration the Cl/Na ratio in these rivers is also higher, averaging 0.9, but is still low relative to that of seawater. The difference between chloride concentration in glacial and non glacial rivers is large, this may be especially true in summer when glacial melting and evaporation are at a maximum. In general it seems unlikely that seawater has any impact on glacial river composition, and despite high levels of evaporation the impact on non glacial rivers is also relatively small.

Because the Kangerlussuaq region is underlain by a zone of monolithological rock (amphibollite grade gneiss) the relative contribution of silicate versus carbonate rocks to the chemical composition of the rivers should be dominated by silicate weathering; this can be checked by calculating major element ratios. The average molar Ca/Na, Mg/Na and Sr/Na ratios (1.6, 0.7 and 3×10^{-3} respectively) reflect the low level of carbonate dissolution in the area and the dominance of silicate weathering (for reference carbonate rivers in Gaillardet et al. (1998) have Ca/Na, Mg/Na and Sr/Na ratios of approximately 50, 10 and 35×10^{-3}). The samples collected either on or adjacent to the ice sheet have higher Ca/Na ratios of 2.3 – 3.8. Further downstream the

level of chemical weathering and the amount of Na^+ that is released into solution increases causing the Ca/Na ratio to fall to ~1.

Relative mobilities of major elements can be estimated by normalising the molar concentration of an element in solution by the molar concentration of that element in the bedload. Elements with a greater mobility will have a higher ratio as more of the element has entered solution relative to the amount in the bedload. Results are plotted in Fig. 3.15, and the elements are ordered with respect to their mobilities in the glacial rivers.

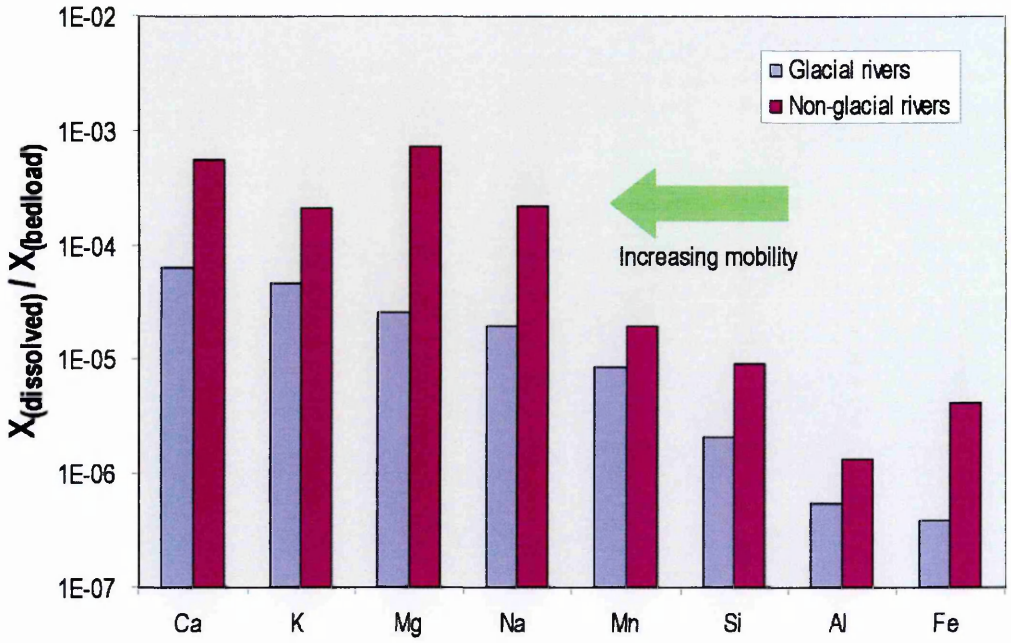

Fig. 3.15 - A graph showing the average relative mobilities of cations in glacial and non glacial rivers from Greenland. The higher the ratio $X_{dissolved}/X_{bedload}$, the more readily the element dissolves.

In the glacial rivers the most mobile elements are calcium and potassium, caused by the preferential release of these elements by weathering of trace carbonates and biotite. The least mobile elements are iron and aluminium which are known to be less mobile during weathering from work on rivers (GISLASON et al., 1996) and from their retention in soils and in some circumstances the formation of laterites and bauxites

(SCHELLMANN, 1994; TARDY, 1997). The final sequence of element mobility in the glacial rivers is (in decreasing order): Ca>K>Mg>Na>Mn>Si>Al>Fe. This pattern of mobility is similar in the non-glacial rivers; again in decreasing order Mg>Ca>Na>K>Mn>Si>Fe>Al. In general all of the elements are more mobile in non-glacial rivers, but particularly magnesium, sodium and iron which reflects the higher chemical weathering intensity in non glacial rivers and the lesser importance of glacial weathering processes that preferentially mobilise K and Ca.

3.5.2.2. Suspended and bedload

The suspended load has been subjected to more weathering than the bedload and as a consequence of this should have a higher clay and secondary mineral content. If the average cation compositions of the bedload and suspended loads are compared to Wells average amphibolite (Fig. 3.8) it shows that with increasing amounts of weathering (i.e bedrock < bedload < suspended sediment) the relative concentrations of Ca^{2+} and Mg^{2+} increase at the expense of Na, Al and Si. Clay minerals have been shown to be effective at adsorbing metal ions in numerous studies (BROWNAWELL et al., 1990; DAVIS and KENT, 1990; PEACOCK and SHERMAN, 2005b; SCHULTHESS and HUANG, 1990; TILLER et al., 1984) and have large surface areas. Clay minerals such as smectites and vermiculites have permanent surface charge which results from the substitution of divalent cations (e.g. Mg^{2+}) for trivalent ions in the octahedral sheet (e.g. Al^{3+}) or the substitution of trivalent cations for Si^{4+} in the tetrahedral layer (DAVIS and KENT, 1990). These substitutions result in a negative surface charge. For this reason clay minerals often take up metal cations such as Mg^{2+}, Ca^{2+} and K^{+}. Iron oxide minerals can also adsorb metal ions but they have no surface charge so adsorption occurs via binding with surface hydroxyl groups (RANDALL et al., 1999). The suspended sediments in the

glacial rivers are enriched in Mg, Ca, K, Li, and Fe; all elements that form cations in solution. Through substitutions into octahedral layers in clays, electrostatic attractions with the clay surfaces and binding with surface hydroxyls on iron oxide minerals these cations can become relatively enriched on suspended sediments. Trace elements also show a substantial enrichment on the suspended sediment in relation to their concentration in the bedload. This is particularly true of the transition metal cations which are readily incorporated into clays (DECARREAU, 1985) and iron oxides (PEACOCK and SHERMAN, 2005a; SHERMAN and PEACOCK, 2004). In this case the adsorption of Ni, Cu and Zn onto the suspended sediment has enriched these elements by ~145, 250 and 140% respectively relative to bedload concentrations.

The suspended sediment is fine grained relative to the bedload (hence it can be transported in suspension by the river). This fine grain size is achieved either by higher levels of chemical weathering or by physical grinding. The relative levels of chemical weathering subjected to the bedload and suspended load can be assessed by using element ratios, in this case the molar ratios of Ca/Na and Mg/Na (STALLARD and EDMOND, 1981). Although relative mobilities of elements in these rivers (Fig. 3.15) show that calcium is the most mobile element (due to its preferential release during weathering of trace carbonates) sodium is usually considered to be the most mobile of the major cations during weathering (GAILLARDET et al., 1999a; GISLASON et al., 1996). Because of this mobility sodium will preferentially enter solution and so with increasing weathering intensity the element ratios should rise. Molar ratios of Ca/Na and Mg/Na in the suspended load average 0.69 and 0.7 respectively, compared to average ratios in the bedload of 0.5 and 0.38 respectively indicating that some chemical weathering has occurred as the more mobile Na is lost into solution and the resulting suspended sediment has proportionally less sodium. Thus suspended sediment has been subjected

to more chemical weathering than the bedload and is likely to contain a higher proportion of alteration minerals such as clays and iron oxide minerals than the less altered bedload. Because the sediment has a finer grain size the total surface area per g available for new minerals to nucleate upon is greater and there is greater potential for further cation exchange reactions to happen. For this reason the bulk composition of the suspended sediment is different from that of the bedload with a greater content of major and trace metal divalent cations. Lithium is also substantially enriched in the suspended phase, this is discussed further in Section 3.5.3.2.

The suspended sediment is the most altered solid phase in the Greenlandic rivers, this can be compared with the composition of suspended sediments in rivers worldwide. A study of suspended sediment (GAILLARDET et al., 1999a) lists compositions of a number of rivers including the Huanghe, Mekong, Niger, St Lawrence and MacKenzie. Calculated Mg/Na ratios for these rivers are 1.6, 1.9, 1.8, 1.1 and 5.3 respectively; Ca/Na ratios for the same rivers are 3.5, 1.9, 0.8, 1.1 and 7.8. In each case the suspended sediment has a higher element ratio when normalised to sodium relative to the ratios obtained in this study from glacial rivers (Fig. 3.16). Another study of suspended sediment from rivers in the Congo Basin have Ca/Na ratios of between 3 and 10 (DUPRE et al., 1996). The relatively high Ca/Na and Mg/Na ratios in these studies suggests that the sediment within these rivers has been subjected to more intense chemical weathering and subsequently a greater loss of sodium into solution.

The bedload is less weathered, is likely to have a low clay content and is closer to the chemical composition of the unaltered bedrock (Appendix B4). The lower amount of weathering of the bedload is highlighted by comparing the silicon composition of the bedload and the silicon concentration in the average amphibollite

(WELLS, 1979); results show that the concentration of bedload Si is almost identical to that in the bedrock at ~31 Wt%. This means that very little Si has been lost and supports the idea that in general the intensity of chemical weathering in these rivers is low.

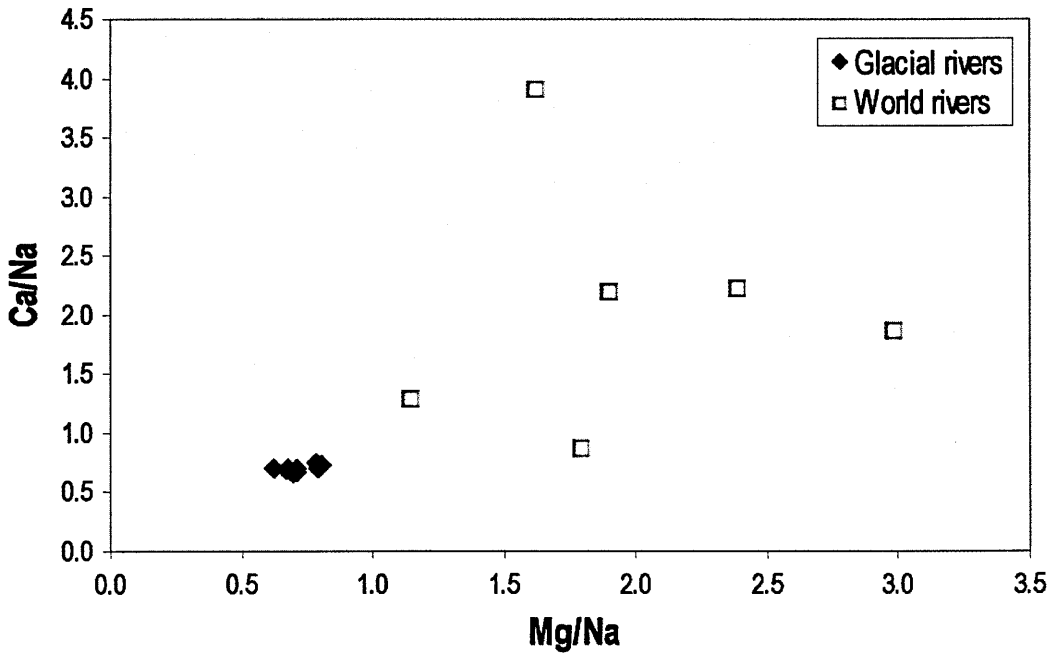

Fig. 3.16 - A graph showing the Ca/Na and Mg/Na ratios of suspended sediment from the glacial rivers in Greenland and from sediment sampled by Gaillardet et al. (1999) from the Huanghe, Changjiang, Xijiang, Mekong, Niger and St Lawrence rivers

3.5.2.3. Colloids

The colloidal fraction of glacial rivers is significantly enriched in iron and aluminium. These are likely to be present in the form of metallic oxyhydroxides or possibly clays. Iron oxyhydroxides can occur in various forms, either attached to particulate grains or as unattached nanoparticles (RAISWELL et al., 2006) so they can affect both the suspended and colloidal phases. Low levels of nitrate and phosphate in the glacial rivers suggests that the formation of organic colloids in these rivers is unlikely.

The colloidal fraction of the non-glacial rivers is also enriched in many elements, including Fe and Al, anion analyses also imply the presence of organics in many of the non glacial rivers. The occurrence of organic colloids such as humic acid is often shown by the brown colour of the water (GAILLARDET et al., 2003) as seen in samples GR11 and GR12. The combination of anion data and observations in the field imply that the dominant colloidal presence in the non glacial rivers is organic. Trace element data also supports this conclusion; comparisons between the concentrations of the biologically important elements Cu, Zn and Ni in the dissolved and ultrafiltered waters of the glacial rivers are similar. In comparison there is a greater concentration difference between phases in the non glacial rivers, with all three elements having lower concentrations in the ultrafiltered phase. Divalent metal cations such as Cu, Ni and Zn are known to form strong complexes with fulvic acid (POKROVSKY et al., 2005) which supports the conclusion that the colloids in the non glacial rivers are organic in origin.

The behaviour of the major cations in the ultrafiltered glacial waters suggests that a high proportion of the 'dissolved' Ca in the <0.2um fraction seems to be present in colloids (Fig. 3.7). While other studies have shown that glacial rivers have high Ca concentrations (ANDERSON et al., 1997; ANDERSON et al., 2003; RAISWELL and THOMAS, 1984; TRANTER et al., 1993; TRANTER et al., 2002) these studies did not separate the colloids from the dissolved load. If a high amount of Ca is present in the colloidal phase in the glacial rivers it suggests that the colloids themselves are Ca rich. One possibility is that the ultrafine material is $CaCO_3$ rich, although calcium-carbonate is only present in trace amounts in the bedrock. Another is that Ca is adsorbed onto the surface of any ultrafine particles or iron oxyhydroxide nanoparticles. The results of the leaching experiments show that ~50% of the total Ca in suspended sediment is leachable, and so can be inferred to be associated with oxyhydroxide minerals.

3.5.3. The behaviour of lithium

3.5.3.1. Riverine δ^7Li

The δ^7Li composition of the dissolved load of Greenland rivers (~27‰) is distinctly different from that of the bedrock from which this lithium was initially derived (~8‰). This difference shows that the dissolved phase is highly enriched in the heavy isotope of lithium and that in order to balance this the light isotope of lithium (^{6}Li) must be preferentially removed from the solution or the heavy isotope (^{7}Li) must be preferentially released during dissolution. Experimental work investigating the dissolution of basalts (PISTINER and HENDERSON, 2003) and work completed during this PhD involving the dissolution of silicate minerals (Chapter 5) show that fractionation of lithium isotopes does not occur during dissolution. Instead this fractionation occurs during secondary mineral formation as proposed in a number of previous studies investigating the behaviour of lithium isotopes (CHAN and HEIN, 2007; HUH et al., 1998; KISAKUREK et al., 2004; PISTINER and HENDERSON, 2003; POGGE VON STRANDMANN et al., 2006). For this reason the δ^7Li composition of the dissolved phase reflects the balance between primary mineral dissolution and secondary mineral formation, this is discussed in Fig. 3.17. The δ^7Li composition of both the glacial rivers (~25‰) and non glacial rivers (~30‰) are higher than the global riverine mean of 23‰ (HUH et al., 1998). The lithium concentrations in the glacial rivers (14-92 nmol/l) are far below the global average (230 nmol/l) while the concentration in the non glacial rivers (14-572 nmol/l) can be far greater. The combination of these lithium data suggests that in both sets of rivers secondary mineral formation dominates over primary mineral dissolution.

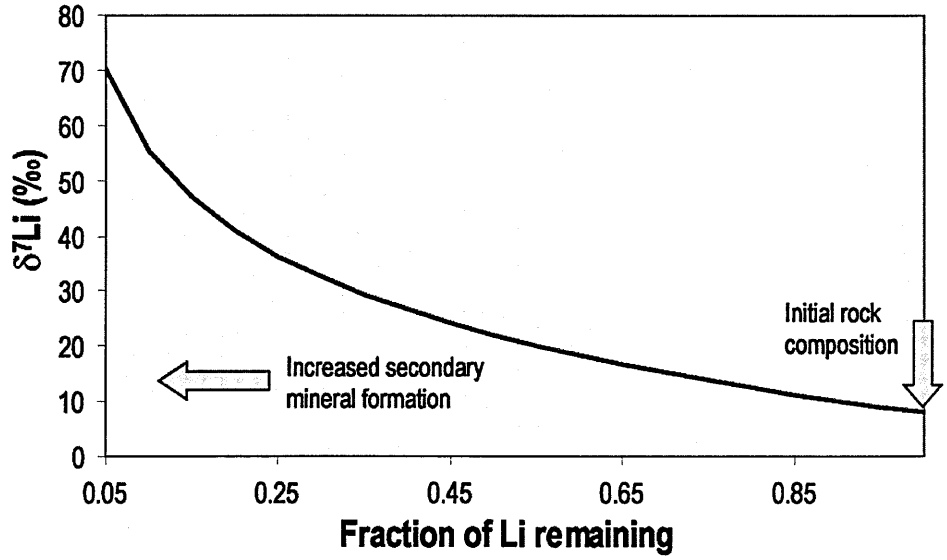

Fig. 3.17 – Rayleigh fractionation curve showing the variation in the value of δ^7Li of the dissolved load as a function of the proportion of lithium that is removed into secondary minerals. The light isotope, ^{6}Li, is preferentially incorporated into secondary minerals leaving the fluid phase enriched in ^{7}Li (Huh et al. 1998). The line represents an isotopic fractionation factor ($\alpha_{mineral\text{-}fluid}$) of 0.980. The initial rock composition used is that of the unaltered bedrock (~8‰).

One sample has a different lithium isotope composition from the glacial and non glacial rivers; GR3 (supraglacial) has an isotopically light δ^7Li ratio of 13.5‰. The fractionation between unaltered bedrock and GR3 is hence relatively small and so suggests that the amount of secondary mineral formation in GR3 is low. Sample GR3 has had no contact with the bedrock, instead its composition is derived from the surface ice and weathering of glacial and aeolian sediment that is entrained within it (FORTNER et al., 2005; TRANTER et al., 1993). GR3 not only has a distinct lithium isotope composition but also has a low pH (6.3) relative to the other waters. This information can help identify the source of the proglacial water, suggesting that while the melting of surface ice must contribute to the composition of the glacial rivers and provide a source of glacial sediment the overall riverine composition is dominated by subglacial water. A river sample from 2km downstream of the ice-sheet such as GR1 has a δ^7Li

composition of 25.4‰. It is unreasonable to suggest that the signal has evolved from a supraglacial value of ~13‰ to 25‰ over 2km when the composition of the solution has remained relatively constant over the 30km stretch of river towards Kangerlussuaq. Instead the high δ^7Li composition of proglacial rivers must be derived from prolonged water-rock contact at the base of the glacier; showing that a significant amount of liquid water must be present here over a long period of time.

3.5.3.2. Suspended and Bedload δ^7Li

The δ^7Li value of the suspended sediments (~3.3‰) in Greenlandic rivers is always lower than the δ^7Li value of the corresponding bedload (~5.2‰) which suggests that it contains a proportionally higher secondary mineral content (HUH et al., 1998). A higher amount of secondary minerals means that more ^{6}Li is taken up out of solution; correspondingly this leaves the dissolved load to be isotopically heavy relative to the bedrock and bedload. The isotopic composition of the dissolved Li in glacial and non glacial rivers is relatively similar (average of 25 to 30‰) compared to a global range of riverine lithium compositions between 6 and 41‰ (HUH et al., 1998; KISAKUREK et al., 2005; POGGE VON STRANDMANN et al., 2006). This requires proportionally similar amounts of ^{6}Li to be taken out of solution by secondary mineral formation. In glacial rivers however, the water is more dilute and rock and particulate phases have been subjected to a lower weathering intensity than in non glacial rivers. For this reason the glacial rivers should be less saturated with respect to secondary minerals and in theory there should be a more pronounced difference between δ^7Li compositions in the two river sets. The fact that there is not suggests that there are different controls on the lithium isotopic composition between glacial and non glacial rivers in Greenland. These controls on lithium behaviour are discussed below.

3.5.4. Controls on the behaviour of lithium

3.5.4.1. Saturation indices of secondary minerals

The potential for formation of secondary minerals can be assessed by calculating their saturation states in the dissolved load using a geochemical modelling program such as PHREEQC (PARKHURST and APPELO, 1999). This program calculates the saturation index (SI) of minerals in solution from the chemical composition of the dissolved load as well as other variables including temperature and pH. The saturation index provides information about the mineral stability, if the SI of a certain mineral is > 0 then that mineral is supersaturated and has the potential to precipitate. If the SI is < 0 then the mineral phase is unstable and will dissolve; if the SI = 0 then the mineral phase is at equilibrium. The units of SI are in a log scale so a SI of 2 is ten times greater than a SI of 1.

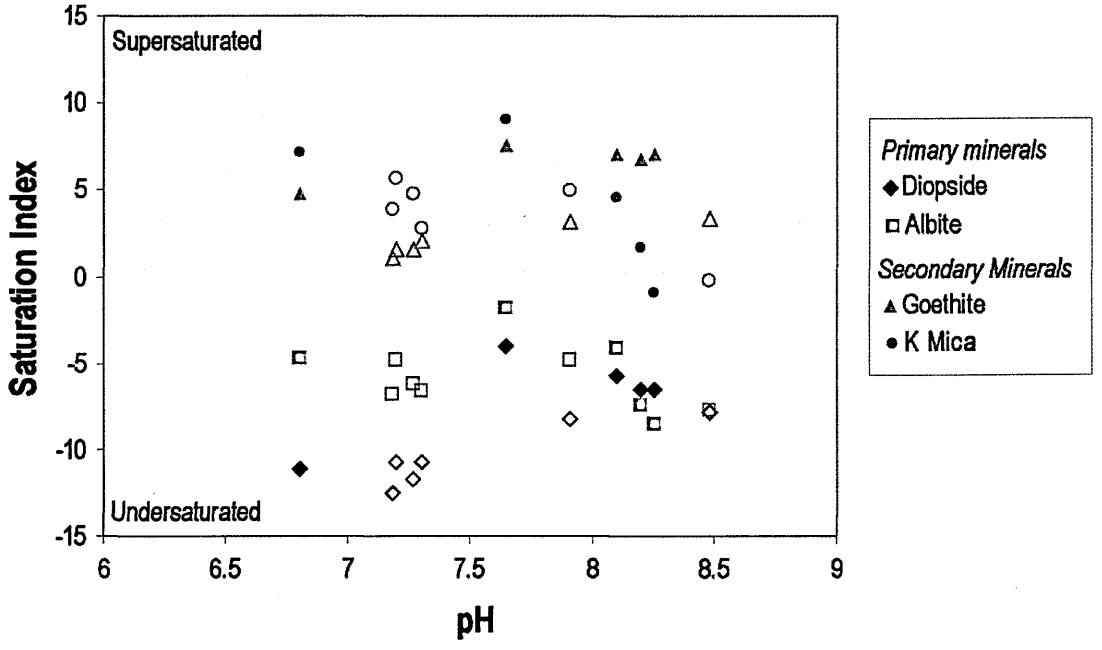

Fig. 3.18 – A graph showing the saturation states of a selection of primary and secondary minerals in ultrafiltered water vs the pH of the sample. Glacial samples are plotted as open symbols, non-glacial samples are plotted as closed symbols. Saturation indices of above 0 indicate that the solution is oversaturated while saturation indices of below 0 indicate that the solution is undersaturated.

Because of the presence of colloidal material in all of the river samples saturation state modelling using dissolved concentrations (<0.2um) gives misleading results. Instead all saturation state modelling has been performed on ultrafiltered water (>10kD) where all of the colloids have been removed; saturation indices calculated for a selection of primary and secondary minerals are presented in Appendix B6. Fig. 3.18 shows the saturation state index as a function of pH for a selection of primary and secondary minerals in the ultrafiltered phase of both the glacial and non glacial rivers. Primary minerals such as diopside and albite are all undersaturated, while some secondary minerals, including goethite and potassium mica are supersaturated. Note that the SI of these minerals is pH dependent; this is because the dissolution mechanism of silicate minerals usually involves metal-proton exchange reactions that break down the crystal lattice (OELKERS, 2001). If the concentration of H^+ increases the potential for exchange reactions increases and mineral stability decreases. On the other hand at high pH high concentrations of OH^- can reduce the mineral stability causing the saturation index of minerals to decrease.

If the formation of secondary minerals is related to ^6Li uptake then a relationship between SI and δ^7Li in the dissolved phase might be expected. However plots of secondary minerals such as ferrihydrite and kaolinite versus δ^7Li show that the relationship in these rivers is small or non existent (Fig. 3.19). This could be because most of the river samples have relatively similar lithium isotope compositions of around 27‰ (±4‰) and that there would be a more significant relationship if there were a wider range of lithium isotope values, or alternatively that secondary mineral formation within these rivers is not driving the shifts in δ^7Li.

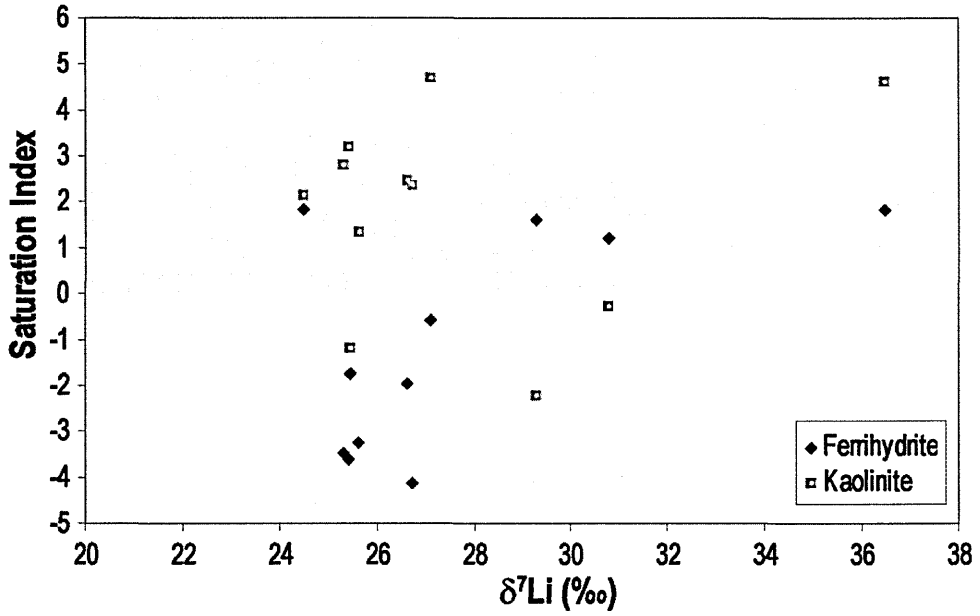

Fig. 3.19 - The relationship between saturation index and δ^7Li of the dissolved phase for the secondary minerals ferrihydrite and kaolinite. There is no significant relationship between saturation index and lithium isotope composition.

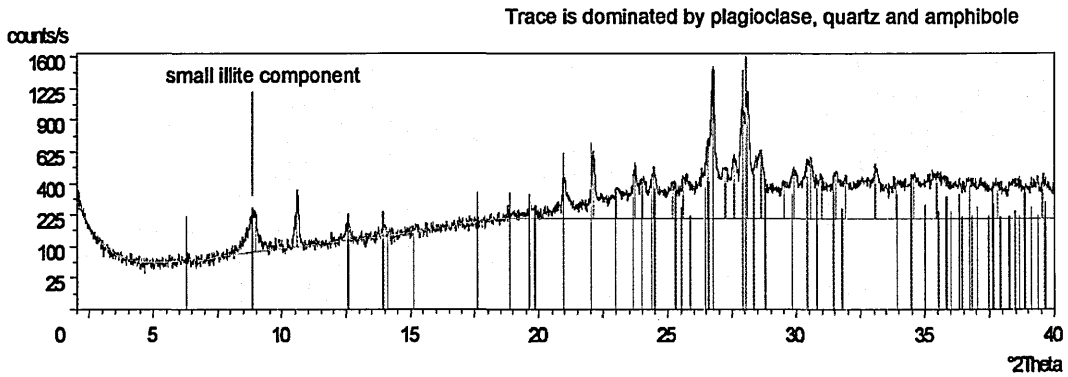

Fig. 3.20 - XRD trace of the suspended sediment from GR2. Results show that the sediment is dominated by plagioclase, amphibole and quartz (i.e. rock flour). There is also a small clay component; mainly illite and kaolinite.

While the relationship between δ^7Li and SI is not significant the results of the saturation state modelling do highlight a difference between the glacial and non glacial rivers. There is a large difference between the saturation states of the glacial and non glacial rivers with respect to the iron oxide minerals. Iron is present almost exclusively

in the colloids in glacial rivers hence the saturation state of iron oxide minerals in the ultrafiltered water is relatively low (e.g. for goethite the SI ranges from -0.9 to 1.3). In contrast a significant proportion of iron is present in the ultrafiltered phase of the non-glacial rivers, so much so that minerals such as haematite and magnetite are highly saturated (SI of up to 17). This suggests that iron oxide formation in the glacial rivers is not important but dominates in the non-glacial rivers. It is a similar story for aluminium; around 90% of aluminium in the dissolved phase is also associated with colloids again suggesting that the likelihood of aluminium silicates and in particular clays forming in the glacial rivers is low. This is supported by XRD analyses of suspended sediment samples (Fig. 3.20) which show that the main constituents of the suspended sediment are amphibole, quartz and plagioclase feldspar. The only traces of secondary minerals are illite and a small component of kaolinite and chlorite.

The results of the saturation state modelling show that essentially the glacial and non glacial rivers have similar mineral saturations except in the case of iron oxide minerals as iron is present only in the colloids in glacial rivers while it is truly dissolved in non glacial rivers. In the non-glacial rivers the formation of these iron oxide minerals could be the mechanism for the removal of ^{6}Li from solution. In general the saturation indices for the glacial rivers are very low, and together with the low TDS it would be predicted that secondary mineral formation was not important. This has been supported by the XRD data. However the relatively high $\delta^{7}Li$ composition of the water (~25‰) compared to the riverine average (23‰ (HUH et al., 1998)) shows that secondary mineral formation must have occurred and removed ^{6}Li from the water in a similar proportion to that removed in the non-glacial rivers (~30‰).

3.5.4.2. Colloidal lithium

One difference between the glacial and non-glacial rivers is the nature of the colloidal material. Anion analyses of the dissolved phases imply that organic molecules are present in the non-glacial rivers while none are present in the glacial rivers. Lithium isotope analyses of the colloidal fraction show that in the non-glacial rivers the colloids have the same δ^7Li value as the dissolved load. In the glacial rivers however the colloids have lower δ^7Li than the river water, indicating that the colloids preferentially incorporate ^{6}Li (Fig. 3.11). In non glacial rivers the colloids are likely to be organic, inferred from the results of the anion analyses, so probably comprised of humic or fulvic acid (GAILLARDET et al., 2003). This suggests that the organic colloids take up lithium from the river water in a way that is indiscriminate of mass. Conversely, in glacial rivers, the colloids are inorganic in origin because of the lack of biological activity in these rivers. The most likely origin for these inorganic colloids is ultrafine particles of suspended sediment that have been ground down by the glacier and possibly further weathered in solution. From analyses of the suspended load these particles will have a lithium composition of ~4‰, and if they have been subjected to further weathering and preferential ^{6}Li uptake they could be even isotopically lighter. The δ^7Li value of the colloidal lithium is not the same as the suspended sediment because each 'colloid' sample is in fact a mixture of dissolved and colloidal phases. These results show that the colloidal fractions are different in the two sets of river and that the colloids in glacial rivers are enriched in ^{6}Li. Nevertheless this has no significant affect on the δ^7Li composition of the dissolved load of the rivers because colloidal lithium concentrations are simply too low – ultrafiltration causes little or no variation in lithium concentration of the dissolved load. This is supported by the lithium isotope composition of the two fluid phases; the lithium in the dissolved phase (<0.2μm) has the

same isotope composition as the lithium in the ultrafiltered phase (<10kD). If there was abundant colloidal lithium present then its removal from the dissolved load should have an affect on the lithium isotopic composition, particularly in glacial rivers.

3.5.4.3. Suspended sediment

Glacial rivers carry far more suspended sediment than non glacial rivers; the average TSS in glacial rivers is ~0.5g/l while in non glacial rivers it is over ten times lower at ~0.045g/l. The suspended sediment carries between 2 and 4 times more Li than the bedload and this lithium is on average 2‰ lighter. As glacial rivers progress downstream the amount of suspended sediment that is carried in the river also increases. Because there is more sediment in suspension this means that more Li can be transported. For example in GR1 the dissolved load carries ~250 ng of lithium per litre. In comparison the suspended sediment carries ~15 μg of lithium per litre, over 60 times more than carried in solution. This can be compared to sample GR2 taken 30km downstream along the Watson River; here the total lithium carried in solution is ~420 ng per litre. In suspension the total lithium is ~17.3 μg per litre, over 40 times more than carried in the dissolved phase. These mass balance calculations show that the suspended load carries far more lithium to the oceans than the dissolved load, although how much of this sediment can be further weathered and release its lithium to the oceans is not known. Further weathering of this sediment in estuaries and deltas may have an impact on the chemistry of seawater lithium similar to that proposed by Gislason et al. (2006) for the Ca flux to seawater carried by Icelandic rivers.

Glacial rivers carry high volumes of sediment that has an isotopically light lithium composition, but it is important to know with what phases this lithium is associated. The most likely minerals to be preferentially taking up ^{6}Li are clay minerals

such as smectites (VIGIER et al., 2008), aluminium oxides such as gibbsite (PISTINER and HENDERSON, 2003), and iron oxyhydroxides (CHAN and HEIN, 2007). However XRD analyses show that the suspended sediment has only trace amounts of clay mineral present (Fig. 3.20). In order to get a better idea of which phases are present on the suspended sediment and how Li is incorporated into these phases leaching experiments were performed (the results of which are described in Section 3.4.4).

The suspended sediment is on average enriched in Fe by ~12% relative to the bedload and contains over twice the amount of Fe present in the bedrock. This means enrichment of Fe on the suspended load must be due to either adsorption processes or the formation of new minerals. The leaching experiments show that almost all (98-100%) of the Fe present in the suspended sediment can be leached by 2M HCl while very little can be removed by the acetic acid buffer. This suggests that little Fe is adsorbed by electrostatic attraction (physisorption) and that there has been significant precipitation of secondary Fe-minerals; the most likely being amorphous Fe-oxyhydroxides that are produced during subglacial sulphide oxidation as explained in Section 3.5.1. (TRANTER, 2003). These secondary minerals will attach to the surface of quartz and clay minerals as patches, aggregates or layers with limited extent (RAISWELL et al., 2006), they may also infill pores on clay mineral surfaces (POULTON and RAISWELL, 2005). Even so, the high percent of Fe that is taken up by growth of Fe-oxyhydroxides is surprising, particularly when the composition of unaltered amphibolite has an Fe content of ~ 2.1 Wt % (WELLS, 1979) of which none will be present as Fe-oxyhydroxides. Because the Fe concentration in suspended sediment is ~ 4.5 Wt % a more reasonable estimate for the percentage of Fe in oxyhydroxide minerals would be 60-70%.

The high concentration of cations that are released along with the iron, such as Ni, Zn, Mn and Li suggest that these elements are also associated with the surface iron oxides. Around 65% of Li from the suspended load is associated with this HCl leach while only ~2% is freely exchangeable. The δ^7Li composition of the fluid from the two leaching stages is also isotopically different. The lithium isotopic composition of the acetate leach is ~15 ‰, this is over 10‰ heavier than the composition of the bulk suspended sediment (~3.5‰). In contrast the HCl leach has a Li isotope composition of ~5‰, much closer to that of the bulk suspended sediment. The reason for this difference is that the lithium in the acetate leach is freely exchangeable; this is lithium that has bonded by electrostatic interactions with no isotopic preferences as shown in previous studies of Li in ferromanganese crusts (CHAN and HEIN, 2007) and Li sorption onto smectite (PISTINER and HENDERSON, 2003). In this case the composition of the lithium reflects that of the river water so is isotopically heavy relative to the suspended sediment. The composition is not identical to that of the river water (in theory it should be ~25‰) but the acetate buffer may have caused a small amount of oxyhydroxide dissolution, particularly if it is poorly crystalline. A relatively minor loss of chemically sorbed lithium from iron or aluminium oxyhydroxides would be enough to significantly offset the lithium composition because the amount of lithium that is freely exchangeable is small (~1.5% of the total Li). The lithium leached by HCl is bound during the formation of secondary minerals such as Fe and Mn-oxyhydroxides (CHAN and HEIN, 2007). This is lithium that has been chemically bound, not attracted by charge imbalance. Recent work into the behaviour of lithium during sorption onto gibbsite has shown that there is an isotopic fractionation associated with the uptake of lithium from solution with a preference for ^{6}Li (PISTINER and HENDERSON, 2003). Gibbsite, like the iron oxide minerals does not have a permanent structural charge at near neutral pH

(DAVIS and KENT, 1990) so this uptake cannot have been caused by electrostatic interaction; the conclusion of the study by Pistiner & Henderson (2001) is that the lithium fractionation occurs during chemical sorption. As a result of this preferential ^{6}Li uptake, the chemically sorbed Li (~5‰) is close in isotopic composition to that of the suspended sediment (~3.5‰) and around 21‰ lower than the river water $\delta^{7}Li$ composition. The difference in the lithium isotope composition between the chemically sorbed Li and the river water can be used to calculate a fractionation factor (CHAN et al., 1992). In this case the fractionation factor ($\alpha_{mineral\text{-}fluid}$) is 0.979, which is similar to the average of the fractionation factors between suspended and dissolved phases in the glacial rivers (range between 0.974 and 0.979). The degree of fractionation is slightly larger than that calculated by Pistiner & Henderson (2003) during the sorption of Li onto gibbsite ($\alpha = 0.986$) but is within the range reported for lithium in ferromanganese crusts ($\alpha = 0.978\text{-}0.999$) (CHAN and HEIN, 2007) and is similar to values obtained in a study of Li sorption from seawater onto kaolinite and vermiculite ($\alpha = 0.979$ and 0.971) (ZHANG et al., 1998).

These results show that the suspended sediment has a relatively high content of easily leachable iron probably in the form of iron oxyhydroxides which preferentially removes ^{6}Li from solution. Saturation state modelling shows that the formation of iron oxides in the glacial rivers is unlikely; there is no free iron in solution. Instead, the formation of Fe-oxyhydroxides must have occurred subglacially, which explains why there is a difference of over 12‰ between the $\delta^{7}Li$ values of the supraglacial and proglacial rivers. The formation of these iron oxyhydroxide minerals occurs in conjunction with the oxidation of sulphides and carbonate hydrolysis (BOTTRELL and TRANTER, 2002; TRANTER, 2003). Most of this Fe-oxyhydroxide will form on the suspended sediment itself, studies of suspended sediment in Arctic, Alpine and

Antarctic locations have all shown the presence of Fe-oxyhydroxide nanoparticles attached to sediment grains (RAISWELL et al., 2006). Because of the low concentration of dissolved lithium and high amount of suspended sediment the formation of these secondary minerals and associated preferential ^{6}Li uptake causes substantial fractionation of the dissolved phase, resulting in a ~21‰ fractionation between dissolved and bedload lithium. As the rivers progress out of the subglacial environment the chemical weathering intensity remains low. Relatively little lithium is released by the weathering of primary minerals and further uptake of lithium onto secondary minerals is limited due to the low amount of clay formation. For this reason the $\delta^{7}Li$ composition of the river water remains high, and does not alter appreciably along the course of the glacial rivers. By this mechanism the composition of lithium in solution can be isotopically heavier than the riverine global average despite these glacial rivers having TDS and dissolved concentrations that are below average.

3.5.5. Global implications

The results from this study show that glacial and non glacial rivers in Greenland have very similar $\delta^{7}Li$ isotope compositions and that these compositions are similar to that of the global riverine mean. In order to assess the impact of glaciation on the behaviour of lithium globally, these results have been compared to results of river analyses worldwide (Fig. 3.21). The comparison shows that the behaviour of Li in glacial rivers from Greenland in this study and from Iceland (POGGE VON STRANDMANN et al., 2006) are similar, having average $\delta^{7}Li$ compositions of 21 and 24 ‰ and Li concentrations of 53 and 40nmol/l. It is also clear that some of the highest $\delta^{7}Li$ values (and relatively low Li concentrations) are recorded in non-glacial rivers in low temperature environments (~30‰). However these high $\delta^{7}Li$ values are not unique to these environments. The

Yangzte and Orinoco rivers also have relatively high δ^7Li because of significant inputs from carbonates that have high δ^7Li (HUH et al., 1998). Generally the glacial and non-glacial rivers carry lithium with an isotopic composition that is either similar to the global mean or within the known range of global rivers. The fact that the isotopic compositions in Greenland are so similar to the lithium compositions in rivers from non-glaciated regions suggests that the onset of glaciation is unlikely to have had a significant impact on the composition of dissolved Li delivered to the oceans.

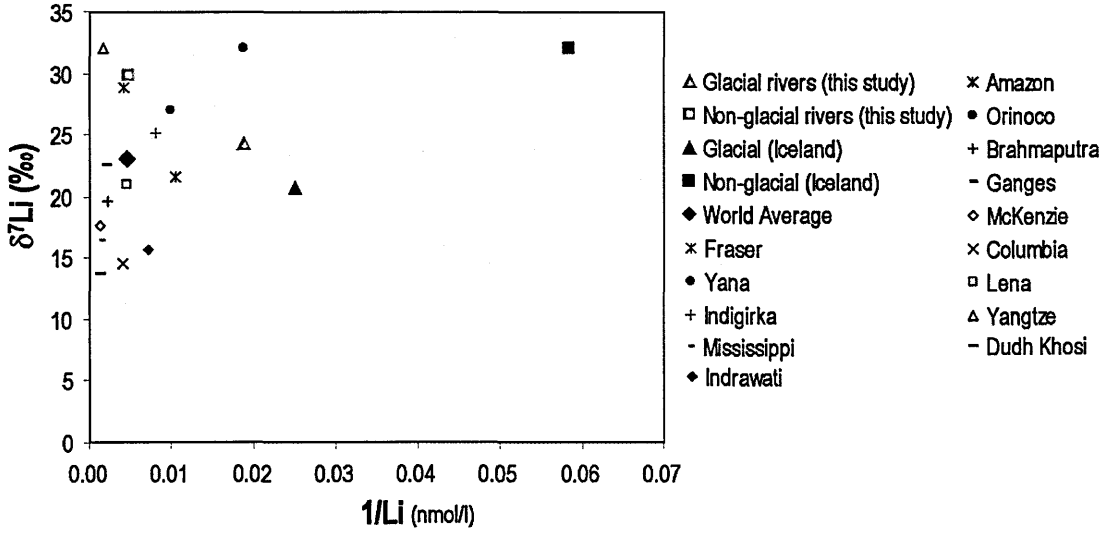

Fig. 3.21 – A compilation of all available Li concentration and Li isotope data for the dissolved load of rivers. Data for Icelandic rivers are from Pogge von Strandmann et al. (2006), the Dudh Khosi and Indrawati are from Kisakurek et al. (2005), and all other river data is from Huh et al. (1998).

While evidence from the dissolved load suggests that glaciation cannot have had an impact on changing oceanic compositions over the last 10Ma, glacial rivers also carry a substantial flux of sediment to the oceans. This sediment has potential to be subsequently reworked and weathered, which would cause further Li uptake and cause further alteration of the δ^7Li composition of seawater. Glacial rivers in this study transport high volumes of suspended sediment (on average 0.5g/l), although if this is compared to rivers globally many carry more sediment such as the Mississippi (0.86g/l), Brahmaputra (1.06g/l) and Ganges (1.1g/l) (GAILLARDET et al., 1999a). Globally rivers

input ~20 billion tonnes of suspended sediment into the oceans per year (MILLIMAN and SYVITSKI, 1992), if the average volume of suspended sediment carried in glacial rivers per litre is taken as 0.5g/l and the annual discharge for all glacial rivers is $\sim 0.5 \times 10^{12} m^3 yr^{-1}$ then the estimated flux of sediment from glacial rivers globally is 250 million tonnes, or 1.25% of the total riverine input. Compositionally this sediment is immature; it has a short rock-water contact time and low weathering intensity. While there are few measurements of the lithium composition in suspended sediments in the literature, data from the Orinoco (HUH et al., 2001), and Himalayan rivers (KISAKUREK et al., 2005) show that suspended sediments in these rivers have higher lithium concentrations (on average 35 and 48ppm respectively) and that the lithium is isotopically lighter (~1.7 and -2.3‰) than in glacial rivers in Greenland (see Fig. 3.22). This could be because the bedrock composition is also isotopically heavy; GR2R and GR6R have δ^7Li values of ~6.5‰. This is higher than the range for continental crust (-5 to +5‰) proposed by Teng et al. (2004). However, other studies have shown that basalts commonly have δ^7Li values up to 6‰ (HUH et al., 2004) and unaltered granites can have a δ^7Li value of ~9‰ (PISTINER and HENDERSON, 2003). If the bedrock does not have an unusually high δ^7Li composition the isotopic composition of the suspended sediment must reflect low secondary mineral formation in the glacial rivers. This supports the idea that glacial sediment is less weathered and less mature. Continued weathering of glacial sediment once it has reached the oceans could cause further preferential uptake of ^{6}Li leaving the dissolved Li isotopically heavy and could contribute to the heavy seawater Li isotope signal. While this mechanism could work in theory global mass balance calculations indicate that the total volume of sediment transported by glacial rivers is relatively small. Moreover, much of this sediment would be trapped in fjords before entering the oceans implying that further weathering of

glacial sediments in seawater is unlikely to have caused a significant alteration in oceanic lithium composition.

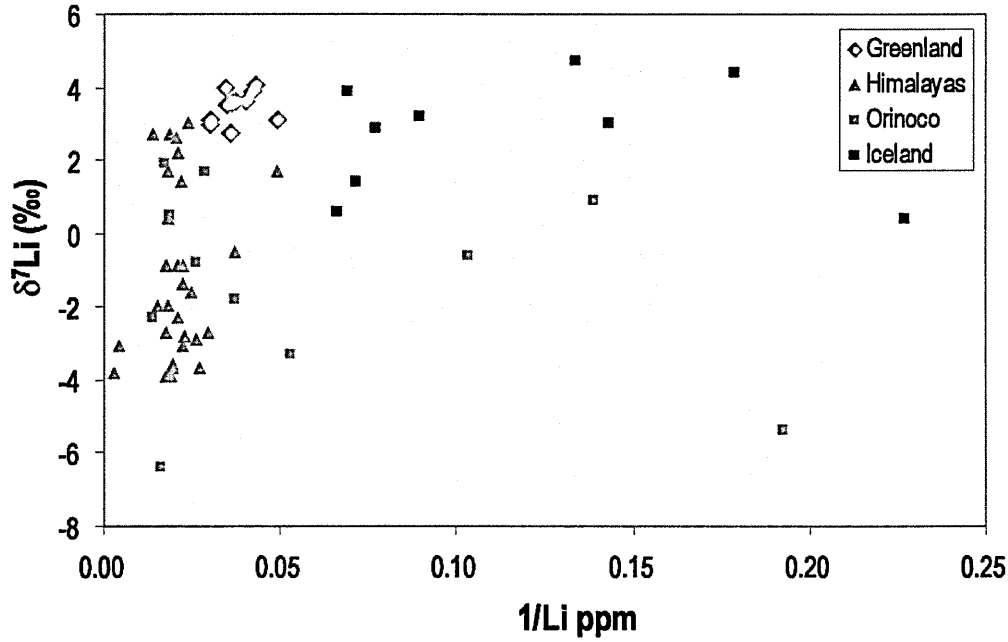

Fig. 3.22 – A comparison of lithium compositions in the suspended sediments of this study, Iceland (Pogge von Strandmann et al. 2006), the Himalayas (Kisakurek et al. 2005) and the Orinoco (Huh et al. 2001).

3.6. Conclusions

The average δ^7Li composition of glacial and non glacial rivers in Greenland are relatively similar to each other (24‰ compared to 29‰) and close to the world average of 23‰ (HUH et al., 1998). Despite the two types of river having similar δ^7Li compositions the controlling processes are different; high δ^7Li in non glacial rivers is caused by high mineral saturation states causing high levels of secondary mineral formation, particularly of iron oxide minerals. Iron is not present in the glacial waters in a truly dissolved form; the iron budget is dominated by colloids. For this reason the formation of iron oxides in the glacial rivers themselves is highly unlikely. XRD

analyses of the suspended sediment carried in glacial rivers also indicates that very little clay formation has occurred. Instead, the high δ^7Li value of these rivers is most likely caused by preferential removal of ^{6}Li from solution in the subglacial environment. High sulphate concentrations in the glacial rivers indicate that sulphide oxidation is an important process; as shown in many other studies of glacial rivers (ANDERSON et al., 2000; TRANTER, 2003). A by product of this process is the formation of Fe-oxyhydoxides, and leaching experiments show that a large quantity of isotopically light lithium is indeed associated with these easily leachable iron phases.

Despite the low chemical weathering intensities and low concentrations of dissolved ions within the glacial rivers the dissolved Li isotope ratios are distinct to that of the bedrock. However, if the δ^7Li values of the glacial rivers (~25‰) are compared to that of the global average (23‰) the values are very similar. From this evidence it seems unlikely that glaciation could influence riverine chemistry enough to cause a significant shift in the oceanic Li isotope composition.

Chapter 4

Magnesium isotope and elemental behaviour in glacial and non-glacial rivers from Greenland

4.1. Introduction

Magnesium is the seventh most abundant element in the Earth's crust by mass and is second only to oxygen in abundance among the rock forming elements (YOUNG and GALY, 2004). It is also the second most abundant cation in seawater; this mostly originates from the weathering of Mg-silicates and Mg-carbonates (MEYBECK, 1987). Once transported to the oceans Mg^{2+} can cause the direct drawdown of CO_2 via combination with HCO_3^- (HOLLAND, 2005), or indirect CO_2 drawdown via exchange for Ca at mid ocean ridges and in detrital sediment (BERNER, 2004; HARDIE, 1996). Magnesium plays a key role in many biological systems; it is at the centre of the chlorophyll pigment which is essential for plants to photosynthesise, and Mg ions are essential for nucleic acids which carry genetic information (SHAUL, 2002). Magnesium has three stable isotopes, ^{24}Mg (78.99%), ^{25}Mg (10.00%), and ^{26}Mg (11.01%) and their relatively large mass differences mean that they are likely to be fractionated by a number of processes in the environment, including weathering, which makes them useful for studies of the Earth system. Magnesium isotope ratios ($\delta^{26}Mg$) are expressed as the ‰ difference between the $^{26}Mg/^{24}Mg$ ratio of a sample and the $^{26}Mg/^{24}Mg$ ratio of a standard (DSM-3), more details are given in Section 1.4.1.2. The $\delta^{26}Mg$ composition of Mg in the oceans of -0.82‰, (CARDER et al., 2004) is controlled by a balance between the input of continentally derived Mg at -1.09‰ (TIPPER et al., 2006b)

and the removal of Mg via hydrothermal exchange at mid ocean ridges, the precipitation of dolomite and exchange reactions with clays (BERNER, 2004; HOLLAND, 2005). Thus, changes in the flux or isotopic composition of Mg that is derived from the continents can have a significant impact on the past composition of Mg in the oceans.

New analytical techniques, in particular the development of MC-ICP-MS technology, means that Mg isotope ratios can now be measured at high precision even in low concentration natural samples. Nevertheless, the number of studies of the behaviour of Mg isotopes during rock-fluid interactions is small. Preliminary data suggest that the Mg composition of the continental weathering flux is controlled by a combination of lithology and weathering processes such as the formation of secondary minerals. Data also suggest that Mg behaves differently in the silicate and carbonate systems; speleothems preferentially incorporate the light isotope relative to drip waters (GALY et al., 2002), while soils are enriched in heavy magnesium relative to silicate rocks (TIPPER et al., 2006a).

The principal control over the Mg isotope composition of large scale rivers appears to be secondary mineral formation, with lithology playing a subsidiary role (TIPPER et al., 2006a; TIPPER et al., 2006b). However, in smaller rivers lithology exerts a greater control (TIPPER et al., 2006b). For example, rivers that drain limestone have a lighter Mg isotope composition (~-2.6‰) than those that exclusively drain silicates (-0.6 to -0.8‰). As well as having chemical controls Mg isotopes are strongly influenced by biological processes. In seawater, organisms such as corals and foraminifera fractionate Mg by preferentially removing the light isotope (CHANG et al., 2004). In plants Mg is the central atom in the chlorophyll molecule and is essential for the function of many enzymes. Plants also have high levels of free Mg^{2+} that is situated in cell vacuoles which regulate its distribution to where it is needed (SHAUL, 2002).

Studies that have extracted chlorophyll-a from cyanobacteria show that the Mg is isotopically light relative to the culture medium, although during the major growth stage of cyanobacteria the δ^{26}Mg composition of the chlorophyll becomes marginally heavier than the initial ratio (BLACK et al., 2006). In contrast, chlorophyll extracted from marine phytoplankton contains Mg that is isotopically heavy relative to the source (seawater). This study also shows that the level of fractionation varies between the different types of chlorophyll (RA and KITAGAWA, 2007). While chlorophyll takes a high proportion of the plants total Mg (~6% in healthy plants) the majority is used elsewhere (SHAUL, 2002). An initial investigation of the Mg composition of higher plants indicates that bulk plant material is isotopically heavy relative to the Mg source; experiments using living roots show the residual solution becomes progressively depleted in heavy Mg with time (BI et al., 2007). The contrasting results of these studies suggest that more research is needed to discern how Mg is taken up into biological systems; however the evidence from higher plants suggests that they preferentially remove heavy Mg from solution.

The importance of both chemical and biological processes in controlling Mg isotope behaviour suggests that interpreting the fractionation in natural samples may be complicated. In this Chapter I extend the work presented in Chapter 3 to an investigation of the controls on the Mg isotope composition of Greenland rivers. The advantage of using glacial rivers for investigations of Mg is that the biological influences such as vegetation are often unimportant (ANDERSON et al., 1997) which means that the isotope data can be interpreted in terms of lithology and weathering processes alone. Moreover, the study area is essentially monolithological (ESCHER and PULVERTAFT, 1995; WELLS, 1979), so any variations due to differences in rock type should be minor. Further details of geological settings and sample locations are given

in Section 3.2 and Figure 3.1. The aim of this work is to compare the behaviour of Mg isotopes in glacial rivers where silicate weathering intensity and secondary mineral formation is low, with non-glacial rivers where these processes are more important. The question is whether a change in the chemical weathering intensity such as that which would accompany glaciation could also cause a change in the composition of Mg that is delivered to the oceans?

While there are as yet very little data concerning the Mg isotope composition of seawater during the Cenozoic studies have shown that the Mg concentration has increased from 35mmol to 52mmol over the last 10Ma (FANTLE and DEPAOLO, 2006). This increase in concentration is thought to have been caused by changes in input from continental weathering possibly driven by mountain building and changes in climate. It seems likely that a change in the flux or composition of continental input would also drive a change in the Mg composition by disturbing the balance between Mg source and sink in a similar way as that observed for Li (HATHORNE and JAMES, 2006) and Sr (PALMER and EDMOND, 1989). The investigation of these glacial rivers and comparison of the behaviour of Mg with that in non glacial rivers may further our understanding of how glaciation could potentially affect the continental Mg signal and thereby alter the oceanic Mg budget.

4.2. Methods for Mg isotope analysis

The sampling procedures and techniques for elemental analysis of major and minor ions in the various river water constituents are described in detail in Chapter 2.

Magnesium is separated from the sample matrix by cation exchange chromatography, similar to the separation of Li described in Chapter 2. The main difference is that all rock samples are additionally processed through an anion column

to minimize any interference from iron (WIECHERT and HALLIDAY, 2007). Details of both column procedures and column calibrations undertaken over the course of this study are given in Section 2.4.3.

Magnesium isotope ratios were measured on a Thermo-Finnegan Neptune MC-ICP-MS. A detailed description of sample analysis is given in Section 2.5.2.3. The internal precision of the Mg isotope measurements was calculated using the technique described in Appendix A10. Typically the internal precision of δ^{26}Mg measurements was better than 0.05‰, and the internal precision of δ^{25}Mg measurements was better than 0.03‰.

In order to monitor the external reproducibility of the Mg isotope measurements the standard CAM-1 was routinely measured at least 2-3 times during a daily analytical session. The average δ^{26}Mg composition of CAM-1 measured over the course of this study (n=24) is -2.62 ±0.13‰ (2σ) while the average δ^{25}Mg composition is -1.35 ±0.06‰ (2σ).

4.3. Results

Magnesium concentrations and Mg isotope ratios for Greenland rivers are presented in Appendix B7.

4.3.1. Magnesium concentrations

The average Mg concentration in the glacial rivers is 0.25ppm compared to 6.1ppm in non glacial rivers; thus, the non glacial rivers have on average over 24 times more Mg. As a proportion of the major cations (Na, Mg, Ca and K) in solution Mg comprises ~12% in the glacial rivers in comparison to ~29% in non glacial rivers (Figure 3.4).

Table 4.1

Magnesium isotope ratios for the dissolved, suspended (SP) and bedload (S) phases in the Greenland rivers.

SAMPLE	[Mg] *ppm*	δ^{26}Mg *(‰)*	Error *(2σ)*	δ^{25}Mg *(‰)*	Error *(2σ)*
GR1	199	-1.04	0.04	-0.52	0.03
GR2	264	-1.07	0.08	-0.54	0.05
GR3	81	-1.31	0.10	-0.67	0.05
GR4	278	-1.12	0.06	-0.56	0.03
GR5	274	-1.17	0.04	-0.58	0.02
GR7	329	-1.19	0.05	-0.64	0.03
GR8	347	-1.18	0.05	-0.59	0.03
GR9	233	-1.06	0.03	-0.54	0.02
GR11	2071	-0.66	0.08	-0.35	0.05
GR12	18622	-0.58	0.07	-0.32	0.04
GR13	2794	-0.65	0.02	-0.34	0.02
GR15	4853	-0.62	0.03	-0.32	0.03
	[Mg] *Wt %*				
GR1-SP	2.07	-0.41	0.03	-0.21	0.02
GR3-SP	1.79	-0.27	0.04	-0.13	0.03
GR5-SP	1.92	-0.44	0.03	-0.23	0.02
GR8-SP	1.97	-0.46	0.03	-0.24	0.03
GR1-S	0.99	-0.53	0.03	-0.25	0.02
GR3-S	1.17	-0.39	0.03	-0.20	0.02
GR5-S	1.20	-0.43	0.03	-0.22	0.02
GR8-S	0.65	-0.44	0.02	-0.22	0.02
GR11-S	1.06	-0.10	0.02	-0.05	0.02
GR12-S	0.94	-0.31	0.02	-0.16	0.02
GR15-S	1.24	-0.34	0.02	-0.18	0.02

Mean Greenland amphibolite (WELLS, 1979) has a Mg concentration of 0.88 Wt%. The Mg concentration of the bedload sampled in this study varies between 0.65 and 1.24 Wt% and there are no clear differences between the glacial and non-glacial rivers. In comparison the suspended sediments (glacial rivers) have a much higher Mg concentration; averaging 1.92 Wt%. Magnesium is present in the colloidal phase of all the rivers, as shown by the higher levels of Mg in the retentate fraction (Appendix B3). However, the total Mg contents in the colloids are likely to be small because the concentrations of dissolved (<0.2μm) and ultrafiltered (>10kD) waters are very similar.

4.3.2. Magnesium isotopes

The $\delta^{26}Mg$ and $\delta^{25}Mg$ values of all samples and standards measured in this study define a line with a gradient of 0.515±0.0032 (R^2 = 0.9994) (Figure 4.1.) similar to the terrestrial equilibrium mass fractionation line defined by Young and Galy (2004) of 0.521. The Mg isotope composition of the dissolved load ranges from $\delta^{26}Mg$ = -1.31‰ in the supraglacial sample (GR3) to $\delta^{26}Mg$ = -0.58‰ in sample GR12. Note that the glacial and non glacial rivers have distinctly different Mg concentrations and Mg isotope compositions (Fig. 4.2) with glacial rivers having both lower Mg and lower $\delta^{26}Mg$ relative to the non-glacial rivers. The average $\delta^{26}Mg$ composition of the dissolved fraction in the glacial rivers is -1.12 ±0.06‰ compared to -0.63 ±0.04‰ in the non glacial rivers. By contrast, the average global riverine $\delta^{26}Mg$ value for rivers has been estimated to be -1.09‰ (TIPPER et al., 2006b) extending from -2.5 to -0.3‰ (TIPPER et al., 2006b).

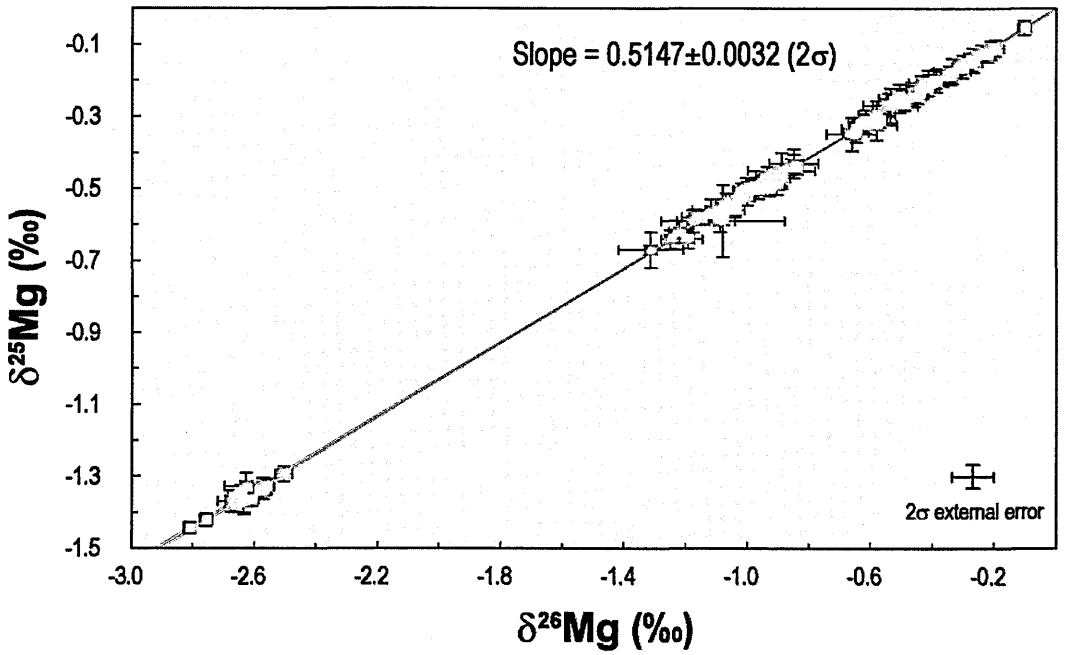

Fig. 4.1 - All Mg isotope ratios lie on a mass fractionation line with a gradient of 0.515

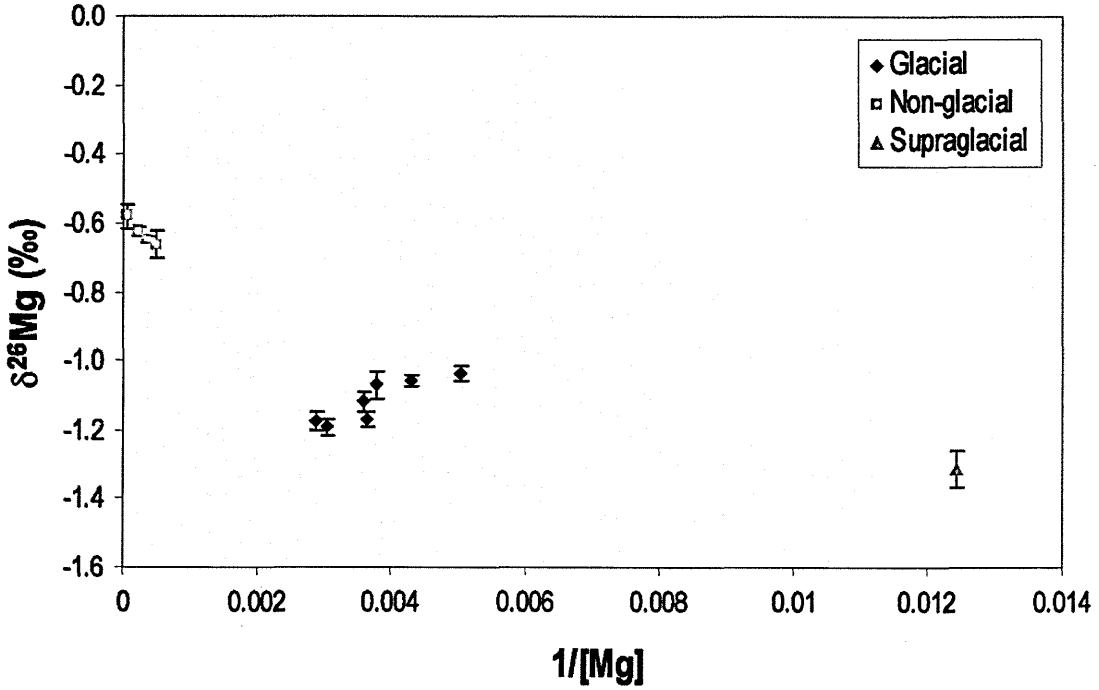

Fig 4.2 - The Mg composition of the dissolved phase plotted versus its Mg concentration. Error bars represent the standard error (2σ) on each isotope measurement.

The suspended sediment in the glacial rivers has an average δ^{26}Mg composition of -0.44‰. This is isotopically heavy relative to the dissolved load carried in these rivers. The suspended sediment in GR3 is slightly heavier than the average (δ^{26}Mg = -0.27‰). The δ^{26}Mg values of the bedload are close to, or very slightly lighter than those of the corresponding suspended sediment; for example in GR1 the bedload has a δ^{26}Mg composition of -0.53‰ compared to -0.41‰ in the suspended load, while at GR3 the bedload is -0.39‰ in comparison to the suspended loads -0.27‰ (Fig. 4.3), but in all cases this difference is little greater than the analytical uncertainty.

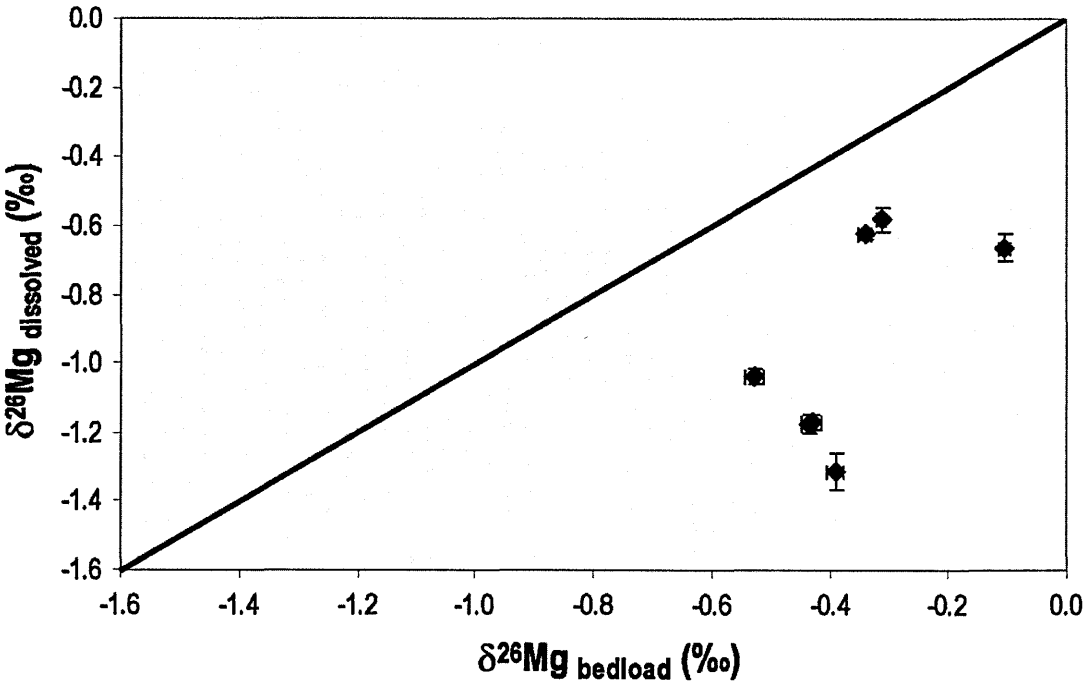

Fig. 4.3 - The Mg isotopic composition of the dissolved phase versus the corresponding composition of the bedload. Error bars represent the standard error (2σ) on each isotope measurement.

4.4. Discussion

4.4.1. Magnesium concentrations

A discussion of the physical and chemical characteristics of the river samples is presented in Chapter 3. In brief, the glacial rivers have low concentrations of dissolved ions, but a high concentration of suspended sediment. The intensity of chemical weathering in the glacial rivers is therefore relatively low, presumably because the water-rock contact time is short. In contrast, the non-glacial rivers have higher concentrations of dissolved ions and lower concentrations of suspended sediments.

With the exception of sample GR10, which contains a seawater component and has a high [Mg^{2+}], Mg concentrations are on average over 24 times greater in the non-glacial rivers than they are in either the supraglacial or glacial rivers. In terms of cation percentage the non-glacial rivers are on average comprised of 29% Mg, compared to 12% in the glacial rivers. To put this in context the average riverine Mg composition is

20% as shown in Figure 3.4 (MEYBECK, 2003). While lithology is often the cause of major cation variation in rivers (MEYBECK, 2003) it seems unlikely to be the cause in this case; there would need to be two separate lithologies, one underlying the glacial rivers and the other underlying the non-glacial rivers. Another possibility proposed from the study of a pingo at Russell's glacier is that deep water from below the permafrost has influenced the surface water composition after travelling along faults (SCHOLZ and BAUMANN, 1997). This hypothesis would need deep water movement along faulting in the vicinity of each non-glacial river while leaving the glacial rivers unaffected, which again seems highly unlikely. Instead, the most reasonable explanation is that the high Mg content of the non-glacial rivers is a result of a higher degree of chemical weathering in these rivers. Glacial rivers preferentially dissolve trace minerals high in Ca and K, hence their compositions are dominated by these ions. Contrastingly, in the non-glacial rivers Mg and Na are more mobile (section 3.5.2.1) because the chemical weathering intensity is much higher and the weathering of silicate minerals is more important.

The Mg concentrations in the solid phases (suspended, bedload and bedrock) range from 0.88 Wt % in amphibolite from the region (WELLS, 1979) to ~1.1 Wt % in the bedload and ~1.9 Wt % in the suspended load. The XRD analyses of the suspended sediment show that the uptake of Mg by clay minerals is likely to be insignificant (because the suspended sediment only contain a small clay mineral component). However, the leaching experiments (section 3.4.4.) show that high levels of Mg^{2+} are released by leaching with 2M HCl. This suggests that a high % of the Mg on the suspended sediment is associated with easily leachable minerals such as iron-oxyhydroxides (CHAN and HEIN, 2007). This is consistent with studies of Mg sorption

onto goethite which show that Mg is mainly adsorbed as a bidentate innersphere complex, with outersphere sorption being less important (RAHNEMAIE et al., 2006).

4.4.2. Magnesium isotopic composition

Glacial, supraglacial and non-glacial rivers have different Mg isotope compositions. The supraglacial river (GR3) has a lighter δ^{26}Mg value (-1.3‰) than the glacial rivers (-1.1‰) and the non-glacial rivers are isotopically the heaviest (-0.6‰). By contrast, excluding sample GR11-S the suspended and bedloads have δ^{26}Mg = -0.40±0.07‰ (Table 4.1). The dissolved load is thus always isotopically lighter than the solid phases, in contrast with Li in which the dissolved phase is always enriched in the heavy isotope in the dissolved phase. In the following sections I explore various ways of explaining these data.

4.4.2.1. Secondary mineral formation

In Chapter 3 it was shown that Li isotopes are fractionated during the formation of secondary minerals, and in particular the formation of iron oxides with preferential uptake of ^{6}Li. By analogy as the δ^{26}Mg value of the river water is always lower than it is in the solid phase it appears that the heavy Mg isotopes are preferentially retained in the solid phase in the Greenland rivers. Other studies have also suggested that Mg isotopes are fractionated during weathering processes: Galy et al. (2002) show that speleothems are isotopically lighter than their dripwaters while Tipper et al. (2006b) show that soils are enriched in ^{26}Mg relative to the source rock, which is in keeping with that data presented here. Nevertheless it is curious that saturation indices (3.5.4.1), leaching experiments and XRD analyses suggest that secondary minerals are far more likely to form in the non-glacial rivers and yet these rivers have δ^{26}Mg values that are

most similar to the source rock. For example, rivers with higher saturation indices for iron oxide minerals such as goethite and haematite have higher δ^{26}Mg values (Fig. 4.4.). Again, this behaviour contrasts with that of the Li isotopes; the non-glacial rivers have δ^{7}Li values (~30‰) that are much higher than that of the source rock (~8‰) whereas the supraglacial sample (GR3) has δ^{7}Li (~13‰) that is closest to the source rock. This suggests that the Mg isotope system is affected by other factors, and these are considered below.

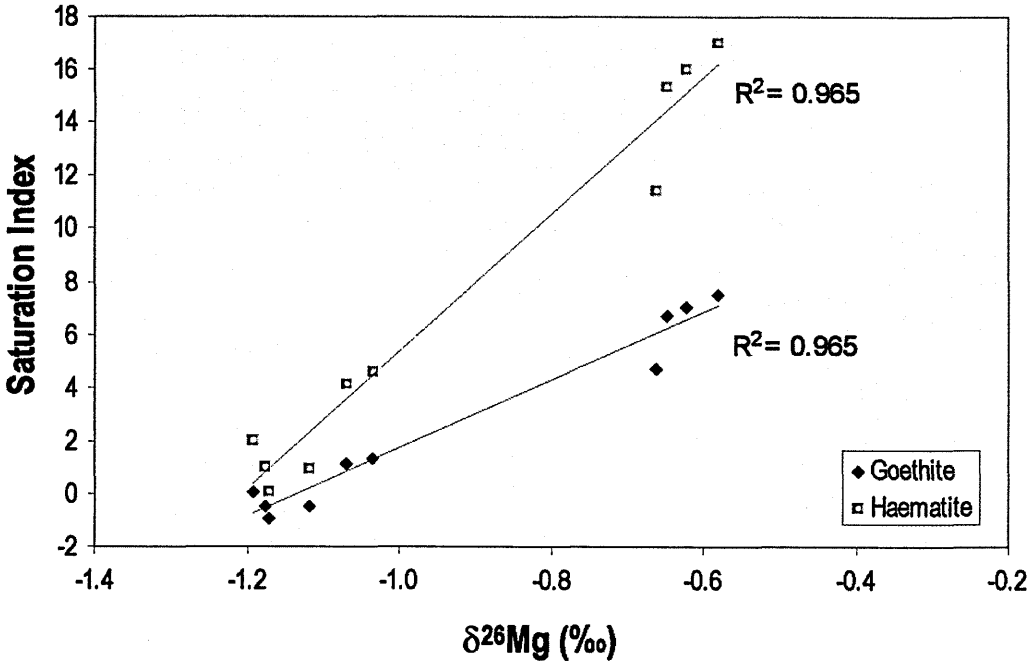

Fig. 4.4 - The magnesium composition of the dissolved phase plotted versus the saturation index with respect to the iron oxide minerals goethite and haematite.

4.4.2.2 Biological controls

Anion analyses of the non-glacial rivers show that they have some organic material present (e.g. the presence of phosphates and nitrates in GR11 and GR12). Biological processes have been shown to utilise magnesium and some of these processes are isotope specific. The water within the non glacial rivers moves at a slow rate, and has a relatively long water-rock contact time in comparison to the glacial rivers

and as a consequence it has a higher TDS. This higher water-rock contact time also means that the water is longer in contact with organic material such as soils and roots. The current understanding of how Mg isotopes behave when taken up into biological systems is described in 4.1. As can be seen the results are mixed; heavy Mg is taken up by chlorophyll in marine phytoplankton while the opposite is the case for chlorophyll in cyanobacteria (BLACK et al., 2006; RA and KITAGAWA, 2007). However, magnesium in chlorophyll is only a fraction of the total Mg in plants (SHAUL, 2002); studies have also shown that the growth of higher plants causes preferential removal of heavy Mg relative to the Mg reservoir (BI et al., 2007). If uptake by plants is the dominant control over Mg in the non glacial rivers then this suggests that the dissolved composition of the water would be isotopically lighter than the glacial rivers where organic influences are negligible. If the behaviour of higher plants is representative of how Mg is taken up by organic material then this suggests that increasing the biological influences should leave the solution isotopically lighter, the opposite of what is observed in the Greenlandic rivers despite the fact that non glacial rivers do have an organic influence.

4.4.2.3 Source controls

It is important to consider whether other sources of Mg (i.e. in addition to rock weathering) could influence the $\delta^{26}Mg$ value of the dissolved load. Seawater has a high $[Mg^{2+}]$ (52mmol/l), and $\delta^{26}Mg$ = -0.82‰ (CARDER et al., 2004; TIPPER et al., 2006b; YOUNG and GALY, 2004). The sample that is most likely to be affected by seawater input is GR3 because it is supraglacial and so has had no contact with bedrock and no biological influence. The Mg isotope composition of this sample (-1.3‰) is lighter than that of seawater and cannot be explained by mixing between seawater and rock (-0.4‰). In addition, the proportion of Mg that could be derived from seawater (estimated using

dissolved Cl^- concentrations) is only ~3%, this is too low to have significantly altered the Mg isotope ratio. The $\delta^{26}Mg$ value of the glacial rivers is also too low to be explained by mixing between Mg derived from rock and Mg derived from seawater. Conversely the composition of the Mg in the non-glacial rivers (-0.6‰) could in theory be produced by a mixing between seawater and rock weathering. However, like the glacial rivers the proportion of Mg that could be derived from seawater is low (~8%); straightforward mixing of Mg derived from seawater (~8%, $\delta^{26}Mg$ -0.82‰) and from rock weathering (~92%, $\delta^{26}Mg$ -0.4‰) would only give a Mg composition of around -0.44‰. This suggests that the impact of Mg derived from seawater is unimportant.

While the Kangerlussuaq region of Greenland is essentially monolithological (ESCHER and PULVERTAFT, 1995; WELLS, 1979) the potential effect of glacial weathering processes on $\delta^{26}Mg$ must be considered. As discussed above, glacial rivers preferentially weather trace phases like carbonates, and leach K from interlayer sites in biotite (ANDERSON et al., 1997; TRANTER, 2003). The Mg isotope composition of carbonate rock is isotopically lighter than silicate. For example carbonate rocks range in composition from -1.1 to -4.8‰ while silicate rocks range from 0.02 to -1.1‰ (YOUNG and GALY, 2004) and the composition of small rivers that drain these two lithologies supports this. For example, in a study by Tipper et al. (2006) the Jura which drains limestone has a $\delta^{26}Mg$ composition of -2.52‰; in comparison, rivers draining basaltic rock have an average composition of -0.6‰ and those draining acidic crystalline rock have an average $\delta^{26}Mg$ value of -0.8‰. This evidence suggests that the preferential dissolution of carbonate material should input Mg which is relatively isotopically light in relation to Mg derived from silicates. This theory can explain why the glacial and supraglacial rivers have higher $\delta^{26}Mg$ compositions (-1.1 and -1.3‰ respectively) than the non-glacial rivers (-0.6‰). As the seawater input is relatively

minor the Mg composition can be modelled simply by two component mixing between carbonate (~-4‰, (YOUNG and GALY, 2004)) and the bedrock (-0.4‰). To achieve Mg compositions of between -1.1 and -1.3‰ then clearly silicate weathering must be dominant source of Mg, the difference in Mg composition must reflect changes in weathering intensity and changes in the ratio between carbonate and silicate derived Mg. The higher chemical weathering intensity in non-glacial rivers means that these rivers will be dissolving more silicate rock than the glacial rivers. This means non-glacial rivers provide more Mg from the dissolution of silicates and so obscure the Mg isotope signal derived from preferential dissolution of trace carbonates and hence have higher δ^{26}Mg ratios.

4.5. Conclusions

The results of this study show that in the Greenland rivers there are two controls on the composition of Mg. These are the formation of secondary minerals, and overprinting this is the preferential dissolution of trace carbonate phases which is a common process in glacial rivers (ANDERSON et al., 1997; ANDERSON et al., 2003; TRANTER, 2003). Carbonate rocks have been shown to be isotopically lighter than silicates with respect to Mg isotopes (TIPPER et al., 2006b; YOUNG and GALY, 2004). Correspondingly the rivers that drain exclusively limestones have isotopically lighter Mg isotope ratios than those that drain exclusively silicate rocks (TIPPER et al., 2006b). The major cation analyses show that the glacial and supraglacial rivers are dominated by Ca (~43% in glacial rivers, 54% in GR3) derived from trace carbonates which dissolve more readily than silicate minerals. Because the water-rock contact time is so low the proportion of silicate rock that can dissolve is very small, so the dissolved load is dominated by those easily dissolvable minerals such as $CaCO_3$. In contrast the non-glacial rivers have a

longer water-rock contact time and silicate mineral dissolution is far more important. This means that the dissolution of easily weathered trace phases will be obscured by the dissolution of silicates; as shown by the lower proportion of Ca that constitute the major cations (~34%) and the higher proportion of Mg (~29%). As a consequence the Mg isotope composition is more reflective of the silicate rock. Thus despite the area being monolithological it is a difference in the dissolving minerals that causes the change in Mg isotope ratio between the glacial and non-glacial rivers. This difference has been caused by variations in the chemical weathering intensity.

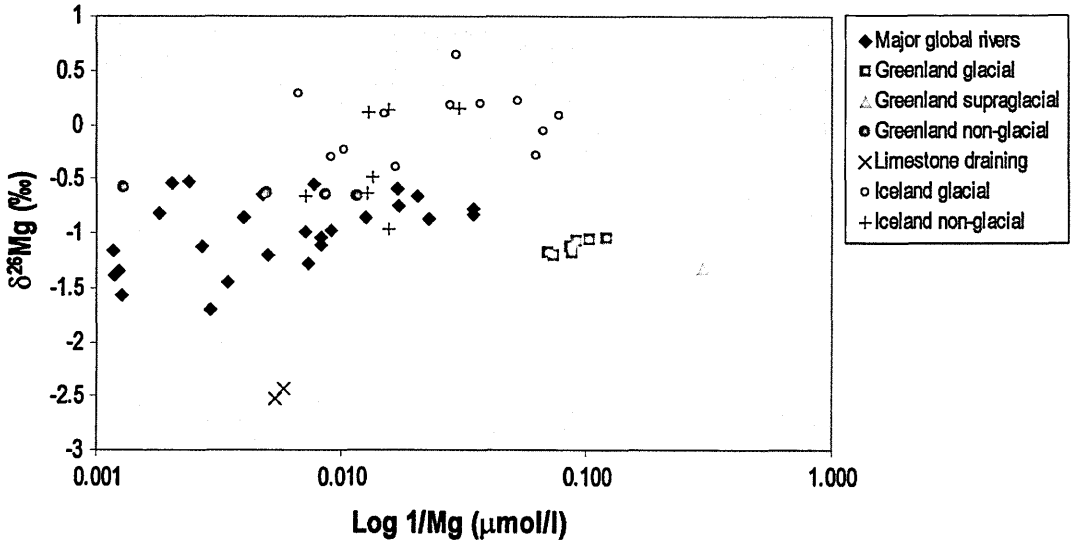

Fig. 4.5 - A comparison of the Mg isotope data from the Greenland rivers with data for global rivers. All global river data and data for limestone draining rivers is from Tipper et al. (2006b), data from Iceland is from Pogge Von Strandmann et al. (2008), data from Greenland rivers is from this study.

The average riverine Mg composition is estimated to be -1.09‰ (TIPPER et al., 2006b). The range of riverine Mg compositions are plotted in Figure 4.5 with most rivers having a Mg isotope composition (δ^{26}Mg) between -0.5 and -1.5‰. The only rivers to significantly deviate from this range are those that drain limestone with much lighter Mg compositions of around -2.5‰ (TIPPER et al., 2006b), and a recent study of

rivers from Iceland with δ^{26}Mg values as high as 0.6‰ (POGGE VON STRANDMANN et al.). These Icelandic rivers are also from glacial regions, but here it is inferred that secondary mineral formation is removing isotopically light Mg, possibly due to the formation of carbonate. The Icelandic rivers are also affected by the input of hydrothermal fluids which have heavy Mg isotope ratios (0.85‰). The Mg isotope compositions of the Greenland rivers fall well within the global riverine range, with the glacial rivers having a Mg isotope ratio that is within error of the estimated global mean (average glacial river composition -1.12‰ ±0.06 (1sd)). This is similar to the findings for Li isotopes, i.e. that the composition of glacial river water is not significantly different to that of rivers with no glacial influence. While it is unknown whether the behaviour of Mg in these rivers is representative of glacially sourced rivers worldwide the difference between Mg composition in glacial and non-glacial rivers in Greenland suggests that glacial processes do have an impact on Mg isotope ratios. However, the similarity between Mg isotope ratios from glacial rivers in Greenland and global rivers suggests that glaciation is likely to have had little measurable affect on the composition of dissolved Mg that has been delivered to the oceans by rivers.

Chapter 5

Isotopic changes accompanying the experimental dissolution of basalt glass and forsterite

5.1. Introduction

The weathering of Ca- and Mg-silicates causes a net drawdown of atmospheric CO_2 which may potentially regulate Earth's climate over geological timescales (BERNER et al., 1983; WALKER et al., 1981). Therefore, quantifying weathering rates of silicate rocks and understanding the processes that control such weathering is fundamentally important because it may improve our understanding of the controls on climate over time. In order to constrain the factors that control weathering rate (such as mineralogy, pH, temperature, CO_2 concentration and organic acid composition) as well as to gain a more complete understanding of water-rock interactions, a number of studies have used experimental techniques to quantify the rates and mechanisms of dissolution of silicate minerals (BRANTLEY and STILLINGS, 1996; CHEN and BRANTLEY, 2000; GISLASON and OELKERS, 2003; OELKERS, 2001a; POKROVSKY and SCHOTT, 2000; STILLINGS and BRANTLEY, 1995). Over the course of these studies a wide range of experimental conditions have been used in order to simulate the wide variety of conditions seen in nature, and so to obtain comprehensive dissolution rate and solubility data for silicate minerals. Particular focus has been on either common rock-forming minerals such as feldspar and quartz (ANBEEK et al., 1994; BLAKE and WALTER, 1999; BRANTLEY and STILLINGS, 1996; CHARDON et al., 2006; PETROVIC, 1976; POULSON et al., 1997; STILLINGS and BRANTLEY, 1995), or on minerals and glasses that have high dissolution rates (BERGER et al., 1994; CROVISIER et al., 1987; DAUX et al., 1997; GISLASON and

OELKERS, 2003; OELKERS and GISLASON, 2001). The latter because if a mineral dissolves rapidly then it can have a disproportionate effect on the weathering signal. In this regard many studies have considered olivine, and in particular the Mg rich end member forsterite due to its abundance in basalts and basic igneous rocks and its relatively high dissolution rate (AWAD et al., 2000; BERGER et al., 1988; BLUM and LASAGA, 1988; CHEN and BRANTLEY, 2000; GIAMMAR et al., 2005; GISLASON and ARNORSSON, 1993; GRANDSTAFF, 1978; HANCHEN et al., 2006; KOBAYASHI et al., 2001; LIU et al., 2006; MURPHY and HELGESON, 1989; OELKERS, 2001a; POKROVSKY and SCHOTT, 2000; ROSSO and RIMSTIDT, 2000; VANHERK et al., 1989; WOGELIUS and WALTHER, 1991; WOGELIUS and WALTHER, 1992).

Another material that has been widely characterised is amorphous silicate glass and in particular basalt glass due to its widespread occurrence at mid ocean ridges and on the ocean floor, together with its relatively rapid dissolution rate when compared to that of crystalline basalt (BERGER et al., 1994; BERGER et al., 1988; CROVISIER et al., 1987; CROVISIER et al., 1983; DAUX et al., 1997; GISLASON and EUGSTER, 1987; GISLASON and OELKERS, 2003; GISLASON et al., 1993; GUY and SCHOTT, 1989; OELKERS and GISLASON, 2001; TECHER et al., 2001; WOLFF-BOENISCH et al., 2006; WOLFF-BOENISCH et al., 2004). The study of amorphous glasses of varying compositions has shown that their dissolution rates are greater relative to a crystalline rock of the same composition (GISLASON and ARNORSSON, 1993; GISLASON et al., 1996; GISLASON and EUGSTER, 1987; WOLFF-BOENISCH et al., 2006). For example basaltic glass dissolves at a rate that is 10 times faster than a crystalline basalt of similar composition (GISLASON and EUGSTER, 1987).

Much of the experimental work has centred on obtaining information on the mechanisms and rates of silicate mineral dissolution. However, more recently there has

been an increasing interest in the behaviour of isotope systems during silicate dissolution and the growth of secondary minerals during weathering. Through the study of certain isotope systems a wide range of information can be gained such as, changes in past weathering processes, weathering rates, variations in redox conditions and changes in the Earths climate. Two isotope systems that have been increasingly used in studies of silicate weathering are those of Li and Mg (CHAN et al., 1992; HUH et al., 2004; HUH et al., 2001; PISTINER and HENDERSON, 2003; POGGE VON STRANDMANN et al., 2008; RUDNICK et al., 2004; TENG et al., 2004; TIPPER et al., 2006b). These are both stable isotope systems, the isotopes of which are readily fractionated during weathering processes due to the large relative mass differences between isotopes (HUH et al., 1998; JAMES and PALMER, 2000; YOUNG and GALY, 2004). In the case of Li this is thought to involve the preferential uptake of the light isotope (^{6}Li) into the solid phase leaving the dissolved phase isotopically heavy (HUH et al., 1998). Contrasting behaviour has been proposed for Mg isotopes where the solution becomes enriched in ^{24}Mg when secondary silicate phases preferentially take up ^{26}Mg (TIPPER et al., 2006a). The particular utility of these isotope systems is that the isotope signal transferred to rivers from the weathering of bedrock is highly dependent on the weathering processes rather than variations in bedrock composition. Thus, an understanding of the behaviour of Li and Mg isotopes during weathering and erosional transport to the oceans may provide key information to aid the interpretation of marine sedimentary records of continental weathering and their relationship to changes in past climate.

The difficulty with interpreting natural systems, such as rivers or soils, is that they are subject to changes in temperature, pH, runoff rate, biological activity and changes in the physical conditions of weathering, for example mechanical grinding by glaciers. All of these variables may cause changes in weathering rate and intensity and

thus can all potentially perturb the isotope signal of systems such as Mg and Li. This makes interpretation of isotope data from natural systems more challenging and quantifying that behaviour very difficult. The benefit of experimental work is that most of these parameters can be controlled and the effect of changing specific parameters on the behaviour of isotopes can be more easily assessed. The aim of this study is to investigate the behaviour of Li and Mg isotopes at far from and near to equilibrium conditions during the dissolution of basalt glass and forsterite. As such this involves the investigation of these systems during primary mineral dissolution and secondary mineral precipitation. These are amongst the most important controls on the chemistry of natural waters so the quantification of their effects on isotope systems is imperative.

Previous experimental investigation of the behaviour of isotope systems during mineral dissolution and precipitation is limited. The incongruent weathering of bulk rocks such as granite causes the Li isotope ratio of the solution to be isotopically distinct, interpreted to be due to the effects of preferential weathering (PISTINER and HENDERSON, 2003). When the same experiment was applied to basalt no fractionation of Li was observed, demonstrating an isotopic homogeneity in Li between the different basaltic minerals and suggesting that the dissolution process does not cause incongruent loss of Li from a single mineral phase. Pistiner & Henderson (2003) also studied the behaviour of lithium isotopes during sorption onto clay minerals and found that the preferential sorption of lithium isotopes was mineral dependent. Adsorption onto minerals with negative surface charge such as smectite caused no fractionation of Li, while adsorption onto minerals with positive surface charge such as gibbsite caused significant fractionation, the sorbed Li being isotopically light relative to the source. This difference is thought to be caused by two different adsorption mechanisms; the former being sorption by weak electrostatic attractions (or physisorption) and the latter

being sorption by chemical bonding (or chemisorption). Only chemisorption is isotope specific. A more recent study has investigated the behaviour of Li during smectite formation (VIGIER et al., 2008), the freely exchangeable Li was removed and the Li incorporated in the octahedral sites was analysed. Results show that octahedrally bonded (or chemisorbed) Li is enriched in ^{6}Li during smectite formation resulting in a 10‰ difference between mineral and solution. Similar results were obtained from experiments investigating sorption of Li onto iron-manganese crusts (CHAN and HEIN, 2007); these are discussed further in Section 3.5.4.3. Many of the other isotope studies investigating isotopic change in laboratory dissolution experiments involve Fe isotopes and their behaviour with precipitating or dissolving secondary minerals. Skulan et al. (2002) found that there is no fractionation of Fe isotopes when haematite precipitates from solution. Similar studies involving the dissolution of goethite showed that Fe will fractionate from its dissolution in certain circumstances including in the presence of bacteria (BRANTLEY et al., 2004). But this occurs only when a specific dissolution mechanism operates; proton donating dissolution will not cause Fe fractionation (WIEDERHOLD et al., 2006).

In summary previous studies of the behaviour of isotope systems in experimental systems suggest that isotopic fractionation can occur, but is more likely when new secondary minerals form. Li analyses suggest that dissolution of single mineral phases will not cause Li fractionation. However, this has not been tested thoroughly for Li and it has never been tested for Mg isotopes, thus assessing the behaviour of these systems at far from equilibrium was the first aim of this study.

The second part of this work involves investigating the process of secondary mineral formation. Dissolution in natural systems may cause a build up of elements in solution. These precipitate as secondary minerals when the solution becomes

oversaturated (saturation also depends on a number of factors such as water temperature and pH). When minerals form they partition certain amounts of an element and certain isotopic compositions that may not necessarily reflect the composition of the solution from which they have formed. Thus, while lithology is important, the Li and Mg isotope signal carried in a river does not simply reflect the composition of the bulk or partially dissolved bedrock, but will also be controlled by the processes of primary mineral dissolution and secondary mineral precipitation. The aim of the precipitation experiments was to quantify the isotope variations associated with secondary mineral formation accompanying the dissolution of forsterite. Forsterite has been chosen for the precipitation experiments because the Mg silicate system is relatively simple; there should be only trace amounts of aluminium present so the range of clay minerals and aluminium silicates that can form is limited. In addition CO_2 input will be limited so no Mg-carbonates can form. The Mg silicate system is shown in Fig. 5.1, and comprises forsterite, talc, chrysotile, brucite and quartz. Consequently, any potential secondary phases are limited and more easily identified. This will be important when interpreting the effect of mineral precipitation, that is, the fractionation can be attributed to the formation of a specific mineral.

Overall, the aim of this investigation is to quantify the effect of dissolution of primary minerals and precipitation of secondary phases in natural waters. This will enable more accurate modelling of water rock interactions. Ultimately such information may better constrain the link between the oceanic isotope record and continental weathering, which, in turn, has consequences for CO_2 drawdown and regulation of Earth's past climate.

Experimental Background

Previous work on olivine and basalt glass dissolution has provided a wide range of data that shows a dependency on factors such as pH, temperature, and solution composition.

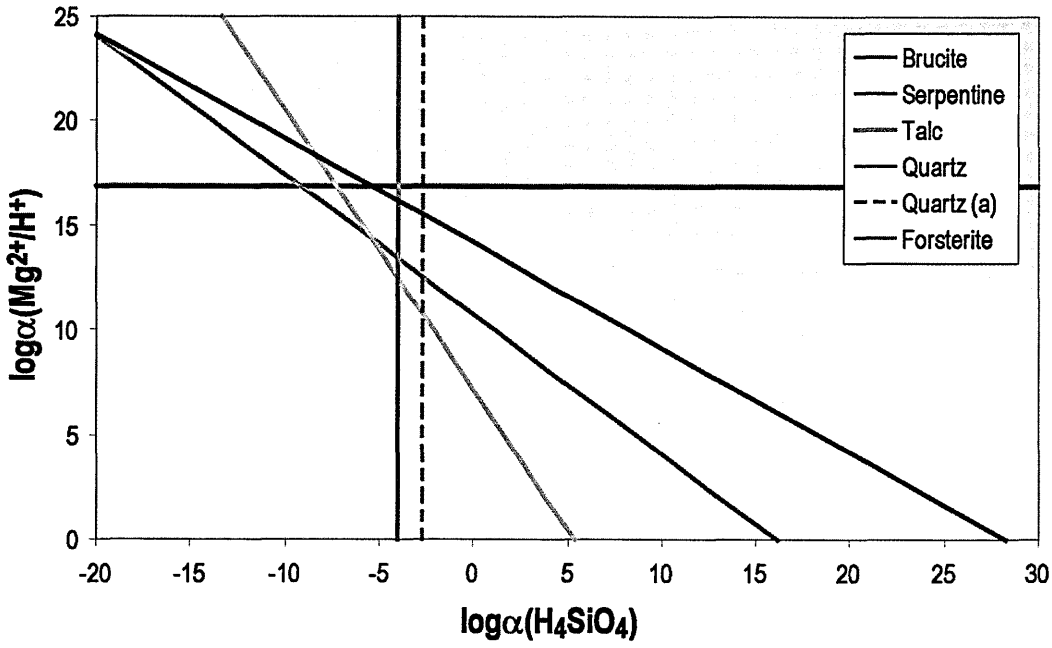

Fig. 5.1 - Magnesium silicate stability diagram, constructed using data from the geochemical modelling program PHREEQC (Parkhurst & Appelo 1997)

Many studies have shown that the dissolution of forsterite is pH dependent (BLUM and LASAGA, 1988; CHEN and BRANTLEY, 2000; GISLASON and ARNORSSON, 1993; MURPHY and HELGESON, 1987; WOGELIUS and WALTHER, 1991; WOGELIUS and WALTHER, 1992) with studies reporting that the dissolution rate increases with decreasing pH in acidic conditions. The dissolution rate of forsterite in high pH solutions is more controversial. Some studies have shown that the dissolution rate increases with increasing pH in basic solutions (BLUM and LASAGA, 1988; WOGELIUS and WALTHER, 1991) but a more recent study by Pokrovsky & Schott (2000) shows that the dissolution rate does not increase with increasing pH, instead it remains relatively constant. The authors explain this discrepancy with the suggestion that the experiments of Blum & Lasaga (1988) and Wogelius & Walther (1991) had not yet reached steady

state, thus dissolution rates are not accurate. High dissolution rates at low pH means that the dissolution of forsterite becomes rapidly stoichiometric (i.e. the system reaches a steady state quickly), lower dissolution rates at high pH means it takes much longer for solution compositions to become stoichiometric. The mechanism of dissolution is also dependent on pH; prior to the solution composition becoming stoichiometric at low pH conditions the dissolution of forsterite involves the preferential loss of Mg, and in high pH solutions involves the preferential loss of Si (POKROVSKY and SCHOTT, 2000). This has been interpreted to indicate that different precursor layers form during dissolution depending on the pH. Further work (OELKERS, 2001a) has investigated the effect of both silica and Mg in solution on forsterite dissolution. The dissolution rate was found to be independent of the concentration of Mg and Si at low pH conditions, suggesting that forsterite dissolution proceeds via two steps; firstly, via protonation forming the rate controlling precursor complex, secondly, by breaking of the octahedral chain that links the Mg-O causing the release of Mg and Si from the forsterite structure.

The dissolution of basalt glass has also been shown to be both pH and temperature dependent (GISLASON and OELKERS, 2003; GUY and SCHOTT, 1989). At low pH the dissolution is controlled by adsorption of H^+ ions onto Al and Fe surface sites while at high pH dissolution is controlled by the adsorption of OH^- ions onto Si surface sites (GISLASON and OELKERS, 2003). The dissolution rate increases rapidly in low pH conditions with decreasing pH, is independent of pH at neutral conditions, and increases slowly at high pH conditions. Studies of the effect of dissolved silica and aluminium concentration and speciation on basaltic glass dissolution rate have enabled an understanding of the mechanism of dissolution (BERGER et al., 1994; DAUX et al., 1997; GISLASON and OELKERS, 2003; OELKERS and GISLASON, 2001; WOLFF-BOENISCH et al., 2004). The proposed mechanism involves: 1) the removal of cations by metal-

proton exchange that leads to the formation of a leached zone, 2) then the substitution of Al^{3+} by substituting three H^+ ions and 3) the liberation of partially detached Si tetrahedra. The concentration of these partially liberated Si-tetrahedra near the glass surface controls the dissolution rate of the glass. In turn the concentration of Si-tetrahedra is controlled by the rate of Al-proton exchange reactions that create the partially liberated Si tetrahedra. Thus the rate of dissolution is dependent on the activity of aqueous Al^{3+} and H^+:

$$r = k\left(\frac{a_{H^+}^3}{a_{Al^{3+}}}\right)^{0.35} \qquad \textit{Equation 5.1}$$

Where r = surface area normalised basaltic glass steady state dissolution rate
k = rate constant equal to $10^{-11.65}$ (mol of Si)/cm^2/s

5.2. Methods

Details of all experimental parameters are given below in Table 5.1.

5.2.1 Experimental minerals and glass

The basaltic glass used in these experiments is from the Stapafell Mountain in south west Iceland, and is the same glass used in similar dissolution experiments involving basalt glass (GISLASON and OELKERS, 2003; OELKERS and GISLASON, 2001).

Forsterite was obtained from Wards Natural Science and has an approximate composition of $Mg_{1.82}Fe_{0.18}SiO_4$ (Fo91). It is similar to forsterite used in dissolution experiments by Pokrovsky & Schott (2000) and Oelkers (2001). More details concerning the compositions of the basalt glass and forsterite and their preparation are given in Section 2.6.1.

Table 5.1 - General parameters for dissolution and precipitation experiments

Experiment	Reactant	Temp *(°C)*	pH	Flow rate *(g/min)*
BG1	Basalt Glass	25	2	1
BG2	Basalt Glass	25	3 & 4	1 - 8.3
BG3	Basalt Glass	25	4	1
BG4	Basalt Glass	35 - 55	4	1
BG5	Basalt Glass	25 - 55	3	5
FO1	Forsterite	25	2,3,4	1 & 3
FO2	Forsterite	25	3 & 2	2 & 3
FO3	Forsterite	25	10	0.15 - 4
FO4	Forsterite	25 - 55	3	1
FO5	Forsterite	25	11	0.2 - 3
FO6	Forsterite	75	10	1 & 2
FO7	Forsterite	75	11	1 & 2

5.2.2 Experimental setup

All dissolution experiments were carried out in titanium mixed flow reactors as illustrated in Fig. 2.5. This reactor enabled control of temperature, pressure, inlet solution flow rate and internal stirring speed. Precipitation experiments were also performed in flow through reactors (Fig. 2.6) though these are constructed from polypropylene. The main difference between experimental setups was that the temperature was controlled during the precipitation experiments by submersing the reactors in a water bath.

More details concerning operation of the dissolution and precipitation experiments are given in Section 2.6.2.

Experimental parameters such as flow rate, stirring rate and solution composition could be changed during the experiment without disruption to the reactors. However in order to assume a steady state had been reached four reactor residence times were allowed to pass before commencement of sampling and whenever these experimental parameters were changed. The reactor residence time being the reactor volume divided by inlet flow rate, high flow rates giving shorter reactor residence times.

At the end of each experiment deionised water was flushed through the system and the rock powder was collected and dried down ready for future analysis. In the event of secondary mineral precipitation reagent grade HCl (1 mol/kg) was pumped through the reactor for 24 hours before cleaning with suprapure HCl (1 mol/kg) for a further 24 hours and a final clean with deionised water.

5.2.3 Major and trace element analyses

Major and trace element concentrations for mineral and glass samples were determined by ICP-MS (Agilent 7500a). Solid material was dissolved following the standard ICP-MS dissolution protocol in Section 2.2.2.

Samples were analysed and calibrated as described in Section 2.5.1.1. The external reproducibility over the course of the investigation are presented for major and minor elements in Appendix A3 and A4. The concentrations of measured standards are mostly close to certified concentrations. The external error for both major and minor elements is better than 6% (2σ).

Aqueous samples were analysed for major cation concentrations by ICP-AES in Iceland and analysed for both major and trace elements by ICP-MS at the Open University. Details of both techniques are presented in 2.5.1.2. Duplicate measurements of the experimental solutions by ICP-AES yielded relative errors of less than 5%. External reproducibility for measurements by ICP-MS are better than 8% (2σ); a comparison of measured SLRS-4 standards with certified values are presented in Appendix A6.

5.2.4. Lithium analysis

The separation of Li for isotope analysis was carried out by ion chromatography following the protocol of James & Palmer (2000) described in Section 2.4.2. Lithium isotope ratios were determined using a combination of a Thermo-Finnegan Neptune and Nu Instruments MC-ICP-MS. The methods of analysis together with the associated internal and external errors are given in 2.5.2.2. The internal error (2σ) of sample measurements was typically better than 0.2‰ with the Nu-Plasma, and better than 0.1‰ on the Neptune. The external reproducibility of the lithium isotope ratios was monitored by routine measurement of IAPSO seawater during sample measurement (see Appendix A8). Over a total of 40 seawater standards that were measured the average δ^7Li value was 31.08 ±0.82‰ (2sd)

5.2.5. Magnesium analysis

The separation of Mg uses cation exchange chromatography similar to that used for the separation of Li; the main difference that an anion column is also used for all rock samples to remove any potential interference from iron (WIECHERT and HALLIDAY, 2007). The full procedure for separation of Mg, including cation and anion column calibrations, is given in Section 2.4.3.

Magnesium isotopes were measured on a Thermo-Finnegan Neptune MC-ICP-MS. The methods of analysis together with the associated internal and external errors are given in 2.5.2.3. The internal precision of the Mg isotope measurements was calculated using the technique in Appendix A10. Typically the internal precision of δ^{26}Mg measurements was better than 0.05‰, and the internal precision of δ^{25}Mg measurements was better than 0.03‰. External reproducibility was monitored by routinely measuring the Mg standard CAM-1 at least 2-3 times for each day of analyses. The average δ^{26}Mg composition of CAM-1 from 20 measurements was -2.62‰ with a

2σ error of 0.13‰ while the average δ^{25}Mg composition was -1.35‰ with a 2σ error of 0.06‰.

5.3. Results

The results of the dissolution experiments involving basalt glass and forsterite are given in Appendices C1 and C2. The results of the precipitation experiments are presented in Appendix C3. All dissolution rates have been calculated using the following equation:

$$r = \frac{Si_{OUT} \times F}{S_{BET}} \qquad \textit{Equation 5.2}$$

Where r = dissolution rate (mol/cm^2/s)
$Si_{(out)}$ = outlet Si concentration (mol/kg)
F = fluid flow rate (g/s)
$S_{(BET)}$ = surface area of sample powder determined by BET method

5.3.1. Mineral phases

Results of the ICP-MS analyses of unreacted and reacted mineral phases are presented in Appendix C4. The dissolution procedure involved the use of HF so silicon concentrations could not be measured. By comparing the concentration of elements in the reacted phase with the concentrations in the unreacted mineral the % loss during dissolution can be calculated. The experiment involving the dissolution of basalt glass at pH2 (experiment BG1) shows the highest % loss of each element; the elements with the greatest % loss were Ba, Li, Al, Sr and Mg with loss of 23, 12, 11.5, 11 and 10.5%, respectively. In general these elements were the most readily lost in all of the basalt glass experiments while Ti and Th concentrations remained similar. Unreacted basalt glass has a Li concentration of 4.7ppm and a Mg concentration of 6 Wt%. In the

forsterite experiments most elements were below detection limits with aluminium, potassium and sodium among the elements unable to be measured. The element with the greatest loss during the experiments was Li with a loss of ~ 17% relative to the levels in the unreacted forsterite. The forsterite Li concentration is lower than that of basalt glass with a concentration of 2ppm.

5.3.2. Dissolution Experiments

The results of the dissolution experiments show that at low pH (2-4) the amount of silica released into solution during the dissolution of both basalt glass and forsterite increases with decreasing pH. For example the concentration of silicon in solution increases from ~1.8ppm in pH 3 solution to 13ppm in pH 2 at the same flow rate and total surface area. As silica concentration is used in the dissolution rate equation this means that the dissolution rate of both minerals also increases with decreasing pH (Figure 5.2). This is consistent with previous experimental work on basalt glass (GISLASON and OELKERS, 2003; OELKERS and GISLASON, 2001; WOLFF-BOENISCH et al., 2004) and forsterite dissolution (CHEN and BRANTLEY, 2000; OELKERS, 2001a; POKROVSKY and SCHOTT, 2000; WOGELIUS and WALTHER, 1992).

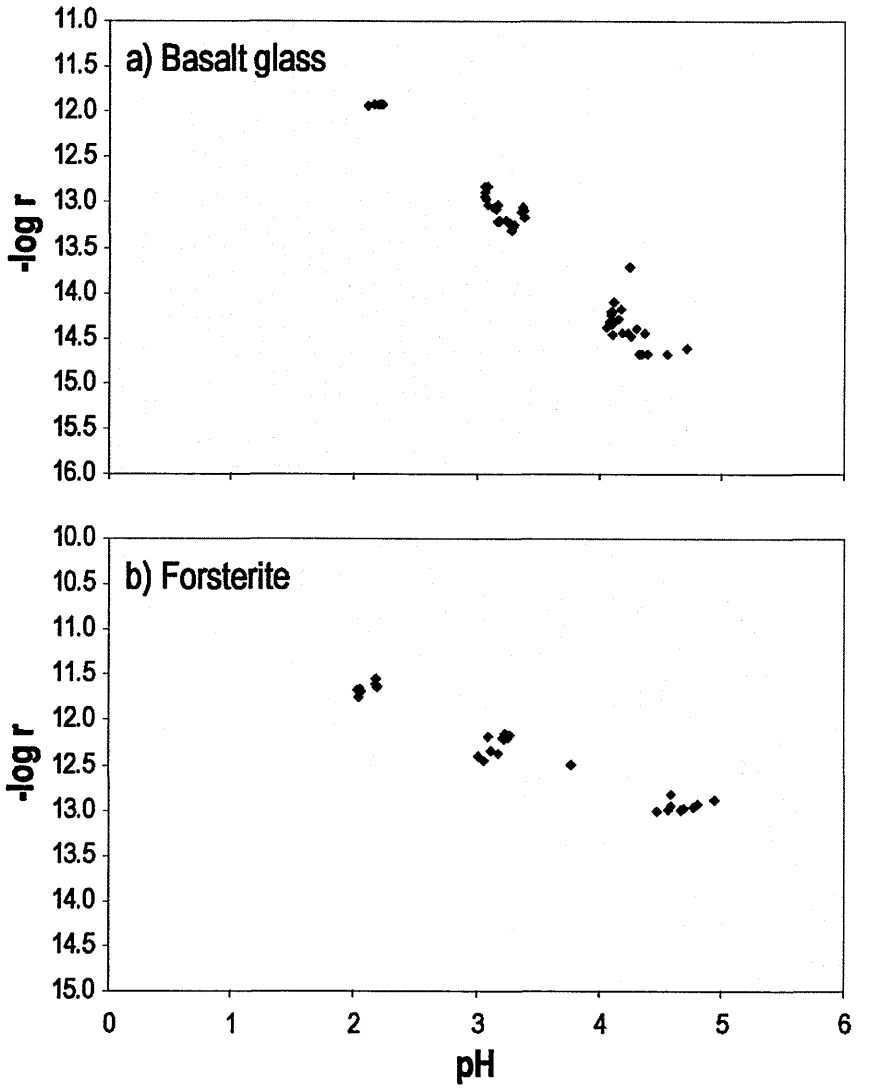

Fig. 5.2 - Graph showing how the dissolution rate (r) changes as a function of pH in basalt glass and forsterite dissolution experiments

The dissolution rates obtained here are almost identical to those reported in the literature (Appendix C5). Changing the experiment temperature also causes changes in the amount of silicon that is released; i.e. temperature regulates the rate of dissolution (Fig. 5.3).

Results show that an increase in temperature from 25°C to 55°C causes the concentration of silicon in the outlet solution to double from ~2ppm to ~4ppm. This causes a concordant increase in the dissolution rate from 5.5×10^{-14} to 1.1×10^{-13} mol/cm^2/s (Fig. 5.4). Changing the solution temperature during the dissolution of

forsterite (experiment FO4, Fig. 5.5) has less of an impact on the concentration of silicon released. An increase in temperature from 35 to 55°C increases the concentration of silicon in the outlet solution by ~1ppm and causes a slight increase in dissolution rate from 7.8×10^{-13} to 9×10^{-13} mol/cm^2/s.

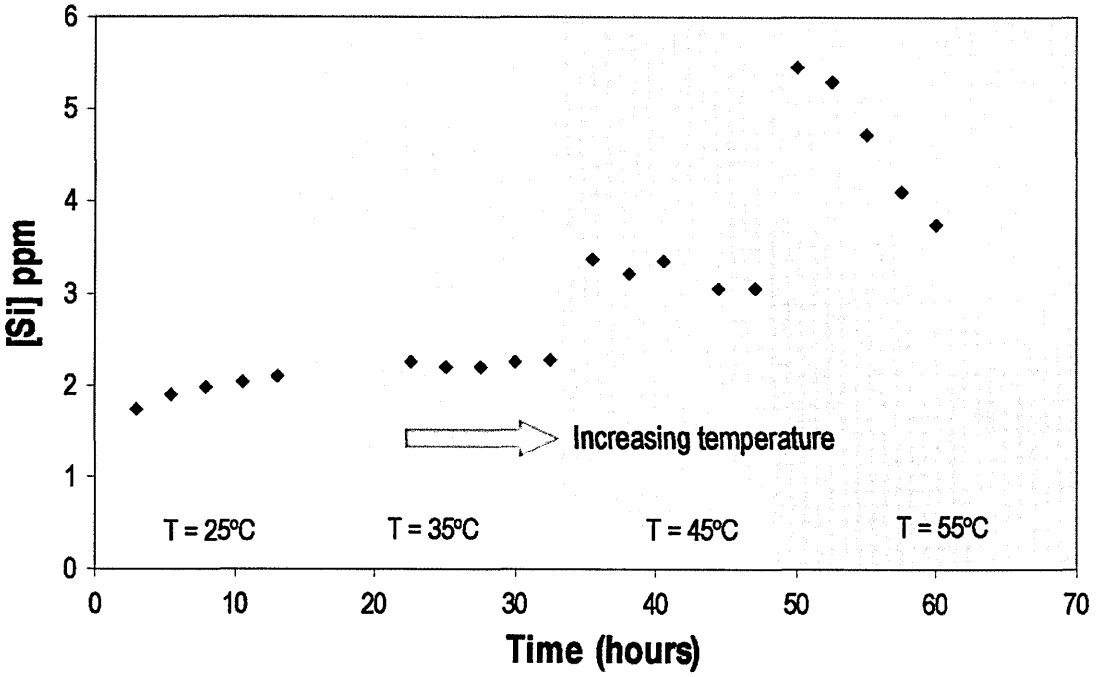

Fig. 5.3 - Concentration of dissolved silicon in solution as a function of time and temperature in experiment BG5

The behaviour of Li is similar to that of silicon, in that the highest Li concentrations coincide with those of silicon in the low pH experiments. Lithium concentrations in solution vary depending on the experiment; low pH experiments involving the dissolution of basalt glass like BG1 have Li concentrations of around 0.5ppb. Experiments involving forsterite have much lower Li concentrations; for example in FO1 initial Li levels were ~0.01ppb. Lithium isotope analyses require a minimum of 5ng in order to make a single measurement thus for many of the samples (those with <0.1ppb Li) isotope analysis was not possible.

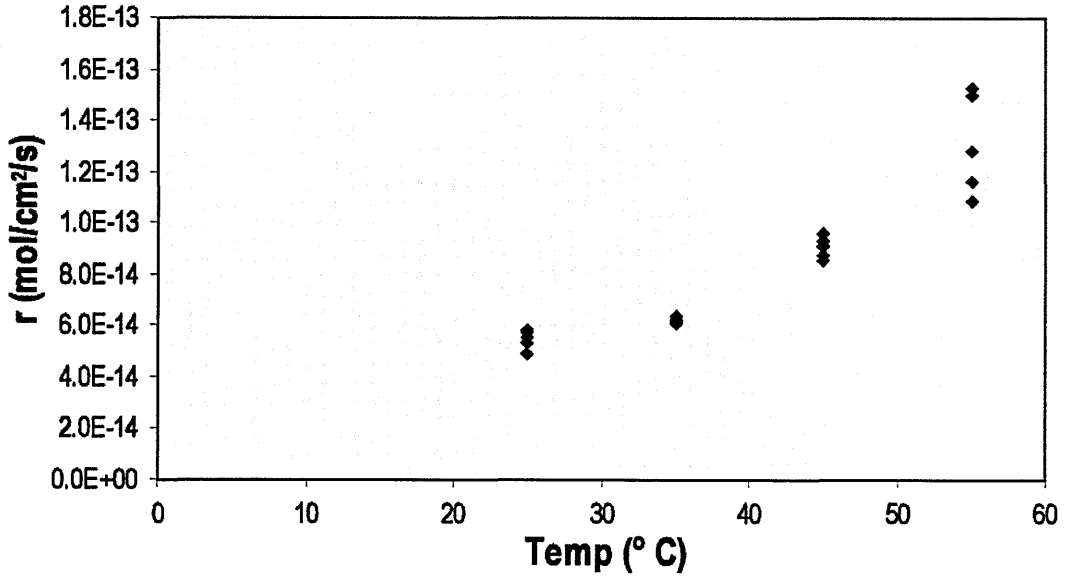

Fig. 5.4 - Graph showing how basaltic glass dissolution rate (r) varies as a function of temperature in experiment BG5 (pH3)

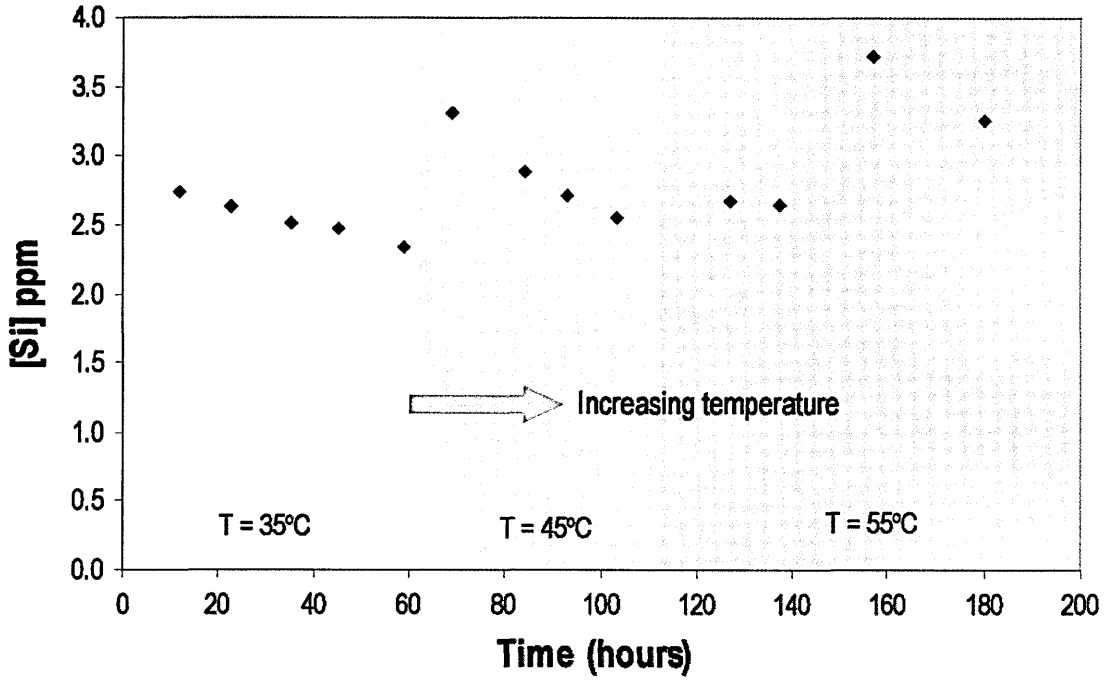

Fig. 5.5 - Concentration of dissolved silicon in solution as a function of time and temperature in experiment FO4 (pH~3.4)

5.3.3. Precipitation experiments

By comparison with the low pH dissolution experiments, at pH10 and 11 the dissolution rate of forsterite is far lower, in agreement with the work of Pokrovsky & Schott (2000).

In experiment FO3 (pH10) the system maintains a relatively constant dissolution rate for over 130 hours at flow rates of 4, 2 and 1g/min; this dissolution rate is 1.62×10^{-14} mol/cm^2/s. When the flow rate drops to 0.15g/min the dissolution rate also falls to 3.16×10^{-15} mol/cm^2/s (see Fig. 5.6). A similar pattern of change is seen during experiment FO5 (pH11), at a flow rate of 3g/min the dissolution rate remained at a constant value of 2.82×10^{-14} for 24 hours, and after dropping the flow rate to 0.2g/min the dissolution rate dropped to 3.16×10^{-15} mol/cm^2/s.

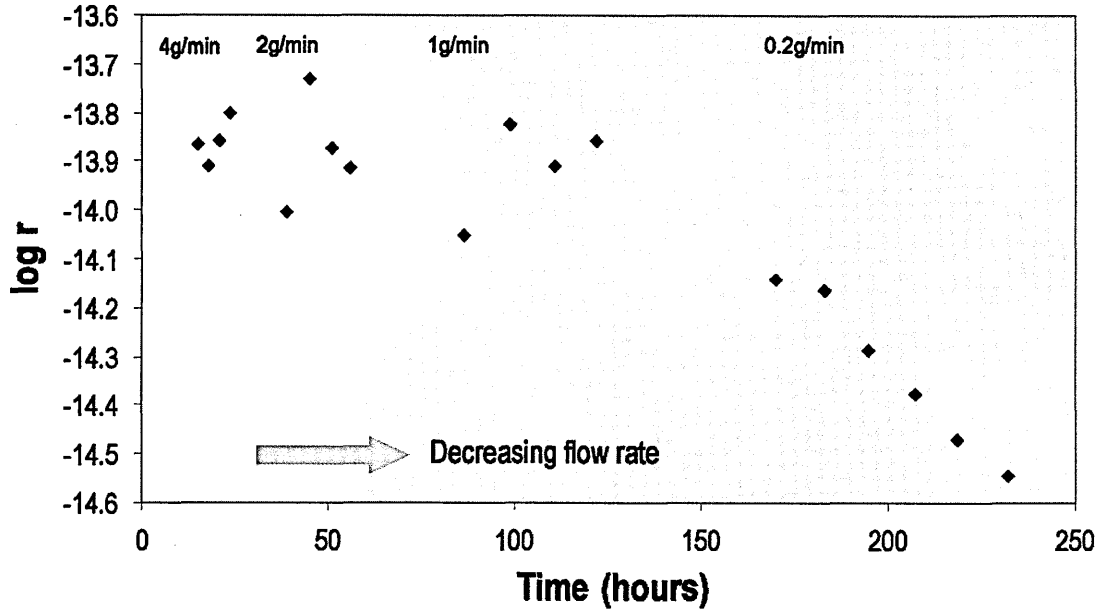

Fig. 5.6 - Change in forsterite dissolution rate (r) with time in experiment FO3 performed at 25°C and pH10

These high pH experiments were repeated at 75°C. The dissolution rate is higher than at 25°C, with the experiment at pH10 having the higher rate of 3.98×10^{-14} mol/cm^2/s compared to 1.41×10^{-14} mol/cm^2/s at pH11.

Lithium concentrations are generally greater than during the dissolution of forsterite at far from equilibrium, with concentrations ranging from 0.1 to 3.8ppb. As a consequence there was potential for a larger number of samples to be analysed than was possible in the dissolution experiments.

5.3.4. Li isotope results

5.3.4.1. Dissolution experiments

Lithium isotope measurements have been made on both experimental solutions (Appendix C6) and experimental minerals (Appendix C4). Results of basalt glass dissolution experiments show that the solutions possess a similar isotopic composition to that of the dissolving mineral. Original basalt glass has a δ^7Li composition of between 5 and 6‰ with solutions from the dissolution experiments ranging in composition from 2.4 to 3.5‰. Unfortunately analyses often involved small sample size so no repeats could be undertaken on many of the samples, while others had a lower Li signal than expected during analysis on the mass spectrometer. The residual glass had δ^7Li compositions that were more consistent with the unaltered basalt glass, BG1 and BG2 all having almost identical Li isotope compositions of ~6‰. Experiments BG3-5 yield slightly lighter isotope ratios of ~4.8‰.

Results from the forsterite experiments show that the solution composition is similar to that of the dissolving mineral. The composition of the forsterite ranges from 1.5 to 2.1‰ while the solutions have a slightly greater range between 0.5 and 2.7‰ (Fig. 5.7). Only four solutions could be measured because the concentration of Li in most of the samples is below the 0.1ppb threshold needed to make one measurement. The δ^7Li isotope composition of unaltered forsterite is ~1.5‰, with the reacted forsterite being slightly heavier between 2 and 2.1‰.

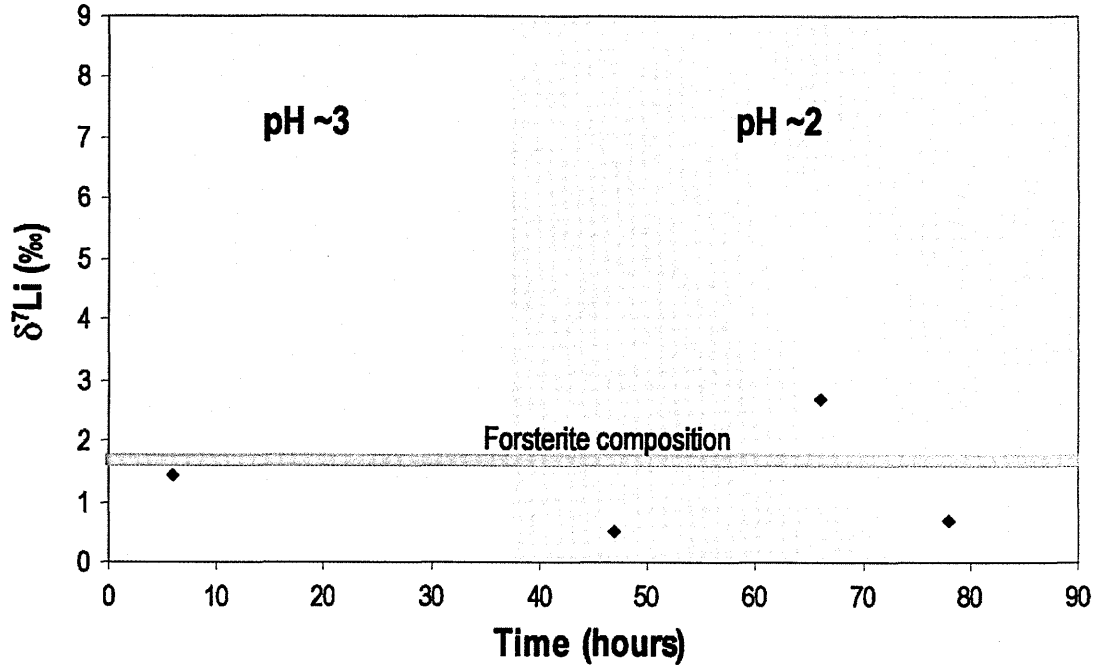

Fig. 5.7 - Variation in the lithium isotope composition of the outlet solution with time in dissolution experiment FO2 (25°C)

5.3.4.2. Precipitation experiments

Results from the precipitation experiments show that the isotope composition of the solutions is much heavier than either the unaltered or experimental forsterite. The δ^7Li value of the solutions ranges from 2 to 12‰, up to 10‰ greater than the values recorded in the fluids produced during the far from equilibrium dissolution experiments. In this case a far greater number of solutions could be analysed because the Li concentration in the precipitation reaction solutions is much higher. For this reason a plot of the δ^7Li composition over time can be made for each experiment (see Fig. 5.8 for FO3). These plots show that the δ^7Li value of the fluid increases over time, for example in FO3 (pH10, 25°C) the δ^7Li value of the solution is 2‰ after 15 hours, increasing to 8.4‰ after 120 hours and remains relatively stable thereafter. Similarly in FO7 (pH11, 75°C) the δ^7Li composition is 7.2‰ after 15 hours and reaches 12.2‰ after 130 hours, remaining constant thereafter.

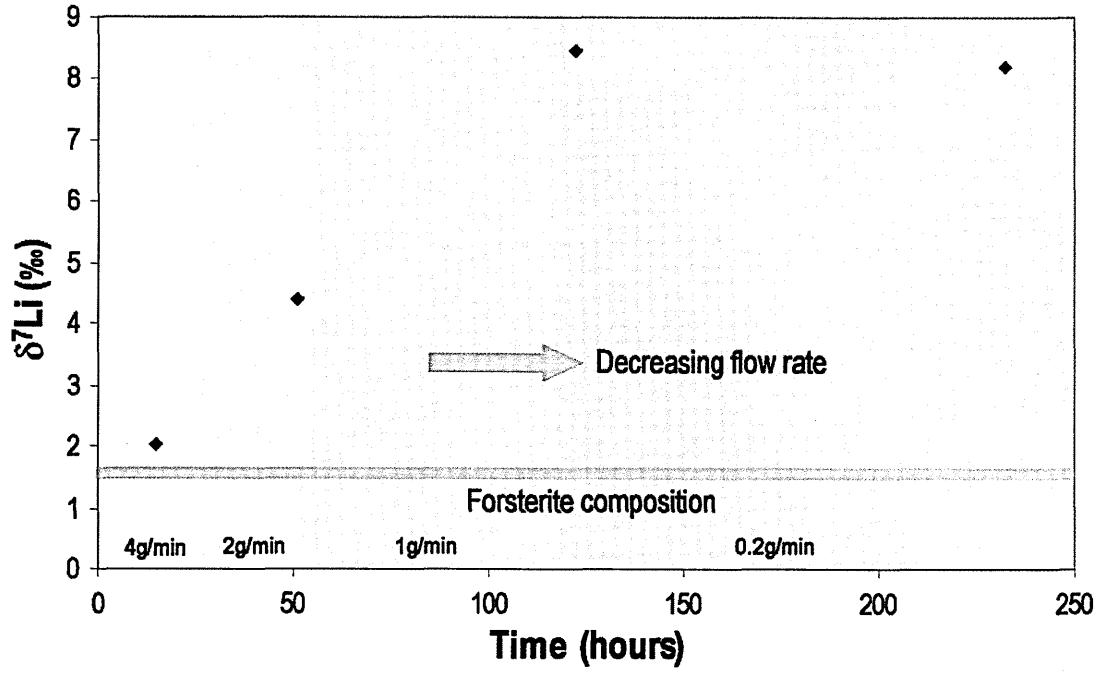

Fig. 5.8 - Change in the lithium isotope composition of the outlet solution with time during precipitation experiment FO3 (25°C).

5.3.5. Mg isotope results

5.3.5.1. Dissolution experiments

Magnesium isotope measurements have been made on the initial mineral phases and the sample solutions for experiments involving both basalt glass and forsterite. The results of these measurements are presented in Appendix C7. In experiments involving both forsterite (FO2) and basalt glass (BG5) the initial solutions have a δ^{26}Mg composition of, respectively -0.45 to -0.5‰ and with time the solutions become isotopically lighter; the final solution of each experiment having a δ^{26}Mg value of -0.62‰. The reproducibility of standards when running experiment BG5 was ~0.1‰ hence all of the samples are within error and any trend cannot be resolved. When running FO2 the reproducibility of the standards was far better; on the order of 0.01‰ and the change in Mg composition with time is illustrated in Fig. 5.9.

The unreacted mineral phases of forsterite and basalt glass have Mg compositions of -0.26 and -0.3‰ respectively. In comparison reacted phases from experiments FO1 and BG1 are isotopically lighter with compositions of -0.34 and -0.35‰ respectively.

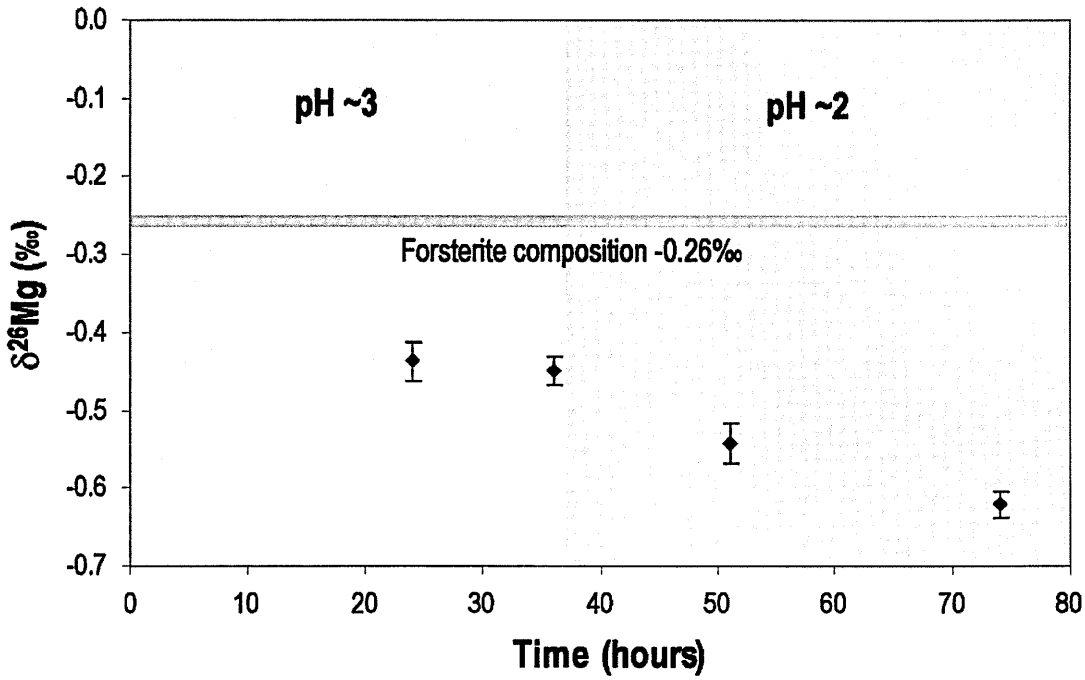

Fig. 5.9 - Change in magnesium isotope composition of the solution with time during the forsterite dissolution experiment FO2 at 25°C. The error bars represent the 2σ error on each sample measurement.

5.3.5.2. Precipitation experiments

In the precipitation experiments the isotope composition of the experimental solutions becomes heavier with time (Fig. 5.10). Three experiments were analysed; FO3, FO5 and FO6 and in each case the first sample had the lightest Mg isotope composition with values of -0.54, -0.65 and -0.30‰, respectively. With time the Mg isotope composition of the fluid phase became increasingly isotopically heavy; the δ^{26}Mg values of the final solutions being -0.34, -0.23 and -0.21‰ respectively. Thus, the Mg isotope composition of the solutions approaches that of forsterite with time. A sample of reacted forsterite from FO5 was also analysed, and the results show it has an Mg isotope

composition of -0.31‰, which is similar to the composition of unreacted forsterite (-0.26‰).

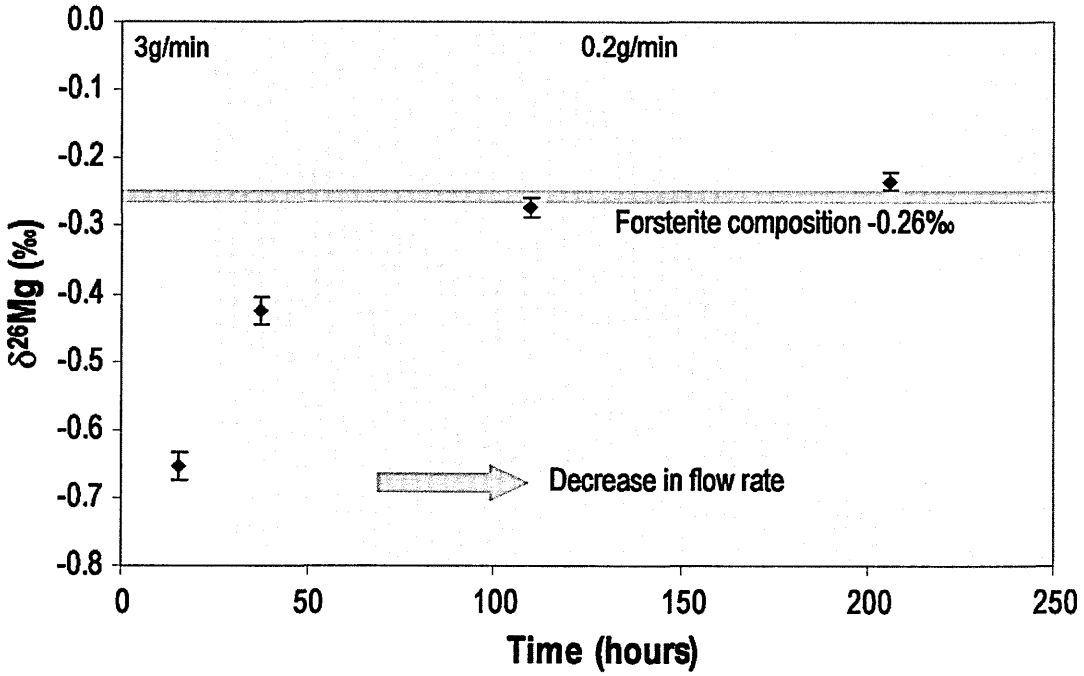

Fig. 5.10 - Change in the magnesium composition of the outlet solution during the precipitation experiment FO5 performed at 25°C and pH11.

5.4. Discussion

5.4.1. Dissolution experiments

5.4.1.1. Dissolution rate

The dissolution rate of both basalt glass and forsterite is dependent on pH, and results from BG4 and BG5 show that basalt glass dissolution is also temperature dependent. This is as expected, the dissolution mechanism of both basalt glass and forsterite involves the exchange of protons for metal cations on the mineral surface (OELKERS, 2001a; OELKERS and GISLASON, 2001; POKROVSKY and SCHOTT, 2000). In the case of basalt glass the dissolution mechanism involves the exchange of protons for aluminium, this partially liberates silica tetrahedra and is the rate limiting step for basalt glass dissolution (OELKERS and GISLASON, 2001). During the dissolution of forsterite at low

pH protons exchange for Mg^{2+} causing the formation of a silica rich layer on the surface, it is the decomposition of this silica rich layer that is the rate limiting step controlling the dissolution rate of forsterite (POKROVSKY and SCHOTT, 2000). For both the glass and olivine decreasing the pH will increase the concentration of protons in solution and so more of these exchange reactions can occur, resulting in a faster breakdown of the mineral lattice which is reflected in higher dissolved silicon concentrations and so higher dissolution rates. Correspondingly, the composition of the reacted mineral is also more depleted in the low pH experiments; for example at pH2 the basalt glass lost ~12% of its lithium into solution while at pH4 the basalt glass lost <1%. Changing the temperature of the system also causes a change in the solution chemistry and reaction rate; this is consistent with the Arrhenius equation:

$$k = A \times \exp\left(\frac{-E_a}{RT}\right) \qquad \textit{Equation 5.3}$$

A is the pre-exponential factor, Ea is the activation energy, R is the gas constant, and T the temperature in K.

Thus reactions such as the hydrolysis of silicates will increase exponentially with increasing temperature. It is predicted that reaction rates will increase by an order of magnitude through an increase in the temperature from 0 to 25°C (WHITE, 2003). Changes in the dissolution rate of basalt glass in this study increase from $\sim 5\times10^{-14}$ to 1.5×10^{-13} mol/cm^2/s as temperature increases from 25 to 55°C. Forsterite behaves slightly differently; in experiment FO4 the dissolution rate increases with temperature but only fractionally from 7.8×10^{-13} to 1×10^{-12} mol/cm^2/s with an increase of temperature by 20°C. This increase is smaller than expected from the Arrhenius equation and from previous work investigating the dissolution of forsterite between 25

and 65°C (OELKERS, 2001a). One possible explanation for the behaviour of FO4 is that it had not yet reached a steady state before the temperature was changed; this is suggested by fluctuations in the silicon concentrations. In general however the dissolution rate of forsterite and basalt glass increases with temperature.

Comparison of the dissolution rate data obtained here with those of previous studies indicates that they are very similar (GISLASON and OELKERS, 2003; POKROVSKY and SCHOTT, 2000; ROSSO and RIMSTIDT, 2000) as shown in Appendix C5. The two exceptions are in the case of forsterite dissolution using variable stir speeds at low pH (this effect is also demonstrated at pH10 and 11). At pH 2-4 the dissolution of forsterite is similar to literature values when the stirring speed is kept constant at 350 rpm. In order to test whether the dissolution is surface reaction controlled the stirring speed was changed during the end of experiments FO1 and FO2 to 500 rpm. This had a dramatic effect on the dissolution rate; increasing it from 2.2×10^{-12} to around 6×10^{-12} mol/cm^2/s. Literature dissolution rates for forsterite range from 7×10^{-13} to 2×10^{-12} mol/cm^2/s (POKROVSKY and SCHOTT, 2000; ROSSO and RIMSTIDT, 2000; WOGELIUS and WALTHER, 1991); so by increasing the stir speed within the reactor the dissolution rate has increased by nearly three times over rates at 350 rpm and up to one order of magnitude over rates reported in the literature. This effect has been shown to occur during the dissolution of basalt glass (GISLASON and OELKERS, 2003) and is attributed to relatively slow diffusional transport of metal ions away from the crystal surface, which limits the diffusion rate at low pH. Gislason & Oelkers (2003) show that a stirring speed of over 550rpm is needed to keep the dissolution rate of basalt glass surface reaction controlled at pH 2, and 325 rpm is needed at pH 3. The results from the present study in pH 2 solutions show that a stir speed of 350 rpm is not sufficient to move metal ions away from the dissolving forsterite surface and as a consequence

dissolution becomes diffusion limited. Determination of the dissolution rate is not the focus of the current investigation. Nevertheless it can be concluded that previous estimates for the dissolution rate of forsterite at low pH and particularly at pH 2 are too low, and on this basis it is recommended that any new studies investigating forsterite dissolution should take diffusional processes into account and use a stir speed of at least 500 rpm at pH 2.

5.4.1.2. Reaction Stoichiometry

The stoichiometry of a reaction is a measure of the molar ratios in solution in comparison to the molar ratios in the dissolving mineral. It is also a good indicator of whether or not the reaction is at a steady state and if dissolution is occurring congruently. This is useful because the mechanisms of dissolution of both basalt glass and forsterite involve preferential loss of a major element and thus can depend on the pH of the solution. In particular, the dissolution of forsterite at low pH involves the formation of a Si rich layer on the surface so preferentially loses Mg, and vice versa at high pH (POKROVSKY and SCHOTT, 2000). Therefore the stoichiometry of dissolution can affect the dissolution rate (e.g. if Si is preferentially lost) and may also affect the isotope composition of material that is lost to solution. Assessing the stoichiometry of basalt glass dissolution is usually performed by analysing the molar ratio of Si:Al (in Stapafell glass this should be 2.77), while the stoichiometry of forsterite dissolution is assessed through the Mg:Si ratio (in this case the Mg:Si ratio should be 1.82). Molar ratios for basalt glass in experiments BG1 to BG5 show that the system is not in a steady state although in most cases the Si:Al ratio is approaching 2.9 (see Fig. 5.11). This is not ideal because it indicates that incongruent dissolution is occurring, and in this case the Li isotope composition will not necessarily reflect the steady state

dissolution of basalt glass. The Si:Al ratio generally starts off lower than 2.77 reflecting the early cation exchange of Al^{3+} for protons, with preferential Al^{3+} release into solution (OELKERS and GISLASON, 2001). Over time and changing conditions the solutions do approach stoichiometry but never completely achieve it, thus it seems likely that a longer time period would have been needed to attain a steady state. In the higher temperature experiments the solutions are also non stoichiometric; each increase in temperature of 10°C causes the Si:Al ratio to increase dramatically. For example as BG4 is increased from 45°C to 55°C the Si:Al ratio increases from ~4 to over 30 before decreasing again with time. The easiest way to explain this is that the increase in temperature causes precipitation of $Al(OH)_3$ which would remove aluminium but not silicon thus increasing the Si:Al ratio. However there is no evidence to support this, saturation state modelling (see Section 5.4.1.3) shows that $Al(OH)_3$ is always undersaturated. Another more complicated explanation involves the dissolution mechanism of basalt glass; basalt glass dissolution involves the removal of Al which causes the partial liberation of silica tetrahedra (OELKERS and GISLASON, 2001). In steady state conditions these partially liberated tetrahedra will be released gradually, but it is possible that the sudden increase in temperature causes a rapid release of these partially attached silica tetrahedra. As time passes at a fixed temperature the Al-proton exchange reaction will re-establish itself and the system can return to steady state conditions.

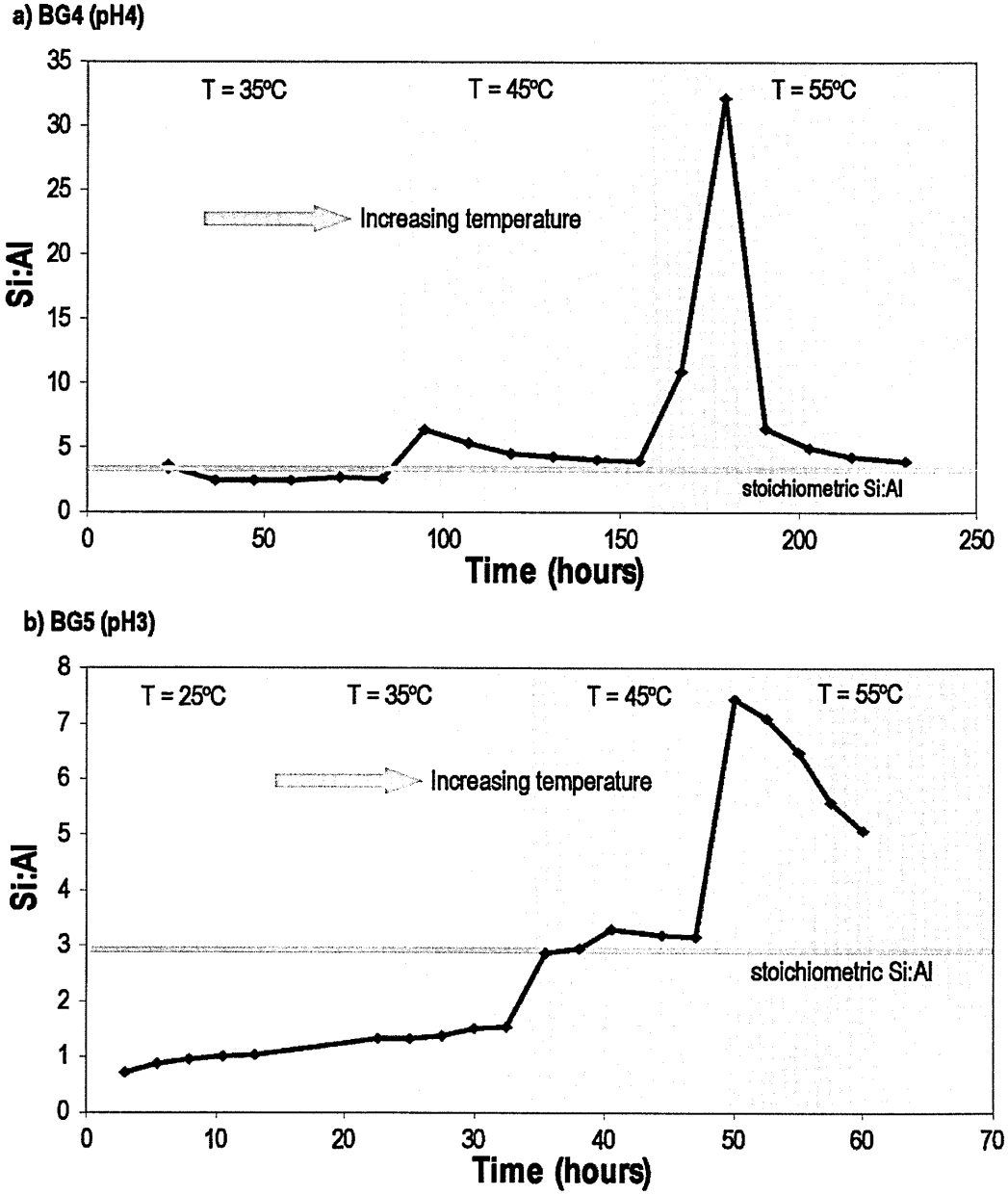

Fig. 5.11 - Graph showing how the Si:Al ratio of the outlet solution changes over time with changing reactor temperature in (a) pH4 (BG4) and in (b) pH3 conditions (BG5). The red line represents the stoichiometric Si:Al ratio in basalt glass of 2.92:1

In contrast to the basalt glass experiments the dissolution of forsterite in FO1 and FO2 achieved stoichiometric ratios of Mg:Si almost immediately, as shown in Fig. 5.12. Initial Mg:Si ratios were slightly higher than stoichiometric (~2) because the dissolution mechanism of forsterite involves the preferential release of Mg in acidic

solutions (OELKERS, 2001a; POKROVSKY and SCHOTT, 2000). With time this ratio approached 1.8 and remains at this level indicating that steady state dissolution has been achieved. On average the Mg:Si ratio was 1.87 ± 0.05 (1σ) over the course of two experiments and a combined total of ten days sampling. This is indistinguishable to the average Mg/Si ratio of 1.84 ± 0.19 recorded by Rosso & Rimstidt (2000) (based on 235 Mg/Si ratios).

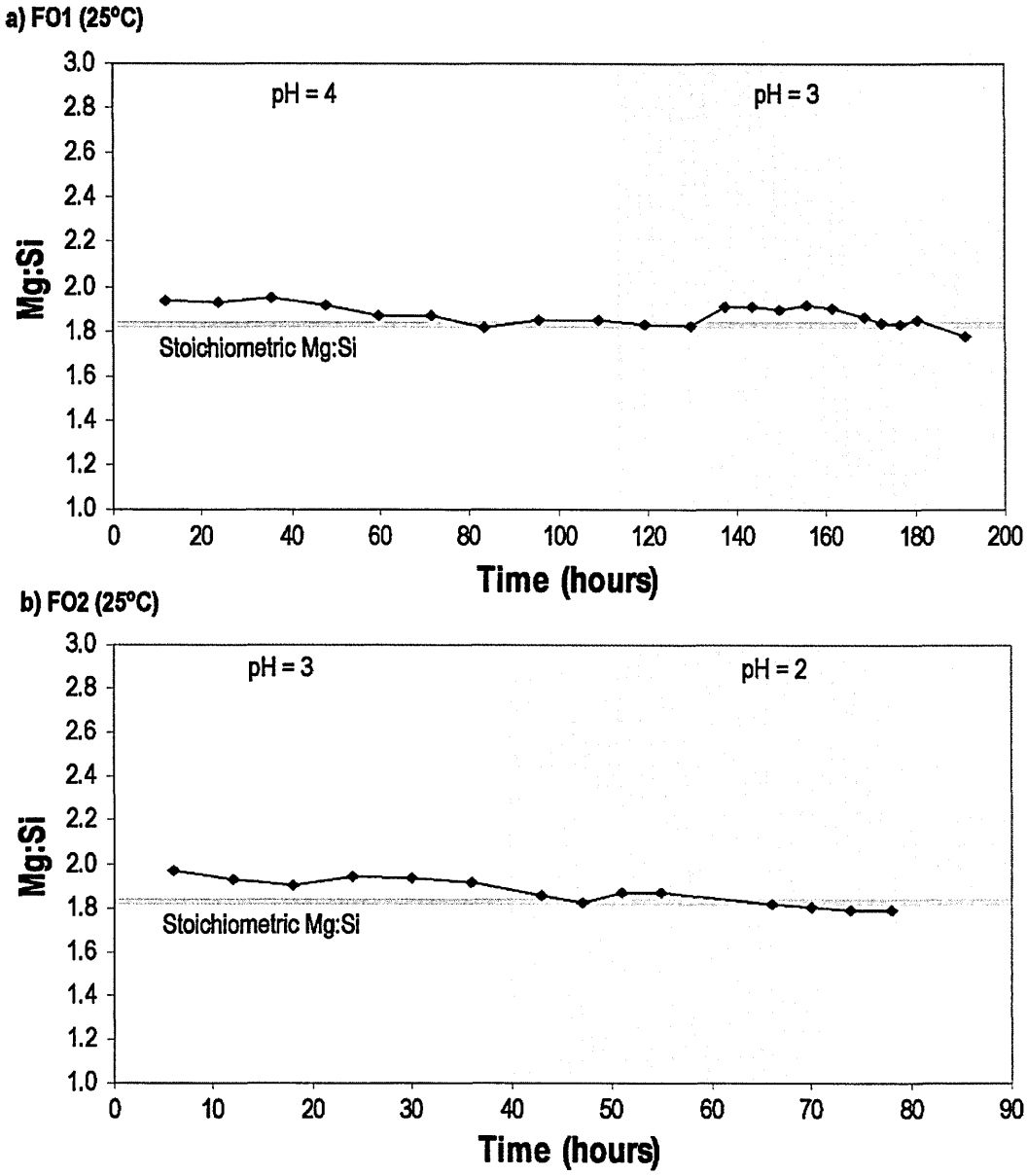

Fig. 5.12 - Graph showing how the Mg:Si ratio of the outlet solution changes with time and changing pH. Red line represents the stoichiometric forsterite ratio of 1.82:1

5.4.1.3. Mineral Saturation

The aim of the dissolution experiments is to assess how Li and Mg isotopes behave during solely dissolution of the primary mineral. For primary mineral dissolution to be the only process that occurs the system needs to be at conditions far from equilibrium so that the reverse reaction cannot easily occur and the likelihood of secondary mineral formation is very low. The saturation state of the system can be estimated with respect to the primary mineral and any potential secondary phases through geochemical modelling. The program PHREEQC (PARKHURST and APPELO, 1999) enables the calculation of saturation states of solutions with respect to specific minerals using the element concentrations of the solutions. The saturation index is an indicator of mineral stability; if it is at zero then the mineral is said to be at equilibrium and should be stable or relatively stable in solution (APPELO and POSTMA, 2005). If the SI is >0 then the mineral is said to be supersaturated and may precipitate, and as the SI increases the mineral in question is increasingly likely to precipitate. If the SI is below zero then the mineral is undersaturated, it is unstable and if present and exposed to such a solution it will have a tendency to dissolve. The predictions of mineral stability obtained from PHREEQC are not definitive but they do provide a useful means of estimating mineral stability within the reactors. Equilibrium constants for each mineral were taken from the Wateq4f database (BALL and NORDSTROM, 1991) within PHREEQC, data for hydrated basalt glass was taken from Oelkers and Gislason (2001), using a log equilibrium constant of 0.079 for the following hydrolysis reaction:

$$SiAl_{0.36}O_2(OH)_{1.08} + 1.08H^+ \rightarrow SiO_2 + 0.36Al^{3+} + 1.08H_2O \qquad \textit{Equation 5.3}$$

The phases that are most at risk of forming in the reactors are amorphous iron and aluminium hydroxides and/or cryptocrystalline goethite and gibbsite (GISLASON and OELKERS, 2003). Results from PHREEQC show that all of these minerals as well as hydrated basalt glass, kaolinite and illite are undersaturated, and that the degree of undersaturation increases at lower pH (Appendices C8 and C9). For this reason it is reasonable to assume that the dissolution experiments are all far from equilibrium and no secondary mineral formation has occurred.

5.4.1.4. Lithium isotope behaviour

As a consequence of the small sample size Li isotope analysis of the experimental solutions was extremely difficult, and no repeat measurements could be made. The Li isotope composition of the basalt glass is ~5.8‰, while the composition of reacted basalt glass ranges from 4.8 to 6‰, these are all within or close to the range of Li compositions documented for MORB (Elliott et al. 2004). The fact that the reacted basalt glass is not identical to unreacted basalt glass could be due to a number of reasons. Firstly, there could be some sample heterogeneity, although the fact that the glass has been powdered and well mixed makes this unlikely. Secondly, samples may have experienced incongruent dissolution or leaching of Li, involving the preferential loss of one isotope. To account for the 1‰ difference between the unreacted basalt glass and basalt glass from experiments BG3, 4 and 5 there would need to be preferential loss of the heavy isotope of Li. However analysis of the solution from BG5 shows that it is in fact isotopically lighter than the original basalt glass by ~2‰. Mass balance calculations suggest that this can only occur if there is another phase present that is preferentially incorporating the ^{7}Li. However, this seems extremely unlikely because all data, thus far, suggest that secondary minerals remove the light isotope of Li

(CHAN and HEIN, 2007; HUH et al., 2001; HUH et al., 1998; KISAKUREK et al., 2005; KISAKUREK et al., 2004; PISTINER and HENDERSON, 2003; POGGE VON STRANDMANN et al., 2006). The most likely explanation is that there have been slight variations generated during the chemical purification of the samples or measurement variations introduced during mass spectrometry. In the context of the very large range of Li isotope compositions observed in nature (e.g. the recorded range of riverine Li is between 6 and 40‰ (HUH et al., 1998; POGGE VON STRANDMANN et al., 2006)), the small variations in isotope ratios observed in these experiments suggest that there is minimal fractionation between mineral and solution at far from equilibrium conditions. This would also be in keeping with the results of basalt leaching experiments by Pistiner and Henderson (2003).

5.4.1.5. Magnesium isotope behaviour

Previous studies of Mg isotopes in crustal and mantle material suggest that there are a wide range of compositions. For example olivine from San Carlos has been measured in several different studies with a range of compositions from -0.73‰ (TENG et al., 2007), to -0.06‰ (WIECHERT and HALLIDAY, 2007). This difference could be due to heterogeneity of the San Carlos olivine (PEARSON et al., 2006) or due to weathering or metasomatic affects (TENG et al., 2007). Alternatively it could be due to problems with Mg isotope analysis. In comparison to these literature values the Mg composition measured in this study falls within the reported range at -0.26‰. The isotopic composition of the phases from the experiments are similar to that of the unaltered forsterite (-0.31 and -0.34‰) although they are slightly lighter, which could result from alteration of the mineral during dissolution but could also be due to sample heterogeneity. This is particularly likely because the forsterite was powdered from

forsterite crystals in batches. Such potential heterogeneity could have been avoided through the use of one large well mixed batch of powder, rather than crushing and sieving in batches.

There are also numerous studies of the composition of basalt; for example the composition of SUNY MORB has been found to be between -0.28 and -0.32‰ (RICHTER et al., 2008; TENG et al., 2007) while the composition of BCR-1 ranges from -0.37 (YOUNG and GALY, 2004) to -0.09‰ (WIECHERT and HALLIDAY, 2007). The Stapafell basaltic glass has a very similar Mg composition to these basalts with a δ^{26}Mg of -0.3‰. The composition of the reacted basalt glass is very similar to this, suggesting that the sample is homogeneous and that there has been no fractionation during dissolution.

The results of Mg isotope analysis from the forsterite dissolution experiments indicate that the dissolution fluid is isotopically light relative to the composition of the forsterite and has become isotopically lighter with time. For the composition of the fluid to be different to that of the mineral there either needs to be fractionation during the dissolution process (i.e. incongruent dissolution with respect to the Mg isotopes) or secondary mineral formation within the reactor causing preferential uptake of the heavy or light isotopes. The latter explanation seems most likely to be the cause of the solutions becoming isotopically light; weathering studies have shown that heavy Mg is preferentially retained in silicate soils (TIPPER et al., 2006a). However, two lines of evidence support the assumption that no secondary mineral formation has occurred. Firstly, modelling of the saturation states shows secondary minerals are undersaturated as discussed in Section 5.4.1.3. Secondly, the solution has a stoichiometric Mg/Si ratio, and any precipitation of silicate minerals will cause the ratio to change. Precipitation of amorphous iron oxyhydroxides and iron oxides would not affect the Mg/Si ratio but

saturation state data show that these minerals are all undersaturated. The Mg/Fe ratio in forsterite is ~10.1, in both experiment FO1 and FO2 the ratio by the end of the experiment is approximately stoichiometric at 10.5 implying that there has been no iron mineral precipitation.

These data suggest that secondary minerals are unlikely to have formed; the only other way to explain the behaviour of Mg isotopes is by the preferential loss of light Mg during forsterite dissolution. If this is the case then it is assumed that if the experiment was to proceed for a longer period of time the fluid composition would become progressively heavier and approach the Mg isotope ratio of forsterite. This is because if dissolution is the only mechanism that occurs then mass balance would require the mineral to preferentially lose heavy Mg at some stage during the dissolution.

5.4.2. Precipitation Experiments

5.4.2.1. Dissolution rate

Dissolution rates at pH 10-11 are far slower than at pH 2-4 as predicted from previous work on forsterite dissolution (POKROVSKY and SCHOTT, 2000; WOGELIUS and WALTHER, 1991).

Results from experiments FO3 and FO5 show that the dissolution rate is highly dependent on the flow rate of the solution pumped into the reactors. For example in FO3 the dissolution rate remains relatively constant at 1.25×10^{-14} mol/cm^2/s for flow rates 4, 2 and 1 g/min. After ~130 hours the experiment was changed to a much lower flow rate of 0.15g/min. This caused the dissolution rate to decrease over the same time period finishing at a rate of 2.82×10^{-15} mol/cm^2/s similar to the results of Pokrovsky & Schott (2000). The system appeared to be at a steady state for the first 130 hours, similarly in FO5 for the initial 24 hours. During this period the dissolution of forsterite

at pH11 was greater than that of forsterite at pH10 (~1.3×10^{-14} at pH10 compared to ~2.9×10^{-14}mol/cm^2/s at pH11). It is only when the flow rates drop to between 0.15 and 0.2 g/min that the dissolution rates at both pH 10 and 11 fall to ~4×10^{-15}mol/cm^2/s similar to results of Pokrovsky & Schott (2000). The fall in dissolution rate could be for two reasons; either the system is still reaching a steady state or the slowdown is related to the increasing concentrations in solution. Studies have shown that it can take as long as 200-300 hours for the dissolution of forsterite to reach steady state at high pH (Pokrovsky & Schott 2000). However, if the drop in dissolution rate is caused by the system reaching steady state conditions the composition of the solution should become more stoichiometric; this is not the case. Instead the falling dissolution rates coincide with falling element concentrations and Mg:Si ratios that are becoming less stoichiometric with time (Fig. 5.13). Initially the decrease in flow rate causes a build up of dissolved solids in the reactor; this may result in the saturation state of secondary minerals like chrysotile and talc also increasing. If secondary minerals were to form they would remove both Mg and Si from solution. Because the dissolution rate is calculated from the dissolved Si concentration this would result in an apparent decrease in dissolution rate. Mineral saturation states and how they may relate to changes in the dissolution rate of forsterite are described in Section 5.4.2.3.

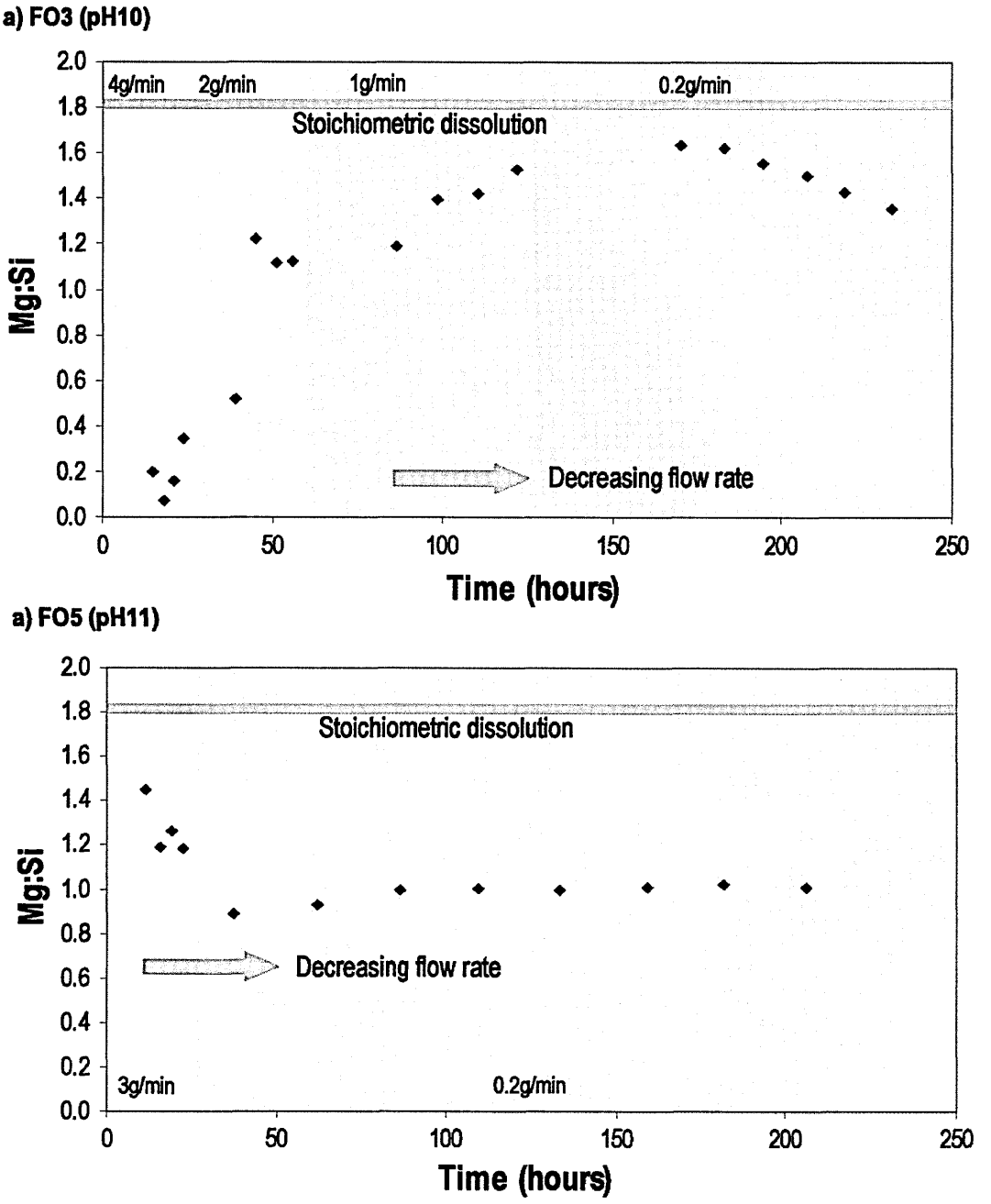

Fig. 5.13 - Graphs showing how the Mg:Si ratio of the outlet solution changes with time and flow rate at (a) pH10 and (b) pH11.

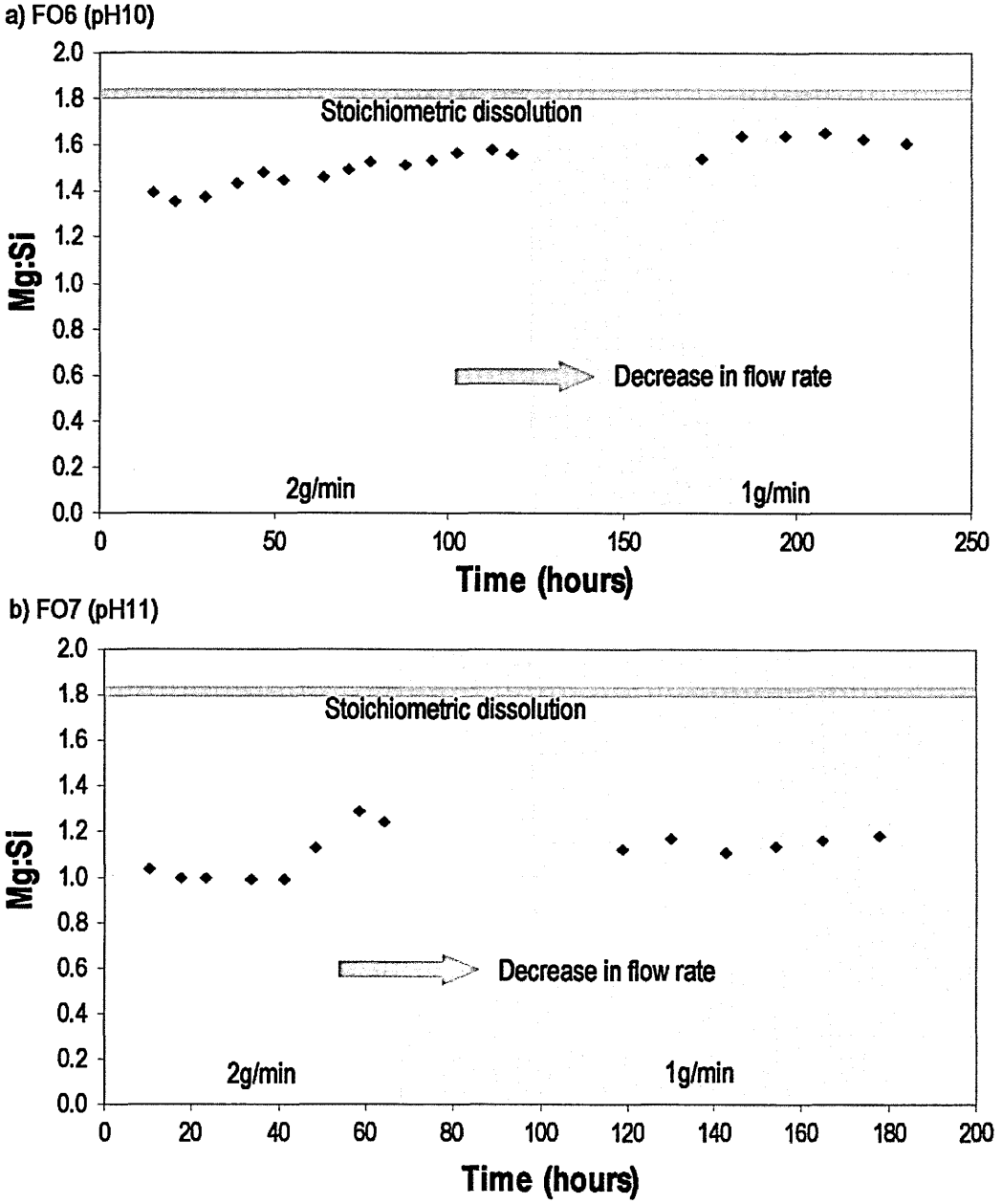

Fig. 5.14 - Graphs showing how the Mg:Si ratio of the outlet solution changes with time and flow rate at 75°C and (a) pH 10 and (b) pH 11

5.4.2.2. Reaction Stoichiometry

Unlike the dissolution experiments where stoichiometric dissolution was quickly attained, this did not occur in any of the experiments at pH 10 and 11 (see Fig. 5.13 and 5.14). An example of this is shown in experiment FO3 (Fig. 5.13), here the Mg:Si solution ratio is initially ~0.1 and steadily rises over time; this is because the mechanism

of dissolution in alkaline conditions involves the formation of a Mg rich layer and the preferential loss of Si into solution (POKROVSKY and SCHOTT, 2000). After ~130 hours the Mg:Si ratio rose to ~1.6; the dissolution of forsterite approached stoichiometry and the system approached a steady state. It is only after the flow rate is decreased to 0.15g/min that the composition of the solution then changes; the Mg:Si ratio starts to decrease away from the stoichiometric ratio for forsterite. A change in the composition of the sample solutions to a lower Mg/Si ratio can result from either a change in the dissolution process (i.e. that forsterite is now dissolving incongruently and preferentially losing Si), or by some other process that preferentially removes Mg from solution. Incongruent dissolution of forsterite is unlikely; it was not observed at far from equilibrium and any initial incongruence will result in the solution becoming relatively enriched in silicon as shown in the early stages of FO3. The other more likely possibility is the formation of secondary minerals; in theory a new mineral could be a Mg silicate such as talc, a Mg hydroxide such as brucite, Mg carbonate (dolomite) or some combination of all three. If concentration data from FO3 is analysed (see Fig. 5.15) it shows that both Mg and Si concentrations increase up to 130 hours but then both concentrations decrease along with the Mg:Si ratio. The fact that both Mg and silicon concentrations decrease show that the drop in Mg/Si is caused by incorporation of both Mg and silica into a new mineral phase(s). The drop in the Mg:Si ratio is caused by the fact that more Mg is removed from solution than Si.

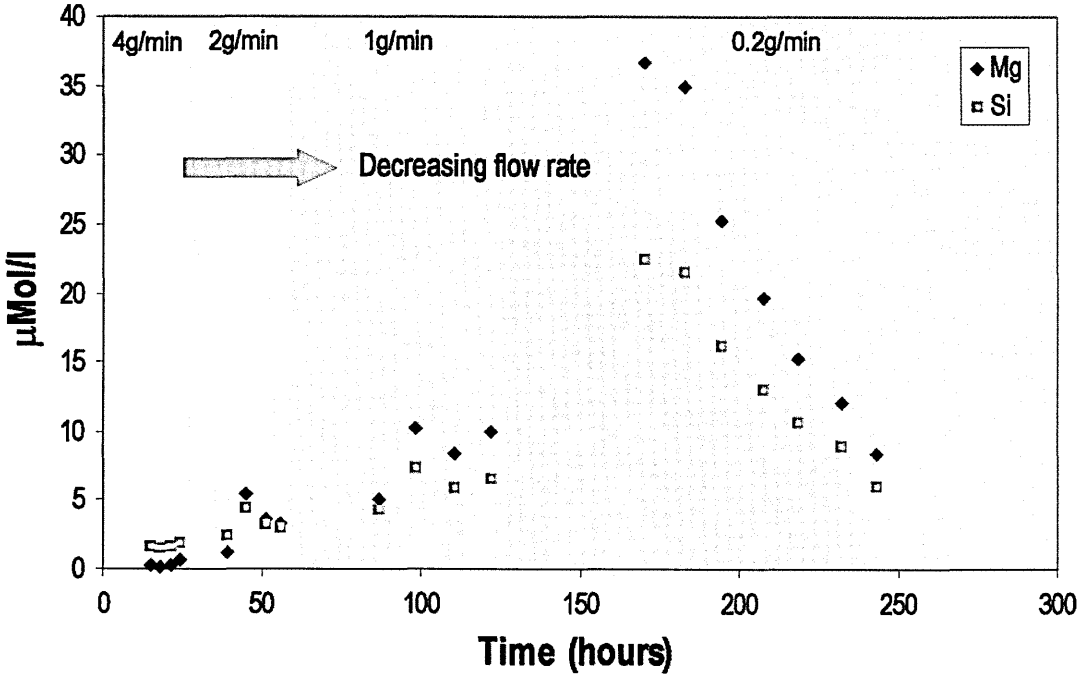

Fig. 5.15 - Change in the concentrations of silica and magnesium in the outlet solution with time in experiment FO3 (25°C, pH10)

If solutions from experiments at pH10 and pH11 are compared, then those at pH10 have Mg:Si ratios that are closer to stoichiometric than pH11 (at pH10 Mg/Si is ~1.5, at pH11 Mg/Si is ~1.1) but despite the running time of these precipitation experiments lasting for far longer than at low pH stoichiometric dissolution is not achieved. The fact that stoichiometric dissolution is not achieved could be due to lower reaction rate at high pH (from $\sim 1\times10^{-13}$ at pH3 to $\sim 2\times10^{-15}$ mol/cm^2/s at pH10) but could also be due to the precipitation of secondary minerals which then affects element ratios. High pH experiments are known to take up to 200-300 hours to reach a steady state (POKROVSKY and SCHOTT, 2000), yet despite experiments such as FO3 and FO5 running for similar periods of time the solutions did not achieve a stoichiometric chemistry. It seems unlikely that if run for longer these solutions would become stoichiometric because the systems appear to have already reached a steady state, in particular those experiments at pH11. If non steady state conditions cannot explain the

offset in the Mg:Si ratio of the solution then the alternative explanation is that secondary mineral formation has occurred and altered the solution chemistry.

5.4.2.3. Mineral saturation states

The calculation of secondary mineral saturation by PHREEQC can yield information on the likelihood of secondary mineral formation. Because the dissolving mineral is forsterite and has a composition of $(Mg_{1.82}Fe_{0.18})SiO_4$ the likely secondary minerals in these experiments are Mg silicates. Iron concentrations in solution are below the detection limits of the ICP-AES so it is assumed that the formation of iron oxyhydroxides will not be important, this is supported by the solution chemistry which shows that both Mg and Si are removed from solution. Figure 5.16 shows the log activities of $(Mg^{2+})/(H^{+})^2$ and silica for experiments FO3 and FO5 (carried out at 25°C). The coloured lines represent the activities in solution needed for the fluid phase to be in equilibrium with respect to the phase in question. For example, a solution that plots on or close to the green line is in equilibrium with talc. A solution that plots below the green line is undersaturated and talc would dissolve if present, while any solution plotting above the green line is supersaturated with respect to talc and so talc has potential to precipitate. Saturation state modelling shows that solutions in both FO3 and FO5 are supersaturated with respect to chrysotile and talc so it is possible that these phases have precipitated from solution. Talc has 3Mg to 4Si so any precipitation should remove more Si than Mg. In contrast chrysotile has 3Mg to 2Si so any precipitation should remove more Mg than Si from solution. Solutions from both FO3 and FO5 have lower Mg:Si ratios than is stoichiometric which suggests that more Mg is being taken out of solution than Si. Of the two supersaturated minerals the evidence from solution chemistry is in favour of chrysotile precipitation over talc. However, in order to prove

this conclusively the secondary phase would need to be identified using SEM analysis, and results so far have proved inconclusive.

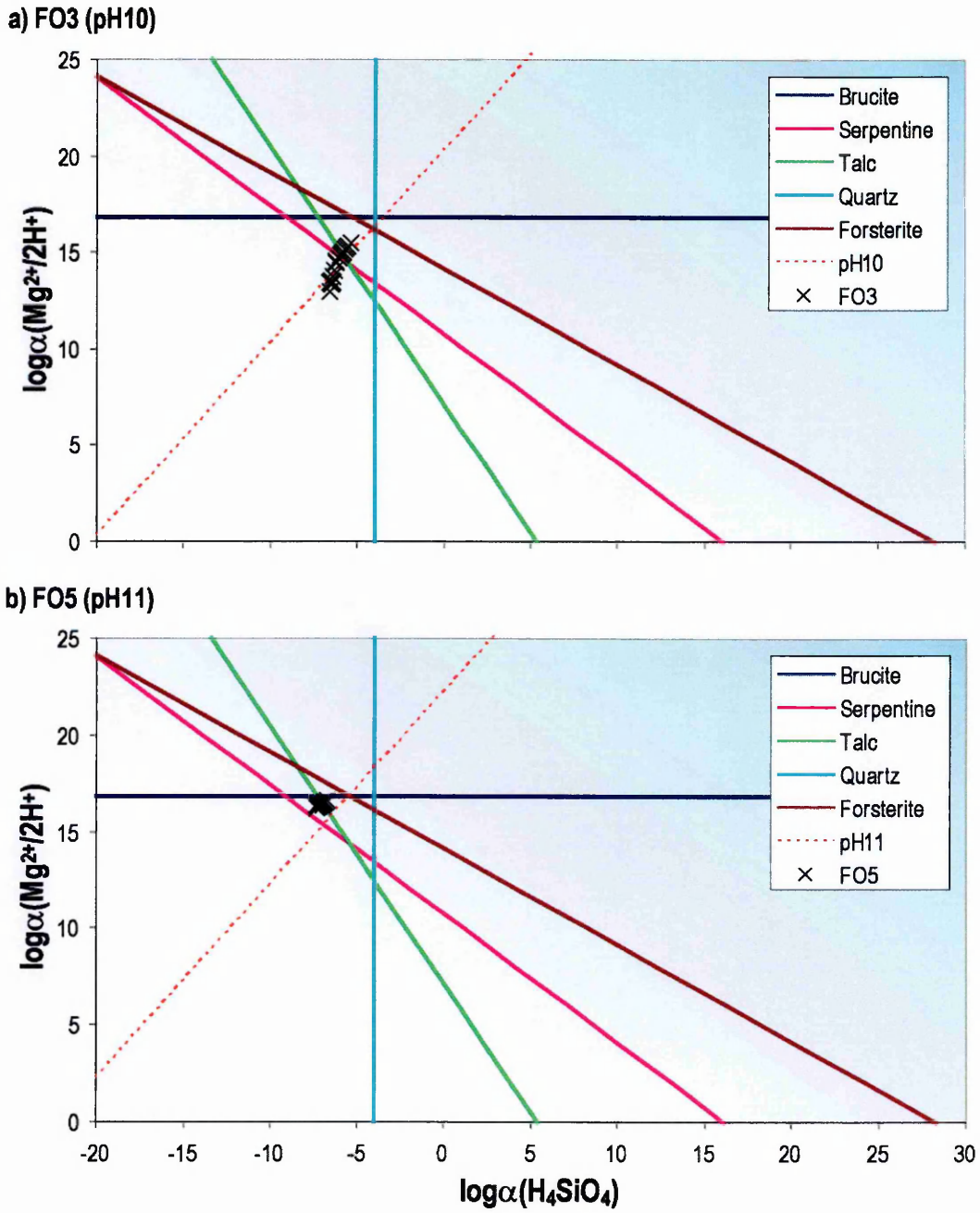

Figure 5.16 - Solubility relationship in the system $MgO\text{-}SiO_2\text{-}H_2O$ using the Wateq4f database (Ball and Nordstrom, 1991). Superimposed on the diagrams are PHREEQC modelling of the aqueous solutions from forsterite experiments at 25°C and pH10 (FO3) and pH11 (FO5). The dashed line represents an estimation of the reaction path during forsterite dissolution at the respective pH assuming stoichiometric dissolution.

If the solutions from the higher temperature experiments (FO6 and FO7) are also analysed in PHREEQC the results are similar to those at 25°C, if slightly less saturated. This is surprising given the greater stability of magnesium silicates at higher temperature. However, increasing the reactor temperature causes the pH of the solution to change; for example a solution that has a pH of ~10 at 25°C will have a pH of ~9 at 75°C. The stability of silicate minerals is highly dependent on the pH of the solution. The magnesium silicates are more stable at high pH so the drop in pH causes the saturation indices of minerals such as chrysotile and talc to be lower than expected. Even so, all solutions at 75°C are saturated with respect to chrysotile and many are saturated with respect to talc.

High saturation indices in solution such as those in FO5 and FO7 suggest firstly, that the formation of secondary minerals is likely, and secondly, that the dissolution rate of the dissolving mineral (in this case forsterite) may be inhibited by its saturation state. When a mineral approaches saturation the total dissolution rate no longer represents just forward dissolution but is also influenced by the reverse reaction (GISLASON and OELKERS, 2003). This means that the dissolution rate will slow down. The braking effect on the dissolution rate can be quantified by using the saturation state (SI) of the mineral in order to calculate the Gibbs free energy of the reaction (ΔG_r kJ/mol).

$$\Delta G_r = \frac{R \times T \times 2.303 \times SI}{1000} \qquad \textit{Equation 5.4}$$

Where R is the gas constant and T is the temperature in K

A dissolution reaction will become dependent on the saturation state of the reactants at ΔG_r values of 0 to -10kJ/mol for basalt glass and ΔG_r values of 0 to -20kJ/mol for forsterite (FLAATHEN and GISLASON, 2007). The braking effect of saturation state on

dissolution rate can be quantified using the following simplified equation to calculate the affinity term:

$$\text{Affinity term} = \left(1 - \exp^{\left[\frac{\Delta G_r}{\sigma RT}\right]}\right) \qquad \textit{Equation 5.5}$$

Where ΔG_r is the Gibbs free energy of reaction, R is the gas constant and T is the temperature (K). σ is Temkins stoichiometric constant and is the ratio of the mineral stoichiometry and the stoichiometry of the activated complex (Oelkers 2001). For basalt glass this value is 1, for forsterite this value is 2.

Equation 5.5 applies to multioxides whose chemical formula has been normalised to the formation of one rate-controlling precursor complex (OELKERS, 2001b). In the experiment FO3 (at 25°C pH10) forsterite has moved from a ΔG_r of around -50 to -15kJ/mol, the increase in concentration causing the dissolution of forsterite to change from being saturation state independent to its saturation state causing a slowdown in the dissolution rate by ~5%. In FO5 (at 25°C and pH11) the pH is greater and forsterite is more stable in solution, consequently the ΔG_r is greater than in FO3 (between -18 and -10kJ/mol) and dissolution of forsterite slows by between 3 and 13%. At 75°C the equilibrium constant (K_{eq}) for forsterite changes as expressed below in Equation 5.6:

$$K_{forsterite} = 2\log\left(\frac{a_{Mg^{2+}}}{a_{H+}^2}\right) + \log a_{H_2SiO_4} \quad = 28.29 \text{ at } 25^\circ\text{C} \qquad \textit{Equation 5.6}$$

$$= 23.19 \text{ at } 75^\circ\text{C}$$

Because $K_{forsterite}$ is lower at 75°C it means that a solution with a given activity of Mg^{2+} and a given pH will be closer to equilibrium at 75°C than at 25°C. However the increase in temperature also acts to lower pH which in turn lowers saturation states; as a

result the dissolution rate of forsterite at 75°C slows down by between 5 and 22% which is comparable with the affect of saturation state at 25°C.

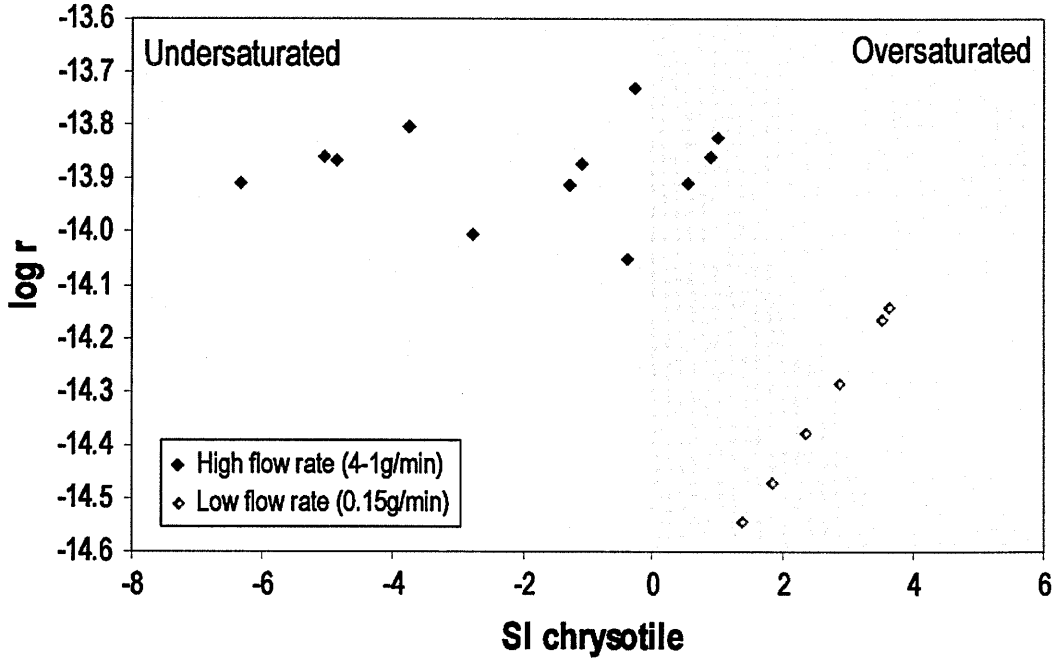

Fig. 5.17 – A graph showing the relationship between the dissolution rate of forsterite (log R) versus the saturation index of solution at different flow rates during experiment FO3 (25°C, pH10).

The use of PHREEQC to obtain saturation state data shows that secondary mineral formation is likely in many of the precipitation experiments, both at 25°C and 75°C. Together with evidence from element concentrations and Mg:Si ratios this strongly implies that the reason for the slowdown in dissolution rate at low flow rates is that secondary minerals have formed and removed Si and Mg from solution. This can be illustrated by plotting the saturation index of a secondary mineral such as chrysotile versus R (Fig. 5.17). The results show that solutions with a higher SI with respect to chrysotile have slower dissolution rates, supporting the suggestion that secondary mineral formation is causing in an apparent change in dissolution rate. For this reason it is assumed that the dissolution rates at pH 10 and 11 obtained with flow rates of ~0.2g/min are not accurate, despite being similar to the rates published by Pokrovsky & Schott (2000) (Fig. 5.18).

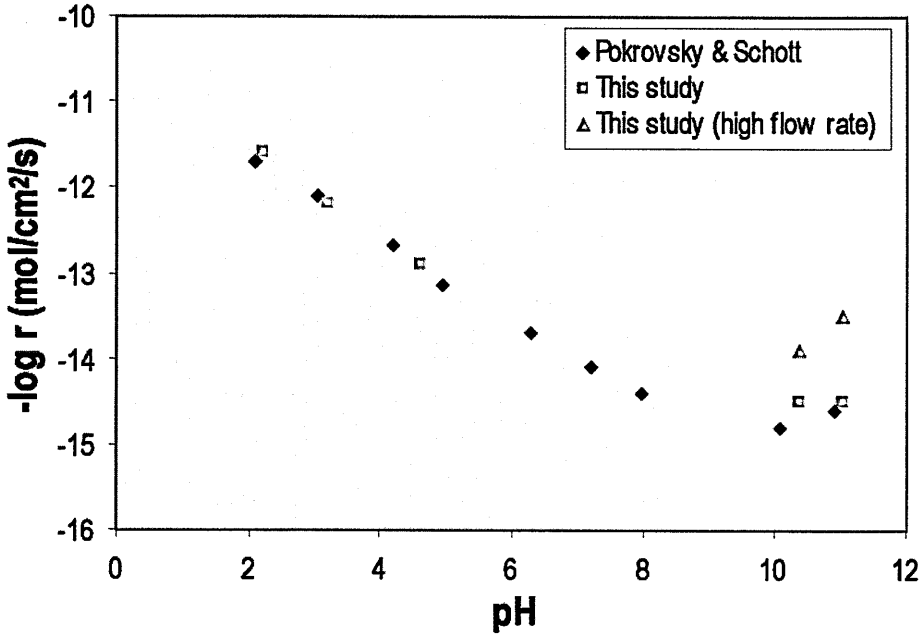

Fig. 5.18 – A comparison of forsterite dissolution rates obtained in this study with those obtained in similar experiments by Pokrovsky & Schott (2000). Also plotted are the results of experiments conducted in this study at high pH, with a high flow rate.

The dissolution rates gained at higher flow rates should, in theory, be more accurate as the solutions are further away from equilibrium. However, it is uncertain whether the systems had attained a steady state; the compositions of the experimental solutions at higher flow rates were not stoichiometric. The fact that the Mg:Si ratios were lower than 1.8 (Fig. 5.13) show that Si was still being preferentially lost, thus Si concentrations would give a dissolution rate that is greater than normal. Even so, solutions from experiment FO3 (pH10) were approaching stoichiometric Mg:Si ratios and the dissolution rate over the first 130 hours remained relatively constant (Fig. 5.6). While the calculated dissolution rate may be an overestimate it is likely to be more accurate than the rates calculated at the end of the experiment where Si has been removed from the system. In FO5 (pH11) inlet rates of 3g/min were maintained for only 24 hours, thus steady state dissolution was almost certainly not attained. Over the 24 hour period the dissolution rate was relatively stable and always faster than

dissolution rates at pH10. However it is unclear how much the dissolution rate may change as the system establishes stability over a period of 200 hours or more.

While these data suggests that the dissolution of forsterite at both pH10 and pH11 is faster than literature rates the fact that the Mg:Si ratios were non-stoichiometric means that steady state, far from equilibrium dissolution was not attained and consequently these results cannot be considered to be reliable. Quantifying the dissolution rate of forsterite was not the primary purpose of this study and more experiments are needed in order to confirm the behaviour of forsterite at high pH. These experiments should run at pH 9-12 with as high a flow rate as possible and the system should be undisturbed for at least 200 hours in order to make sure that it is at a steady state. Such experiments would verify whether the dissolution rates obtained here at high flow rates are accurate and whether the dissolution rate of forsterite continues to decrease as pH increases from 9 to 12 as stated in Pokrovsky & Schott (2000) or whether there is an increase in dissolution rate at high pH as previously proposed by Blum and Lasaga (1988) and Wogelius and Walther (1991). The results from the high flow rate solutions provide support for the latter (Fig. 5.18).

5.4.2.4. Lithium isotope behaviour

During the precipitation experiments the Li isotope composition of the solutions became increasingly heavy. This behaviour contrasts with that of the dissolution experiments where the Li isotope compositions of the solutions remained relatively constant and similar to that of the dissolving forsterite ($\delta^7Li \approx 2‰$). The fact that the solutions are isotopically heavy suggests that ^7Li is preferentially lost into solution, consistent with previous work on weathering in natural waters (HUH et al., 2001; KISAKUREK et al., 2004; PISTINER and HENDERSON, 2003; SEYFRIED et al., 1998). The

enrichment of ^{7}Li in solution is usually attributed to the preferential retention of ^{6}Li during secondary mineral formation and/or by adsorption onto clays. The simplest explanation for the Li composition of the fluid phase becoming isotopically heavy is that the mineral preferentially loses ^{7}Li into solution when it dissolves. However this hypothesis can be discounted for two reasons; a) the isotopic composition of the fluid in the dissolution experiments is similar to the composition of the dissolving mineral, and b) the mineral phase at the end of the experiments has a $\delta^{7}Li$ composition that is indistinguishable from that of an unaltered sample.

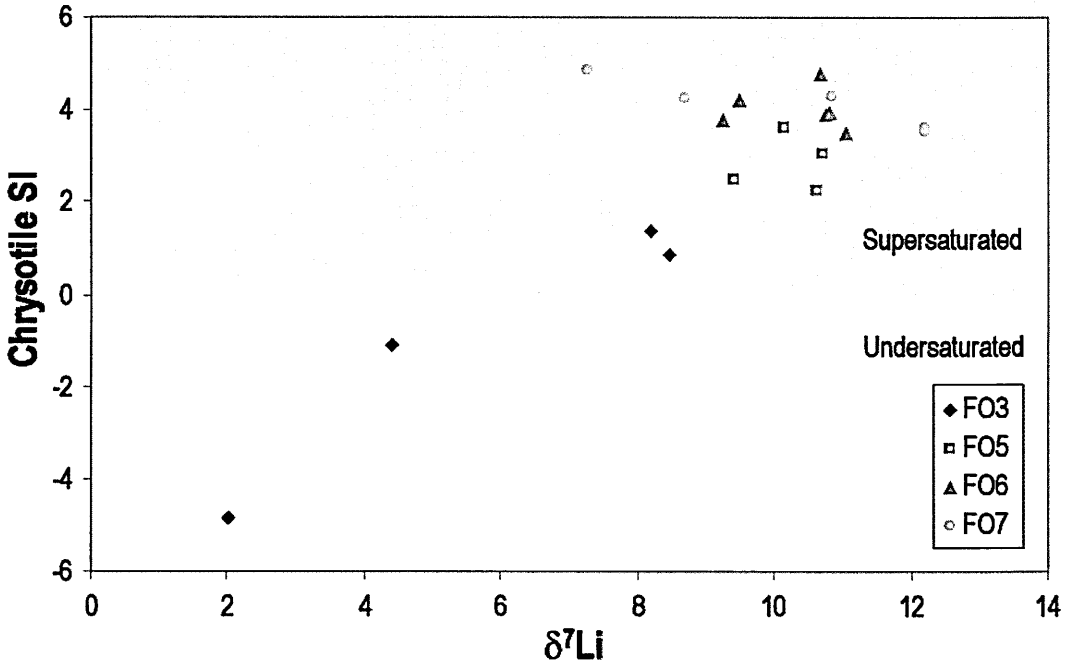

Fig. 5.19 - A graph showing the saturation indices of chrysotile vs the $\delta^{7}Li$ (‰) composition of the solutions

The only difference between the dissolution and precipitation experiments was that the latter were set up to run at near to equilibrium conditions so that the precipitation of secondary minerals was encouraged. If the behaviour of Li is compared with mineral saturation for all four precipitation experiments (as in Fig. 5.19 for

chrysotile), then this shows that as the mineral saturation increases the δ^7Li composition of the solution also increases. Analysis of the end-forsterite sample indicates that it is compositionally similar to or slightly heavier than the unaltered forsterite. Thus, in order to satisfy the mass balance there must be a solid present with a Li isotope composition of <2‰. That the molar ratios of Mg:Si have also decreased throughout the course of the precipitation experiments suggests that if a secondary mineral has formed it is chrysotile. This can only be unambiguously confirmed by analysis of the solid phase by SEM. However, initial analysis by SEM has been unable to show evidence for secondary mineral formation associated with the forsterite grains. The problem is that the mass of any secondary mineral that has precipitated is likely to be very low. The change in solution chemistry during FO3 can be used to predict just how much chrysotile may have formed by using the change in dissolution rate (Fig. 5.6) to calculate just how much Si may have been removed from solution. In this case the amount of Si that has been removed is ~0.14mg which equates to ~0.7mg of chrysotile which is ~0.007% of the total mass of forsterite in the reactor (10g). Such a small mass would be difficult to identify, even by SEM.

5.4.2.5. Magnesium isotope behaviour

The Mg composition of the San Carlos forsterite is -0.26‰; in comparison the results from the precipitation experiments show that the solutions are initially isotopically light, and become isotopically heavy with time. The evidence presented in this discussion from solution stoichiometry and Li isotope data implies that secondary minerals have formed, although the identity of the secondary phase has proven to be elusive. The use of nitrogen gas to prevent CO_2 dissolving into the solution should prevent the formation of carbonates. This leaves the formation of silicate minerals or metal oxides to be the

most likely cause of the changes in solution composition with time. As the concentration of both Mg and Si decrease with time it seems likely that both are incorporated in the formation of a new mineral. The sense of fractionation observed here, where the light isotope of Mg is preferentially incorporated into the secondary phase is the opposite to that observed by Tipper et al. (2006) who consider that the heavy isotope of Mg is retained in soils and secondary minerals leaving the dissolved phase to be isotopically light. This interpretation is based on results from rivers in the Himalayas where the composition of the river water is ~1.1‰ lighter than that of the source rocks. However, in a more recent study it was found that soils with an increasing clay content (dominantly allophane) possessed systematically lighter Mg isotope compositions, suggesting that, at least, some secondary minerals preferentially incorporate the light isotope of Mg (POGGE VON STRANDMANN et al., 2008). Furthermore, in both this study of Icelandic rivers (POGGE VON STRANDMANN et al., 2008) and another on Himalayan rivers (KISAKUREK et al., 2005), waters were found to possess Mg isotope compositions both lighter and heavier than the bed load or suspended load, suggesting that fractionation may occur in both senses. Work of Galy et al. (2002) showed that during carbonate precipitation as a speleothem the drip water is isotopically heavy relative to the speleothem, whereas in another study of the Mg composition of coral and foraminifera also show that the light isotope is preferentially incorporated into their shells (CHANG et al., 2004). Overall, these studies suggest that the Mg isotope system appears to behave in a less predictable manner than for example Li isotopes, where it is always the light isotope that is preferentially incorporated into secondary minerals irrespective of the type of mineral that is forming. Carbonate formation in these reactors is unlikely but not impossible; flow rates during the experiment are very low (down to 0.2ml/min) and the reacting solution travels through

plastic tubing to enter the reactor. There may be time for some CO_2 to dissolve into solution through the tubing, and the high pH (10-11) means that H_2CO_3 would dissociate to CO_3^{2-}. While this could account for the drop in Mg concentration by formation of $MgCO_3$, it cannot explain the accompanying fall in Si concentration. It is far more likely for the secondary mineral forming being a Mg silicate, and if so these results suggest that secondary Mg silicate minerals incorporate preferentially the light isotope of Mg.

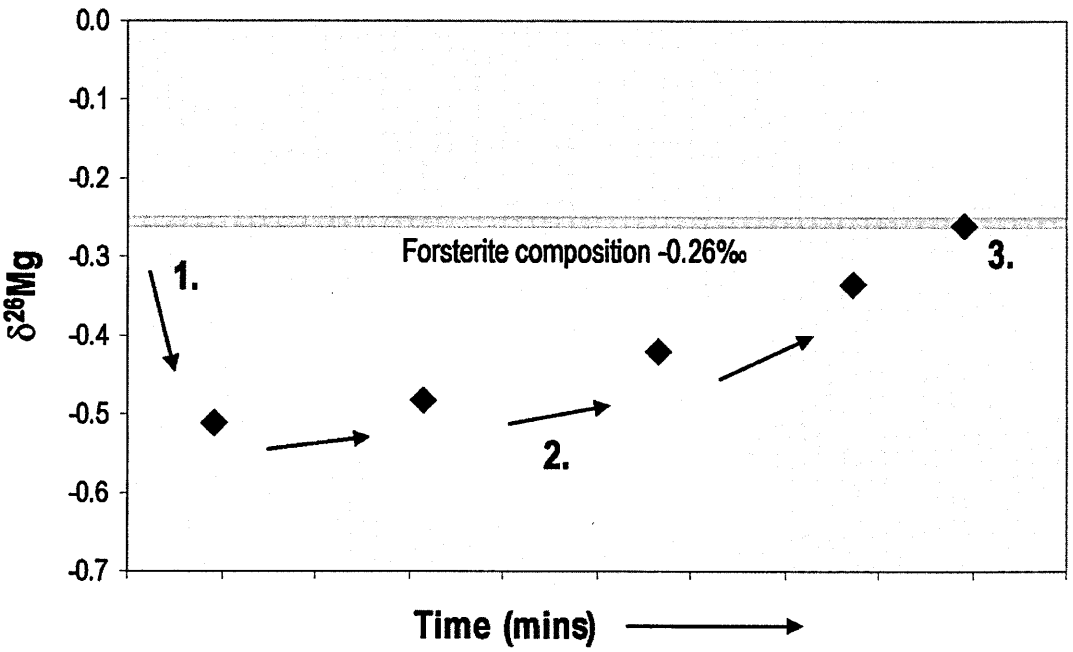

Fig. 5.20 - A diagram showing the theoretical evolution of the magnesium isotopic composition of the dissolved phase during the dissolution of a mineral grain. The fluid develops light Mg isotope ratios relative to the dissolving forsterite as it begins to dissolve (1), as inferred from results of the dissolution experiments. As the mineral continues to dissolve mass balance requires the solution to become isotopically heavier (2) and eventually as the entire mineral dissolves the composition of the fluid will match that of the dissolving mineral (3).

There is one other possible explanation for the behaviour of Mg isotopes observed in this study that is linked to the process of dissolution. During dissolution the isotope composition of the solution becomes lighter with time, but this cannot continue

at conditions far from equilibrium. If the entire mineral was to dissolve then the solution has to have the same composition as the dissolving mineral (see Fig. 5.20) and so mass balance dictates that the mineral must at some point release isotopically heavy Mg. If it is a question of time then the precipitation experiments are on average three times longer than those carried out at far from equilibrium. It is possible that the progression to increasingly isotopically heavy fluid is a result of an initial loss of light Mg and the reestablishment of the system towards congruent loss of Mg. However a major difference between the experiments at far-from and near-to equilibrium are the varying dissolution rates; between pH 2-4 the dissolution rate of forsterite is around 2 orders of magnitude faster than at pH 10 and 11 (POKROVSKY and SCHOTT, 2000). For this reason the total amount of forsterite dissolved at high pH should be much lower than that at low pH despite the experiments lasting for much longer. Taken together with evidence that secondary mineral formation has occurred (from solution chemistry and Li isotopes), and that Mg isotope fractionation is associated with secondary mineral formation (GALY et al., 2002; TIPPER et al., 2006b) it is most likely that this trend towards isotopically heavy Mg is caused by preferential uptake of light ^{24}Mg into secondary phases.

5.5. Implications for natural systems

The results of the dissolution experiments have implications for the way we interpret how Li and Mg isotopes behave in the natural environment. In Chapters 3 and 4 these isotope systems were analysed in rivers from Greenland. In the laboratory the Li isotope composition of fluid at far from equilibrium is similar to the composition of the dissolving mineral; there is no fractionation associated with dissolution. On the other hand precipitation of secondary minerals causes preferential uptake of ^{6}Li from solution.

The Greenland rivers illustrate the control of secondary mineral formation on the Li composition of the dissolved load. The most dilute river with the lowest amount of secondary mineral formation (GR3) has the Li isotope composition that is closest to that of the bulk rock. The non-glacial rivers are more concentrated and have probably experienced the highest level of secondary mineral formation, hence their dissolved Li compositions are most fractionated from the bulk rock. Although the story is complicated by subglacial processes, it is still true that the primary control on Li isotope composition is secondary mineral formation.

The magnesium system is more complicated than that of lithium; magnesium fractionates differently during the formation of carbonates and silicates, and is affected by biology. If secondary mineral formation is the dominant control over the Mg system (as is the case for Li) then the precipitation experiments suggest that rivers with more secondary mineral formation should have higher δ^{26}Mg ratios, and rivers should have a δ^{26}Mg composition that is close to or heavier than the bedrock. However this is not the case in the Greenland rivers. Instead all dissolved phases are isotopically light relative to the bedrock. This evidence suggests that a) secondary mineral formation is not the dominant process in the Greenland rivers or b) any secondary mineral formation is fractionating magnesium in the opposite sense to that observed in the laboratory.

The major control over the magnesium isotopes in Greenland is the chemical weathering intensity and the incongruent dissolution of trace phases such as carbonates (see Chapter 4). Thus the experimental work has little relevance to this natural system. In regions that are controlled by weathering process the experimental work may be more relevant. However, because magnesium behaves differently depending on the secondary mineral that is forming, characterisation of the secondary phase is essential.

Without this information it is impossible to apply experimental results to natural studies concerning the behaviour of magnesium isotopes.

5.6. Conclusions

The results of these laboratory experiments have implications for the interpretation of Li and Mg isotope data in natural waters. The behaviour of Li isotopes is consistent with previous experimental work (PISTINER and HENDERSON, 2003) and with predictions from the study of the different riverine phases; suspended sediment that is enriched in secondary minerals is always isotopically lighter than the bedload of a river (HUH et al., 2001; KISAKUREK et al., 2005; POGGE VON STRANDMANN et al., 2006). One question that had not been answered was whether individual mineral phases dissolve congruently. Experimental work involving the dissolution of whole rocks suggests that minerals do dissolve congruently with respect to Li (PISTINER and HENDERSON, 2003), and the results from this study support this hypothesis.

While the results of Li analyses confirm established understanding the behaviour of the Mg isotope system is more complicated. Unlike Li, which fractionates from solution in the same sense for all secondary minerals, the response of Mg appears to be dependent on the mineral type (GALY et al., 2002; TIPPER et al., 2006a). An aim of this study was to precipitate Mg silicate minerals by dissolving forsterite at near to equilibrium conditions. Previous studies suggest that silicate formation should cause the heavy isotope of Mg to be incorporated into new minerals (TIPPER et al., 2006b), while carbonate incorporates the light isotope (GALY et al., 2002). In practise the results of this study show that the light isotope of Mg is preferentially lost during the dissolution of forsterite, and that during secondary mineral formation the light isotope is preferentially incorporated leaving the solution isotopically heavy. The most likely

secondary phase to have formed is a Mg silicate mineral. If so then this suggests that different silicate minerals incorporate different compositions of Mg. The results highlight the present difficulties in interpreting variations in Mg isotopes in natural systems because, in addition to fractionation caused by primary mineral weathering and the formation of secondary phases, natural waters (in soils and rivers) will also be affected by removal and fractionation accompanying biomass activity, in soils and vegetation. More research into the behaviour of Mg isotopes during weathering processes in the laboratory and natural environments is needed to fully understand the way that this system behaves.

Chapter 6

The dissolution of basalt glass and forsterite in seawater

6.1. Introduction

Chapter 1 describes the weathering of Ca-Mg silicates and the associated drawdown of CO_2 that helps to control climate over geological timescales. While the weathering of Ca-silicates directly removes atmospheric CO_2 via the formation of $CaCO_3$ in the oceans the link between weathering of Mg-silicates and CO_2 is only indirect. In the modern oceans the formation of dolomite is unimportant; instead Mg in solution exchanges with Ca in mid ocean ridge basalts and in detrital sediments. This process is thought to be so efficient that it is thought by some that there is an indirect link between Mg-silicate dissolution and CO_2 drawdown (GISLASON et al., 2006).

Basalts are among the most easily weathered crystalline silicate rocks (DESSERT et al., 2003), they are mostly comprised of plagioclase and pyroxene but may also contain a significant proportion of the Mg-rich olivine, forsterite, which is one of the most readily weathered rock forming minerals (BRANTLEY, 2003). The ease of weathering of mafic minerals and glass means that chemical erosion rates are high in basaltic regions. For example rates of erosion in SW Iceland, Reunion and the Deccan Traps range between 20 and 170t/km^3/yr (DESSERT et al., 2001; GISLASON et al., 1996; LOUVAT and ALLEGRE, 1997). In comparison, chemical erosion rates in mixed silicate terrains such as the Congo (GAILLARDET et al., 1995), Amazon (GAILLARDET et al., 1997) and Ganges (SUMMERFIELD and HULTON, 1994) are generally lower (0.6-42t/km^3/yr). Rates of CO_2 consumption are also high in basaltic regions ranging from

0.3×10^6mol/km^2/yr in the Massif Central (NEGREL and DESCHAMPS, 1996) to 6.4×10^6mol/km^2/yr in Java (DESSERT et al., 2003). Such is the susceptibility of basalt to weathering that the emplacement of large igneous provinces like Columbia River may have caused an increase in the global level of CO_2 drawdown of up to 2% over a period of ~3 million years (TAYLOR and LASAGA, 1999).

It is not just on the continents that the weathering of basalt has important consequences for long term climate change. Low temperature alteration of calcium bearing silicates in basalt, and of basalt glass itself, in seawater are estimated to release as much calcium to the oceans as continental weathering (BRADY and GISLASON, 1997; STAUDIGEL et al., 1989). Much of this alteration takes place at mid ocean ridges and on the ocean floor; however rivers also transport around 20,000 million tonnes of sediment from the continents to the oceans per year (HAY, 1998; MILLIMAN and SYVITSKI, 1992) which may experience continued weathering in the oceans. Not all of this material will simply be buried, as deltas and estuaries can act as fluidised bed reactors that are driven by riverine input, with tides extensively reworking this sediment over a timescale of hundreds to thousands of years (ALLER, 1998; ALLER and BLAIR, 2004). If such reworking is common then the continued weathering of continentally-derived sediment in the oceans is likely to affect the chemistry of seawater. It has been suggested that high relief volcanic and tectonically active islands provide ~45% of this flux of river suspended sediment, much of which consists of basaltic glass (GISLASON et al., 2006; MILLIMAN and SYVITSKI, 1992). For Icelandic rivers, Gislason et al. (2006) estimated just how much calcium could be delivered to the oceans via suspended material (mostly basalt glass) versus the volume delivered in the dissolved load. This study showed that a combination of ion exchange on clays (Ca for Na), diffusive flux from ocean sediments, and dissolution of suspended Ca-bearing silicates could supply enough Ca to

match the dissolved Ca flux. Furthermore, because the flux of suspended Ca is more dependent on changes in river runoff (and hence climate) than dissolved Ca then the suspended load may have a stronger link to CO_2 drawdown than the dissolved load (GISLASON et al., 2006). Clearly the interaction of detrital sediment with seawater could affect the chemistry of the oceans and the behaviour of rock types such as basaltic glass that are susceptible to dissolution in seawater is particularly important to characterise.

Natural glasses comprise ~12% of the average exposed continental crust (NESBITT and YOUNG, 1984) and over one billion cubic metres of volcanic glass is produced each year, mostly as basalt glass along the mid ocean ridge system (WOLFF-BOENISCH et al., 2004). Natural glasses are less stable than crystalline igneous minerals at the Earth's surface partly because the glass retains more of the energy from the parent magma (GISLASON and ARNORSSON, 1993; GISLASON and EUGSTER, 1987a; WOLFF-BOENISCH et al., 2006; WOLFF-BOENISCH et al., 2004). Basalt glass dissolves over an order of magnitude faster than crystalline basalt at pH 9-10 (GISLASON and EUGSTER, 1987b) and volcanic glasses of rhyolitic to basaltic compositions dissolve a factor of 1-2 faster than crystalline rocks of the same composition at 25°C and pH4 (WOLFF-BOENISCH et al., 2004). Basalt glass also enhances the flux of mobile elements by 2-5 times where present in river catchments in Iceland (STEFANSSON and GISLASON, 2001). The high reactivity of basalt glass, both on the continents and potentially in the deep ocean (at mid-ocean ridges) suggests that its dissolution may have a significant affect on seawater chemistry, and may also have some impact on the drawdown of atmospheric CO_2 over long time periods. Similarly on the scale of an individual mineral the high reactivity of forsterite olivine, coupled with its commonly high abundance in basalts and ultramafic rocks, suggests that the dissolution of this mineral may exert a disproportionate influence on seawater, which it is important to quantify.

There are many experimental studies involving the dissolution of basalt glass and forsterite at far from equilibrium conditions (CROVISIER et al., 1987; GISLASON and OELKERS, 2003; OELKERS, 2001; OELKERS and GISLASON, 2001; POKROVSKY and SCHOTT, 2000; TECHER et al., 2001; WOGELIUS and WALTHER, 1991; WOGELIUS and WALTHER, 1992; WOLFF-BOENISCH et al., 2006; WOLFF-BOENISCH et al., 2004) so the rate and mechanism of dissolution of these phases have been deduced for a range of pH, temperature and solution chemistries. Experimental studies involving the low temperature dissolution of basalt glass or forsterite in seawater are less common. Crovisier et al. (1987) used both natural and artificial basalt glass to estimate its dissolution mechanism and rate of dissolution in seawater. However, because this study focussed on the altered layer (palagonite) that develops on the glass they were performed on centimetre sized pieces of glass, rather than the powdered samples that are more usually used, and this difference in the available surface area makes direct comparison of dissolution rate difficult. Brady & Gislason (1996) undertook dissolution experiments using unaltered pillow basalt in artificial seawater at low temperature (between 25 and 50°C). They obtained a dissolution rate for such basalt of 4.47×10^{-15} moles/cm^2/s at 25°C. In comparison the dissolution of basalt glass in pH8 freshwater solutions is ~7.4×10^{-15} mol/cm^2/s (GISLASON and OELKERS, 2003). Studies of olivine dissolution in seawater are rarer still and confined to dissolution at higher temperatures (BERGER et al., 1988) representative of hydrothermal conditions. Therefore the principal aim of this study is to assess the dissolution rate of basalt glass and forsterite in seawater with particular emphasis on comparing the results here with those obtained for freshwater solutions.

While the low temperature interaction of basalt glass with seawater has been poorly studied, even less is known about how isotope tracers of continental weathering

such as the magnesium and lithium isotope systems might behave. These are both stable isotope systems that have been shown to fractionate by mass during weathering processes (HUH et al., 1998; TIPPER et al., 2006a). In the case of magnesium the seawater composition ($\delta^{26}Mg$ = -0.82‰) is largely controlled by continental input with subsequent removal of Mg by carbonate precipitation and exchange with oceanic basalts and detrital sediments. The global average isotope composition of the dissolved flux carried by rivers is -1.09‰ (TIPPER et al., 2006b) and rivers are thought to be the most important source of magnesium to the oceans. The offset between seawater and riverine Mg isotope compositions must mean that either the oceans are not at a steady state with respect to Mg or that fractionation is occurring during removal of Mg from seawater. The lithium isotope composition of seawater ($\delta^{7}Li$ = 31‰) is maintained by inputs of hydrothermal fluids at mid ocean ridges ($\delta^{7}Li$ = 6.7‰) and dissolved lithium from rivers ($\delta^{7}Li$ = 23‰) (HATHORNE and JAMES, 2006). Seawater is isotopically heavier than its sources because secondary mineral formation preferentially removes ^{6}Li from solution. Because materials like basalt and basaltic glass are so common in the oceans (on the seafloor and as products of continental weathering), and are relatively reactive, their interaction with seawater is likely to have a significant and measurable effect on the behaviour of isotope systems like Li and Mg. This work should help to shed some light on how the processes of dissolution, ion exchange and secondary mineral formation can affect the Li and Mg isotope composition of seawater.

6.2. Method

The seawater experiments were performed on basaltic glass and forsterite, the basalt glass used was identical to that used by Gislason & Oelkers (2003) while the forsterite was similar to that used by Pokrovsky & Schott (2000) (that is, the same as that used in Chapter 5). A detailed description of the composition and preparation of both mineral phases are given in Section 2.6.1, and the experimental technique is explained in Section 2.6.3. The seawater experiments were carried out using one litre polypropylene batch reactors, at temperatures between 4 and 25°C. The seawater was taken from the North Atlantic (STEFANSDOTTIR and GISLASON, 2005) and from the Southern Ocean (JONES and GISLASON, 2008). All seawater was filtered and then irradiated using UV radiation prior to experimentation. Basalt glass and forsterite sample size varied from between 10 and 30g in each reactor and temperature was regularly monitored, with fluctuations of ± 0.2°C. Samples (of ~40ml) were taken by pumping solution out of the reactors, each sample was filtered and subsequently pH was measured. At the end of the experiments a sample was taken to measure alkalinity and the glass and minerals were drained and collected.

Element concentrations in solution were determined by ICP-AES at the Science Institute in Reykjavik and by ICP-MS at the Open University (see Section 2.5.1.2). The high concentration of dissolved solids (~3.5% TDS) in seawater means that the sample matrix is very different to that of freshwater samples so a different set of standards was used. For the ICP-AES analyses in Reykjavik a seawater standard and a groundwater standard (Selsund 03) were used, whereas for the ICP-MS analyses at the Open University artificial seawater was prepared using pure salts partly following the method by Kester et al. (1978). The major constituents of this standard were NaCl, KCl and Na_2SO_4, other elements were added to this in the form of ICP standard solutions (1000ppm). The final standard TDS from the dissolved salts was ~2.9%.

Lithium and magnesium isotope ratios were determined by MC-ICP-MS and cation chromatography was used to purify the solutions, as described in Sections 2.4.2 and 2.4.3, respectively. Details of isotope analytical procedures, and the internal and external precision of the isotope measurements, are given in Section 2.5.2.

6.3. Results

6.3.1. Major elements

Experimental parameters and results of pH measurements are given in Appendix C10. Results of major element analyses and dissolution rates are given in Appendix C11, and changes in pH and Si concentration are plotted in Figs. 6.1 and 6.3. During all of the experiments the solution pH initially increased by between 0.1 (FOSW-1) and 0.5 pH units (BGSW-2). The pH then dropped from 7.9 to 7.69 over the first 40 days of the experiment and then rose steadily, reaching 8.18 at the end of the experiment at 270 days. This is illustrated in Figure 6.1 for experiment BG-SW1, but the same pattern is observed in all of the seawater experiments.

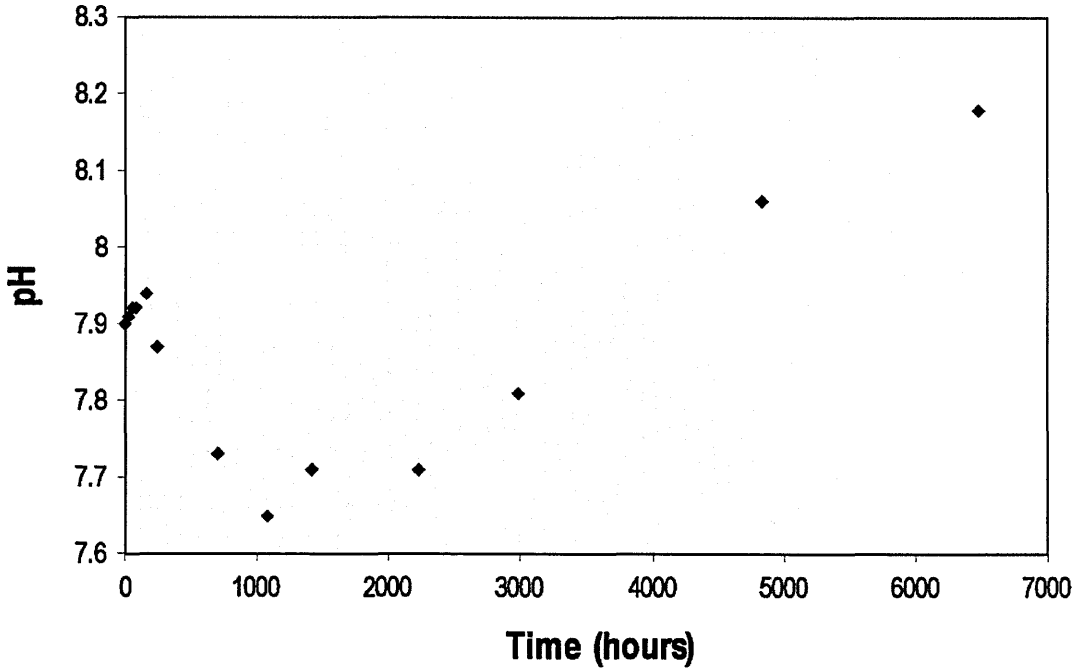

Fig. 6.1 - Change in solution pH with time during the dissolution of basalt glass in seawater (BGSW-1)

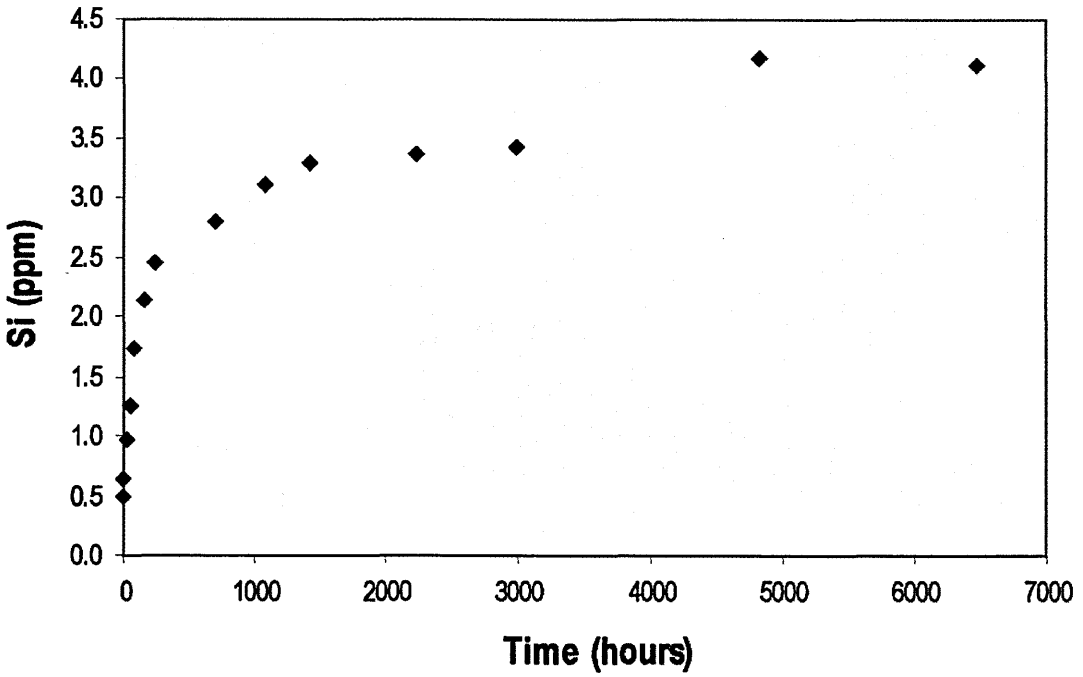

Fig. 6.2 - Change in the dissolved silicon concentration of the solution with time during the dissolution of basaltic glass in seawater (BGSW-1)

The initial alkalinity of the seawater was 2.19 meq/l for Atlantic seawater and 2.01 meq/l for Southern Ocean seawater. At the end of the experiments, alkalinities

ranged from 2.08 to 2.33 meq/l; the largest increase in alkalinity was measured in experiment BG-SW2 (0.25 meq/l).

Major element concentrations (Na, Ca, Mg and K) remained relatively constant throughout each experiment. On the other hand, the concentration of silicon in seawater is low (~0.5ppm) so any silicon released during basalt glass dissolution will make a significant difference to the overall concentration. Therefore, changes in silicon concentration have been used to estimate the dissolution rate of the glass.

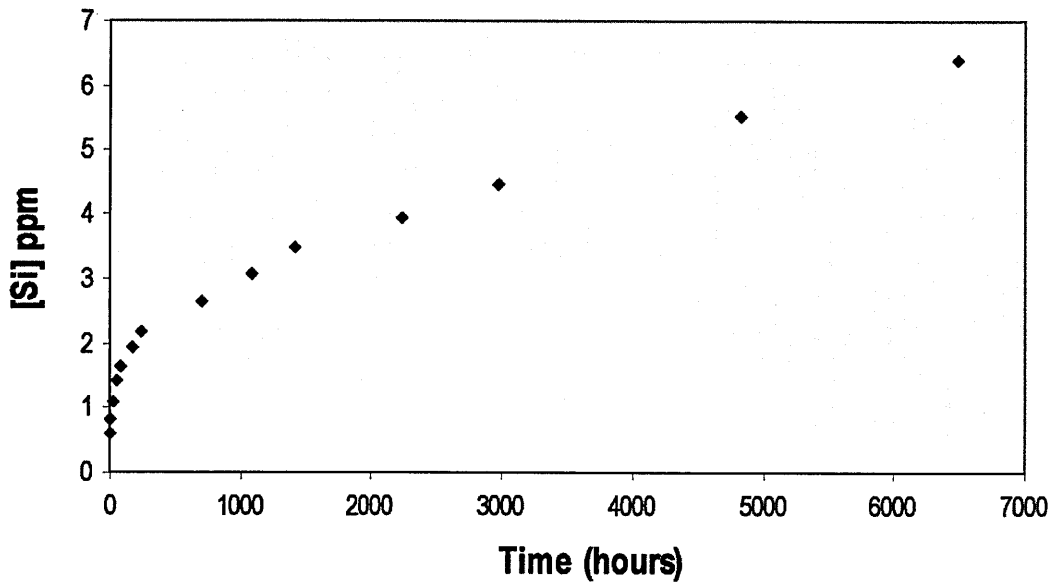

Fig. 6.3 - Change in the dissolved silicon concentration of the solution with time during the dissolution of forsterite in seawater (FOSW-1)

Results show that Si concentration increases with time (see experiment BG-SW1, Fig. 6.2). The increase in silicon during the dissolution of basalt glass is not linear. Dissolved silicon concentrations rise rapidly at the beginning of each experiment, slow after ~500 hours and reach a plateau at ~4000 hours. The dissolution of forsterite also begins with rapid release of silicon during the first 240 hours, but the increase in concentration of dissolved silicon becomes linear from that point on until the end of the experiment. Experiment BG-SW4 (using 30g of basalt glass) was the

experiment that attained a plateau in the rate of silicon release most rapidly, with a concentration of 4.4ppm reached after 700 hours. Experiment BG-SW5 (at 4°C) was run for the shortest length of time but over the 3000 hours it was running it reached a maximum Si concentration of 2.2 ppm. In comparison experiments at room temperature had Si concentrations of 3.4ppm (BG-SW1) and 3.5ppm (BG-SW2) after 3000 hours. The dissolution rate of forsterite is faster than that of basalt glass in the same way as seen in the freshwater experiments (Chapter 5) and illustrated by a dissolved silica concentration in FO-SW1 at 3000 hours of 4.48ppm (Fig. 6.3).

6.3.2. Lithium and lithium isotopes

The experimental solutions were analysed for both Li and Mg isotopes, the results of which are tabulated in Appendices C12.

Lithium concentrations remained constant throughout the experiments, staying at around 0.165ppm which is consistent with literature values of ~0.18ppm (CHAN and EDMOND, 1988).

Three experiments were analysed for Li isotopes; BGSW1, BGSW4 and FOSW1. These results show that in each experiment the Li isotope composition does not vary significantly from that of seawater (δ^7Li of ~31‰). The external reproducibility of the Li isotope measurements (2σ) is 0.84‰; the only experiment where the solution composition is statistically different from that of seawater is in BGSW1. Here the δ^7Li value remains constant (at around 31‰) up until BGSW1-K where there is a slight increase of ~0.5‰. After 4800 hours (BGSW1-M) the composition had increased to 32.4‰ (Fig. 6.4.).

During the measurement of solutions from FOSW1 the Nu-Plasma yielded a δ^7Li value of 30.6‰ for seawater. Samples FOSW1-A and FOSW1-I have similar δ^7Li values, while the δ^7Li value of FOSW1-M was slightly heavier at 31.1‰.

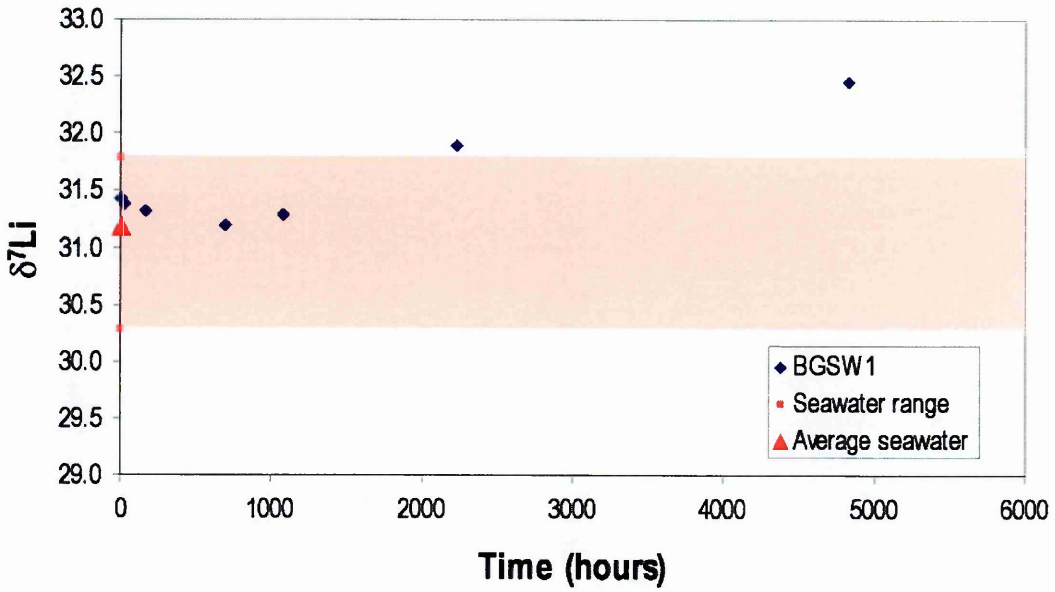

Fig. 6.4 - Change in the isotopic composition of dissolved lithium during experiment BGSW-1. The shaded zone is the range of IAPSO seawater lithium compositions measured during this part of the study.

6.3.3. Magnesium and magnesium isotopes

Magnesium concentrations are also constant throughout the experiments with the solutions having average Mg concentrations of 1280ppm ±25 (1σ).

The results of Mg isotope analyses also show that there is little variation from the seawater value. The Mg isotopes were measured in two stages; initially three experimental samples were analysed (BGSW1-A, D and G) and each sample was measured between 4 and 6 times so that an average isotopic composition could be calculated. The average composition of these samples was then compared to the average of seven IAPSO seawater standard measurements. Literature values for seawater are δ^{26}Mg of -0.82‰ (TIPPER et al., 2006b), the average composition of IAPSO seawater (n=7) in this initial study was -0.88 ± 0.04‰. In comparison the

experimental samples are on average within 0.06‰ of the seawater standard. The external reproducibility (2σ) during magnesium isotope analyses is 0.1‰ (calculated from 20 measurements of CAM-1). Therefore the experimental samples have $\delta^{26}Mg$ compositions that are within error of seawater.

All other samples were run at a later date; at this time the average composition of seawater was -1‰, and the compositions of the experimental solutions were again within error of this value.

6.4. Discussion

6.4.1. pH and alkalinity

Changes in pH in natural waters reflect either proton consumption during the weathering of silicate rocks or proton production during the dissolution of CO_2 into water, the formation of secondary –OH bearing minerals and biomass activity. Seawater pH is controlled by two buffering systems; on relatively short timescales it is primarily buffered by the carbonic acid system, while on longer timescales pH is regulated by ion exchange reactions between seawater and aluminium silicates (MARTIN, 1970; RILEY and CHESTER, 1971; SILLEN, 1967). As a result, the pH of seawater is relatively stable and rarely falls outside the range 7.8-8.2 except in restricted basins. However, in an experimental system holding only one litre of seawater, the buffering capacity is much more limited. The bicarbonate ion concentration in seawater is around 2.5×10^{-3}M; if just 3×10^{-3}moles of HCl is added to one litre of seawater it is enough to lower the pH to <6 (RILEY and CHESTER, 1971). In the present study the pH of the experimental solution rose from around 7.9 in the North Atlantic seawater and 7.7 in the Southern Ocean seawater to between pH 8 and pH 8.4. The rise in pH is due to

the dissolution of the reacting mineral/glass, a process which involves the consumption of protons (GISLASON and ARNORSSON, 1993; GISLASON and EUGSTER, 1987a; GISLASON and OELKERS, 2003). Nevertheless, the rise in pH is not continuous; there is an initial rise in pH over the first week, which is probably due to the removal of partially attached silica tetrahedra from the surface of the basalt glass or forsterite. These silica tetrahedra are initially abundant on the edges and sharp tips of the crystals (GISLASON and OELKERS, 2003; OELKERS and GISLASON, 2001; WOLFF-BOENISCH et al., 2004). After this rise there is a general decrease in pH possibly due to buffering by the carbonic acid system and/or precipitation of secondary minerals. Over time however the pH generally rises as the minerals continue to dissolve and the surface area of the minerals increases (because of an increase in surface roughness) as shown during extended basalt glass dissolution experiments (GISLASON and OELKERS, 2003).

Alkalinity should, in theory, also increase with time; one of the main sources of alkalinity is its production during the dissolution of silicate minerals, although it can also be consumed during the precipitation of secondary minerals. While two of the experiments show an increase in alkalinity (BGSW1 and BGSW2), this increase is small (up to 0.16mmol/l) and in the other experiments the alkalinity decreased by similar amounts. Taking the precision of the analyses into account, it thus appears that seawater alkalinity has remained relatively constant over the course of the 8 month experiments.

6.4.2. Major elements

The major cations Mg^{2+}, K^{+} and Ca^{2+} show little variation in concentration over time, remaining close to the average for North Atlantic seawater used in these experiments (STEFANSDOTTIR and GISLASON, 2005). In the freshwater experiments the solution

becomes enriched in the major cations with time. Data from Chapter 5 shows that during the dissolution of basalt glass the concentration of magnesium in solution can increase by over 5ppm. While the amount of magnesium that will enter solution is likely to be even more in seawater experiments (because they are run for a longer time and the system is closed) even if 50 mg of magnesium was to dissolve this would only constitute ~1% of the total Mg concentration in seawater. As a consequence any change in concentration linked to mineral dissolution is likely to be within the error of the analysis by ICP-MS. This problem does not affect the measurement of Si; seawater has a relatively low Si concentration (~0.5 ppm) hence any Si that is added to the system can be observed. The Si concentration initially rises rapidly (Fig. 6.1) due to the initial dissolution of crystal edges and partially attached silica tetrahedra (OELKERS and GISLASON, 2001). However the rate of release of Si then slows and the resulting Si concentrations do not exceed 4.6ppm in the basalt glass experiments and 6.4ppm in the forsterite experiments. This apparent slow down in the release rate of Si could be caused by the system reaching steady state with respect to the dissolving material or could be caused by Si being taken out of solution by secondary mineral formation. This will be discussed further in the following sections.

6.4.3. Dissolution rate

These experiments were performed in a closed system so that estimating the dissolution rate is difficult. This is because as the experiment (and time) progresses, more of the mineral dissolves and with successive samples being taken the remaining volume of solution will decrease. As a consequence the solution becomes more concentrated and the saturation state of the solution will change, increasing the potential for secondary mineral formation. These high concentrations also mean that dissolution of the primary

mineral may be inhibited by an increasing saturation state, and the precipitation of secondary phases. In either case the dissolution rate is no longer representative of the far from equilibrium dissolution rate, and is likely to be significantly slower than that rate.

The dissolution rate is calculated using the following equation:

$$R = \frac{Si_{out}}{(SA \times t)} \qquad \textit{Equation 6.1}$$

Where R = dissolution rate (mol/cm^2/s)
$Si_{(out)}$ = the total silicon in solution (mol)
SA = the BET surface area of basalt glass or forsterite (cm^2)
t = time (s)

The silicon out value must take into account the concentration of silicon and volume of solution in the reactor, but also has to account for the concentration of silicon and volume of solution that is removed. If not the final dissolution rate will be an underestimate.

Dissolution rates obtained using this equation are presented in Appendix C12. The dissolution rate of forsterite in seawater is faster than that of basalt glass, in agreement with the findings in Chapter 5 and dissolution rates obtained for the same two phases in the literature (GISLASON and OELKERS, 2003; POKROVSKY and SCHOTT, 2000). There are a range of dissolution rates, with log r for basalt glass between -12.7 and -16 and rates for forsterite between -12.1 and -15.1. Over time, the dissolution rate changes from initially high values before decreasing by 2 orders of magnitude over the first 1000 hours of the experiment and continuing to decrease by another half order of magnitude over the next 5000 hours (Fig. 6.5). This suggests that the system is

approaching a steady state and that the initial rapid dissolution rates are too fast to be representative.

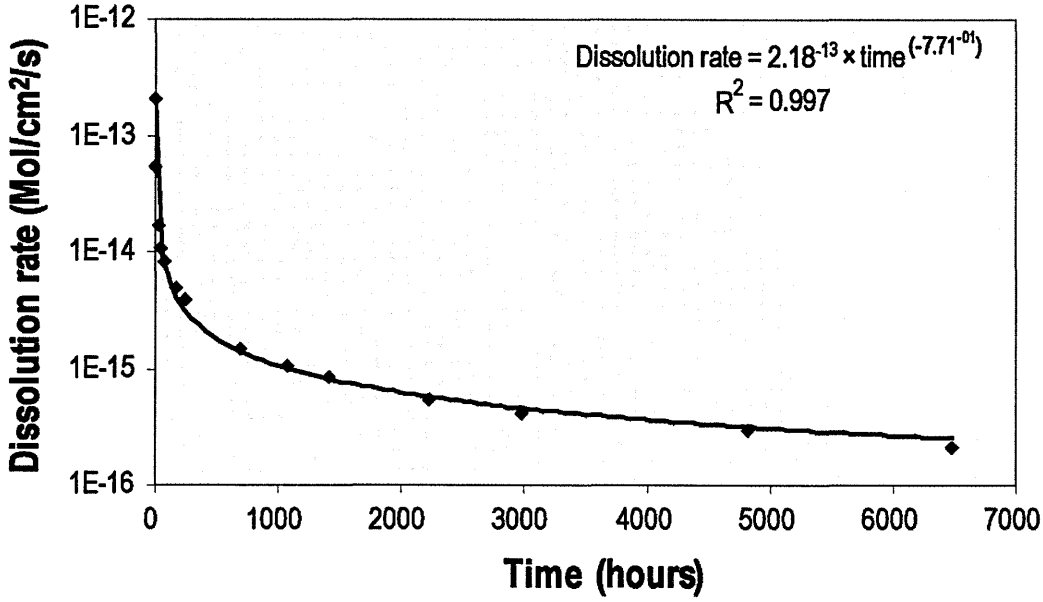

Fig. 6.5 - The dissolution rate of basalt glass during experiment BGSW-1

Dissolution rates often slow down in batch reactors for two reasons; firstly, there will be an initial rapid dissolution of ultrafine particles adsorbed on the larger grains and over time the grains become more rounded (this also applies to through flow reactors). Secondly, as the concentration in the solution increases the saturation state of the dissolving mineral changes so that it could inhibit dissolution, as discussed previously in Section 5.4.2.3 .

Although equation 6.1 can be used to show how the rate of dissolution changes with time it cannot be used to generate a dissolution rate that is representative of the mineral for the entire experiment. However, dissolution rate can be estimated by plotting the total silicon lost from the solution versus time (Fig. 6.6).

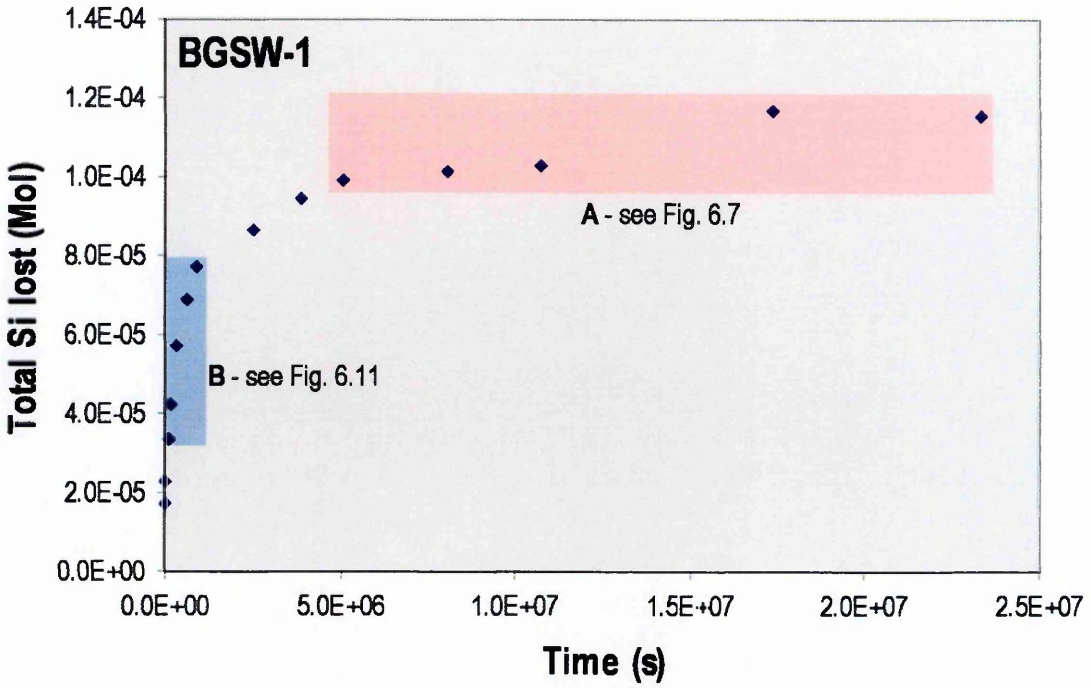

Fig. 6.6 - A graph showing the change in the total number of moles of dissolved silicon with time during experiment BGSW-1. Dissolution rates were estimated for two time periods. The first, Zone A, consists of 5 sample points at the end of the experiment where it is inferred a steady state has been reached. The second, Zone B, consists of 5 samples recovered in the early stages of the experiment. Dissolution rates estimated for zone A are described in 6.4.3. and those estimated for zone B are described in 6.4.5.

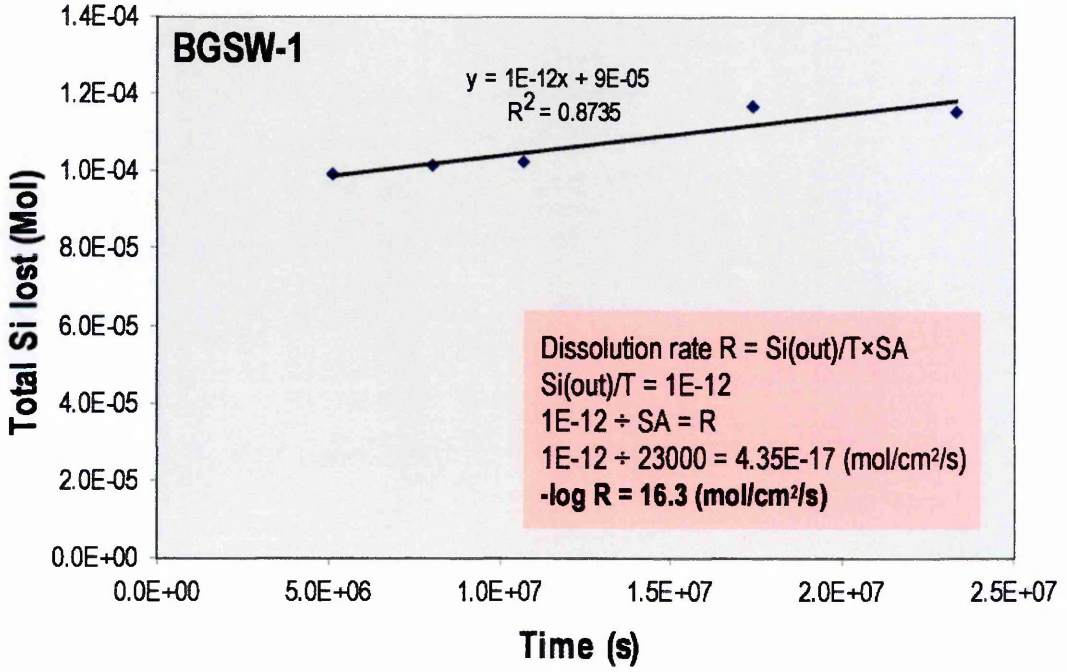

Fig. 6.7 - A graph using the last five sample points from BGSW-1 (see Figure 6.6, zone A) to calculate the dissolution rate based on change in silicon concentration

This is different from the silicon concentration of the solution because it is cumulative and takes into account the mass of silicon removed by sampling. As Fig. 6.6 shows the rate of silicon loss is initially rapid for the first 10 days and then the rate of release decreases until reaching a steady state after 59 days. By drawing a straight line through this steady state region (Zone A, Fig. 6.6) the dissolution rate can be estimated from the rate at which the silicon concentration increases (Fig. 6.7). This gives a dissolution rate (log R) of -16.3 mol/cm^2/s, in comparison the rate calculated by Gislason et al. (2003) in a freshwater solution at pH 8 and 25°C is -14.55 mol/cm^2/s, over one order of magnitude higher. The same calculation gives similar results for the dissolution of forsterite, the last five points show the system to be at steady state (Zone A, Fig. 6.8.), a straight line drawn through these points yields a dissolution rate (log R) of -15.4 (Fig. 6.9) in comparison to the rate calculated by Pokrovsky & Schott (2000) at pH8 and 25°C which is an order of magnitude higher at -14.4. These results show that by the end of the experiment the dissolution rates of both basalt glass and forsterite are slower than those measured in freshwater at the same temperature and similar pH. There are two possible reasons for this: a) high concentrations in the batch reactors are inhibiting the dissolution process, or causing formation of secondary minerals that alter the chemistry of the solution, or b) the seawater is inhibiting the dissolution process.

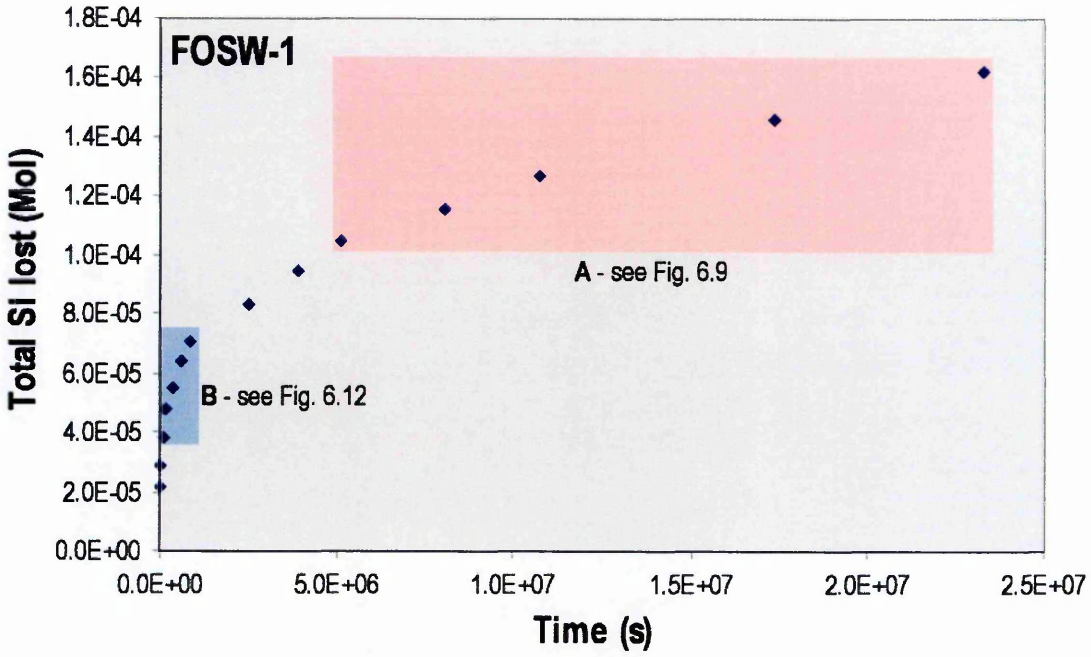

Fig. 6.8 - A graph showing the change in total number of moles of dissolved silicon with time during FOSW-1. Dissolution rates were estimated for two time periods. The first, Zone A, consists of 5 sample points at the end of the experiment where it is inferred a steady state has been reached. The second, Zone B, consists of 5 samples recovered during the early stages of the experiment. Dissolution rates estimated for zone A are described in 6.4.3 and those estimated for zone B are described in 6.4.6.

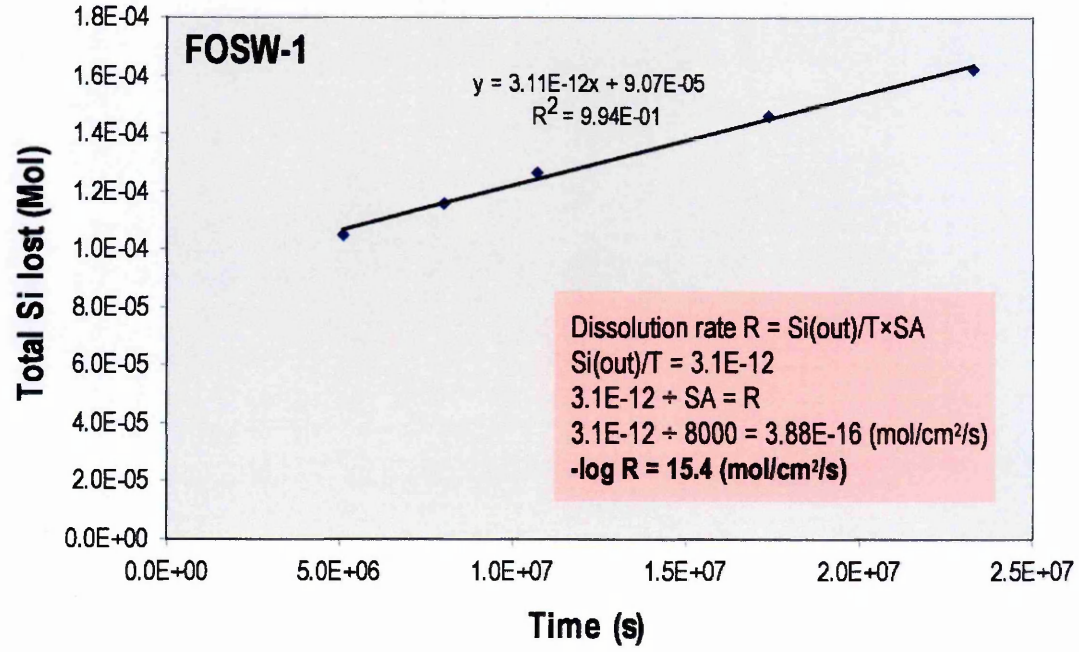

Fig. 6.9 - A graph using the last five sample points from FOSW-1 (see Figure 6.8, zone A) to calculate the dissolution rate based on change in silicon concentration

The first hypothesis is that the closed system causes build up of dissolved solids which in turn inhibits dissolution or promotes secondary mineral formation as described earlier in 6.4.3. Also by changing the saturation state of the dissolving mineral (i.e. the solution becomes more and more saturated) the dissolution rate can become saturation state dependent. The inhibiting effect of saturation state can be evaluated by calculating the affinity term (see Section 5.4.2.3). A dissolution reaction will become dependent on the saturation state of the reactants at ΔG_r values of between 0 and -10kJ/mol (FLAATHEN and GISLASON, 2007). In this case it will cause a slowdown in the forward reaction. In the current experiments modelling of the seawater saturation states (PHREEQC) and calculation of ΔG_r gives ΔG_r values that range from -18.5 to -10.7kJ/mol. Because the ΔG_r values are lower than -10kJ/mol they suggest that the impact of saturation state on dissolution rate is negligible. However, although saturation state itself does not appear to be inhibiting the dissolution of mineral phases this does not imply that secondary minerals have not formed.

6.4.4. Saturation state modelling

The saturation states of the solutions can be modelled by geochemical modelling software such as PHREEQC; further details of the modelling procedure are presented in 5.4.1.3 and results of the modelling are given in Appendices C13 and C14.

Saturation state modelling suggests that the fluid phase becomes supersaturated with respect to many secondary minerals during the seawater experiments. This is particularly true of clay minerals such as pyrophyllite, K-mica, illite and kaolinite (Fig. 6.10) which all become highly saturated. For example, over the course of the experiment, the saturation index of K-Mica changes from 2 to 8, while kaolinite is initially undersaturated (-1.1) but becomes oversaturated (reaching 3.2) over time.

Carbonate minerals such as calcite and dolomite are also oversaturated in solution although their saturation states do not change over the course of the experiments (as alkalinity remains relatively constant). High saturation states in seawater are unsurprising; seawater has a high solute content. The formation of silicate minerals is controlled by the relatively low concentration of aluminium and silicon in seawater. Thus, initially the saturation state of secondary minerals is low or undersaturated but as silicon enters the solution through the dissolution of basalt glass or forsterite the secondary mineral saturation state will rise. By the end of the experiments the dissolved silicon concentrations are at their highest level and saturation state modelling suggests that by this time the likelihood of clay formation is high. The formation of secondary minerals would then account for the "apparent" slowing of the dissolution rate by removing silicon from the solution.

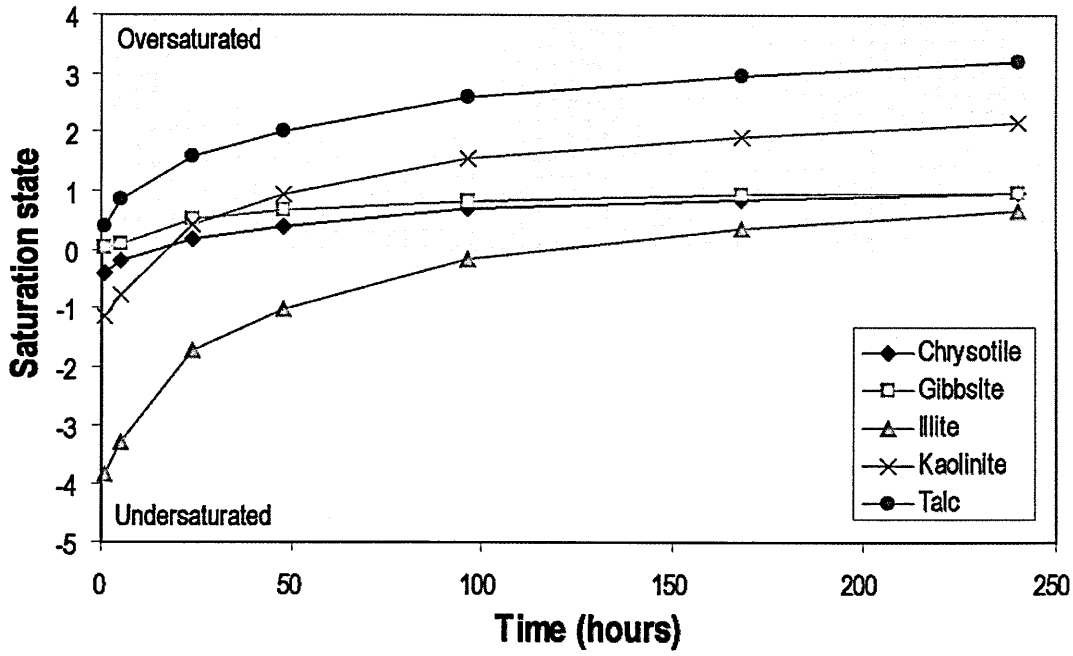

Fig. 6.10 - The change in saturation state with time for a selection of secondary minerals during experiment BGSW-1.

6.4.5. Inhibition by seawater

The second hypothesis is that seawater itself could cause a slowdown in the rate of dissolution; either because the high element concentrations in solution inhibit the hydrolysis reactions that cause the breakdown of basalt glass and forsterite, or because the high concentrations mean that the dissolution is always inhibited by the high saturation states. Experiments have been performed upon basalt glass using high concentrations of dissolved species such as Si and Al. The dissolution rate of basalt glass has the potential to be dependent on the concentration of these two elements because dissolution involves the removal of Al, then the removal of Si tetrahedra. Studies have shown that Si concentration has no effect on the dissolution rate, while Al can inhibit dissolution at low and high pH (OELKERS and GISLASON, 2001). The aluminium concentration in seawater is ~8ppb, which is too low to have any impact on the dissolution rate of basalt glass. For this reason there does not appear to be any reason why seawater should inhibit the dissolution rate of basalt glass. The dissolution of forsterite involves the formation of Si-rich or Mg-rich surface layers depending on the pH of the solution (POKROVSKY and SCHOTT, 2000). At low pH forsterite initially preferentially loses Mg into solution so high concentrations of Mg in solution could potentially affect the rate of dissolution. However, a recent study of forsterite dissolution rates as a function of aqueous Si and Mg concentrations shows that the rate of dissolution is independent of solution composition (OELKERS, 2001). In summary, there is no evidence to support the notion that seawater could inhibit basalt glass or forsterite dissolution rates. Instead there is good evidence from saturation state modelling to suggest that secondary minerals have formed within the reactors and it is the removal of silicon from seawater during this secondary mineral formation, not the seawater itself which is causing the low dissolution rates.

6.4.6. Far from equilibrium dissolution rates

If secondary mineral formation has affected the dissolution rates as indicated by the saturation state modelling then one way to overcome this is by calculating the rate (using equation 6.1) based upon the early stages of the experiment where the saturation states will be lower and the system should be further from equilibrium. The problem with doing this is that the system may not have attained a steady state and consequently the calculated dissolution rate may be incorrect. The experiments of Gislason & Oelkers (2003) involving basalt glass at pH 7, took 16 hours for the dissolution to reach a steady state. Whereas, experiments involving the dissolution of forsterite show that steady state can take between 6 and 100 hours (POKROVSKY and SCHOTT, 2000), the system taking far longer to reach a steady state at high pH. The pH of seawater is ~8 so the dissolution of basalt glass will be faster than at pH 7 (GISLASON and OELKERS, 2003) and as a consequence steady state will take less time to attain. Thus for dissolution rate estimates from these experiments it is reasonable to exclude the first two samples of BGSW1 and FOSW1 and use the solutions that were sampled between 24 and 240 hours into the experiment. Using these samples (Zone B, Fig. 6.6 and 6.8) a modified dissolution rate can be estimated for both materials. This new estimate for the dissolution rate of basalt glass is (log R) -14.66 mol/cm^2/s (Fig. 6.11), which is very close to the rate estimated by Gislason & Oelkers (2003) of -14.55 mol/cm^2/s. The new estimate for the dissolution rate of forsterite is (log R) -14.3 mol/cm^2/s (Fig. 6.12), which is also close to that determined by Pokrovsky & Schott (2000) with dissolution rates of -14.4 mol/cm^2/s.

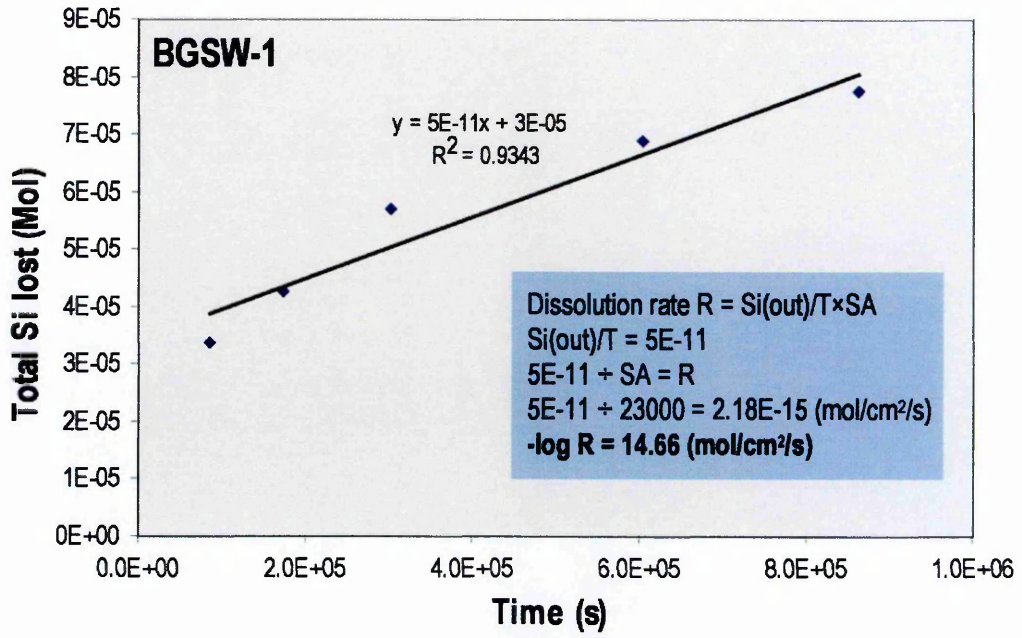

Fig. 6.11 - A graph using the first five sample points from BGSW-1 (see Figure 6.6, zone B) to calculate the dissolution rate based on change in silicon concentration

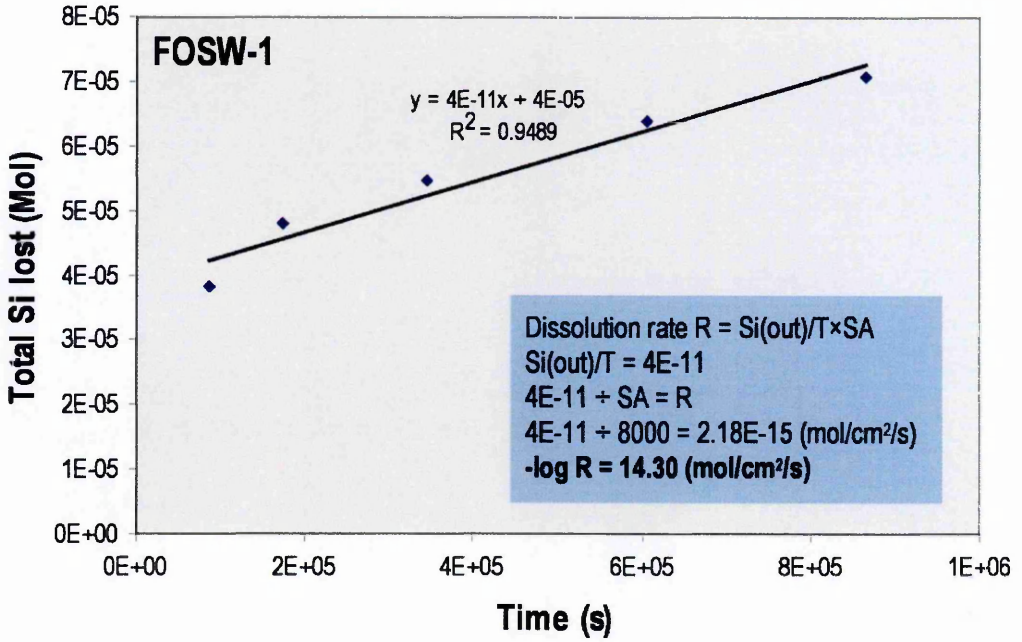

Fig. 6.12 - A graph using the first five sample points from FOSW-1 (see Figure 6.8, zone B) to calculate the dissolution rate based on change in silicon concentration

These results suggest that in the early stages of the experiments the system was at far from equilibrium conditions and that the dissolution rates of both basalt glass and

forsterite are close to the rates obtained from similar experiments with non seawater solutions. Consequently, these results support the hypothesis that seawater itself does not inhibit the dissolution rate of either basalt glass or forsterite and that the slow dissolution rates at the end of each experiment were caused by either high saturation indices of the dissolving mineral or secondary mineral formation.

Despite the similarity between these results and literature values it should be noted that the dissolution rates are estimates, and that they carry a significant uncertainty, because the system may not have reached a steady state even after 24 hours. In an ideal world, an open system experiment should be set up; this would enable far from equilibrium conditions to be maintained over a long period of time so that the systems can reach steady state without the occurrence of secondary mineral formation.

6.4.7. Isotopic changes

The results of the isotope analyses (see 6.3.2 and 6.3.3) show that there has been very little change in the Mg and Li isotope composition of the solution. The reasons for this are the relatively high concentrations of both Li and Mg in seawater. There are two ways that the isotopic composition of the fluid phase could alter with time. Firstly, Li or Mg that is isotopically different from the fluid phase could be added to solution during dissolution. Seawater has a δ^7Li value of 31‰, in comparison basalt glass and forsterite have much lighter Li isotope compositions (δ^7Li values of ~5 and 2‰ respectively). A significant input of Li from the dissolution of these minerals would lead to the solution becoming isotopically lighter, assuming that there is no fractionation of Li during mineral dissolution (as indicated in Chapter 5). Similarly the δ^{26}Mg values of basalt glass and forsterite are -0.3 and -0.26‰ respectively (Chapter 5) so any input of Mg should drive the isotopic composition of the solution to values higher than -

0.82‰. While this mechanism has the potential to drive isotopic change, a high concentration of Mg or Li would need to be added to the system to cause a detectable change in the isotopic composition of seawater. The concentration of Li in seawater is ~0.18ppm; therefore in a 1 litre reactor there are 0.18mg of Li in solution. In comparison the basalt glass has a Li concentration of 4.7ppm; this means that in 10g of basalt glass there is a total of 0.047mg of Li or 25% of the total Li in one litre of seawater. Using a dissolution rate for basalt glass of 3.16×10^{-15}mol/cm^2/s for pH8 and 25°C (GISLASON and OELKERS, 2003), a total of 0.048μg will be released into solution over 6000 hours, which is only ~0.03% of the total Li in the seawater solution. Similar results are obtained for Mg; even though silicates contain far higher Mg (particularly forsterite), Mg is also far more abundant in seawater. Assuming stoichiometric dissolution and using dissolution rates from freshwater experiments (GISLASON and OELKERS, 2003; POKROVSKY and SCHOTT, 2000) the dissolution of basalt glass will provide ~0.84% of the total Mg in seawater and forsterite will provide ~4.4% of total Mg from seawater. Therefore it is unlikely that the either the Li or Mg isotope composition of the experimental solution could be altered by straightforward mineral dissolution.

The second way in which the Li and Mg isotope compositions may be altered would be via the formation of secondary minerals. Previous work has shown that both isotope systems can be fractionated during weathering processes (HUH et al., 1998; TIPPER et al., 2006a), as has also been observed in laboratory experiments (Chapter 5) and in the Greenland rivers studied here (Chapters 3 and 4). In principle, secondary mineral formation should cause the solution to become isotopically heavy in the case of Li as ^{6}Li is preferentially removed from solution into the solid phase. Lithium isotope values show little variation; solutions from BGSW-1 change from ~31‰ to 32.5‰ over

the course of the experiment. This change is small; the average IAPSO standard measured over the course of this work is 31.2 ± 0.84 (2σ), so statistically it is only just outside the range of the seawater standards. Assuming that secondary minerals have indeed formed, the reason that the amount of Li fractionation from IAPSO seawater is so small is because of the high Li concentration in seawater. A relatively large amount of ^{6}Li would need to be removed from solution by secondary minerals to cause a change in the $\delta^{7}Li$ composition of seawater. Similarly for Mg isotopes the ratios of the solutions do not change over time. The relative mass difference between Mg isotopes is far less than that for Li isotopes and as a consequence the degree of Mg fractionation will also be less. For example the range of riverine Li compositions in Greenland (Chapter 3) is 23‰, yet the same rivers have a range of Mg isotope compositions of 0.8‰. Any variation in the Mg isotopic composition of the experimental waters would be lower than the external reproducibility of the analysis (which is 0.11‰ (2σ)).

6.5. Conclusions and future work

The aims of this study were to investigate the dissolution rate of easily weathered basaltic phases, such as glass and forsterite, in seawater and to assess the effect of this (as well as the formation of secondary minerals) on the Li and Mg isotope composition of the fluid phase. To this end, a number of experiments were conducted but the results have proved rather inconclusive for two reasons.

First, the experiments were conducted in a closed system, which though ideal for the precipitation of secondary minerals is less suited to the determination of dissolution rates at far from equilibrium conditions because of the build-up of high concentrations in solution. This is illustrated by the high secondary mineral saturation states and the

observation that the dissolution rate at steady state was over an order of magnitude slower than the dissolution rate at far from equilibrium conditions obtained by Gislason & Oelkers (2003). Dissolution rates were also calculated using samples from the first two weeks of the experiment in order to attempt to obtain far from equilibrium dissolution rates. The results showed similar dissolution rates to experimental results carried out in freshwater solutions suggesting that the dissolution of basalt glass and forsterite is not inhibited by seawater. However these solutions may not have attained a steady state and as such the results cannot be seen as being entirely reliable.

Secondly, the amount of Li and Mg released into solution was low in relation to the amount of Li and Mg in the seawater solution, which meant that any isotope changes accompanying basalt glass dissolution and/or the precipitation of secondary minerals were obscured. This problem could be overcome by the use of an artificial seawater solution containing all of the major cations, but with no Mg^{2+} or Li^{+}.

The most effective way to run these experiments would be to use a through flow reactor (see Chapter 5) and using artificial seawater, so that both far from equilibrium dissolution rates and high concentrations in solution could be achieved, while changes in $\delta^{26}Mg$ and $\delta^{7}Li$ could be measured. The only complicating issue with such a setup would be the amount of artificial seawater that would be needed (especially if experiments were to last for 8 months or longer), and the through flow reactor itself. It would not be wise to use a reactor that is mostly used for low concentration far from equilibrium experiments because of the risk of secondary mineral formation and the high dissolved solid content of the seawater contaminating the apparatus.

Chapter 7

Rhenium and osmium isotope and elemental behaviour accompanying laterite formation in the Deccan region of India

This chapter contains work investigating rhenium and osmium behaviour in two laterite profiles from India. This was originally written up in paper format and submitted to EPSL in October 2006. After going to review some parts were rewritten and the manuscript was resubmitted in June 2007 when it was accepted for publication.

7.1. Introduction

The continental crust is severely depleted in many platinum group elements (PGE: Ru, Rh, Pd, Os Ir and Pt) relative to the Earth's core and mantle, and contains less than 0.01% of the terrestrial PGE budget (e.g. (ESSER and TUREKIAN, 1993; PEUCKER-EHRENBRINK and JAHN, 2001; SCHMIDT et al., 1998; TAYLOR and MCLENNAN, 1995; WEDEPOHL, 1995)). This depletion, in part, reflects the siderophile and chalcophile behaviour of these elements, which means that they are highly concentrated in the Earth's metallic core (SHIREY and WALKER, 1998; WANKE, 1981), but also, in part, because some of these elements are compatible during silicate melting, and hence are preferentially retained in the residual mantle (ALLEGRE and LUCK, 1980; SHIREY and WALKER, 1998).

Osmium (Os) is a platinum group element that is related to rhenium (Re) through the beta decay of ^{187}Re to form ^{187}Os. During partial melting Os behaves as a compatible element, whereas Re is moderately incompatible and enters the melt

(SHIREY and WALKER, 1998). Consequently, the Earth's crust (continental and oceanic) possesses high Re/Os (parent/daughter) ratios and develops radiogenic Os isotope compositions over time, relative to contemporaneous mantle. Under normal circumstances the Os isotope composition of the continental crust is controlled by the Re/Os ratio and age of a given rock type (ESSER and TUREKIAN, 1993). However, estimates for the average $^{187}Os/^{188}Os$ isotope composition of the upper continental crust are variable, ranging from 1.4 to 1.9 (from loess (PEUCKER-EHRENBRINK and JAHN, 2001) and river sediments (LEVASSEUR et al., 1999), respectively) while rivers themselves yield a global mean value of ~1.4 (LEVASSEUR et al., 1999; PEUCKER-EHRENBRINK and RAVIZZA, 2000b).

The behaviour of Re and Os during continental weathering is unusual because these elements are often highly concentrated in accessory phases or else in particular rock types. At the mineral scale in silicate rocks, a significant proportion of the Re and Os present is located in phases present at trace levels (accessory phases) such as sulphide and PGE-alloys (BURTON et al., 1999; HART and RAVIZZA, 1996). It is these phases that control the Os isotope composition and elemental abundance of Re and Os in the whole-rock, and often their behaviour during weathering that determines the composition of waters and soils. Similarly, certain rock types such as organic-rich sediments are highly concentrated in Re and Os, possess very high Re/Os ratios, and thus with time develop highly radiogenic Os isotope compositions, relative to average continental crust (JAFFE et al., 2002; PEUCKER-EHRENBRINK and HANNIGAN, 2000; SINGH et al., 1999). Such sediments are also highly susceptible to weathering and readily release their radiogenic Os, and this weathering signal may strongly influence the marine Os isotope composition, despite comprising less than 1% of the continental crust (PEUCKER-EHRENBRINK and HANNIGAN, 2000). Notwithstanding, the concentration of Re and Os

in accessory phases and particular rock types, under certain circumstances both elements may be highly mobile during weathering, and readily transported in natural waters (i.e. ground and river waters).

Laterites result from extreme weathering of the continental crust in tropical or sub tropical climates, they are estimated to cover 30% of the exposed continental crust, and nearly 50% of continental drainage flows through laterite covered terrain (TARDY, 1997). Laterites are commonly over 20m thick and can have thicknesses of up to 100 m (BRIMHALL et al., 1991). Laterite profiles generally show a progression from unaltered bedrock to increasingly altered rock above with an iron rich crust or duricrust at or close to the surface. Laterites are formed during continuous in situ weathering of bedrock (BRIMHALL et al., 1991; SCHELLMANN, 1981; TARDY, 1997; WIDDOWSON and COX, 1996), which acts to strip away less resistant elements (such as silica, and the mobile elements Na, Mg, Ca) leaving secondary minerals enriched in Fe_2O_3 and Al_2O_3. There is also some evidence to suggest that they are, at least in part, modified by external input and redistribution processes (BRIMHALL et al., 1991; KISAKUREK et al., 2004) and that their formation may be initiated by changing weathering conditions (DEQUINCEY et al., 2002).

It has long been known that laterite soils may be enriched in platinum group elements, located in PGE-rich alloys and associated sulphides and iron-oxides (e.g. (BOWLES, 1986)). Early work suggested that these PGE-rich minerals were present as resistant phases residual from weathering of the parent rock (e.g. (CABRI and HARRIS, 1975)). However, it is now established that under the conditions prevalent in laterite soils (that is, low pH and high Eh) some platinum group elements may be taken into solution, transported and redeposited (BOWLES, 1986; BOWLES et al., 1994), consistent with textural evidence indicating that PGE-minerals in laterites have grown in situ

(BOWLES, 1986; MANN, 1984). Thus far there have been few published Re-Os isotope measurements for laterites. The data that have been obtained indicate a depletion of Re and enrichment of Os in the topsoil part of the profile, and consequently a relatively unradiogenic Os isotope composition, relative to the parent rock (SHARMA et al., 1998). These results were taken to indicate that the weathering of laterite soils will yield relatively unradiogenic Os which may control the composition of dissolved and aeolian material delivered to the oceans (SHARMA et al., 1998).

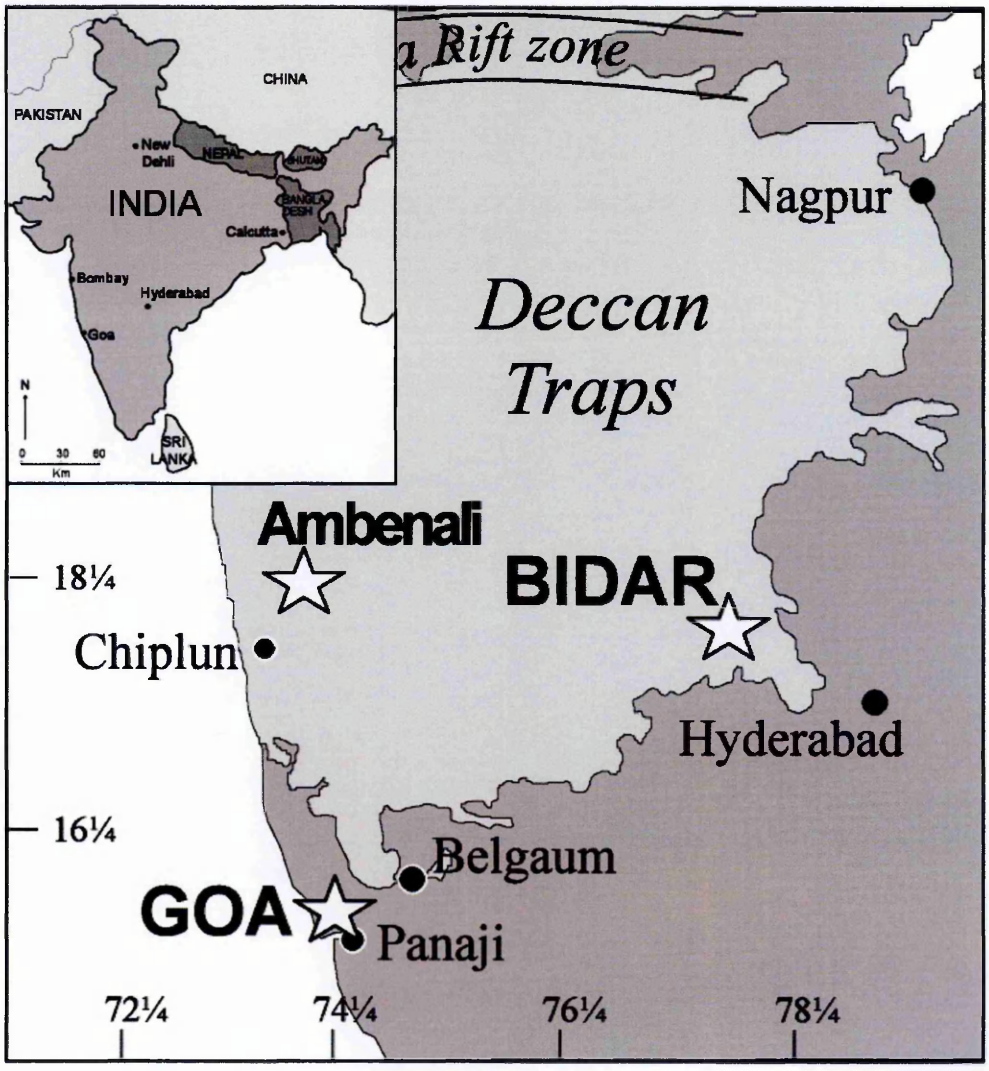

Fig. 7.1. Location map showing the two laterite study sites. Bidar is in central India in the Deccan CFBP, Goa is on the west coast of India on the Dharwar Craton.

This study presents major-, trace element, and Re-Os isotope and elemental data for two laterite profiles from a similar climatic regime, but having different parent rock types, from Bidar and Goa in India. These results provide information on the distribution and mobility of Re and Os during laterite formation and groundwater movement, the consequences for the Os isotope evolution of laterites (compared to parent rock types), and the implications for the behaviour of these elements during weathering in tropical and sub-tropical climates.

7.2. Geological setting and Background

7.2.1. Geological setting

Two laterite profiles from the Deccan region have been studied here; the first is from Bidar in central India, and the second is from Goa on the west coast (Fig. 7.1). Bidar is located near the present-day edge of the Deccan Traps Continental Flood Basalt Province (CFBP). The Deccan Traps were erupted during a ~3-4 Ma period straddling the Cretaceous-Tertiary boundary (e.g. (COURTILLOT et al., 1988; WIDDOWSON et al., 2000)), onto a complex Archean-Proterozoic basement comprising part of the Dharwar craton (CHADWICK et al., 2000). Today the Deccan Traps cover an area of over 500,000km^2, and have a maximum thickness of ~2km (MITCHELL and WIDDOWSON, 1991). Each lava package (or formation) has a distinct chemical and isotopic signature, reflecting different stages of the eruptive history (KALE et al., 1992). Of these different lavas the Ambenali formation is the most volumetric and geographically widespread (WIDDOWSON et al., 2000), and forms the upper flow units that have been subsequently laterised at Bidar (KISAKUREK et al., 2004). The second profile at Goa developed on a Proterozoic greywacke that forms part of the Dharwar supergroup.

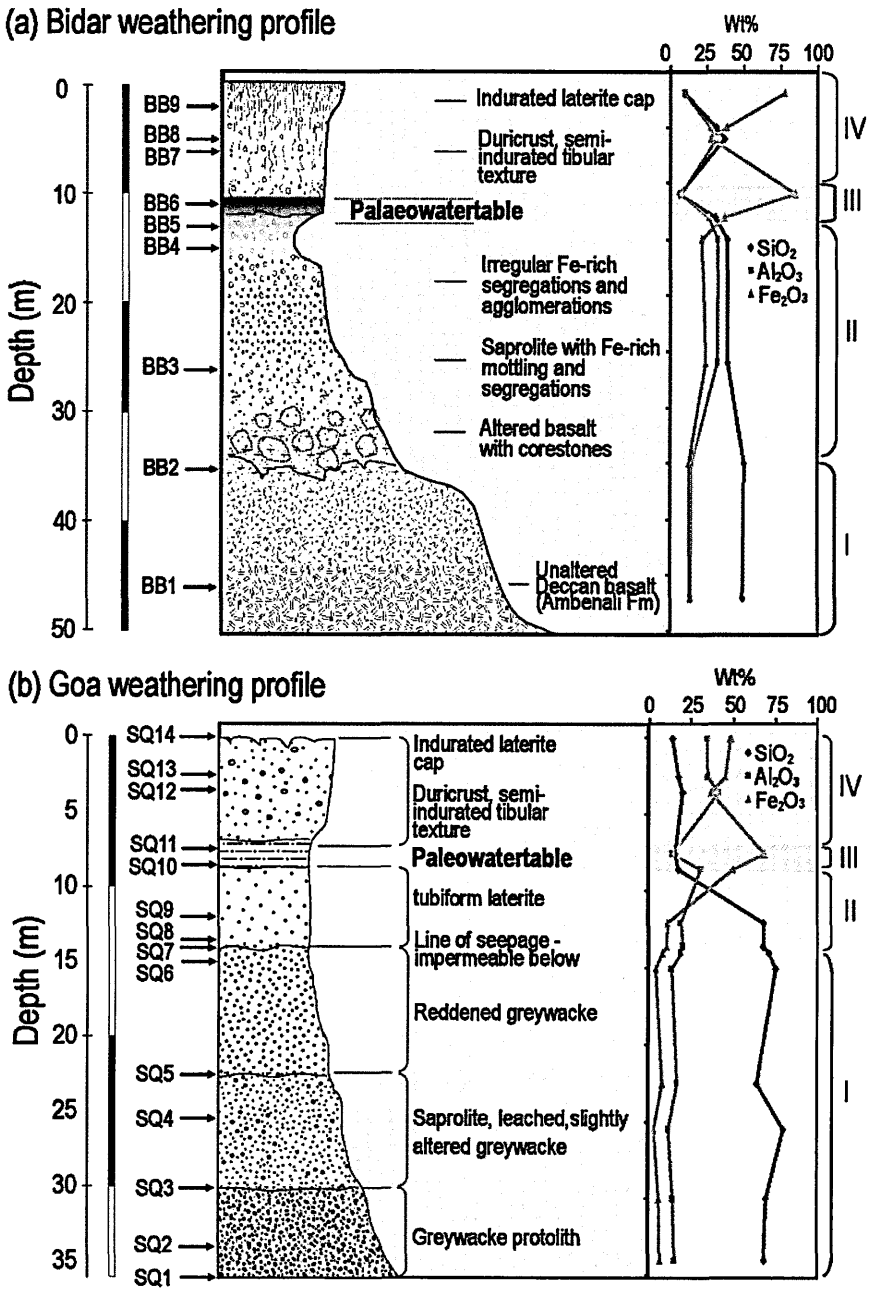

Fig. 7.2. Schematic profiles of the studied laterites at (a) Bidar and (b) Goa. Both profiles show progression from unaltered rock at the base to increasingly altered rock towards the surface, and both have a hard indurated iron cap at the surface and a distinct paleowatertable horizon. Zones I–IV illustrate the progressive lithological changes within the laterite. Zone I - unaltered or little altered bedrock, Zone II - high alteration bedrock/ laterite (saprolite), Zone III - paleowatertable, Zone IV - Fe rich laterite cap (see text). Includes major element profiles that are characterised by a general decrease in Si, and relative enrichment in Fe and Al contents. This pattern of chemical change is interrupted at the paleowatertable where there is considerable enrichment of Fe, and depletion of both Si and Al.

During the later stages of eruption of the Deccan Traps, northwest drift of India, across the equator (KLOOTWIJK and PEIRCE, 1979), exposed the Deccan (CFBP) to intensive weathering leading to the development of deep weathering profiles capped by a regional laterite (WIDDOWSON and COX, 1996). At the Bidar site, this major period of laterite formation was brought to a close between 55 and 45 Ma (SCHMIDT et al., 1983), when regional uplift raised the laterite above the watertable (WIDDOWSON, 1997), possibly as a result of the collision of India and Asia, thereby preserving this ancient weathering profile. In contrast, the site at Goa did not experience this uplift, and paleomagnetic data suggest that laterite formation occurred during the late Tertiary, ~20 Ma, and is ongoing today.

The profile at Bidar extends to a depth of ~50 m where unaltered basalt is located (Fig. 7.2). In the region of the Bidar profile the Ambenali formation represents the uppermost flow units of the Deccan, constructed at the highest elevations, and not overlain by later eruption. Consequently, any extraneous groundwater influence from different lithologies at higher levels can be discounted. Rather, the huge lateral extent and thickness of the Ambenali formation suggests that the majority of elements mobilised and transported by groundwaters were ultimately derived from the breakdown of this tholeiitic precursor. Moreover, the uniform composition of the Ambenali formation offers an ideal substrate for assessing the chemical variations accompanying laterite formation, because any changes in chemistry are unlikely to be a result of parent rock heterogeneity. Moreover, the intracontinental location precludes any marine influence on the chemistry, through aerosols or precipitation, but does not rule out the presence of continental derived aeolian material. The profile at Goa is a ~35 m thick and developed on a Proterozoic greywacke that forms part of the Dharwar supergroup. By contrast to the site at Bidar, the relatively low topography of the laterite

and the heterogeneity of the Dharwar craton raises the possibility of lateral input of groundwater potentially sourced by a range of lithologies. Moreover, unlike the Ambenali formation, the parent greywacke shows some chemical variation both laterally and vertically.

7.2.2. Sample Description

The two profiles are shown in detail in Fig. 7.2 and sample depths and descriptions of their lithology and mineralogy given in Appendix E1 (previously reported in (BORGER and WIDDOWSON, 2001; KISAKUREK et al., 2004)). Both show progression from unaltered rock at the base to increasingly altered rock towards the surface, and both have a hard indurated iron cap at the surface ("cuirasse") together with distinct paleowatertable horizon a few meters below the cap. The laterite profiles can be divided into zones based on the level of alteration reflected in their physical properties, mineralogy and elemental behaviour (Fig. 7.2). Zone I is unaltered or slightly altered bedrock. Zone II is altered bedrock increasingly so up the profile. At Bidar the crystalline groundmass of the basalt is initially replaced by illite and kaolinite clay, similarly at Goa primary quartz, biotite and feldspar are also replaced by clays in this zone. Moving up, the primary mineralogy is lost, and the groundmass becomes mottled due to the development of Fe and Al oxides and oxyhydroxides. Zone III is the paleowatertable horizon, and Zone IV is the Fe-rich indurated laterite crust. Within Zone IV no remnant of the protolith texture or primary mineralogy remains. The high haematite content of these samples indicates that well drained oxidizing conditions prevailed.

There is no petrographic evidence for significant input of aeolian material to either profile, this supporting the view that the laterite profiles across the Deccan region

were predominantly formed by in situ alteration of the underlying bedrock. However, for the profile at Bidar, Sr, Nd and Li isotope data have been taken to indicate aeolian input of weathered continental material to the top of the profile (KISAKUREK et al., 2004; MASON, 2000). Consequently, a number of potential sources of local aeolian material have been examined here including basement granite, banded iron formation (BIF) and a limestone all from the Dharwar craton.

Finally, a sequence of Deccan 'bole' samples have also been analysed. These are highly weathered basaltic material or basaltic ash that developed between successive lava flows (i.e. during a hiatus in eruption). The Bole samples studied are from a locality close to the village of Ambenali, and comprise a ~1.4 m profile sandwiched between two massive lava flows. The base of the profile is marked by weathered flow top material that is overlain by fine-grained ash which is increasingly weathered towards the top of the bole horizon. These bole samples serve to illustrate the behaviour of Re and Os in weathered basalt that has not had sufficient time to develop into a laterite.

7.3. Methods

7.3.1. Sampling and sample preparation

Samples were taken from each of the profiles (sample locations shown in Fig. 7.2) chosen as representative of each key horizon, or else taken immediately above or below (i.e. bracketing) levels where distinct textural changes are observed. Because the weathering profiles are highly heterogeneous large samples (between 1 and 3 kg) were taken, and these large samples were then homogenised by milling in agate.

7.3.2. Major and trace element analysis

Bulk materials from the weathering profiles and surrounding basement rocks were analysed by XRF for major elements and ICP-MS for minor and trace elements. Full details of the analytical procedures are given in Section 2.2 and 2.5.

7.3.3. Re-Os isotopic analysis

Rhenium and Os were separated from laterite and rock samples using techniques previously described (BIRCK et al., 1997) and given in Section 2.4.1. Re and Os samples were analysed as OsO_3^- and ReO_4^- oxides by negative TIMS (Section 2.5.2.1). The average total procedural blank for the Bidar samples was 0.41 pg for Os and 4.75 pg for Re; the Os isotopic composition of the blank ($^{187}Os/^{188}Os$) was 0.179 ± 0.005. Corresponding blanks for Goa were 0.22 pg for Os and 4.42 pg for Re; the Os isotopic composition of the blank was 0.186 ± 0.007.

7.4. Results

7.4.1. Major and trace element data

Major and trace element data for both profiles are given in Appendices E2 and E3. Above the zone of unaltered bedrock (zone I) both profiles show a decrease in the concentration of the more mobile elements (e.g. Ca, Na, K and Mg) relative to the parent rock, towards the surface (zones II, III and IV). The decrease in mobile elements is accompanied by a decrease in SiO_2, and relative enrichments in Fe and Al contents (Fig. 7.2). This pattern of chemical change is interrupted at the level of the paleowatertable (~11-14m depth at Bidar, ~7-8.5m depth at Goa) where there is considerable relative enrichment of Fe, and a relative depletion of both Si and Al.

The variation of trace elements with depth is also similar for both profiles. The concentration of mobile trace elements, such as Sr and Rb, is highest in the unaltered bedrock and decreases as the rock becomes more altered (and permeability increases) (Appendix D3). At Goa there is a sharp change in permeability at 15m depth that is marked by a line of seepage and loss of the mobile elements. Relatively immobile transition elements such as Cu, V, Sc and Cr are enriched in the upper half of the laterite profile, and have lowest concentrations in the unaltered bedrock (Fig. 7.3).

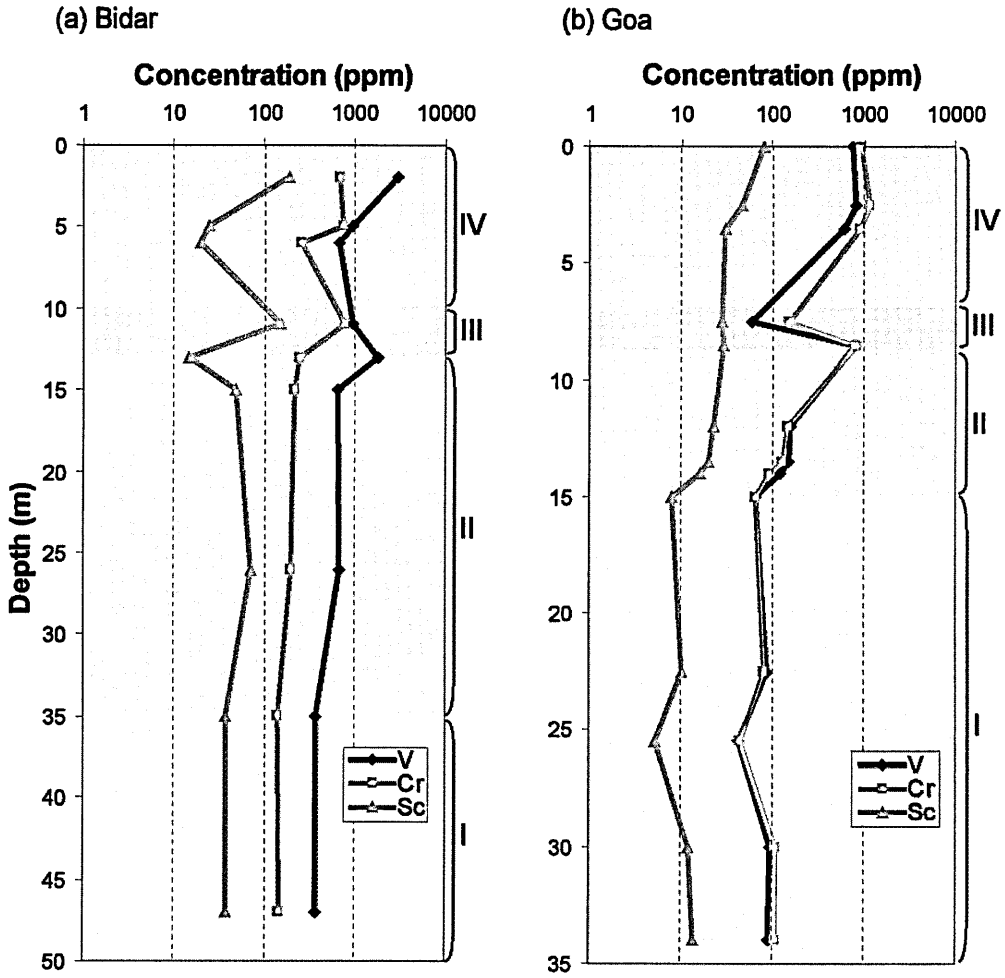

Fig. 7.3. Trace element profiles for (a) Bidar and (b) Goa, showing that the immobile trace elements V, Cr and Ni are enriched in laterite compared to the parent rock.

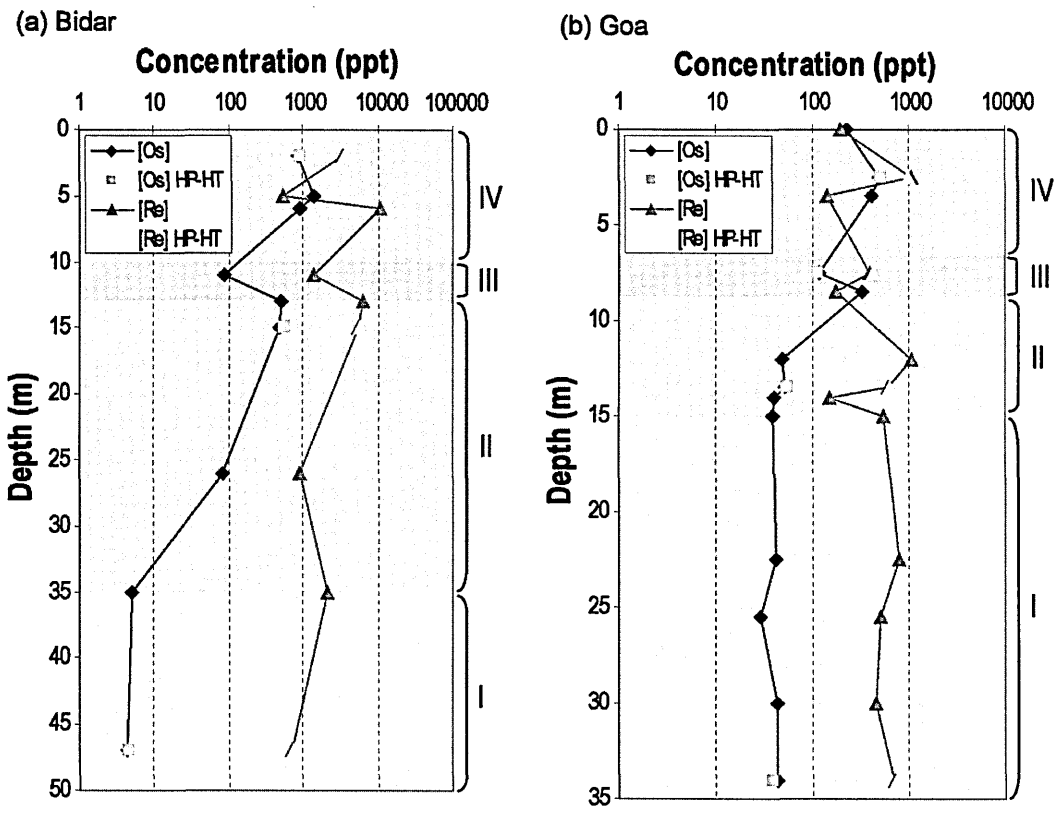

Fig. 7.4. Re and Os concentration profiles for (a) Bidar and (b) Goa. The parent rocks have relatively low Re and Os concentrations. However, both profiles show a significant increase in Re and Os concentration with increasing alteration, with the highest values being seen in the Fe-rich laterite cap. For both profiles enrichment of Os is always greater than Re, consistent with previous work. In addition, both profiles show a decrease in the concentration of Re and Os at the level of the paleowatertable.

7.4.2. Re-Os elemental data

The concentrations of Os and Re at Bidar show significant variation with depth (Fig. 7.4). Osmium concentrations increase from 4ppt at 47m depth to 1410ppt at 5m depth, a 300-fold increase. Rhenium concentrations are higher than those of Os, increasing from 0.7 ppb at 47m depth to 10 ppb at 6m depth, but the level of enrichment is much lower (some 14-fold). Similar Re and Os variations are observed at Goa. Osmium concentrations increase from 43 ppt at 34 m depth to 492 ppt at 2.5 m depth, an enrichment factor of >11. Rhenium has higher concentrations than Os, increasing from 0.7 ppb at 34 m depth to 1 ppb at 2.5 m depth, an enrichment factor of 1.4. The pattern

of increasing Re and Os concentration towards the top of the profile is interrupted by a sharp decrease in the concentration of both elements at the level of the paleowatertable.

7.4.3. Re-Os isotope data

For both profiles parent rock $^{187}Re/^{188}Os$ ratios are greater than those of the overlying laterite and $^{187}Os/^{188}Os$ ratios are also in general more radiogenic; the least radiogenic ratios being found at the surface (Fig. 7.5). At Bidar, $^{187}Re/^{188}Os$ drops from 2286 at 35m depth to 2 at 5m depth. $^{187}Os/^{188}Os$ ratios show a similar pattern, falling from 0.98 at 45m depth to 0.33 at 2m. Both isotope ratios shift to lower values where the Os concentration starts to increase (between 35 and 26m depth). A similar pattern is observed in the Goa profile; both $^{187}Re/^{188}Os$ and $^{187}Os/^{188}Os$ ratios shift to lower values towards the surface. The parent rock has a $^{187}Re/^{188}Os$ ratio of ~100, and a $^{187}Os/^{188}Os$ ratio of ~4.5; these values are far more radiogenic than those of Deccan basalt. Both ratios fall as the Os concentration starts to rise at 12m depth. The $^{187}Re/^{188}Os$ ratio at the surface is 4.4 and the $^{187}Os/^{188}Os$ ratio is 0.48, similar to the values recorded at Bidar.

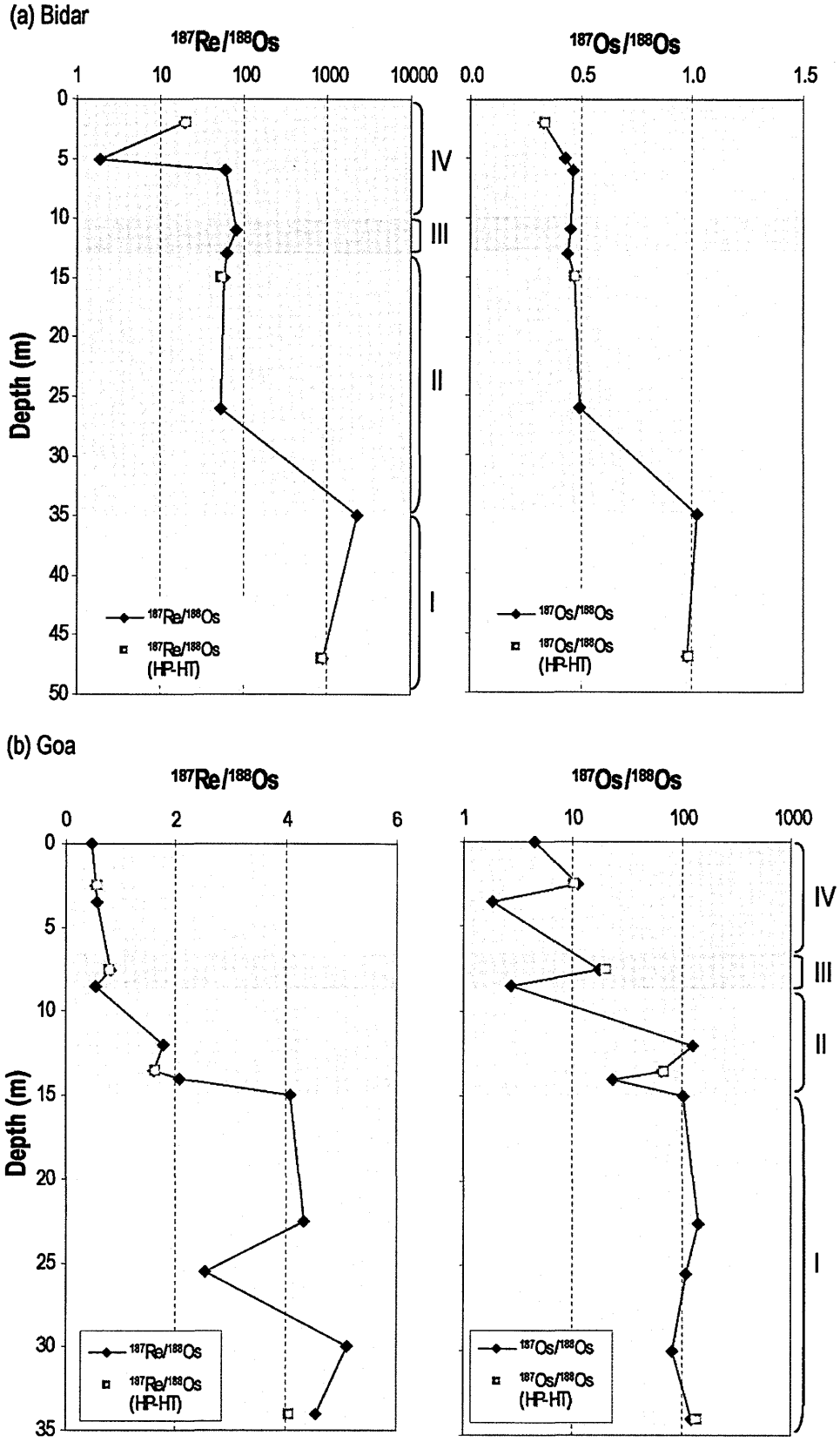

Fig. 7.5. $^{187}Re/^{188}Os$ and $^{187}Os/^{188}Os$ ratios shown against depth at (a) Bidar and (b) Goa. The $^{187}Re/^{188}Os$ and ratios of the laterite are, with one exception, always lower than the those of the parent rock. The measured $^{187}Os/^{188}Os$ isotope ratios are also always less radiogenic than the parent rock

7.4.4. Basement lithologies and Bole samples

The three granite samples analysed have Os concentrations of ~4 ppt; similar to the unaltered basalt at Bidar but far lower than the laterites at both Bidar and Goa. $^{187}Os/^{188}Os$ isotope compositions of the granites range from 0.74 to 1.77; these compositions are more radiogenic than the surface compositions of either laterite profile. The BIF and limestone samples from the Dharwar craton have Os concentrations of between 20 and 31 ppt, an order of magnitude lower than the highest concentrations recorded at Goa and two orders of magnitude lower than recorded at Bidar. The $^{187}Os/^{188}Os$ isotope ratio of the Bhima limestone is relatively unradiogenic (0.175) while the $^{187}Os/^{188}Os$ ratio of the BIF is relatively radiogenic (1.345). The basalt bole samples have Os concentrations between 20 and 44 ppt, and $^{187}Os/^{188}Os$ ratios of between 0.157 and 0.171. The concentration of Re is variable ranging from 97 to 1080 ppt, and consequently the $^{187}Re/^{188}Os$ ratio also shows wide variation from 23 to 119.

7.5. Discussion

7.5.1. Elemental variations

The variation in the chemical composition of both profiles is very similar, and consistent with previous studies of laterite formation on comparable protoliths (e.g. (BRIMHALL et al., 1991; TARDY, 1997; WIDDOWSON and COX, 1996)). The data indicate loss of the more mobile elements (e.g. Ca, Na, Mg, K, Rb and Sr) in the earlier stages of weathering, followed by a decrease in silica content, facilitated initially by the breakdown of the primary mineralogy, and subsequently by the breakdown of neo-formed clay minerals. The depletion in mobile elements is accompanied by a concomitant increase in the concentration of less mobile elements within the developing

laterite profile, in particular Fe, Al and Ti, typically considered as residual. Superimposed on this pattern of enrichment and depletion is element behaviour at the watertable, since many elements are controlled by the change in redox conditions at this level. For example, iron can exist as reduced Fe^{2+} that is mobile or oxidised Fe^{3+} that is immobile. The paleowatertable marks a change in the redox conditions from sub-oxic to oxic so that Fe^{2+} is oxidised to immobile Fe^{3+} that is then deposited as oxides or oxyhyroxides.

At both Bidar and Goa high Re and Os concentrations occur in the upper parts of the profile, coinciding with significant Fe_2O_3 enrichment and SiO_2 depletion. Enrichment of trace metals, in particular the rare earth elements (REE) in heavily weathered and lateritized soils has been widely recognised (BRAUN et al., 1998; KOPPI et al., 1996; NESBITT and MARKOVICS, 1997; WALTER et al., 1995). REE's form mobile complexes with phosphates, fluorides and carbonates (WALTER et al., 1995), can be mobilized by organic matter (BRAUN et al., 1998) and can be trapped by Fe- and Mn-oxides (KOPPI et al., 1996; WALTER et al., 1995). Substantial PGE enrichment in lateritic soils has also been documented (BOWLES, 1986; BOWLES et al., 1994; BROWN et al., 2003; ELIOPOULOS and ECONOMOU-ELIOPOULOS, 2000; MANN, 1984; ROQUIN et al., 1990; TOPP et al., 1984) and attributed to supergene enrichment and co-precipitation of PGE-rich alloys with iron and manganese oxides. Lateritic soils are considered to develop in a high Eh (+200 – +800mV) and low pH (2-5) environment (BOWLES, 1986; MANN, 1984), and these conditions are thought to arise because cations such as Fe^{2+} are removed from solution under increasingly oxidising conditions (MANN, 1984). The release of protons into solution causes pH to decrease; and where Fe^{2+} concentrations are high, such as just below the water table, pH can be as low as 2 (BOWLES, 1986). Under these conditions the PGEs become mobile by forming complexes with species

such as chlorides, oxides and hydroxides as well as with organic matter such as oxalates and humic acid (BAKER, 1978; BOWLES, 1986; BOWLES et al., 1994; MOUNTAIN and WOOD, 1988). However, not all of the PGEs have the same mobility: for example Pd is considered to be more mobile than Pt (MOUNTAIN and WOOD, 1988; OBERTHUR et al., 2003; TRAORE et al., 2006) and more readily enters the aqueous phase in solution (BOWLES et al., 1994), whilst available data suggest that Os is amongst the most soluble (BOWLES, 1986). The PGEs are then progressively removed from solution as conditions become increasingly oxidising and pH increases towards the surface. Here there are high concentrations of poorly crystalline secondary phases such as Mn- and Fe-oxyhydroxides that act as scavengers of metal ions in solution (KUHNEL, 1987). This secondary mineral crystallisation accounts for the high PGE, Au and Ag concentrations in a number of weathering profiles (BOWLES, 1986; BOWLES et al., 1994; BROWN et al., 2003; MANN, 1984; ROQUIN et al., 1990) and the same processes can also account for the high Re and Os concentrations seen in the laterites studied here. That is, high Eh and low pH conditions cause Re and Os dissolution, and redistribution occurs via groundwaters. Subsequently with increasing pH in the upper part of the laterite profile, both elements are scavenged out of solution and precipitate either as PGE-rich alloys or are strongly partitioned into oxides or oxyhydroxides.

The variation in Re and Os, in particular those seen at the level of the paleowatertable (Fig. 7.4, zone III) indicates that they are mobile. The extent of this mobility can be assessed by comparison with an 'immobile' index element. Elements such as Ti, Th and Zr are considered relatively immobile in surface weathering environments because of their relatively high field strength and low solubility in water, for this reason they have been used previously in many studies of weathering profiles and processes (BRIMHALL and DIETRICH, 1987; BROWN et al., 2003). Nevertheless it

should be remembered that they are not totally immobile and that they can be mobilised in extreme weathering conditions or in the presence of high organic matter (HODSON, 2002; OLIVA et al., 1999). In this study Zr has been used as the index element because its concentration shows the least variation over the two profiles, when compared to concentration in the parent rock (Fig. 7.6). Re and Os concentrations normalised to Zr and Ti show little difference in patterns of enrichment or depletion (Figures 7.7 and 7.8), where enrichment or depletion can be defined by:

$$\%\ \text{enrichment/depletion} = 100 \times \frac{R_n - R_i}{R_i} \qquad \textit{Equation 7.1}$$

In equation 7.1 R is the ratio of the element concentration to the Zr concentration and the subscripts i and n indicate the bedrock and weathered horizon respectively. At Bidar there are substantial enrichments of both Os and Re. The highest Os enrichment occurs at 5m depth where the laterite is ~19,000 % enriched relative to the parent rock, and Re is enriched by 920 %. At Goa most samples are enriched in Os relative to the bedrock, the sample at 2-5m depth being enriched by 630%. Concentrations of Re are very variable; some horizons contain higher Re and some lower Re than the parent rock. It is important to note that the Zr content at the level of the watertable is ~40% lower than the parent basalt, suggesting that this element may also have been mobilised. The net effect of this relative mobilisation of Zr will be to enhance the relative depletion of Re and Os. However, throughout the remainder of the profile the trends revealed by Zr normalisation remain unaffected.

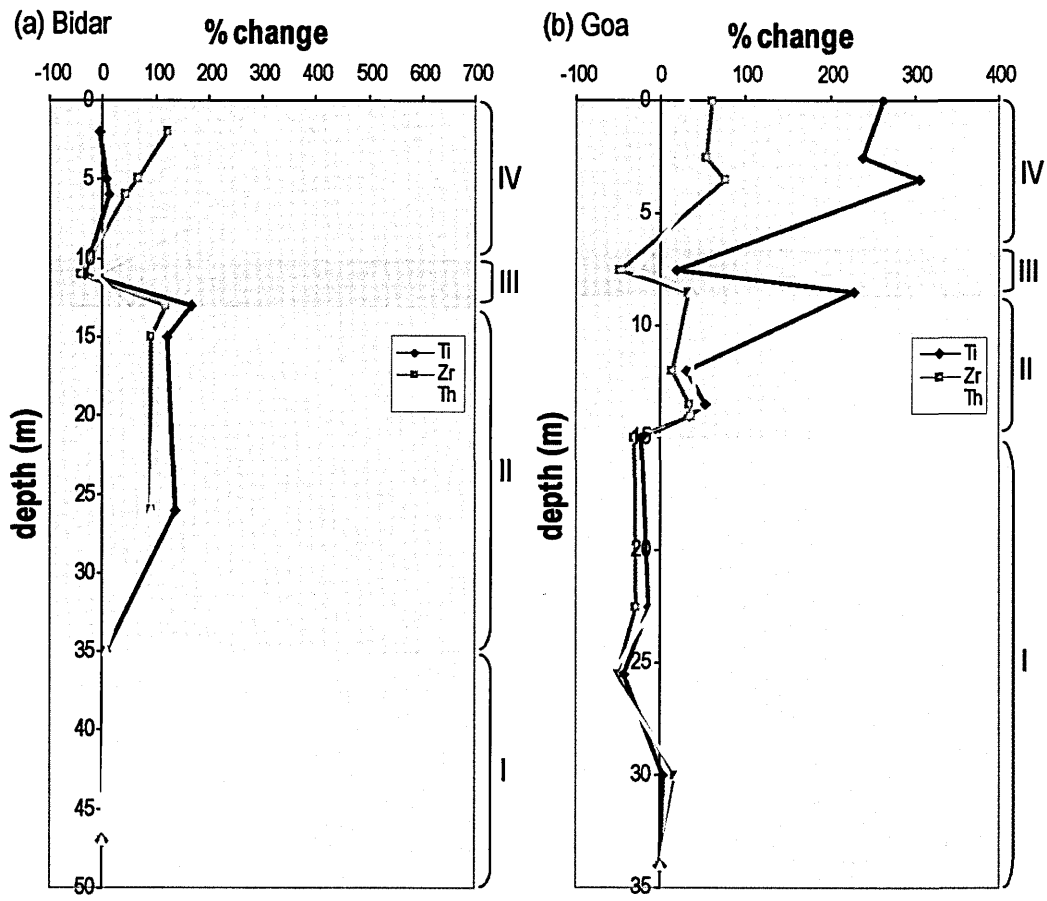

Fig. 7.6. - Percentage change for concentrations of Ti, Zr and Th relative to parent concentrations at (a) Bidar and (b) Goa.

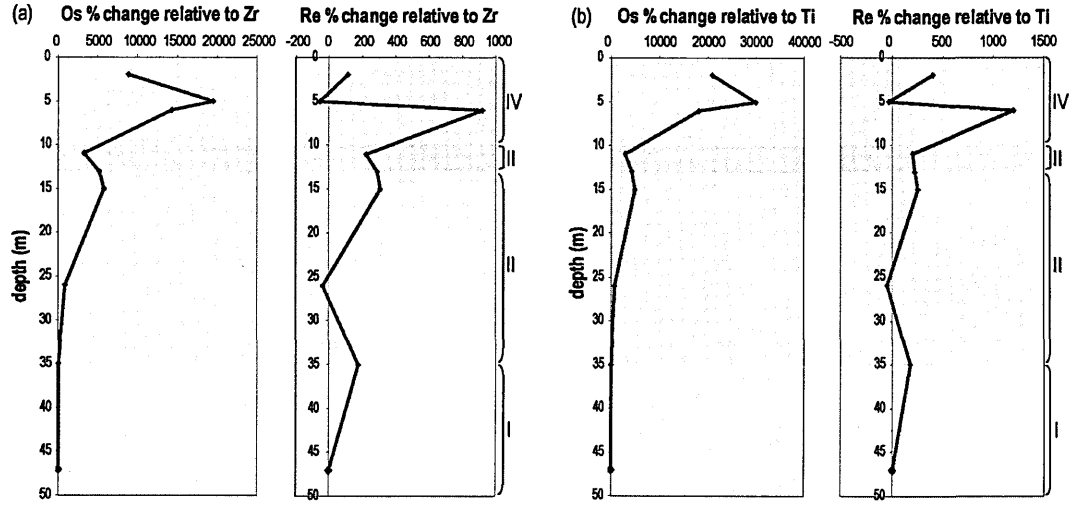

Fig. 7.7. Re and Os concentrations for Bidar shown relative to (a) zirconium and (b) titanium. Since both trace elements are considered to be immobile, this serves to illustrate the degree of enrichment of Re and Os in both laterite profiles, relative to their parent-rock.

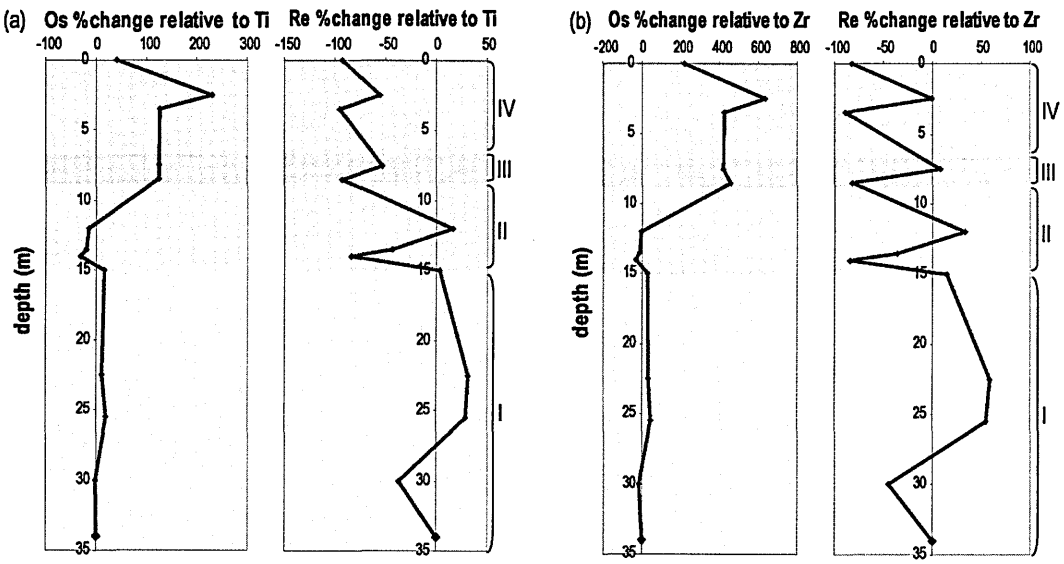

Fig. 7.8. Re and Os concentrations for Goa shown relative to (a) zirconium and (b) titanium. Since both trace elements are considered to be immobile this serves to illustrate the degree of enrichment of Re and Os in both laterite profiles, relative to their parent-rock.

The pattern of increasing enrichment in Os towards the laterite surface has also been observed in a laterite with a granodiorite parent rock from Burkina Faso, west Africa (SHARMA et al., 1998) but these authors report low levels of Re at the surface (lower even than the parent rock) which is in contrast to the profiles at Bidar and Goa.

7.5.2. Re-Os isotope variations

Elemental enrichment of Os relative to Re in both profiles has an impact on the measured parent/daughter $^{187}Re/^{188}Os$ ratios. Both profiles show a decrease in $^{187}Re/^{188}Os$ with increasing alteration. Because ^{187}Os is produced from the β-decay of ^{187}Re it can be anticipated that with time the altered laterite samples will develop a less radiogenic $^{187}Os/^{188}Os$ isotope composition than the parent rock. Accordingly both profiles show $^{187}Os/^{188}Os$ values that are significantly less radiogenic than the parent rock with increasing alteration (i.e. up the profile). As will be seen for the profile at Goa this is not simply due to in situ decay of ^{187}Re but reflects the sources and distribution of

Re and Os. Therefore, for the profiles studied here and elsewhere (SHARMA et al., 1998) the data indicate that laterites possess a less radiogenic $^{187}Os/^{188}Os$ isotope composition that the parent rock from which they were formed, and this relationship appears to hold irrespective of rock type or age, or the timing of laterite formation.

7.5.3. Basalt Bole samples

The basaltic red 'boles' are relatively short lived weathering profiles that developed between successive lava flows in the uppermost lava sequences of the Deccan. These boles have been subject to intense tropical weathering (hence their red colour), but laterite formation *sensu-stricto* did not occur (SCHELLMANN, 1981), and thus they serve to distinguish the affects of element transport in a low pH, high Eh environment from straightforward basalt weathering at higher pH conditions. The Os concentrations in the boles are higher than the parent basalt at Bidar, but within the range observed for other Deccan basalts. However, the Os concentrations remain much lower than those observed in the laterite at Bidar. Rhenium concentrations are high at the base of the bole profile, similar to concentrations in unaltered basalt, but Re contents decline at higher levels where they are lower (in most cases) than the laterite at Bidar. The low Re and relatively low Os concentration results in generally low $^{187}Re/^{188}Os$ ratios and relatively unradiogenic $^{187}Os/^{188}Os$ isotope compositions, but all are within the range observed for unaltered Deccan basalt (ALLEGRE et al., 1999).

Thus, overall the bole samples appear to have experienced Re loss, with perhaps some slight Os enrichment, relative to the unweathered parent basalt. However, they do not show the either the extreme or differential enrichment of Os > Re seen in the laterite samples. This is presumably because there has been little external input of Re or Os to

the profile, and pH and Eh conditions have not resulted in significant mobility of these elements.

7.5.4. Origin of elemental and isotope variations

7.5.4.1. In situ parent rock weathering

There are a number of possible processes that may have been responsible for the high levels of Re and Os found in the laterites studied here. It is possible that this enrichment is simply due to in situ weathering of the parent rock, where Re and Os are located in weathering resistant minerals retained in the residue.

In order to estimate the amount of parent rock needed to supply the Re and Os found in the laterite, the Os (and Re) content of each horizon (Os_n) is weighted by the horizon thickness (h_n) and its absolute density (ρ_n).

$$Os = \sum_{n=1}^{n=x} [Os]_n h_n \rho_n \qquad \textit{Equation 7.2}$$

Using equation 7.2 the total Os content of the Bidar profile is 3×10^{-5} kg/m^2 and at Goa it is 7.6×10^{-6} kg/m^2. The total mass of Os that can be supplied from parent basalt to the Bidar profile is 5.8×10^{-7} kg/m^2, which is 1.9% of the estimated Os. Using the same method for Re then the precursor basalt can contribute 35% of the total Re, emphasising the greater level of Os enrichment in the profile. At Goa, the parent greywacke can supply 45% of the Os and all of the Re measured in the profile.

The same approach can be used to calculate the mass of Re or Os in 1 m of bedrock to give an estimate of the number of metres of parent rock that would have to be weathered and removed in order to concentrate the estimated masses of Re and Os. The high Os enrichment in the laterite at Bidar demands the weathering and erosion of some 2600 m of parent basalt to account for the laterite Os content; while 42m of

vertical loss are required at Goa. It has been suggested that some two thirds of the initial volume of the Deccan basalt may have been removed by weathering and erosion over the past 65 Ma (COURTILLOT et al., 1988). However, the Ambenali formation at Bidar represents the uppermost flow units of the Deccan eruptions (WIDDOWSON et al., 2000) and such volumes of basalt loss seem unlikely. Therefore, the elemental data appear to suggest that a direct, vertical, contribution by weathering and removal of the parent rock, concentrating Re and Os in the residue, is unlikely to supply the Re and Os at Bidar. However, such a process could potentially provide much of the Re and Os in the laterite at Goa.

The Os isotope data can also be used to evaluate whether the relatively unradiogenic Os at both sites could be derived from the parent rock. Laterite formation at Bidar is thought to have commenced at or soon after the final Deccan eruptions at ~65 Ma, and ceased sometime between 55 and 45 Ma, when the profile was elevated above the level of the watertable (WIDDOWSON, 1997). At first sight it would appear that laterite and parent rock at this locality possess very different $^{187}Os/^{188}Os$ isotope compositions. However, the laterite has a much lower parent/daughter $^{187}Re/^{188}Os$ ratio and thus growth of radiogenic ^{187}Os from the decay of ^{187}Re may have been very different both over the 10-20 Ma of laterite formation, and up to the present-day. Assuming that there has been no recent mobility of Re or Os calculations indicate that the Os isotope compositions of the laterites has not changed significantly over the past 65 Ma. Initial $^{187}Os/^{188}Os$ isotope ratios have also been calculated for the parent basalt to take into account the amount of ^{187}Os growth since between 65 and 45 Ma, and are shown against Os concentration in Fig. 7.9. The $^{187}Os/^{188}Os$ of the parent basalt was relatively unradiogenic at the time of eruption at 65 Ma ($^{187}Os/^{188}Os \approx 0.128$; this study and (ALLEGRE et al., 1999)). However, over the timescale of laterite formation the

basalts will have evolved to much more radiogenic values such that the Os isotope composition of the parent basalt at 55 to 45 Ma could have sourced the laterite at that time.

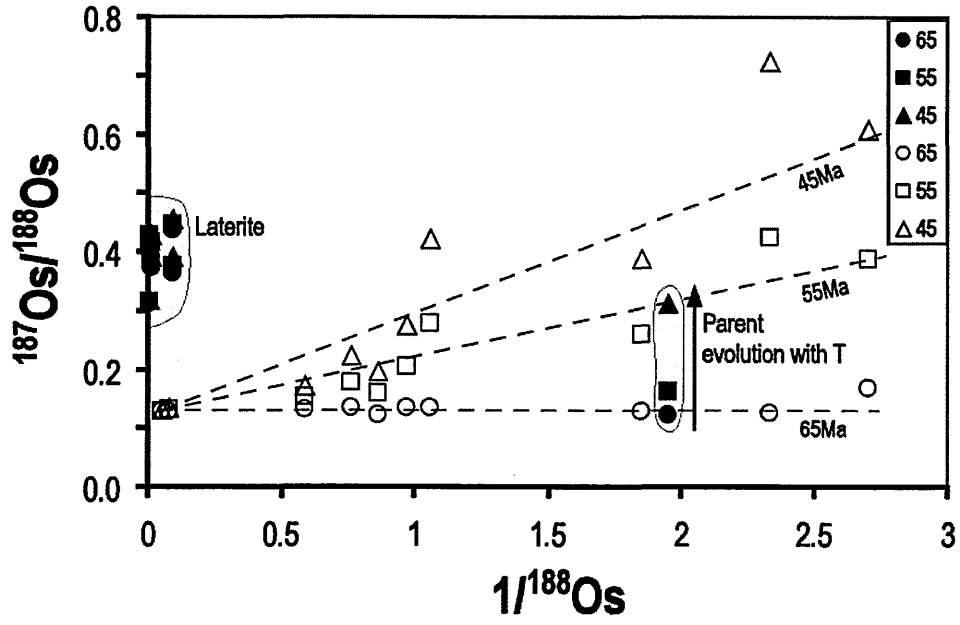

Fig. 7.9. Initial $^{187}Os/^{188}Os$ ratios against Os concentration (shown as $1/[^{188}Os]$) for the laterite and parent rock at Bidar (open symbols) and previously published data for the Deccan basalts (filled symbols). For the laterite samples there is no significant change in $^{187}Os/^{188}Os$ composition over the 20 Ma between basalt eruption and the end of laterite formation. However the parent basalt (and other Deccan basalts) rapidly evolve to radiogenic Os isotope values and may have possessed an appropriate composition at 45 Ma to source the laterite, albeit that the laterite is significantly enriched in Os. Initial ratios calculated using: $(^{187}Os/^{188}Os)_i = (^{187}Os/^{188}Os)_a - [(^{187}Re/^{188}Os)_a \times e^{(\lambda t-1)}]$ where λ is the decay constant of Os (taken as 1.66×10^{-11} yr^{-1}).

At Goa the parent greywacke again possesses much more radiogenic $^{187}Os/^{188}Os$ isotope compositions than the overlying laterite and higher $^{187}Re/^{188}Os$ ratios. Laterite formation at Goa occurred during the late Tertiary (between 20 and 30 Ma) and is ongoing today, providing a 30 Ma maximum timescale for the radiogenic growth of ^{187}Os. However, calculations indicate that even if laterite formation started at 30 Ma the greywacke will have been only slightly less radiogenic than at the present-day, and there will have been little resolvable change in the composition of the laterite (Fig. 7.10).

Therefore these calculations indicate that the unradiogenic Os isotope compositions of the laterite at Goa cannot have been simply acquired from the parent greywacke.

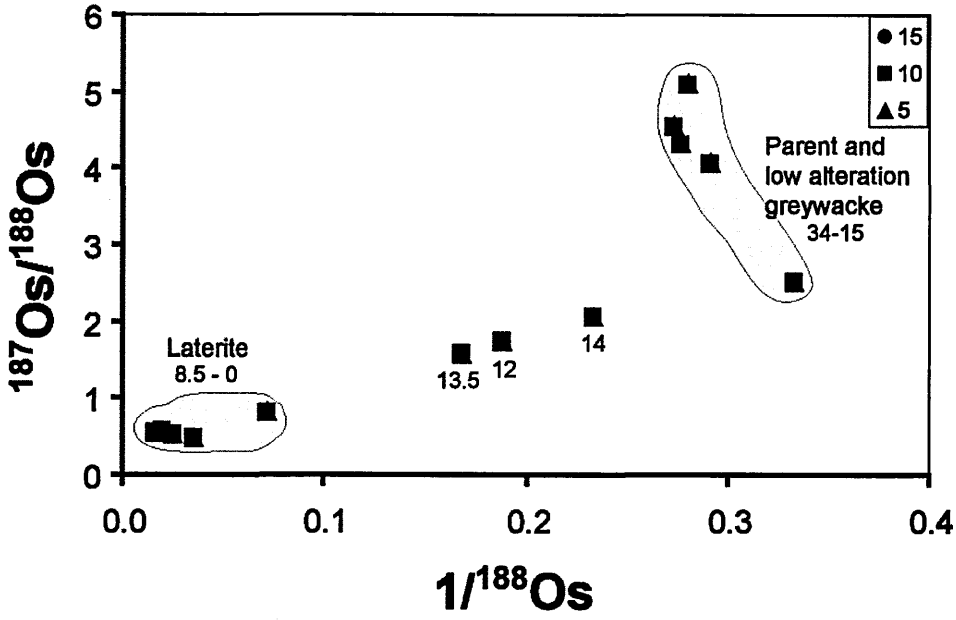

Fig. 7.10. Initial $^{187}Os/^{188}Os$ ratios against Os concentration (shown as $1/[^{188}Os]$) for the laterite and parent rock at Goa. The initial Os isotope compositions have been calculated for 5, 10 and 15 Ma of radiogenic growth of ^{187}Os. In contrast, to Bidar there is no significant change in $^{187}Os/^{188}Os$ ratios of the parent greywacke over these time intervals, and its composition is too radiogenic to exclusively source the laterite material, indicating that there must have been some external source of Os.

Overall, these data indicate that there must have been some form of external input of Re and Os to both profiles. While the Os isotope composition of the laterites at Bidar can be explained by ageing of the parent rock, the level of Os enrichment cannot be attributed to concentration (in residual minerals) through massive vertical weathering and erosion. At Goa, the level of Os enrichment is lower, and could conceivably be supplied by the parent greywacke. However, the parent greywacke at Goa possesses Os that is too radiogenic to account for the unradiogenic Os isotope compositions seen in the overlying laterites.

7.5.4.2 Aeolian input

Previous isotope studies of the laterite at Bidar have concluded that some degree of aeolian input to the top of the soil profile must have occurred. With increasing laterite alteration $^{87}Sr/^{86}Sr$ isotope composition becomes more radiogenic, shifting from 0.704249 to 0.710099 while $^{143}Nd/^{144}Nd$ becomes less radiogenic, shifting from 0.512818 to 0.512437. This variation far exceeds the natural variation of the Ambenali basalt, and is too extreme to be explained by fractionation induced by weathering. Instead these isotope shifts can be explained by aeolian input of ancient continental material such as the neighbouring Dravidian Shield (MASON, 2000). Li isotope data suggests that this continental material must have been weathered prior to aeolian transport and deposition (KISAKUREK et al., 2005). Redistribution of aeolian material input to the top of the profile could occur via dissolution and transport in groundwater and the subsequent precipitation of secondary minerals.

The Archean to Proterozoic Dharwar craton is one possible source of aeolian material. For the locality at Bidar, during the main period of laterite formation India was located to the south of the equator, and so southeast trade winds could have carried dust from this terrain (KALE et al., 1992). A number of potential source rocks have been studied from the Dharwar craton including granites, banded iron formation and limestone. However, while some rock types (or mixture of rock types) possess the appropriate Os isotope compositions, none have a sufficiently high Os concentration to account for those measured in the laterite. Further afield another potential source is loess, and samples from China, Europe and S. America give an average $^{187}Os/^{188}Os$ composition of 1.05 ± 0.23, and Os and Re concentrations of 31pg/g and 198pg/g respectively (PEUCKER-EHRENBRINK and JAHN, 2001). If it is assumed that the present day dust flux of 1-10 $g/m^2/yr$ (DUCE et al., 1991) is similar to that during the ~15-20 Ma

period over which both profiles developed then it is possible to estimate the potential mass of aeolian derived Os. If it is further assumed that all this Os dissolved and entered the laterite then such aeolian sources can account for a maximum of 20% of the total Os at Bidar and 81% of the total Os at Goa. This suggests that aeolian material with an average continental crustal Os composition and radiogenic $^{187}Os/^{188}Os$ isotope ratio cannot by itself account for all of the Os in these laterites, although it could account for much of the Os seen in the profile at Goa. Cosmic (interplanetary) dust is also known to have a high Os concentration and very unradiogenic $^{187}Os/^{188}Os$ isotope composition. The average flux of cosmic dust to Earth is 40-80 $g/km^2/yr$ (PEUCKER-EHRENBRINK and RAVIZZA, 2000a) with an Os concentration of ~50ng/g and $^{187}Os/^{188}Os$ composition of ~0.127 (ANDERS and GREVESSE, 1989). Over 20 Ma a maximum of $8x10^{-5}g$ of Os could be input to the laterite profiles, accounting for 0.26% and 1% of the total Os at Bidar and Goa, respectively. This suggests that despite the high Os concentrations of cosmic dust it is unlikely to be solely responsible for the enrichment seen in the laterite profiles.

These results highlight the fundamental difficulty of sourcing the Os isotope and elemental signature seen in the laterites directly from crustal rocks. This is because first, average continental crust has a much lower Os concentration (~50 ppt) (ESSER and TUREKIAN, 1993; PEUCKER-EHRENBRINK and JAHN, 2001; PEUCKER-EHRENBRINK and RAVIZZA, 2000b) than that seen in the laterites (80 to 1400 ppt). Second, average continental crust also has a relatively high $^{187}Re/^{188}Os$ ratio (ESSER and TUREKIAN, 1993; PEUCKER-EHRENBRINK and JAHN, 2001; PEUCKER-EHRENBRINK and RAVIZZA, 2000b) and thus ancient continental crust would be expected to develop a radiogenic $^{187}Os/^{188}Os$ isotope composition, consistent with the measurements for some of the Dharwar lithologies. It is possible to invoke the input of specific rock types, for

example, the weathering and erosion of ultramafic peridotites which possess high Os concentrations and radiogenic Os compositions (e.g. (REISBERG and LORAND, 1995; SNOW and REISBERG, 1995)). However, such peridotites do not normally possess unradiogenic Sr and radiogenic Nd compositions and so are unlikely to account for the variations seen in those systems (e.g. (JACOBSEN et al., 1984; RAMPONE et al., 1996). Alternatively it is possible that if the aeolian material was weathered prior to deposition then the Os concentration and isotope concentration in this residual material may be very different from that of the bulk rock from which it was sourced.

Therefore, while aeolian input is likely to have had some influence on the Re-Os isotope system in the laterites, the nature and extent of this input is difficult to assess. In any event, if aeolian deposition is responsible for the external input to the laterites then this must have occurred while the groundwaters were still actively redistributing elements within the profile or else the patterns of change, including that at the watertable would be obscured.

7.5.4.3. Groundwater input

The chemical variations observed in both profiles provide clear evidence of the role of groundwater in the redistribution of elements. In particular, the oxic-suboxic stratification provides a means for dissolution, transport and precipitation of both Re and Os. This raises the possibility that material may be gained or lost from the profile, not only by vertical movement from in situ weathering or aeolian input, but also by lateral movement of solute-laden groundwaters. The laterite at Bidar is remote from basement lithologies and developed upon the highest elevations. Consequently, there is no topography or adjacent rock types to drive a flow of externally sourced groundwater towards the profile. However, this does not preclude the input of groundwaters from the

breakdown of the Ambenali formation itself. As was shown in section 7.5.3.1 the Os isotope composition of the laterite at Bidar can be accounted for by derivation from the parent basalt, but does demand Os enrichment which could have been facilitated by Os-rich groundwaters.

Groundwaters carrying externally derived Os are much more likely to be present in the laterite at Goa, not only because of the low lying topographic position but also the presence of diverse surrounding rock types. Many of the surrounding rocks are from Archean and Proterozoic lithologies of the Dharwar craton, and therefore be expected to possess radiogenic Os isotope compositions. However, some lithologies do possess less radiogenic compositions and it is possible that Os could be input via groundwater derived from a mixture of these sources. Alternatively, the chemical signature of the groundwaters may have been derived from the nearby Deccan basalts.

7.6. Laterites and the surficial Os cycle

The results presented here, together with those of reported previously (SHARMA et al., 1998) suggest that laterites commonly possess much less radiogenic Os isotope compositions than their parent rock, and may also have much higher Os concentrations. Significantly, the laterites are also much less radiogenic and have much higher Os concentrations than average upper continental crust. Given the extensive geographical coverage of laterites (~30% of the exposed continental crust (TARDY, 1997), and their influence on the surface water cycle (nearly 50% of continental drainage flows through laterite terrain (TARDY, 1997) it seems likely that they will exert a significant influence on the movement of Re and Os between the continents, oceans and atmosphere.

During their formation laterite soils may initially act to sequester Os mobilised by weathering (either from groundwaters or aeolian input). However, over time the

relatively unradiogenic Os isotope composition from the weathering and erosion of laterite topsoils is likely to influence the composition of rivers and dust that they source. There is little detailed data for rivers draining laterite terrains, but, in general global river data suggest that the riverine $^{187}Os/^{188}Os$ isotope composition is actually more radiogenic than the average continental crust (LEVASSEUR et al., 1999; PEUCKER-EHRENBRINK and RAVIZZA, 2000b), possibly due to the effects of incongruent weathering. An upper limit of the Os contribution to the oceans from mineral aerosols can be calculated, from estimates of the global aerosol flux (e.g. (DUCE et al., 1991) and the Os content of average continental crust (ESSER and TUREKIAN, 1993; PEUCKER-EHRENBRINK and JAHN, 2001; PEUCKER-EHRENBRINK and RAVIZZA, 2000b), which suggests about a 10% contribution from aerosols (e.g. (PEUCKER-EHRENBRINK and RAVIZZA, 2000b). However, if 30% of that aeolian flux is derived from laterite topsoils (reflecting the continental coverage) then at least some aerosols may contain a much higher Os content than has previously been considered.

Changes in the balance of Os sequestered or released by laterites might be expected to accompany tectonic or climatic change. For example, uplift or cooling may lead to their enhanced physical weathering, and in particular, periods of global aridity will result in an enhanced dust flux from the continents. Conversely, during periods of global warming laterite formation may be enhanced (DEQUINCEY et al., 2002).

7.7. Summary

Laterite weathering profiles at Bidar and Goa developed on different rock types, with different ages and a time interval of ~40 Ma between periods of laterisation. Nevertheless, the profiles are very similar, progressing from unaltered bedrock upwards to increasingly altered saprolite and an uppermost Fe-rich iron crust. Both profiles also

preserve a watertable that is coincident with significant major and trace element variation.

Platinum Group element enrichment in laterites is well documented, and the data from this study confirms that both Re and Os are highly enriched in the laterite relative to the parent rock. The pattern of Re and Os enrichment and depletion, particularly at the level of the watertable indicates that both elements are mobile. The level of Os enrichment is far greater than that of Re, which is reflected in the decreasing $^{187}Re/^{188}Os$ ratio and corresponding decrease in $^{187}Os/^{188}Os$ up profile. Laterite $^{187}Os/^{188}Os$ ratios are always less radiogenic than the parent bedrock that they developed from, consistent with previous work (SHARMA et al., 1998).

The origin of the high Re and Os concentrations in the laterites remains unclear. Previous isotope studies of the laterite at Bidar have concluded that aeolian input to the profile must have occurred. Nd and Sr isotope data suggest that the source of this material was ancient continental crust (MASON, 2000), while Li isotopes indicate that this material has experienced significant weathering prior to deposition (KISAKUREK et al., 2004). However, for Os most potential crustal sources have low Os concentrations demanding significant aeolian deposition or the pre-concentration of Os in aerosols (perhaps as residues from weathering). Similarly average crustal sources are too radiogenic to account for the unradiogenic $^{187}Os/^{188}Os$ compositions observed in both laterites. Alternatively, the Re and Os may have been transported into the profile by the lateral movement of solute-laden groundwaters.

The Os concentration in laterites is similar to that found in Os-rich rock types, such as organic-rich sediments (JAFFE et al., 2002; PEUCKER-EHRENBRINK and HANNIGAN, 2000; SINGH et al., 1999) and ultramafic peridotites (REISBERG and LORAND, 1995; SNOW and REISBERG, 1995), but in contrast to those lithologies laterites

comprise a significant part of the continental land surface, and play an active role in the surface water cycle. Under those circumstances laterite formation or weathering is likely to exert a significant influence on Os behaviour in the surface environment, and that influence is itself likely to be highly sensitive to climatic or tectonic change (cf. (DEQUINCEY et al., 2002).

References

Allaart J. H. (1982) Map sheet no. 2, Frederikshåb Isblink -Søndre Strømfjord. Geological Survey of Denmark and Greenland (GEUS).

Allegre C. J., Birck J. L., Capmas F., and Courtillot V. (1999) Age of the Deccan traps using Re-187-Os-187 systematics. *Earth and Planetary Science Letters* **170**(3), 197-204.

Allegre C. J. and Luck J. M. (1980) Osmium Isotopes as Petrogenetic and Geological Tracers. *Earth and Planetary Science Letters* **48**(1), 148-154.

Aller R. C. (1998) Mobile deltaic and continental shelf muds as suboxic, fluidized bed reactors. *Marine Chemistry* **61**(3-4), 143-155.

Aller R. C. and Blair N. E. (2004) Early diagenetic remineralization of sedimentary organic C in the Gulf of Papua deltaic complex (Papua New Guinea): Net loss of terrestrial C and diagenetic fractionation of C isotopes. *Geochimica et Cosmochimica Acta* **68**(8), 1815-1825.

Anbeek C., Vanbreemen N., Meijer E. L., and Vanderplas L. (1994) The Dissolution of Naturally Weathered Feldspar and Quartz. *Geochimica Et Cosmochimica Acta* **58**(21), 4601-4613.

Anders E. and Grevesse N. (1989) Abundances of the elements: Meteoritic and solar. *Geochimica et Cosmochimica Acta* **53**(1), 197-214.

Anderson N. J., Harriman R., Ryves D. B., and Patrick S. T. (2001) Dominant Factors Controlling Variability in the Ionic Composition of West Greenland Lakes. *Arctic, Antarctic, and Alpine Research* **33**(4), 418-425.

Anderson S. P. (2005) Glaciers show direct linkage between erosion rate and chemical weathering fluxes. *Geomorphology* **67**(1-2), 147-157.

Anderson S. P., Drever J. I., Frost C. D., and Holden P. (2000) Chemical weathering in the foreland of a retreating glacier. *Geochimica Et Cosmochimica Acta* **64**(7), 1173-1189.

Anderson S. P., Drever J. I., and Humphrey N. F. (1997) Chemical weathering in glacial environments. *Geology* **25**(5), 399-402.

Anderson S. P., Longacre S. A., and Kraal E. R. (2003) Patterns of water chemistry and discharge in the glacier-fed Kennicott River, Alaska: evidence for subglacial water storage cycles. *Chemical Geology* **202**(3-4), 297-312.

Andersson P. S., Dahlqvist R., Ingri J., and Gustafsson O. (2001) The isotopic composition of Nd in a boreal river: A reflection of selective weathering and colloidal transport. *Geochimica et Cosmochimica Acta* **65**(4), 521-527.

Appel F., Moorbath, Myers,. (1998) Recognizable primary volcanic and sedimentary features in a low-strain domain of the highly deformed, oldest known Greenstone Belt, Isua, West Greenland. *Terra Nova* **10**(2), 57-62.

Appelo C. A. J. and Postma D. (2005) *Geochemistry, groundwater and pollution.* A.A. Balkema.

Armstrong R. l. (1971) Glacial Erosion and Variable Isotopic Composition of Strontium in Sea Water. *Nature-Physical Science* **230**(14), 132-&.

Awad A., van Groos A. F. K., and Guggenheim S. (2000) Forsteritic olivine: Effect of crystallographic direction on dissolution kinetics. *Geochimica et Cosmochimica Acta* **64**(10), 1765-1772.

Ball J. W. and Nordstrom D. K. (1991) User's manual for WATEQ4F, with revised thermodynamic data base and text cases for calculating speciation of major, trace, and redox elements in natural waters, pp. 193.

Bell R. E. (2008) The role of subglacial water in ice-sheet mass balance. **1**(5), 297-304.

Berger A. (1988) Milankovitch Theory and Climate. *Reviews of Geophysics* **26**(4), 624-657.

Berger G., Claparols C., Guy C., and Daux V. (1994) Dissolution Rate of a Basalt Glass in Silica-Rich Solutions - Implications for Long-Term Alteration. *Geochimica et Cosmochimica Acta* **58**(22), 4875-4886.

Berger G., Schott J., and Guy C. (1988) Behavior of Li, Rb and Cs During Basalt Glass and Olivine Dissolution and Chlorite, Smectite and Zeolite Precipitation from Seawater - Experimental Investigations and Modelization between 50-Degrees and 300-Degrees-C. *Chemical Geology* **71**(4), 297-312.

Berner R. A. (2003) The long-term carbon cycle, fossil fuels and atmospheric composition. *Nature* **426**(6964), 323-326.

Berner R. A. (2004) A model for calcium, magnesium and sulfate in seawater over Phanerozoic time. *American Journal of Science* **304**(5), 438-453.

Bi E. B. B., Poszwa A., and Vigier N. (2008) Experimental determination of magnesium isotope fractionation during higher plant growth. *Geophysical Research Abstracts* **10**(EGU 2008).

Bi E. B. B., Vigier N., Poszwa A., and Brenot A. (2007) Compared Mg isotope compositions of plants, rocks and waters. *Geochimica et Cosmochimica Acta* **71**(15), A106-A106.

Birck J. L., Barman M. R., and Capmas F. (1997) Re-Os isotopic measurements at the femtomole level in natural samples. *Geostandards Newsletter-the Journal of Geostandards and Geoanalysis* **21**(1), 19-27.

Black J. R., Yin Q.-z., and Casey W. H. (2006) An experimental study of magnesium-isotope fractionation in chlorophyll-a photosynthesis. *Geochimica et Cosmochimica Acta* **70**(16), 4072-4079.

Blake R. E. and Walter L. M. (1999) Kinetics of feldspar and quartz dissolution at 70-80 degrees C and near-neutral pH: Effects of organic acids and NaCl. *Geochimica et Cosmochimica Acta* **63**(13-14), 2043-2059.

Blum J. D., Gazis C. A., Jacobson A. D., and Chamberlain C. P. (1998) Carbonate versus silicate weathering in the Raikhot watershed within the high Himalayan crystalline series. *Geology* **26**(5), 411-414.

Blum A. and Lasaga A. (1988) Role of Surface Speciation in the Low-Temperature Dissolution of Minerals. *Nature* **331**(6155), 431-433.

Borger H. and Widdowson M. (2001) Indian laterites, and lateritious residues of southern Germany: A petrographic, mineralogical, and geochemical comparison. *Zeitschrift Fur Geomorphologie* **45**(2), 177-200.

Bottrell S. H. and Tranter M. (2002) Sulphide oxidation under partially anoxic conditions at the bed of the Haut Glacier d'Arolla, Switzerland. *Hydrological Processes* **16**(12), 2363-2368.

Bowles J. F. W. (1986) The Development of Platinum-Group Minerals in Laterites. *Economic Geology* **81**(5), 1278-1285.

Bowles J. F. W., Gize A. P., and Cowden A. (1994) The Mobility of the Platinum-Group Elements in the Soils of the Freetown Peninsula, Sierra-Leone. *Canadian Mineralogist* **32**, 957-967.

Brady P. V. and Gislason S. R. (1997) Seafloor weathering controls on atmospheric CO2 and global climate. *Geochimica et Cosmochimica Acta* **61**(5), 965-973.

Brantley S. L., Liermann L. J., Guynn R. L., Anbar A., Icopini G. A., and Barling J. (2004) Fe isotopic fractionation during mineral dissolution with and without bacteria. *Geochimica et Cosmochimica Acta* **68**(15), 3189-3204.

Brantley S. L. and Stillings L. (1996) Feldspar dissolution at 25 degrees C and low pH. *American Journal of Science* **296**(2), 101-127.

Braun J. J., Viers J., Dupre B., Polve M., Ndam J., and Muller J. P. (1998) Solid/liquid REE fractionation in the lateritic system of Goyoum, east Cameroon: The implication for the present dynamics of the soil covers of the humid tropical regions. *Geochimica et Cosmochimica Acta* **62**(2), 273-299.

Bray A. M., Chan L. H., and Von Damm K. L. (2001) Constancy of the Li-Isotopic Signature in Mid-Ocean Ridge Hydrothermal Fluids: Evidence for Equilibrium Control. *Eos Trans. AGU* **82**(47), OS41A-0440.

Brimhall G. H. and Dietrich W. E. (1987) Constitutive Mass Balance Relations between Chemical-Composition, Volume, Density, Porosity, and Strain in Metasomatic Hydrochemical Systems - Results on Weathering and Pedogenesis. *Geochimica et Cosmochimica Acta* **51**(3), 567-587.

Brimhall G. H., Lewis C. J., Ford C., Bratt J., Taylor G., and Warin O. (1991) Quantitative Geochemical Approach to Pedogenesis - Importance of Parent Material Reduction, Volumetric Expansion, and Eolian Influx in Lateritization. *Geoderma* **51**(1-4), 51-91.

Brown D. J., Helmke P. A., and Clayton M. K. (2003) Robust geochemical indices for redox and weathering on a granitic laterite landscape in central Uganda. *Geochimica et Cosmochimica Acta* **67**(15), 2711-2723.

Brownawell B. J., Chen H., Collier J. M., and Westall J. C. (1990) Adsorption of Organic Cations to Natural Materials. *Environmental Science & Technology* **24**(8), 1234-1241.

Brunauer S., Emmett P. H., and Teller E. (1938) Adsorption of Gases in Multimolecular Layers. *J. Am. Chem. Soc.* **60**(2), 309-319.

Buhl D., Immenhauser A., Smeulders G., Kabiri L., and Richter D. K. (2007) Time series delta Mg-26 analysis in speleothem calcite: Kinetic versus equilibrium fractionation, comparison with other proxies and implications for palaeoclimate research. *Chemical Geology* **244**, 715-729.

Burton K. W. (2006) Global weathering variations inferred from marine radiogenic isotope records. *Journal of Geochemical Exploration* **88**(1-3), 262-265.

Burton K. W., Schiano P., Birck J. L., and Allegre C. J. (1999) Osmium isotope disequilibrium between mantle minerals in a spinel-lherzolite. *Earth and Planetary Science Letters* **172**(3-4), 311-322.

Cabri L. and Harris D. (1975) Zoning in Os-Ir alloys and the relation of the geological and tectonic environment of the source rocks to the bulk Pd: Pt+ Ir+ Os ratio for placers. *The Canadian Mineralogist* **13**, 266–274.

Carder E. A., Galy A., and Elderfield H. (2004) The magnesium isotopic composition of oceanic water masses. *Geochimica et Cosmochimica Acta* **68**(11), A329.

Chadwick B., Vasudev V. N., and Hegde G. V. (2000) The Dharwar craton, southern India, interpreted as the result of Late Archaean oblique convergence. *Precambrian Research* **99**(1-2), 91-111.

Chan L. H. and Edmond J. M. (1988) Variation of Lithium Isotope Composition in the Marine-Environment - a Preliminary-Report. *Geochimica et Cosmochimica Acta* **52**(6), 1711-1717.

Chan L. H., Edmond J. M., Thompson G., and Gillis K. (1992) Lithium Isotopic Composition of Submarine Basalts - Implications for the Lithium Cycle in the Oceans. *Earth and Planetary Science Letters* **108**(1-3), 151-160.

Chan L. H., Gieskes J. M., You C. F., and Edmond J. M. (1994) Lithium Isotope Geochemistry of Sediments and Hydrothermal Fluids of the Guaymas Basin, Gulf of California. *Geochimica et Cosmochimica Acta* **58**(20), 4443-4454.

Chan L. H. and Hein J. R. (2007) Lithium contents and isotopic compositions of ferromanganese deposits from the global ocean. *Deep-Sea Research Part Ii-Topical Studies in Oceanography* **54**(11-13), 1147-1162.

Chang V. T. C., Williams R. J. P., Makishima A., Belshawl N. S., and O'Nions R. K. (2004) Mg and Ca isotope fractionation during CaCO3 biomineralisation. *Biochemical and Biophysical Research Communications* **323**(1), 79-85.

Chardon E. S., Livens F. R., and Vaughan D. J. (2006) Reactions of feldspar surfaces with aqueous solutions. *Earth-Science Reviews* **78**(1-2), 1-26.

Chen J. L., Wilson C. R., and Tapley B. D. (2006) Satellite gravity measurements confirm accelerated melting of Greenland ice sheet. *Science* **313**(5795), 1958-1960.

Chen Y. and Brantley S. L. (2000) Dissolution of forsteritic olivine at 65 degrees C and $2 < pH < 5$. *Chemical Geology* **165**(3-4), 267-281.

Clarke G. K. C. (2005) Subglacial processes. *Annual Review of Earth and Planetary Sciences* **33**(1), 247-276.

Courtillot V., Feraud G., Maluski H., Vandamme D., Moreau M. G., and Besse J. (1988) Deccan Flood Basalts and the Cretaceous Tertiary Boundary. *Nature* **333**(6176), 843-846.

Crovisier J. L., Honnorez J., and Eberhart J. P. (1987) Dissolution of Basaltic Glass in Seawater - Mechanism and Rate. *Geochimica et Cosmochimica Acta* **51**(11), 2977-2990.

Crovisier J. L., Thomassin J. H., Juteau T., Eberhart J. P., Touray J. C., and Baillif P. (1983) Experimental Seawater Basaltic Glass Interaction at 50-Degrees-C - Study of Early Developed Phases by Electron-Microscopy and X-Ray Photoelectron Spectrometry. *Geochimica et Cosmochimica Acta* **47**(3), 377-387.

Das S. B., Joughin I., Behn M. D., Howat I. M., King M. A., Lizarralde D., and Bhatia M. P. (2008) Fracture Propagation to the Base of the Greenland Ice Sheet During Supraglacial Lake Drainage 10.1126/science.1153360. *Science* **320**(5877), 778-781

Daux V., Guy C., Advocat T., Crovisier J. L., and Stille P. (1997) Kinetic aspects of basaltic glass dissolution at 90 degrees C: role of aqueous silicon and aluminium. *Chemical Geology* **142**(1-2), 109-126.

Davis J. A. and Kent D. B. (1990) Surface complexation modeling in aqueous geochemistry. *Reviews in Mineralogy and Geochemistry* **23**(1), 177-260.

De La Rocha C. L., Brzezinski M. A., and DeNiro M. J. (2000) A first look at the distribution of the stable isotopes of silicon in natural waters. *Geochimica et Cosmochimica Acta* **64**(14), 2467-2477.

de Villiers S., Dickson J. A. D., and Ellam R. M. (2005) The composition of the continental river weathering flux deduced from seawater Mg isotopes. *Chemical Geology* **216**(1-2), 133-142.

Decarreau A. (1985) Partitioning of Divalent Transition-Elements between Octahedral Sheets of Trioctahedral Smectites and Water. *Geochimica et Cosmochimica Acta* **49**(7), 1537-1544.

Depaolo D. J. and Ingram B. L. (1985) High-Resolution Stratigraphy with Strontium Isotopes. *Science* **227**(4689), 938-941.

Dequincey O., Chabaux F., Clauer N., Sigmarsson O., Liewig N., and Leprun J. C. (2002) Chemical mobilizations in laterites: Evidence from trace elements and U-

238-U-234-Th-230 disequilibria. *Geochimica et Cosmochimica Acta* **66**(7), 1197-1210.

Dessert C., Dupre B., Francois L. M., Schott J., Gaillardet J., Chakrapani G., and Bajpai S. (2001) Erosion of Deccan Traps determined by river geochemistry: impact on the global climate and the Sr-87/Sr-86 ratio of seawater. *Earth and Planetary Science Letters* **188**(3-4), 459-474.

Dessert C., Dupre B., Gaillardet J., Francois L. M., and Allegre C. J. (2003) Basalt weathering laws and the impact of basalt weathering on the global carbon cycle. *Chemical Geology* **202**(3-4), 257-273.

Dickin A. P. (1995) *Radiogenic Isotope Geology*. Cambridge University Press.

Drever J. I. and Stillings L. L. (1997) The role of organic acids in mineral weathering. *Colloids and Surfaces a-Physicochemical and Engineering Aspects* **120**(1-3), 167-181.

Duce R., Liss P., Merrill J., Atlas E., Buat-Menard P., Hicks B., Miller J., Prospero J., Arimoto R., and Church T. (1991) The atmospheric input of trace species to the world ocean. *Global Biogeochemical Cycles* **5**(3), 193-259.

Dupre B., Dessert C., Oliva P., Godderis Y., Viers J., Francois L., Millot R., and Gaillardet J. (2003) Rivers, chemical weathering and Earth's climate. *Comptes Rendus Geoscience* **335**(16), 1141-1160.

Dupre B., Gaillardet J., Rousseau D., and Allegre C. J. (1996) Major and trace elements of river-borne material: The Congo Basin. *Geochimica et Cosmochimica Acta* **60**(8), 1301-1321.

Dupre B., Viers J., Dandurand J. L., Polve M., Benezeth P., Vervier P., and Braun J. J. (1999) Major and trace elements associated with colloids in organic-rich river waters: ultrafiltration of natural and spiked solutions. *Chemical Geology* **160**(1-2), 63-80.

Eliopoulos D. G. and Economou-Eliopoulos M. (2000) Geochemical and mineralogical characteristics of Fe-Ni- and bauxitic-laterite deposits of Greece. *Ore Geology Reviews* **16**(1-2), 41-58.

Escher J. C. and Pulvertaft T. C. R. (1995) Geological Map of Greenland 1:2500000. Geological Survey of Denmark and Greenland (GEUS).

Esser B. K. and Turekian K. K. (1993) The Osmium Isotopic Composition of the Continental-Crust. *Geochimica et Cosmochimica Acta* **57**(13), 3093-3104.

Fantle M. S. and DePaolo D. J. (2006) Sr isotopes and pore fluid chemistry in carbonate sediment of the Ontong Java Plateau: Calcite recrystallization rates and evidence for a rapid rise in seawater Mg over the last 10 million years. *Geochimica et Cosmochimica Acta* **70**(15), 3883-3904.

Flaathen T. K. and Gislason S. R. (2007) The effect of volcanic eruptions on the chemistry of surface waters: The 1991 and 2000 eruptions of Mt. Hekla, Iceland. *Journal of Volcanology and Geothermal Research* **164**(4), 293-316.

Fortner S. K., Tranter M., Fountain A., Lyons W. B., and Welch K. A. (2005) The geochemistry of supraglacial streams of Canada Glacier, Taylor Valley (Antarctica), and their evolution into proglacial waters. *Aquatic Geochemistry* **11**(4), 391-412.

Gaillardet J., Dupre B., and Allegre C. J. (1995) A Global Geochemical Mass Budget Applied to the Congo Basin Rivers - Erosion Rates and Continental-Crust Composition. *Geochimica et Cosmochimica Acta* **59**(17), 3469-3485.

Gaillardet J., Dupre B., Allegre C. J., and Negrel P. (1997) Chemical and physical denudation in the Amazon River basin. *Chemical Geology* **142**(3-4), 141-173.

Gaillardet J., Dupre B., and Allegre C. J. (1999a) Geochemistry of large river suspended sediments: Silicate weathering or recycling tracer? *Geochimica et Cosmochimica Acta* **63**(23-24), 4037-4051.

Gaillardet J., Dupre B., Louvat P., and Allegre C. J. (1999b) Global silicate weathering and CO2 consumption rates deduced from the chemistry of large rivers. *Chemical Geology* **159**(1-4), 3-30.

Gaillardet J., Viers J., and Dupre B. (2003) Trace Elements in River Waters. Treatise on Geochemistry (ed. H. D. Holland and K. K. Turekian), pp. 225-272. Pergamon.

Galy A., Bar-Matthews M., Halicz L., and O'Nions R. K. (2002) Mg isotopic composition of carbonate: insight from speleothem formation. *Earth and Planetary Science Letters* **201**(1), 105-115.

Galy A., Belshaw N. S., Halicz L., and O'Nions R. K. (2001) High-precision measurement of magnesium isotopes by multiple-collector inductively coupled plasma mass spectrometry. *International Journal of Mass Spectrometry* **208**(1-3), 89-98.

Galy A., Yoffe O., Janney P. E., Williams R. W., Cloquet C., Alard O., Halicz L., Wadhwa M., Hutcheon I. D., Ramon E., and Carignan J. (2003) Magnesium

isotope heterogeneity of the isotopic standard SRM980 and new reference materials for magnesium-isotope-ratio measurements. *Journal of Analytical Atomic Spectrometry* **18**(11), 1352-1356.

Gannoun A., Burton K. W., Thomas L. E., Parkinson I. J., van Calsteren P., and Schiano P. (2004) Osmium Isotope Heterogeneity in the Constituent Phases of Mid-Ocean Ridge Basalts 10.1126/science.1090266. *Science* **303**(5654), 70-72.

Gannoun A., Burton K. W., Vigier N., Gislason S. R., Rogers N., Mokadem F., and Sigfusson B. (2006) The influence of weathering process on riverine osmium isotopes in a basaltic terrain. *Earth and Planetary Science Letters* **243**(3-4), 732-748.

Garrels R. M. and Mackenzie F. T. (1971) *Evolution of Sedimentary Rocks*. WW Norton and Co.

Georg R. B., Reynolds B. C., Frank M., and Halliday A. N. (2006) New sample preparation techniques for the determination of Si isotopic compositions using MC-ICPMS. *Chemical Geology* **235**(1-2), 95-104.

Georg R. B., Reynolds B. C., West A. J., Burton K. W., and Halliday A. N. (2007) Silicon isotope variations accompanying basalt weathering in Iceland. *Earth and Planetary Science Letters* **261**(3-4), 476-490.

Giammar D. E., Bruant R. G., and Peters C. A. (2005) Forsterite dissolution and magnesite precipitation at conditions relevant for deep saline aquifer storage and sequestration of carbon dioxide. *Chemical Geology* **217**(3-4), 257-276.

Gislason S. R. and Arnorsson S. (1993) Dissolution of Primary Basaltic Minerals in Natural-Waters - Saturation State and Kinetics. *Chemical Geology* **105**(1-3), 117-135.

Gislason S. R., Arnorsson S., and Armannsson H. (1996) Chemical weathering of basalt in southwest Iceland: Effects of runoff, age of rocks and vegetative/glacial cover. *American Journal of Science* **296**(8), 837-907.

Gislason S. R. and Eugster H. P. (1987) Meteoric water-basalt interactions. II: A field study in N.E. Iceland. *Geochimica et Cosmochimica Acta* **51**(10), 2841-2855.

Gislason S. R. and Hans P. E. (1987) Meteoric water-basalt interactions. I: A laboratory study. *Geochimica et Cosmochimica Acta* **51**(10), 2827-2840.

Gislason S. R. and Oelkers E. H. (2003) Mechanism, rates, and consequences of basaltic glass dissolution: II. An experimental study of the dissolution rates of basaltic

glass as a function of pH and temperature. *Geochimica Et Cosmochimica Acta* **67**(20), 3817-3832.

Gislason S. R., Oelkers E. H., and Snorrason A. (2006) Role of river-suspended material in the global carbon cycle. *Geology* **34**(1), 49-52.

Gislason S. R., Veblen D. R., and Livi K. J. T. (1993) Experimental Meteoric Water-Basalt Interactions - Characterization and Interpretation of Alteration Products. *Geochimica Et Cosmochimica Acta* **57**(7), 1459-1471.

Grandstaff D. E. (1978) Changes in Surface-Area and Morphology and Mechanism of Forsterite Dissolution. *Geochimica Et Cosmochimica Acta* **42**(12), 1899-1901.

Guy C. and Schott J. (1989) Multisite Surface-Reaction Versus Transport Control During the Hydrolysis of a Complex Oxide. *Chemical Geology* **78**(3-4), 181-204.

Hanchen M., Prigiobbe V., Storti G., Seward T. M., and Mazzotti M. (2006) Dissolution kinetics of fosteritic olivine at 90-150 degrees C including effects of the presence of CO2. *Geochimica Et Cosmochimica Acta* **70**(17), 4403-4416.

Hardie L. A. (1996) Secular variation in seawater chemistry: An explanation for the coupled secular variation in the mineralogies of marine limestones and potash evaporites over the past 600 my. *Geology* **24**(3), 279-283.

Hart S. and Ravizza G. (1996) Os partitioning between phases in lherzolite and basalt. *Geophysical monograph* **95**, 123-134.

Harris N., Bickle M., Chapman H., Fairchild I., and Bunbury J. (1998) The significance of Himalayan rivers for silicate weathering rates: evidence from the Bhote Kosi tributary. *Chemical Geology* **144**(3-4), 205-220.

Hasholt B. (1996) Sediment Transport In Greenland. In *Erosion And Sediment Yield: Global And Regional Perspectives*, Vol. 236, pp. 105-114. IAHS.

Hathorne E. C. and James R. H. (2006) Temporal record of lithium in seawater: A tracer for silicate weathering? *Earth and Planetary Science Letters* **246**(3-4), 393-406.

Haug G. H., Ganopolski A., Sigman D. M., Rosell-Mele A., Swann G. E. A., Tiedemann R., Jaccard S. L., Bollmann J., Maslin M. A., Leng M. J., and Eglinton G. (2005) North Pacific seasonality and the glaciation of North America 2.7 million years ago. *Nature* **433**(7028), 821-825.

Hay W. W. (1998) Detrital sediment fluxes from continents to oceans. *Chemical Geology* **145**(3-4), 287-323.

Hay W. W., Sloan J. L., and Wold C. N. (1988) Mass Age Distribution and Composition of Sediments on the Ocean-Floor and the Global Rate of Sediment Subduction. *Journal of Geophysical Research-Solid Earth and Planets* **93**(B12), 14933-14940.

Hess J., Bender M. L., and Schilling J. G. (1986) Evolution of the Ratio of Sr-87 to Sr-86 in Seawater from Cretaceous to Present. *Science* **231**(4741), 979-984.

Hodson M. E. (2002) Experimental evidence for mobility of Zr and other trace elements in soils. *Geochimica Et Cosmochimica Acta* **66**(5), 819-828.

Holdren G. R. and Speyer P. M. (1986) Stoichiometry of Alkali Feldspar Dissolution at Room Temperature and Various pH Values. In *Rates of Chemical Weathering of Rocks and Minerals* (ed. S. M. Colman and D. P. Dethier), pp. 61-81. Academic Press.

Holland H. D. (2005) Sea level, sediments and the composition of seawater. *American Journal of Science* **305**(3), 220-239.

Holland H. D. and Zimmerman H. (2000) The dolomite problem revisited. *International Geology Review* **42**(6), 481-490.

Huh Y., Chan L. H., and Chadwick O. A. (2004) Behavior of lithium and its isotopes during weathering of Hawaiian basalt. *Geochemistry Geophysics Geosystems* **5**.

Huh Y., Chan L. H., and Edmond J. M. (2001) Lithium isotopes as a probe of weathering processes: Orinoco River. *Earth and Planetary Science Letters* **194**(1-2), 189-199.

Huh Y., Chan L. H., Zhang L., and Edmond J. M. (1998) Lithium and its isotopes in major world rivers: Implications for weathering and the oceanic budget. *Geochimica Et Cosmochimica Acta* **62**(12), 2039-2051.

Jacobsen S. B., Quick J. E., and Wasserburg G. J. (1984) A Nd and Sr Isotopic Study of the Trinity Peridotite - Implications for Mantle Evolution. *Earth and Planetary Science Letters* **68**(3), 361-378.

Jaffe L. A., Peucker-Ehrenbrink B., and Petsch S. T. (2002) Mobility of rhenium, platinum group elements and organic carbon during black shale weathering. *Earth and Planetary Science Letters* **198**(3-4), 339-353.

James R. H. and Palmer M. R. (2000) The lithium isotope composition of international rock standards. *Chemical Geology* **166**(3-4), 319-326.

Jones M. T. and Gislason S. R. (2008) Rapid releases of metal salts and nutrients following the deposition of volcanic ash into aqueous environments. *Geochimica et Cosmochimica Acta* 72(15), 3661-3680.

Jorgensen A. S. and Andreasen F. (2007) Mapping of permafrost surface using ground-penetrating radar at Kangerlussuaq Airport, western Greenland. *Cold Regions Science and Technology* **48**(1), 64-72.

Kale V., Kulkarni H., Peshwa V., Widdowson M., and Mitchell C. (1992) Discussion on a geological map of the southern Deccan Traps, India and its structural implications. Reply. *Journal of the Geological Society(London)* **149**, 473-478.

Kisakurek B., James R. H., and Harris N. B. W. (2005) Li and delta Li-7 in Himalayan rivers: Proxies for silicate weathering? *Earth and Planetary Science Letters* **237**(3-4), 387-401.

Kisakurek B., Widdowson M., and James R. H. (2004) Behaviour of Li isotopes during continental weathering: the Bidar laterite profile, India. *Chemical Geology* **212**(1-2), 27-44.

Klootwijk C. T. and Peirce J. W. (1979) Indias and Australias Pole Path since the Late Mesozoic and the India-Asia Collision. *Nature* **282**(5739), 605-607.

Kobayashi M., Sawada A., Tani Y., Soma M., Tanaka A., Honma T., Seyama H., and Theng B. K. G. (2001) Acid dissolution of olivines, feldspars and dunite. *Water Air and Soil Pollution* **130**(1-4), 757-762.

Koppi A. J., Edis R., Field D. J., Geering H. R., Klessa D. A., and Cockayne D. J. H. (1996) Rare earth element trends and cerium-uranium-manganese associations in weathered rock from Koongarra, northern territory, Australia. *Geochimica Et Cosmochimica Acta* **60**(10), 1695-1707.

Krabill W., Hanna E., Huybrechts P., Abdalati W., Cappelen J., Csatho B., Frederick E., Manizade S., Martin C., Sonntag J., Swift R., Thomas R., and Yungel J. (2004) Greenland Ice Sheet: Increased coastal thinning. *Geophysical Research Letters* **31**(24).

Kuhnel R. A. (1987) The Role of Cationic and Anionic Scavengers in Laterites. *Chemical Geology* **60**(1-4), 31-40.

Leeder M. (1999) *Sedimentology and Sedimentary Basins: From Turbulence to Tectonics*. Blackwell Science.

Levasseur S., Birck J.-L., and Allègre C. J. (1998) Direct Measurement of Femtomoles of Osmium and the 187Os/186Os Ratio in Seawater 10.1126/science.282.5387.272. *Science* **282**(5387), 272-274.

Levasseur S., Birck J. L., and Allegre C. J. (1999) The osmium riverine flux and the oceanic mass balance of osmium. *Earth and Planetary Science Letters* **174**(1-2), 7-23.

Liu Y., Olsen A. A., and Rimstidt J. D. (2006) Mechanism for the dissolution of olivine series minerals in acidic solutions. *American Mineralogist* **91**(2-3), 455-458.

Louvat P. and Allegre C. J. (1997) Present denudation rates on the island of Reunion determined by river geochemistry: Basalt weathering and mass budget between chemical and mechanical erosions. *Geochimica Et Cosmochimica Acta* **61**(17), 3645-3669.

Mann A. W. (1984) Mobility of Gold and Silver in Lateritic Weathering Profiles - Some Observations from Western-Australia. *Economic Geology* **79**(1), 38-49.

Martin D. (1970) Marine Chemistry, Vol. 2, pp. 451. Marcel Dekker.

Mason T. F. D., Widdowson, M., Ellam, R. M., Oxburgh, R.,. (2000) Isotopic Variability of Sr and Nd in laterites from the deccan Traps, India: Evidence for an Aeolian Input to a Weathering profile.

Maslin M. A., Li X. S., Loutre M. F., and Berger A. (1998) The contribution of orbital forcing to the progressive intensification of Northern Hemisphere glaciation. *Quaternary Science Reviews* **17**(4-5), 411-426.

McArthur J. M., Howarth R. J., and Bailey T. R. (2001) Strontium isotope stratigraphy: LOWESS version 3: Best fit to the marine Sr-isotope curve for 0-509 Ma and accompanying look-up table for deriving numerical age. *Journal of Geology* **109**(2), 155-170.

McMillan M., Nienow P., Shepherd A., Benham T., and Sole A. (2007) Seasonal evolution of supra-glacial lakes on the Greenland Ice Sheet. *Earth and Planetary Science Letters* **262**, 484-492.

Meisel T., Reisberg L., Moser J., Carignan J., Melcher F., and Brügmann G. (2003) Re-Os systematics of UB-N, a serpentinized peridotite reference material. *Chemical Geology* **201**(1-2), 161-179.

Meybeck M. (1987) Global Chemical-Weathering of Surficial Rocks Estimated from River Dissolved Loads. *American Journal of Science* **287**(5), 401-428.

Meybeck M. (2003) Global Occurrence of Major Elements in Rivers. Treatise on Geochemistry (ed. H. D. Holland and K. K. Turekian), pp. 207-223. Pergamon.

Milliman J. D. and Syvitski J. P. M. (1992) Geomorphic Tectonic Control of Sediment Discharge to the Ocean - the Importance of Small Mountainous Rivers. *Journal of Geology* **100**(5), 525-544.

Millot R., Gaillardet J., Dupre B., and Allegre C. J. (2002) The global control of silicate weathering rates and the coupling with physical erosion: new insights from rivers of the Canadian Shield. *Earth and Planetary Science Letters* **196**(1-2), 83-98.

Mitchell C. and Widdowson M. (1991) A Geological Map of the Southern Deccan Traps, India and Its Structural Implications. *Journal of the Geological Society* **148**, 495-505.

Molnar P. (2004) Late cenozoic increase in accumulation rates of terrestrial sediment: How might climate change have affected erosion rates? *Annual Review of Earth and Planetary Sciences* **32**, 67-89.

Mountain B. W. and Wood S. A. (1988) Chemical Controls on the Solubility, Transport, and Deposition of Platinum and Palladium in Hydrothermal Solutions - a Thermodynamic Approach. *Economic Geology* **83**(3), 492-510.

Murphy W. M. and Helgeson H. C. (1987) Thermodynamic and Kinetic Constraints on Reaction-Rates among Minerals and Aqueous-Solutions .3. Activated Complexes and the Ph-Dependence of the Rates of Feldspar, Pyroxene, Wollastonite, and Olivine Hydrolysis. *Geochimica Et Cosmochimica Acta* **51**(12), 3137-3153.

Murphy W. M. and Helgeson H. C. (1989) Thermodynamic and Kinetic Constraints on Reaction-Rates among Minerals and Aqueous-Solutions .4. Retrieval of Rate Constants and Activation Parameters for the Hydrolysis of Pyroxene, Wollastonite, Olivine, Andalusite, Quartz, and Nepheline. *American Journal of Science* **289**(1), 17-101.

Negrel P. and Deschamps P. (1996) Natural and anthropogenic budgets of a small watershed in the massif central (France): Chemical and strontium isotopic characterization of water and sediments. *Aquatic Geochemistry* 2(1), 1-27.

Nesbitt H. W. and Markovics G. (1997) Weathering of granodioritic crust, long-term storage of elements in weathering profiles, and petrogenesis of siliciclastic sediments. *Geochimica Et Cosmochimica Acta* **61**(8), 1653-1670.

Newman A. C. D. and Brown G. (1969) Delayed Exchange of Potassium from Some Edges of Mica Flakes. *Nature* **223**(5202), 175-&.

Oberthur T., Weiser T. W., and Gast L. (2003) Geochemistry and mineralogy of platinum-group elements at Hartley Platinum Mine, Zimbabwe Part 2: Supergene redistribution in the oxidized Main Sulfide Zone of the Great Dyke, and alluvial platinum-group minerals. *Mineralium Deposita* **38**(3), 344-355.

Oelkers E. H. (2001) General kinetic description of multioxide silicate mineral and glass dissolution. *Geochimica Et Cosmochimica Acta* **65**(21), 3703-3719.

Oelkers E. H. (2001) An experimental study of forsterite dissolution rates as a function of temperature and aqueous Mg and Si concentrations. *Chemical Geology* **175**(3-4), 485-494.

Oelkers E. H. and Gislason S. R. (2001) The mechanism, rates and consequences of basaltic glass dissolution: I. An experimental study of the dissolution rates of basaltic glass as a function of aqueous Al, Si and oxalic acid concentration at 25 degrees C and pH=3 and 11. *Geochimica Et Cosmochimica Acta* **65**(21), 3671-3681.

Oelkers E. H. and Schott J. (1995) Experimental study of anorthite dissolution and the relative mechanism of feldspar hydrolysis. *Geochimica Et Cosmochimica Acta* **59**(24), 5039-5053.

Oelkers E. H. and Schott J. (1998) Does organic acid adsorption affect alkali-feldspar dissolution rates? *Chemical Geology* **151**(1-4), 235-245.

Oliva P., Viers J., Dupre B., Fortune J. P., Martin F., Braun J. J., Nahon D., and Robain H. (1999) The effect of organic matter on chemical weathering: Study of a small tropical watershed: Nsimi-Zoetele site, Cameroon. *Geochimica Et Cosmochimica Acta* **63**(23-24), 4013-4035.

Palmer M. R. and Edmond J. M. (1989) The Strontium Isotope Budget of the Modern Ocean. *Earth and Planetary Science Letters* **92**(1), 11-26.

Palmer M. R. and Edmond J. M. (1992) Controls over the Strontium Isotope Composition of River Water. *Geochimica Et Cosmochimica Acta* **56**(5), 2099-2111.

Parkhurst D. L. and Appelo C. A. J. (1999) User's guide to PHREEQC (version 2)--A computer program for speciation, batch-reaction, one-dimensional transport, and inverse geochemical calculations. In *U.S. Geological Survey Water-Resources Investigations Report*, pp. 312.

Peacock C. L. and Sherman D. M. (2004) Vanadium(V) adsorption onto goethite ([alpha]-FeOOH) at pH 1.5 to 12: a surface complexation model based on ab initio molecular geometries and EXAFS spectroscopy. *Geochimica et Cosmochimica Acta* **68**(8), 1723-1733.

Peacock C. L. and Sherman D. M. (2005) Surface complexation model for multisite adsorption of copper(II) onto kaolinite. *Geochimica Et Cosmochimica Acta* **69**(15), 3733-3745.

Peacock C. L. and Sherman D. M. (2005a) Copper(II) sorption onto goethite, hematite, and lepidocrocite: A surface complexation model based on ab initio molecular geometries and EXAFS spectroscopy (vol 68, pg 2623, 2004). *Geochimica Et Cosmochimica Acta* **69**(21), 5141-5142.

Peacock C. L. and Sherman D. M. (2005b) Surface complexation model for multisite adsorption of copper(II) onto kaolinite. *Geochimica Et Cosmochimica Acta* **69**(15), 3733-3745.

Pearson N. J., Griffin W. L., Alard O., and O'Reilly S. Y. (2006) The isotopic composition of magnesium in mantle olivine: Records of depletion and metasomatism. *Chemical Geology Special Issue in Honour of R.K. O'Nions* **226**(3-4), 115-133.

Pearson P. N. and Palmer M. R. (2000) Atmospheric carbon dioxide concentrations over the past 60 million years. *Nature* **406**(6797), 695-699.

Pegram W. J. and Turekian K. K. (1999) The osmium isotopic composition change of Cenozoic sea water as inferred from a deep-sea core corrected for meteoritic contributions. *Geochimica Et Cosmochimica Acta* **63**(23-24), 4053-4058.

Petrovic R. (1976) Rate Control in Feldspar Dissolution .2. Protective Effect of Precipitates. *Geochimica Et Cosmochimica Acta* **40**(12), 1509-1521.

Petrovic R., Berner R. A., and Goldhaber M. B. (1976) Rate Control in Dissolution of Alkali Feldspars .1. Study of Residual Feldspar Grains by X-Ray Photoelectron-Spectroscopy. *Geochimica Et Cosmochimica Acta* **40**(5), 537-548.

Petrovich R. (1981) Kinetics of Dissolution of Mechanically Comminuted Rock-Forming Oxides and Silicates in the Laboratory and at the Earths Surface. *Geochimica Et Cosmochimica Acta* **45**(10), 1675-1686.

Peucker-Ehrenbrink B. and Blum J. D. (1998) Re-Os isotope systematics and weathering of Precambrian crustal rocks: Implications for the marine osmium isotope record. *Geochimica Et Cosmochimica Acta* **62**(19-20), 3193-3203.

Peucker-Ehrenbrink B. and Hannigan R. E. (2000) Effects of black shale weathering on the mobility of rhenium and platinum group elements. *Geology* **28**(5), 475-478.

Peucker-Ehrenbrink B. and Jahn B. M. (2001) Rhenium-osmium isotope systematics and platinum group element concentrations: Loess and the upper continental crust. *Geochemistry Geophysics Geosystems* **2**.

Peucker-Ehrenbrink B. and Ravizza G. (2000a) The effects of sampling artifacts on cosmic dust flux estimates: A reevaluation of nonvolatile tracers (Os, Ir). *Geochimica Et Cosmochimica Acta* **64**(11), 1965-1970.

Peucker-Ehrenbrink B. and Ravizza G. (2000b) The marine osmium isotope record. *Terra Nova* **12**(5), 205-219.

Pierson-Wickmann A. C., Reisberg L., and France-Lanord C. (2002) Behavior of Re and Os during low-temperature alteration: Results from Himalayan soils and altered black shales. *Geochimica Et Cosmochimica Acta* **66**(9), 1539-1548.

Pistiner J. S. and Henderson G. M. (2003) Lithium-isotope fractionation during continental weathering processes. *Earth and Planetary Science Letters* **214**(1-2), 327-339.

Pogge von Strandmann P. A. E., Burton K. W., James R. H., van Calsteren P., Gislason S. R., and Mokadem F. (2006) Riverine behaviour of uranium and lithium isotopes in an actively glaciated basaltic terrain. *Earth and Planetary Science Letters* **251**(1-2), 134-147.

Pogge von Strandmann P. A. E., Burton K. W., James R. H., van Calsteren P., Gislason S. R., and Sigfússon B. The influence of weathering processes on riverine magnesium isotopes in a basaltic terrain. *Earth and Planetary Science Letters* **In Press, Corrected Proof.**

Pogge von Strandmann P. A. E., James R. H., van Calsteren P., Gíslason S. e. u. R., and Burton K. W. (2008) Lithium, magnesium and uranium isotope behaviour in the estuarine environment of basaltic islands. *Earth and Planetary Science Letters* **274**(3-4), 462-471.

Pokrovsky O. S., Dupre B., and Schott J. (2005) Fe-Al-organic colloids control of trace elements in peat soil solutions: Results of ultrafiltration and dialysis. *Aquatic Geochemistry* **11**(3), 241-278.

Pokrovsky O. S. and Schott J. (2000) Kinetics and mechanism of forsterite dissolution at 25 degrees C and pH from 1 to 12. *Geochimica Et Cosmochimica Acta* **64**(19), 3313-3325.

Pokrovsky O. S. and Schott J. (2002) Iron colloids/organic matter associated transport of major and trace elements in small boreal rivers and their estuaries (NW Russia). *Chemical Geology* **190**(1-4), 141-179

Poulson S. R., Drever J. I., and Stillings L. L. (1997) Aqueous Si-oxalate complexing, oxalate adsorption onto quartz, and the effect of oxalate upon quartz dissolution rates. *Chemical Geology* **140**(1-2), 1-7.

Poulton S. W. and Raiswell R. (2005) Chemical and physical characteristics of iron oxides in riverine and glacial meltwater sediments. *Chemical Geology* **218**(3-4), 203-221.

Ra K. and Kitagawa H. (2007) Magnesium isotope analysis of different chlorophyll forms in marine phytoplankton using multi-collector ICP-MS. *Journal of Analytical Atomic Spectrometry* **22**(7), 817-821.

Raiswell R. and Thomas A. G. (1984) Solute Acquisition in Glacial Melt Waters .1. Fjallsjokull (Southeast Iceland) - Bulk Melt Waters with Closed-System Characteristics. *Journal of Glaciology* **30**(104), 35-43.

Raiswell R., Tranter M., Benning L. G., Siegert M., De'ath R., Huybrechts P., and Payne T. (2006) Contributions from glacially derived sediment to the global iron (oxyhydr)oxide cycle: Implications for iron delivery to the oceans. *Geochimica Et Cosmochimica Acta* **70**(11), 2765-2780.

Rampone E., Hofmann A. W., Piccardo G. B., Vannucci R., Bottazzi P., and Ottolini L. (1996) Trace element and isotope geochemistry of depleted peridotites from an N-MORB type ophiolite (Internal Liguride, N Italy). *Contributions to Mineralogy and Petrology* **123**(1), 61-76.

Randall S. R., Sherman D. M., Ragnarsdottir K. V., and Collins C. R. (1999) The mechanism of cadmium surface complexation on iron oxyhydroxide minerals. *Geochimica Et Cosmochimica Acta* **63**(19-20), 2971-2987.

Ravizza G. and Turekian K. K. (1992) The Osmium Isotopic Composition of Organic-Rich Marine-Sediments. *Earth and Planetary Science Letters* **110**(1-4), 1-6.

Ravizza G. E. and Zachos J. C. (2003) Records of Cenozoic Ocean Chemistry. Treatise on Geochemistry (ed. H. D. Holland and K. K. Turekian), pp. 551-581. Pergamon.

Raymo M. E., Ruddiman W. F., and Froelich P. N. (1988) Influence of Late Cenozoic Mountain Building on Ocean Geochemical Cycles. *Geology* **16**(7), 649-653.

Reisberg L. and Lorand J. P. (1995) Longevity of Sub-Continental Mantle Lithosphere from Osmium Isotope Systematics in Orogenic Peridotite Massifs. *Nature* **376**(6536), 159-162.

Richter F. M. and Depaolo D. J. (1988) Diagenesis and Sr Isotopic Evolution of Seawater Using Data from Dsdp-590b and Dsdp-575. *Earth and Planetary Science Letters* **90**(4), 382-394.

Richter F. M., Watson E. B., Mendybaev R. A., Teng F.-Z., and Janney P. E. (2008) Magnesium isotope fractionation in silicate melts by chemical and thermal diffusion. *Geochimica et Cosmochimica Acta* **72**(1), 206-220.

Riley J. P. and Chester R. (1971) *An Introduction To Marine Chemistry*. Academic Press.

Riotte J., Chabaux F., Benedetti M., Dia A., Gerard M., Boulegue J., and Etame J. (2003) Uranium colloidal transport and origin of the U-234-U-238 fractionation in surface waters: new insights from Mount Cameroon. *Chemical Geology* **202**(3-4), 365-381.

Roquin C., Freyssinet P., Zeegers H., and Tardy Y. (1990) Element Distribution Patterns in Laterites of Southern Mali - Consequence for Geochemical Prospecting and Mineral Exploration. *Applied Geochemistry* **5**(3), 303-315.

Rosso J. J. and Rimstidt J. D. (2000) A high resolution study of forsterite dissolution rates. *Geochimica Et Cosmochimica Acta* **64**(5), 797-811.

Ruddiman W. F. and Prell W. L. (1997) Introduction to the Uplift-Climate Connection. In *Tectonic Uplift and Climate Change* (ed. W. F. Ruddiman), pp. 535. Springer.

Rudnick R. L., Tomascak P. B., Njo H. B., and Gardner L. R. (2004) Extreme lithium isotopic fractionation during continental weathering revealed in saprolites from South Carolina. *Chemical Geology* **212**(1-2), 45-57.

Russell A. J. (2007) Controls on the sedimentology of an ice-contact jokulhlaup-dominated delta, Kangerlussuaq, west Greenland. *Sedimentary Geology* **193**(1-4), 131-148.

Schellmann W. (1981) Considerations on the definition and classification of laterites. *International Seminar on Laterisation Processes*, 1-10.

Schellmann W. (1994) Geochemical Differentiation in Laterite and Bauxite Formation. *Catena* **21**(2-3), 131-143.

Schmidt G., Palme H., and Kratz K. (1998) Fractionation of highly siderophile elements in the Earth's upper continental crust. *Eos, Trans. Am. geophys. Un.* **79**, 354.

Schmidt P. W., Prasad V., and Ramam P. K. (1983) Magnetic Ages of Some Indian Laterites. *Palaeogeography Palaeoclimatology Palaeoecology* **44**(3-4), 185-202.

Scholz H. and Baumann M. (1997) An 'open system pingo' near Kangerlussuaq (Søndre Strømfjord),West Greenland. *Geology of Greenland Survey Bulletin* **176**, 104–108.

Schulthess C. P. and Huang C. P. (1990) Adsorption of Heavy-Metals by Silicon and Aluminum-Oxide Surfaces on Clay-Minerals. *Soil Science Society of America Journal* **54**(3), 679-688.

Seitz H.-M., Brey G. P., Lahaye Y., Durali S., and Weyer S. (2004) Lithium isotopic signatures of peridotite xenoliths and isotopic fractionation at high temperature between olivine and pyroxenes. *Chemical Geology Lithium Isotope Geochemistry* **212**(1-2), 163-177.

Seyfried W. E., Chen X., and Chan L. H. (1998) Trace element mobility and lithium isotope exchange during hydrothermal alteration of seafloor weathered basalt: An experimental study at 350 degrees C, 500 bars. *Geochimica Et Cosmochimica Acta* **62**(6), 949-960.

Sharma M., Clauer N., and Toulkeridis T. (1998) Rhenium-osmium isotopic systematics of an ancient laterite profile. *Mineralogical magazine* **62A**, 1373-1374.

Sharma M., Papanastassiou D. A., and Wasserburg G. J. (1997) The concentration and isotopic composition of osmium in the oceans. *Geochimica et Cosmochimica Acta* **61**(16), 3287-3299.

Sharma M., Wasserburg G. J., Hoffmann A. W., and Chakrapani G. J. (1999) Himalayan uplift and osmium isotopes in oceans and rivers. *Geochimica Et Cosmochimica Acta* **63**(23-24), 4005-4012.

Sharp M. and Gomez B. (1986) Processes of Debris Comminution in the Glacial Environment and Implications for Quartz Sand-Grain Micromorphology. *Sedimentary Geology* **46**(1-2), 33-47.

Sharp M., Tranter M., Brown G. H., and Skidmore M. (1995) Rates of Chemical Denudation and Co2 Drawdown in a Glacier-Covered Alpine Catchment. *Geology* **23**(1), 61-64.

Shaul O. (2002) Magnesium transport and function in plants: the tip of the iceberg. *Biometals* **15**(3), 309-323.

Sherman D. M. and Peacock C. L. (2004) Metal sorption to iron(III) (hydr)oxides: The first surface complexation models consistent with spectroscopy and quantum chemistry. *Geochimica Et Cosmochimica Acta* **68**(11), A370-A370.

Snow J. E. and Reisberg L. (1995) Os Isotopic Systematics of the Morb Mantle - Results from Altered Abyssal Peridotites. *Earth and Planetary Science Letters* **133**(3-4), 411-421.

Shirey S. B. and Walker R. J. (1998) The Re-Os isotope system in cosmochemistry and high-temperature geochemistry. *Annual Review of Earth and Planetary Sciences* **26**, 423-500.

Shotyk W. and Nesbitt H. W. (1992) Incongruent and Congruent Dissolution of Plagioclase Feldspar - Effect of Feldspar Composition and Ligand Complexation. *Geoderma* **55**(1-2), 55-78.

Sillen L. G. (1967) The Ocean as a Chemical System 10.1126/science.156.3779.1189. *Science* **156**(3779), 1189-1197.

Sivry Y., Riotte J., and Dupre B. (2006) Study of exchangeable metal on colloidal humic acids and particulate matter by coupling ultrafiltration and isotopic tracers: Application to natural waters. *Journal of Geochemical Exploration* **88**(1-3), 144-147.

Skulan J. L., Beard B. L., and Johnson C. M. (2002) Kinetic and equilibrium Fe isotope fractionation between aqueous Fe(III) and hematite. *Geochimica Et Cosmochimica Acta* **66**(17), 2995-3015.

Stallard R. F. (1995) Relating chemical and physical erosion. In *Chemical Weathering Rates of Silicate Minerals*, Vol. 31, pp. 543-564.

Stallard R. F. and Edmond J. M. (1981) Geochemistry of the Amazon .1. Precipitation Chemistry and the Marine Contribution to the Dissolved-Load at the Time of Peak Discharge. *Journal of Geophysical Research-Oceans and Atmospheres* **86**(NC10), 9844-9858.

Stanley S. M. and Hardie L. A. (1999) Hypercalcification: Paleontology Links Plate Tectonics and Geochemistry to Sedimentology. *GSA Today* **9**(2), 2-7.

Staudigel H., Hart S. R., Schmincke H. U., and Smith B. M. (1989) Cretaceous Ocean Crust at Dsdp Site-417 and Site-418 - Carbon Uptake from Weathering Versus Loss by Magmatic Outgassing. *Geochimica Et Cosmochimica Acta* **53**(11), 3091-3094.

Staudigel H., Yayanos A., Chastain R., Davies G., Verdurmen E. A. T., Schiffman P., Bourcier R., and De Baar H. (1998) Biologically mediated dissolution of volcanic glass in seawater. *Earth and Planetary Science Letters* **164**(1-2), 233-244.

Stefansdottir M. B. and Gislason S. R. (2005) The erosion and suspended matter/seawater interaction during and after the 1996 outburst flood from the Vatnajokull Glacier, Iceland. *Earth and Planetary Science Letters* **237**(3-4), 433-452.

Stefánsdóttir M. B. and Gíslason S. R. (2006) Suspended basaltic glass-seawater interactions. *Journal of Geochemical Exploration Extended Abstracts presented at the 7th Symp. on the Geochemistry of the Earth's Surface (GES-7)* **88**(1-3), 332-335.

Stefansson A. and Gislason S. R. (2001) Chemical weathering of basalts, Southwest Iceland: Effect of rock crystallinity and secondary minerals on chemical fluxes to the ocean. *American Journal of Science* **301**(6), 513-556.

Stillings L. L. and Brantley S. L. (1995) Feldspar Dissolution at 25-Degrees-C and Ph 3 - Reaction Stoichiometry and the Effect of Cations. *Geochimica Et Cosmochimica Acta* **59**(8), 1483-1496.

Stillings L. L., Drever J. I., Brantley S. L., Sun Y. T., and Oxburgh R. (1996) Rates of feldspar dissolution at pH 3-7 with 0-8 mM oxalic acid. *Chemical Geology* **132**(1-4), 79-89.

Summerfield M. A. and Hulton N. J. (1994) Natural Controls of Fluvial Denudation Rates in Major World Drainage Basins. *Journal of Geophysical Research-Solid Earth* **99**(B7), 13871-13883.

Tajika E. (1998) Climate change during the last 150 million years: reconstruction from a carbon cycle model. *Earth and Planetary Science Letters* **160**(3-4), 695-707.

Tardy Y. (1997) *Petrology of Laterites and Tropical Soils*. A.A. Balkema, 1997.

Taylor A. S. and Lasaga A. C. (1999) The role of basalt weathering in the Sr isotope budget of the oceans. *Chemical Geology* **161**(1-3), 199-214.

Taylor S. R. and McLennan S. M. (1995) The Geochemical Evolution of the Continental-Crust. *Reviews of Geophysics* **33**(2), 241-265.

Techer I., Advocat T., Lancelot J., and Liotard J. M. (2001) Dissolution kinetics of basaltic glasses: control by solution chemistry and protective effect of the alteration film. *Chemical Geology* **176**(1-4), 235-263.

Teng F.-Z., Wadhwa M., and Helz R. T. (2007) Investigation of magnesium isotope fractionation during basalt differentiation: Implications for a chondritic composition of the terrestrial mantle. *Earth and Planetary Science Letters* **261**(1-2), 84-92.

Tiller K. G., Gerth J., and Brummer G. (1984) The Relative Affinities of Cd, Ni and Zn for Different Soil Clay Fractions and Goethite. *Geoderma* **34**(1), 17-35.

Tipper E. T., Galy A., and Bickle M. J. (2006a) Riverine evidence for a fractionated reservoir of Ca and Mg on the continents: Implications for the oceanic Ca cycle. *Earth and Planetary Science Letters* **247**(3-4), 267-279.

Tipper E. T., Galy A., Gaillardet J., Bickle M. J., Elderfield H., and Carder E. A. (2006b) The magnesium isotope budget of the modem ocean: Constraints from riverine magnesium isotope ratios. *Earth and Planetary Science Letters* **250**(1-2), 241-253.

Tomascak P. B. (2004) Developments in the understanding and application of lithium isotopes in the earth and planetary sciences. *Geochemistry of Non-Traditional Stable Isotopes* **55**, 153-195.

Topp S. E., Salbu B., Roaldset E., and Jorgensen P. (1984) Vertical-Distribution of Trace-Elements in Laterite Soil (Suriname). *Chemical Geology* **47**(1-2), 159-174.

Tranter M. (2003) Geochemical Weathering in Glacial and Proglacial Environments Treatise on Geochemistry (ed. H. D. Holland and K. K. Turekian), pp. 189-205. Pergamon.

Tranter M., Brown G., Raiswell R., Sharp M., and Gurnell A. (1993) A Conceptual-Model of Solute Acquisition by Alpine Glacial Meltwaters. *Journal of Glaciology* **39**(133), 573-581.

Tranter M., Huybrechts P., Munhoven G., Sharp M. J., Brown G. H., Jones I. W., Hodson A. J., Hodgkins R., and Wadham J. L. (2002) Direct effect of ice sheets on terrestrial bicarbonate, sulphate and base cation fluxes during the last glacial cycle: minimal impact on atmospheric CO2 concentrations. *Chemical Geology* **190**(1-4), 33-44.

Traore D., Beauvais A., Auge T., Chabaux F., Parisot J. C., Cathelineau M., Peiffert C., and Colin F. (2006) Platinum and palladium mobility in supergene environment: The residual origin of the Pirogues River mineralization, New Caledonia. *Journal of Geochemical Exploration* **88**(1-3), 350-354.

Trivedi P., Axe L., and Dyer J. (2001) Adsorption of metal ions onto goethite: single-adsorbate and competitive systems. *Colloids and Surfaces A: Physicochemical and Engineering Aspects* **191**(1-2), 107-121.

Urey H. C. (1952) On the Early Chemical History of the Earth and the Origin of Life. *Proceedings of the National Academy of Sciences of the United States of America* **38**(4), 351-363.

Vance D. and Burton K. (1999) Neodymium isotopes in planktonic foraminifera: a record of the response of continental weathering and ocean circulation rates to climate change. *Earth and Planetary Science Letters* **173**(4), 365-379.

Vanherk J., Pietersen H. S., and Schuiling R. D. (1989) Neutralization of Industrial-Waste Acids with Olivine - the Dissolution of Forsteritic Olivine at 40 Degrees-C70 Degrees-C. *Chemical Geology* **76**(3-4), 341-352.

Viers J., Dupre B., Braun J. J., Deberdt S., Angeletti B., Ngoupayou J. N., and Michard A. (2000) Major and trace element abundances, and strontium isotopes in the Nyong basin rivers (Cameroon): constraints on chemical weathering processes and elements transport mechanisms in humid tropical environments. *Chemical Geology* **169**(1-2), 211-241.

Vigier N., Decarreau A., Millot R., Carignan J., Petit S., and France-Lanord C. (2008) Quantifying Li isotope fractionation during smectite formation and implications for the Li cycle. *Geochimica et Cosmochimica Acta* **72**(3), 780-792.

Walker J. C. G., Hays P. B., and Kasting J. F. (1981) A Negative Feedback Mechanism for the Long-Term Stabilization of Earths Surface-Temperature. *Journal of Geophysical Research-Oceans and Atmospheres* **86**(NC10), 9776-9782.

Walter A. V., Nahon D., Flicoteaux R., Girard J. P., and Melfi A. (1995) Behaviour of major and trace elements and fractionation of REE under tropical weathering of a typical apatite-rich carbonatite from Brazil. *Earth and Planetary Science Letters* **136**(3-4), 591-602.

Wanke H. (1981) Constitution of Terrestrial Planets. *Philosophical Transactions of the Royal Society of London Series a-Mathematical Physical and Engineering Sciences* **303**(1477), 287-302.

Wedepohl K. H. (1995) The Composition of the Continental-Crust. *Geochimica Et Cosmochimica Acta* **59**(7), 1217-1232.

Welch S. A. and Ullman W. J. (1996) Feldspar dissolution in acidic and organic solutions: Compositional and pH dependence of dissolution rate. *Geochimica Et Cosmochimica Acta* **60**(16), 2939-2948.

Wells P. R. A. (1979) Chemical and Thermal Evolution of Archaean Sialic Crust, Southern West Greenland. *Journal of Petrology* **20**(2), 187-226.

West A. J., Galy A., and Bickle M. (2005) Tectonic and climatic controls on silicate weathering. *Earth and Planetary Science Letters* **235**(1-2), 211-228.

White A. F. (2003) Natural Weathering Rates of Silicate Minerals Treatise on Geochemistry (ed. H. D. Holland and K. K. Turekian), pp. 133-168. Pergamon.

White A. F., Bullen T. D., Schulz M. S., Blum A. E., Huntington T. G., and Peters N. E. (2001) Differential rates of feldspar weathering in granitic regoliths. *Geochimica Et Cosmochimica Acta* **65**(6), 847-869

Widdowson M. (1997) Tertiary palaeosurfaces of the SW Deccan, Western India: implications for passive margin uplift. *Palaeosurfaces: Recognition, Reconstruction and Palaeoenvironmental Interpretation.*

Widdowson M. and Cox K. G. (1996) Uplift and erosional history of the Deccan Traps, India: Evidence from laterites and drainage patterns of the Western Ghats and Konkan Coast. *Earth and Planetary Science Letters* **137**(1-4), 57-69.

Widdowson M., Pringle M. S., and Fernandez O. A. (2000) A post K-T boundary (Early Palaeocene) age for Deccan-type feeder dykes, Goa, India. *Journal of Petrology* **41**(7), 1177-1194.

Wiechert U. and Halliday A. N. (2007) Non-chondritic magnesium and the origins of the inner terrestrial planets. *Earth and Planetary Science Letters* **256**(3-4), 360-371.

Wiederhold J. G., Kraemer S. M., Teutsch N., Borer P. M., Halliday A. N., and Kretzschmar R. (2006) Iron isotope fractionation during proton-promoted, ligand-controlled, and reductive dissolution of goethite. *Environmental Science & Technology* **40**(12), 3787-3793.

Williams L. B. and Hervig R. L. (2005) Lithium and boron isotopes in illite-smectite: The importance of crystal size. *Geochimica Et Cosmochimica Acta* **69**(24), 5705-5716.

Willemse N. W., Koster E. A., Hoogakker B., and van Tatenhove F. G. M. (2003) A continuous record of Holocene eolian activity in West Greenland. *Quaternary Research* **59**(3), 322-334.

Wogelius R. A. and Walther J. V. (1991) Olivine Dissolution at 25-Degrees-C - Effects of Ph, Co2, and Organic-Acids. *Geochimica Et Cosmochimica Acta* **55**(4), 943-954.

Wogelius R. A. and Walther J. V. (1992) Olivine Dissolution Kinetics at near-Surface Conditions. *Chemical Geology* **97**(1-2), 101-112.

Wolff-Boenisch D., Gislason S. R., and Oelkers E. H. (2006) The effect of crystallinity on dissolution rates and CO2 consumption capacity of silicates. *Geochimica Et Cosmochimica Acta* **70**(4), 858-870.

Wolff-Boenisch D., Gislason S. R., Oelkers E. H., and Putnis C. V. (2004) The dissolution rates of natural glasses as a function of their composition at pH 4 and 10.6, and temperatures from 25 to 74 degrees C. *Geochimica Et Cosmochimica Acta* **68**(23), 4843-4858.

Yde J. C. and Knudsen N. T. (2004) The importance of oxygen isotope provenance in relation to solute content of bulk meltwaters at Imersuaq Glacier, West Greenland. *Hydrological Processes* **18**(1), 125-139.

Yde J. C., Knudsen N. T., and Nielsen O. B. (2005) Glacier hydrochemistry, solute provenance, and chemical denudation at a surge-type glacier in Kuannersuit Kuussuat, Disko Island, West Greenland. *Journal of Hydrology* **300**(1-4), 172-187.

Young E. D. and Galy A. (2004) The isotope geochemistry and cosmochemistry of magnesium. *Geochemistry of Non-Traditional Stable Isotopes* **55**, 197-230.

Zachos J., Pagani M., Sloan L., Thomas E., and Billups K. (2001) Trends, rhythms, and aberrations in global climate 65 Ma to present. *Science* **292**(5517), 686-693.

Zhang L. B., Chan L. H., and Gieskes J. M. (1998) Lithium isotope geochemistry of pore waters from Ocean Drilling Program Sites 918 and 919, Irminger Basin. *Geochimica Et Cosmochimica Acta* **62**(14), 2437-2450.

Zwally H. J., Abdalati W., Herring T., Larson K., Saba J., and Steffen K. (2002) Surface Melt-Induced Acceleration of Greenland Ice-Sheet Flow 10.1126/science.1072708. *Science* **297**(5579), 218-222.

Appendix A

Analytical techniques and experimental methods

Appendix A provides supporting data for Chapter 2 and includes:

- *Column calibrations for Mg isotope analyses (Appendices A1 and A2)*
- *Data regarding reproducibility of standards for rock analysis by XRF and ICP-MS and water analysis by ICP-MS (Appendices A3 to A9)*
- *Reproducibility of standards during Li isotope analyses (Appendix A10)*
- *Reproducibility of standards during Mg isotope analyses (Appendices A11 and A12)*
- *Solution and total procedural blanks during the dissolution experiments (Appendix A13)*

Appendix A1

Column calibration for the separation of magnesium from iron using an anion column. The sample was eluted using 2ml aliquots of 6N TD HCl. Concentrations are in ppb. Yields are calculated by comparing the total of each element that is recovered with the elemental abundances in the standard (Wt %).

BIR-1							
vol (ml)	**Na**	**Mg**	**Al**	**K**	**Ca**	**Ti**	**Fe**
2	16.3	79.4	123	0	111	8.54	0.35
4	6.58	16.1	29.6	0	20.8	1.91	2.87
6	3.79	0.21	4.00	0	0.50	0.04	0.45
8	4.69	2.16	27.0	0.43	0.41	0.22	7.25
10	3.76	0.19	3.90	0	0.45	0.04	0.33
12	4.09	0.18	4.06	0	0.16	0.04	0.58
14	3.09	0.13	3.19	0	0.33	0.04	0.38
Total (ng)	84.6	197	389	0.86	268	21.7	24.4
Yield (%)	**157**	**84**	**119**	**100**	**91**	**94**	**8**

AGV-1							
vol (ml)	**Na**	**Mg**	**Al**	**K**	**Ca**	**Ti**	**Fe**
2	256	88.6	895	226	311	60.5	1.48
4	15.2	5.27	39.6	6.58	17.7	6.55	1.52
6	3.50	0.14	3.36	0	0.57	0.03	1.17
8	3.91	0.13	2.45	0	0.82	0.03	1.16
10	3.52	0.13	3.60	0	0.27	0.02	1.03
12	3.14	0.18	1.82	0	2.28	0.07	0.90
14	5.09	0.22	5.12	0	0.68	0.07	1.10
Total (ng)	581	189	1900	435	667	134	16.7
Yield (%)	**84**	**93**	**95**	**82**	**110**	**97**	**2**

Appendix A2

Column calibration for the separation of magnesium using a cation column and 2.5ml aliquots.

DSM-3	Cation concentration (ppb)							
2M HCl (ml)	**Na**	**Mg**	**Al**	**K**	**Ca**	**Ti**	**Cr**	**Fe**
2.5	0	0.00	0	1.94	0	0.03	6.84	1.00
5	0	0.08	0	2.93	0	0.06	8.98	0.99
7.5	0	31.7	0	2.71	0	0.05	8.23	0.84
10	0	29.7	0	2.95	0	0.05	6.75	0.93
12.5	0	0.11	0	3.21	0	0.06	6.66	0.52
15	0	0	0	3.25	0	0.04	6.85	0.79
17.5	0	0	0	2.27	0	0.04	6.67	0.38
20	0	0	0	2.70	0	0.03	7.12	39.5
22.5	0	0	0	2.65	0	0.03	6.14	0.92
25	0	0	0	2.93	0.29	0.03	5.69	0.83
yield (%)		**102**						

BG1-A								
2M HCl (ml)	**Na**	**Mg**	**Al**	**K**	**Ca**	**Ti**	**Cr**	**Fe**
2.5	1.3	0.2	0.1	2.4	1.6	0.33	8.4	1.5
5	0	0.0	0	3.0	2.4	8.14	9.1	1.1
7.5	0	45.1	0	2.1	2.8	0.51	9.9	7.4
10	0	44.0	0	2.4	2.5	0.06	8.1	108
12.5	0	0.1	0	5.8	2.9	0.05	6.5	36.9
15	0	0	0	2.8	1.4	0.05	6.6	1.5
17.5	0	0	1.6	2.8	1.3	0.04	6.8	0.6
20	0	0	16.0	2.0	0.7	0.03	6.8	0.5
22.5	0	0	51.8	2.3	0.2	0.02	6.3	0.7
25	0	0	48.6	2.8	0.0	0.03	6.6	0.7
yield (%)		**99**						

Appendix A3

Standards run during XRF analyses.

Wt. %	WS-E 1	WS-E 2	WS-E recommended	OUG94 1	OUG94 2	OUG94 recommended
SiO_2	51.25	51.24	51.10	70.05	70.17	69.95
TiO_2	2.416	2.424	2.400	0.309	0.313	0.314
Al_2O_3	13.84	13.80	13.78	14.51	14.57	14.66
Fe_2O_3	13.22	13.23	13.15	3.04	3.05	3.05
MnO	0.170	0.170	0.171	0.075	0.074	0.075
MgO	5.56	5.59	5.55	1.06	1.06	1.04
CaO	8.95	8.89	8.95	1.35	1.34	1.34
Na_2O	2.46	2.47	2.47	4.60	4.59	4.60
K_2O	1.01	0.99	1.00	2.98	2.99	2.96
P_2O_5	0.299	0.299	0.302	0.163	0.168	0.165
LOI	0.85	0.85	0.85	1.97	1.97	1.97

Appendix A4

Major element analyses of JB-2 (JGS) measured by ICP-MS over the course of this study. Concentrations are in Wt %.

	Na	Mg	Al	K	Ca	Mn	Fe
Standard	JB-2	JB-2	JB-2	JB-2	JB-2	JB-2	JB-2
Average	1.57	2.94	8.21	0.35	5.71	0.17	10.06
2σ (abs)	0.05	0.11	0.29	0.02	0.28	0.007	0.43
2σ (%)	3.4	3.6	3.5	5.5	4.8	4.3	4.3
Certified	1.51	2.79	7.75	0.35	7.02	0.169	9.97

Appendix A5

Minor element analyses of the rock standards JB-2 (JGS) and BIR-1 (USGS) over the course of this study. Concentrations are in ppm.

	Li	Ti	V	Cr	Co	Ni	Cu
Standard	BIR-1	BIR-1	BIR-1	BIR-1	BIR-1	BIR-1	BIR-1
Average	3.33	6030	341	428	52	181	119
2σ (abs)	0.113	320	18.6	20.4	2.1	8	4.6
2σ (%)	3.38	5.30	5.46	4.78	4.02	4.43	3.89
Certified	3.6 ± 0.2	5760 ± 60	310 ± 11	370 ± 8	52 ± 2	170 ± 6	125 ± 4
Standard	JB-2	JB-2	JB-2	JB-2	JB-2	JB-2	JB-2
Average	8.67	6860		26.1	37.8		
2σ (abs)	0.4	375		2.4	2		
2σ (%)	4.57	5.46		9.19	5.40		
Certified	7.78	7100	575	28.1	38	16.6	225

	Zn	Rb	Sr	Zr	Ba	Th	U
Standard	BIR-1	BIR-1	BIR-1	BIR-1	BIR-1	BIR-1	BIR-1
Average	69.7	0.21	109	14.7	6.6	0.03	0.01
2σ (abs)	1.7	0.01	2.8	0.39	0.2	0.002	0.001
2σ (%)	2.49	3.63	2.60	2.63	3.04	5.35	5.56
Certified	70 ± 9		110 ± 2	18 ± 1	7 (± nd)		
Standard	JB-2	JB-2	JB-2	JB-2	JB-2	JB-2	JB-2
Average	109	6.32	177		227	0.25	0.15
2σ (abs)	3.87	0.32	6.97		8.7	0.02	0.02
2σ (%)	3.55	5.01	3.93		3.81	9.53	13.74
Certified	108	7.37	178	51.2	222	0.35	0.18

Appendix A6

Major and minor element analyses of the river water standard SLRS-1 during this study. Concentrations are in ppb.

	Date	Li	Na	Mg	Al	Si	K	Ca	Mn	Fe	Ni	Cu	Zn	Sr	Ba
SLR-S4	15/11/2007	0.49	1960	1410	46.1	2034	561	5250	3.19	86.5	0.71	1.73	1.02	37.9	12.5
SLR-S4	15/11/2007	0.50	2110	1500	48.0	2158	592	5450	3.30	92.1	0.74	1.81	1.07	39.7	12.9
SLR-S4	15/11/2007	0.51	2130	1520	50.2	1930	608	5600	3.31	93.5	0.77	1.86	1.07	40.5	12.7
AVERAGE		0.50	2060	1480	48.1	2040	587	5430	3.27	90.7	0.74	1.80	1.05	39.4	12.7
2SD		0.01	185	121	4.14	114	47.9	355	0.13	7.43	0.06	0.13	0.06	2.66	0.35
2SD (%)		2.4	8.9	8.2	8.6	2.3	8.2	6.5	4.0	8.2	8.0	7.0	5.7	6.8	2.8
SLR-S4	21/11/2007	0.49	1960	1410	46.1		561	5250	3.19	86.5	0.71	1.73	1.02	37.9	12.5
SLR-S4	21/11/2007	0.50	2110	1500	48.0		592	5450	3.30	92.1	0.74	1.81	1.07	39.7	12.9
SLR-S4	21/11/2007	0.51	2130	1520	50.2		608	5600	3.31	93.5	0.77	1.86	1.07	40.5	12.7
SLR-S4	21/11/2007	0.52	2190	1530	50.9		609	5640	3.36	99.5	0.77	1.92	1.12	41.4	12.8
SLR-S4	21/11/2007	0.53	2150	1530	51.7		620	5750	3.46	103	0.79	1.94	1.12	40.4	13.0
SLR-S4	21/11/2007	0.52	2180	1550	52.6		629	5750	3.47	97.4	0.79	1.91	1.10	40.2	13.0
SLR-S4	21/11/2007	0.51	2220	1580	56.2		624	5680	3.42	98.4	0.78	1.85	1.09	38.1	12.8
SLR-S4	21/11/2007	0.53	2160	1550	54.2		622	5690	3.42	99.0	0.79	1.87	1.06	38.4	12.9
AVERAGE		0.52	2160	1540	52.0		615	5650	3.39	97.6	0.78	1.88	1.09	39.8	12.9
2SD		0.02	75.9	49.7	5.38		25.9	208	0.14	7.62	0.03	0.09	0.06	2.36	0.22
2SD (%)		4.4	3.5	3.2	10.3		4.2	3.7	4.0	7.8	4.4	4.8	5.1	5.9	1.7
CERTIFIED	Concentration	0.54	2400	1600	54	1860	680	6200	3.37	103	0.67	1.81	0.93	26.3	12.2
SLRS-4	(±)	0.07	0.2	0.1	4	0.05	0.02	0.2	0.08	5	0.08	0.08	0.1	3.2	0.6

Appendix A7

Major and minor element analyses of the in house river standard Sco2/15 during this study. Concentrations are in ppb.

	Date	Li	Na	Mg	Al	Si	K	Ca	Sc	Mn	Fe	Ni	Cu	Zn	Sr	Ba
Sco2/15	11/11/2006	0.38	2981	691	50.3	2171	363	3325	2279	1.48	20020	0.16	0.37	0.62	17.0	9.60
Sco2/15	11/11/2006	0.38	3276	755	55.3	2360	424	3889	2591	1.66	23160	0.19	0.43	0.68	18.5	11.1
Sco2/15	11/11/2006	0.35	3191	739	53.5	2232	405	3804	2482	1.55	22720	0.18	0.37	0.42	17.4	10.5
Sco2/15	11/11/2006	0.34	3269	748	54.4	2233	410	3947	2628	1.58	24660	0.17	0.40	0.42	17.9	11.0
Sco2/15	11/11/2006	0.32	3475	806	58.5	2189	422	3950	2751	1.60	25250	0.17	0.41	0.47	18.3	11.4
Sco2/15	11/11/2006	0.33	3577	831	60.5	2172	422	4077	2784	1.61	26120	0.18	0.43	0.40	18.2	11.8
Sco2/15	11/11/2006	0.33	3550	815	57.9	2085	399	3966	2743	1.57	25020	0.17	0.40	0.40	18.4	11.3
AVERAGE		0.35	3331	769	56	2206	406	3851	2608	1.58	23850	0.17	0.40	0.49	18.0	11.0
2SD		0.05	431	99.6	6.9	168	42.5	492	360	0.11	4128	0.02	0.05	0.23	1.14	1.44
2SD (%)		14.0	12.9	12.9	12.4	7.6	10.5	12.8	13.8	7.1	17.3	11.2	12.3	47.2	6.3	13.2
Sco2/15	16/11/2006	0.49	3070	712	52.6	2280	360	3120	2540	1.40	41.5	0.17	0.39	0.94	16.8	9.58
Sco2/15	16/11/2006	0.50	3180	731	53.5	2330	355	3270	2300	1.48	39.7	0.18	0.41	0.93	17.7	10.1
Sco2/15	16/11/2006	0.51	3220	730	54.1	2320	367	3230	2590	1.47	40.9	0.16	0.40	0.89	17.1	9.79
Sco2/15	16/11/2006	0.51	3310	742	55.2	2390	373	3310	2650	1.45	41.3	0.18	0.40	0.98	17.6	10.2
Sco2/15	16/11/2006	0.50	3110	721	52.9	2240	355	3290	2630	1.50	44.6	0.17	0.42	0.91	17.4	9.94
Sco2/15	16/11/2006	0.48	3080	702	50.9	2240	337	3160	2450	1.45	40.0	0.17	0.37	0.85	16.9	9.75
Sco2/15	16/11/2006	0.49	3090	705	51.6	2220	345	3160	2530	1.48	41.1	0.18	0.38	0.89	17.5	9.94
Sco2/15	16/11/2006	0.49	3110	719	53.1	2290	353	3240	2600	1.48	41.6	0.17	0.43	1.01	17.7	10.1
Sco2/15	16/11/2006	0.49	3130	702	53.7	2300	362	3230	2530	1.43	40.1	0.17	0.41	0.93	17.3	9.95
AVERAGE		0.50	3140	718	53.1	2290	356	3220	2540	1.46	41.2	0.17	0.40	0.93	17.4	9.92
2SD		0.02	158	28.7	2.62	105	21.9	127	212	0.06	2.89	0.01	0.04	0.10	0.65	0.37
2SD (%)		4.1	5.0	4.0	4.9	4.6	6.1	3.9	8.4	4.2	7.0	7.7	9.5	10.5	3.8	3.7

Appendix A8

Major and minor element analyses of the river water standard SLRS-4 measured during this study (n=11).

	Cation concentrations						
	Li (ppb)	**Na (ppm)**	**Mg (ppm)**	**Al (ppb)**	**Si (ppm)**	**K (ppm)**	**Ca (ppm)**
Measured	0.51	2.1	1.5	51	2.04	0.60	5.5
(±) SD	0.01	0.08	0.05	3.2	0.11	0.02	0.18
Certified	0.54	2.4	1.6	54	1.86	0.68	6.2
(±) SD	0.07	0.2	0.1	4	0.05	0.02	0.20
	Mn (ppb)	**Fe (ppb)**	**Ni (ppb)**	**Cu (ppb)**	**Zn (ppb)**	**Sr (ppb)**	**Ba (ppb)**
Measured	3.3	96.5	0.8	1.84	1.1	39.5	12.8
(±) SD	0.1	5.4	0.03	0.07	0.04	1.24	0.16
Certified	3.37	103	0.67	1.81	0.93	26.3	12.2
(±) SD	0.08	5.0	0.08	0.08	0.10	3.20	0.60

Appendix A9

Standard anion analyses (n=4).

Anions (ppm)	**chloride**	**nitrate**	**phosphate**	**sulphate**
concentration	50	10	10	50
measured (n=4)	51.01	10.02	10.04	50.44
(±) 2SD	7.3	1.1	0.8	6.3

Appendix A10

Error propagation using the standard-sample bracketing technique

1. The standard-sample bracketing technique normalises the isotope ratio of a sample (S) to the mean value of the isotope ratio of the bracketing standards (X).
Thus the final ratio (Y) = S/X.

2. The total error associated with the two standards, (ΔX), is:

$$\Delta X = \frac{\sqrt{(\Delta A)^2 + (\Delta B)^2}}{2}$$

where ΔA and ΔB are the errors on standards A and B respectively.

3. The error on the sample measurement (ΔS) can be combined with the error on the standard measurements (ΔX) to find the total error on the isotope ratio (ΔY):

$$\Delta Y = Y \times \sqrt{\left(\frac{\Delta S}{S}\right)^2 + \left(\frac{\Delta X}{X}\right)^2}$$

Example:	**7/6Li**	**error**
LSVEC	13.94251	0.00083
Sample	14.37965	0.00073
LSVEC	13.94383	0.00098

$$\Delta X = \frac{\sqrt{(0.00083)^2 + (0.00098)^2}}{2} = 0.00064$$

Y = 14.37965/13.94317 = 1.0313

$$\Delta Y = 1.0313 \times \sqrt{\left(\frac{0.00073}{14.37965}\right)^2 + \left(\frac{0.00064}{13.94317}\right)^2} = 0.000074$$

So the δ^7Li isotope ratio = 31.3±0.07‰ (1σ)

So the δ^7Li isotope ratio = 31.3±0.07‰ (1σ)

Appendix A11

Compilation of seawater standards (IAPSO) run during lithium isotope analyses on Neptune and Nu-Plasma (*) MC-ICP-MS.

Date	δ^7Li (‰)	Error (2σ)	Date	δ^7Li (‰)	Error (2σ)
*22/02/2007**	30.28	0.11	*06/02/2008*	30.82	0.14
*22/02/2007**	31.13	0.12	*07/02/2008*	30.80	0.18
*01/03/2007**	31.02	0.16	*09/02/2008**	31.72	0.2
08/11/2007	30.67	0.09	*10/02/2008**	31.45	0.17
08/11/2007	30.36	0.05	*10/02/2008**	31.71	0.16
12/11/2007	31.10	0.07	*02/04/2008**	30.43	0.19
22/11/2007	31.82	0.15	*02/04/2008**	31.11	0.18
23/11/2007	31.38	0.25	*02/04/2008**	30.74	0.16
24/11/2007	31.13	0.07	*02/04/2008**	30.57	0.17
24/11/2007	31.43	0.09	*02/04/2008**	30.71	0.15
24/11/2007	31.39	0.05	*02/04/2008**	30.80	0.21
24/11/2007	31.32	0.06	*08/05/2008**	30.71	0.17
24/11/2007	31.20	0.09	*08/05/2008**	30.97	0.14
24/11/2007	31.74	0.02	*08/05/2008**	31.18	0.14
24/11/2007	30.95	0.08	*09/05/2008**	30.76	0.11
24/11/2007	31.38	0.09	*09/05/2008**	31.11	0.17
24/11/2007	31.28	0.08	*09/05/2008**	31.24	0.24
25/11/2007	31.63	0.09			
26/11/2007	31.78	0.07			
26/11/2007	31.36	0.10			
17/12/2007	30.92	0.11	**Average**	31.08	(n=40)
18/12/2007	30.62	0.14	**2σ**	0.823	
18/12/2007	30.54	0.17			

Appendix A12

Compilation of CAM-1 standards run during magnesium isotope analyses on Neptune MC-ICP-MS.

Date	δ^{26}Mg (‰)	Error (2σ)	δ^{25}Mg (‰)	Error (2σ)	δ^{25}Mg:δ^{26}Mg
26/02/2008	-2.60	0.05	-1.35	0.03	0.521
26/02/2008	-2.60	0.03	-1.36	0.02	0.521
26/02/2008	-2.51	0.04	-1.33	0.02	0.530
26/02/2008	-2.60	0.07	-1.34	0.04	0.514
27/02/2008	-2.74	0.11	-1.41	0.05	0.512
27/02/2008	-2.54	0.04	-1.30	0.02	0.511
27/02/2008	-2.63	0.03	-1.37	0.02	0.521
13/05/2008	-2.52	0.04	-1.29	0.03	0.512
14/05/2008	-2.57	0.06	-1.33	0.03	0.517
15/05/2008	-2.50	0.07	-1.29	0.04	0.516
16/05/2008	-2.76	0.03	-1.42	0.03	0.516
16/05/2008	-2.66	0.04	-1.38	0.03	0.518
16/05/2008	-2.61	0.03	-1.37	0.02	0.523
17/05/2008	-2.66	0.03	-1.37	0.02	0.515
17/05/2008	-2.66	0.04	-1.36	0.02	0.510
05/06/2008	-2.63	0.02	-1.33	0.03	0.505
05/06/2008	-2.63	0.02	-1.37	0.02	0.521
06/06/2008	-2.68	0.04	-1.37	0.03	0.512
06/06/2008	-2.66	0.03	-1.36	0.02	0.512
07/06/2008	-2.66	0.03	-1.38	0.03	0.517
07/06/2008	-2.58	0.02	-1.34	0.03	0.520
07/06/2008	-2.64	0.02	-1.35	0.02	0.511
09/07/2008	-2.56	0.03	-1.33	0.03	0.519
09/07/2008	-2.57	0.02	-1.33	0.02	0.519
Average (n=24)	-2.62		-1.35		0.516
2σ	0.13		0.06		0.011

Appendix A13

Compilation of IAPSO seawater standards run during magnesium isotope analyses on Neptune MC-ICP-MS.

Date	$\delta^{26}Mg$ (‰)	Error (2σ)	$\delta^{25}Mg$ (‰)	Error (2σ)	$\delta^{25}Mg:\delta^{26}Mg$
26/02/2008	-1.22	0.02	-0.62	0.01	0.510
26/02/2008	-1.25	0.05	-0.64	0.03	0.510
26/02/2008	-0.95	0.08	-0.49	0.04	0.515
12/09/2007	-0.86	0.02	-0.44	0.02	0.514
12/09/2007	-0.85	0.02	-0.43	0.02	0.504
12/09/2007	-0.89	0.03	-0.47	0.02	0.523
13/09/2007	-0.93	0.2	-0.50	0.1	0.540
13/09/2007	-0.84	0.03	-0.43	0.02	0.516
12/05/2008	-1.04	0.02	-0.55	0.02	0.526
12/05/2008	-1.05	0.03	-0.55	0.02	0.523
12/05/2008	-1.09	0.11	-0.59	0.05	0.543
12/05/2008	-0.85	0.26	-0.43	0.12	0.504
13/05/2008	-0.84	0.19	-0.44	0.11	0.525
16/05/2008	-1.15	0.05	-0.58	0.03	0.499
16/05/2008	-1.12	0.05	-0.57	0.03	0.508
05/06/2008	-1.08	0.02	-0.59	0.02	0.544
05/06/2008	-1.04	0.03	-0.56	0.02	0.536
06/06/2008	-1.08	0.02	-0.56	0.02	0.519
06/06/2008	-1.00	0.02	-0.50	0.02	0.500
07/06/2008	-0.89	0.02	-0.45	0.02	0.509
Average (n=20)	-1.14		-0.58		0.518
2σ	0.33		0.16		0.028

Appendix A14

Experimental solution blanks (ppb). (TPB = total procedural blank)

	Li	Na	Mg	Al	Si	K	Ca	Ti	Mn	Fe	Rb	Sr
2% HNO_3 blank	0.35	10.7	0.9	0.6	-0.4	7.6	19.9	0.08	0.05	1.0	0.032	0.024
pH2 TPB	0.28	26.2	3.5	6.3	-24.2	27.0	1.8	0.94	0.06	-0.2	0.051	0.023
pH3 TPB	0.22	12.9	36.7	34.0	24.7	2.2	14.4	4.81	0.75	41.3	0.016	0.095
pH2 BG1	0.18	5.8	0.7	2.0	-25.5	-2.4	2.5	-0.04	0.04	-0.6	0.008	0.024
pH2 29/11/2006	0.17	25.9	4.1	2.2	-28.3	21.4	39.2	-0.10	0.10	-2.3	0.041	0.112
pH3 23/11/2006	0.15	343	8.2	13.9	-24.4	527	12.9	-0.04	0.11	-0.3	0.581	0.096
pH3 27/11/2006	0.15	4.0	1.6	0.9	-27.9	-7.1	0.6	0.00	0.01	-2.6	0.007	0.007
pH3 15/12/2006	0.14	1.8	1.6	0.2	-27.2	-7.1	-0.3	-0.10	0.00	-2.8	0.006	0.002
pH4 TPB	0.14	7.9	2.3	6.6	-23.9	0.9	3.0	-0.11	0.51	1.4	0.015	0.050
pH10 5/4/2007	0.12	1.1	0.1	0.8	100	-7.9	-0.5	0.10	0.01	-3.1	0.006	-0.001
pH10 16/5/2007	0.12	35.0	451	1.9	263	31.0	2.1	0.02	1.72	104	0.042	0.020
pH11 30/4/2007	0.10	4.1	0.0	1.1	109	-1.9	-0.4	0.01	-0.01	-3.3	0.009	-0.001
pH11 16/5/2007	0.11	51.0	640	5.4	403	41.4	3.9	0.12	2.58	156	0.053	0.030

Appendix B

Greenland Rivers

Appendix B provides supporting data for Chapters 3 and 4 concerning the analyses of glacial rivers in Greenland and includes:

- *Field measurements for Greenland river samples (Appendix B1)*
- *Cation measurements for all phases (Appendices B2 to B4)*
- *Results of leaching experiments carried out on the suspended sediment (Appendix B5)*
- *Li isotope results for all phases and for leaching experiments (Appendices B2 to B5)*
- *Saturation indices of the ultrafiltered Greenland river waters (Appendix B6)*

Appendix B1

Field measurements for Greenland river samples.

Sample	Latitude	Longitude	Origin	pH	T (°C)	TDS (µS)	TSS (g/l)	Alkalinity (meq/l)
GR1	N 67°04.666'	W 50°16.935'	Glacial	8.48	4.2	9.21	0.435	0.073
GR2	N 67°01.745'	W 50°35.683'	Glacial	7.91	4.2	14.4	0.598	0.098
GR3	N 67°09.129'	W 50°02.790'	Glacial	6.32	0.6	2.6	0.229	0.023
GR4	N 67°01.057'	W 50°39.869'	Glacial	7.11	6	17.8	0.846	0.119
GR5	N 67°01.172'	W 50°40.747'	Glacial	7.18	3	9.77	0.399	0.145
GR6	N 66°59.057'	W 50°27.051'	Non-glacial	7.61	12.62	61.6		0.133
GR7	N 66°59.243'	W 50°26.962'	Glacial	7.3	8.6	12.7	0.545	0.151
GR8	N 67°03.269'	W 50°24.644'	Glacial	7.2	5.5	10.7	0.444	0.099
GR9	N 67°09.060'	W 50°13.101'	Glacial	7.18	5.3	6.77		0.266
GR10	N 66°58.09'	W 50°57.101'	Non-glacial	6.96	10.5	2650	0.162	0.358
GR11	N 66°55.915'	W 50°46.448'	Non-glacial	6.81	10	25.1	0.004	1.74
GR12	N 67°03.606'	W 50°25.983'	Non-glacial	7.65	19.3	198	0.014	0.532
GR13	N 66°59.089'	W 50°41.864'	Non-glacial	8.23	14.2	55.3		0.556
GR14	N 66°57.096'	W 53°39.940'	Non-glacial	8.1	7.5	120	0.002	0.784
GR15	N 67°05.945'	W 50°15.950'	Non-glacial	8.25	12.3	106		0.073

Appendix B2

Cation, anion and Li isotope data for the dissolved load (<0.2m) of the Greenland river samples . * Denotes sample is above detection limits. + All errors are 2σ

Sample	Major cations (μmol/l)					Minor cations (nmol/l)					Anions (μmol/l)			Li	δ^7Li
	Si	Al	Na	Ca	Mg	K	Fe	Mn	Ni	Cu	Zn	Sr	HCO_3^-	Cl^-	SO_4^{2-}	(nmol/l)	(‰)+
GR1	19.6	1.64	11.6	24.8	8.28	12.2	229	131	6.9	10.0	4.9	59.6	72.8	1.95	8.29	49	25.4±0.11
GR2	21.6	0.73	29.9	32.9	11.0	18.2	117	108	4.7	10.4	4.1	58.6	98.5	5.97	13.4	69	26.6±0.08
GR3	6.14	0.10	2.99	11.1	3.3	4.54	55.5	54.4	8.6	4.9	6.1	15.7	23.3	1.75	7.06	14	13.5±0.09
GR4	25.7	0.57	32.2	40.8	11.6	20.2	87	94.3	7.5	6.2	3.1	66.9	119	4.31	19.5	75	25.3±0.09
GR5	24.8	0.72	30.2	39.2	11.4	18.6	98.9	92.2	7.2	4.0	3.7	64.4	145	5.15	16.8	67	26.7±0.10
GR7	28.7	1.08	35.4	42.4	13.7	21.6	132	87.8	8.3	6.9	3.9	73.0	133	4.13	19.3	91	25.6±0.08
GR8	42.1	5.34	37.7	40.6	14.4	22.9	693	150	9.1	18.8	11.5	77.8	151	3.18	17.9	92	25.4±0.10
GR9	21.7	1.18	8.01	31.1	9.71	9.75	176	69.5	10.4	15.7	14.5	53.8	99.3		10.7	31	25.9±0.12
GR10	26.6	0.71	*	615	2940	586	427	159	15.1	311	39.9	5050	266	42300	1890	1810	30.4±0.09
GR11	76.1	3.40	99.1	105	86.3	15.6	1440	178	64.9	103	24.7	307	358	94	17.2	51	27.1±0.10
GR12	323	8.62	539	665	775	142	12700	1080	587	873	66.5	1070	1740	596	263	569	36.5±0.10
GR13	6.88	0.77	136	148	116	40.5	179	8.0	65.8	73.2	15.7	441	532	105	22	83	30.8±0.11
GR14	59.5	0.53	362	229	91.1	11.2	249	8.0	7.0	36.7	5.4	1150	556	324	72	14	24.5±0.11
GR15	4.17	0.08	171	181	202	82.7	173	4.7	44.5	29.2	4.3	285	784	119	28.4	195	29.3±0.09

Appendix B3

Cation and Li isotope composition of ultrafiltered and colloidal fractions. + All errors are 2σ

Sample	Major cations (μmol/l)						Minor cations (nmol/l)						Li	δ^7Li
	Si	Al	Na	Ca	Mg	K	Fe	Mn	Ni	Cu	Zn	Sr	(nmol/l)	(‰)+
Ultrafiltered														
GR1	18.6	0.04	30.9	16.8	8.9	9.9	N.D.	5.59	0.27	0.22	0.11	3.42	44	
GR2	121	0.10	28.8	24.8	9.5	16.4	N.D.	5.74	0.71	0.19	0.72	4.9	73	
GR4	40.3	0.09	30.7	32.8	10.8	17.0	N.D.	4.52	0.41	0.2	0.4	5.34	61	
GR5	35.6	0.09	29.2	29.7	10.2	16.0	N.D.	4.25	0.38	0.17	0.37	4.93	64	
GR7	51.7	4.01	32.5	32.7	10.8	19.2	N.D.	4.18	0.42	0.21	0.33	5.72	81	22.9 ± 0.21
GR8	31.7	0.29	860	52.8	110	38.7	N.D.	6.81	0.34	0.97	0.23	19.8	133	24.0 ± 0.14
GR10	48.4	0.73		621	2790	605	754	8.09	1.18	20.3	2.11	419	1620	
GR11	83.7	0.65	73.7	75.3	69.3	13.5	218	7.69	1.23	1.62	0.78	21.2	44	
GR12	352	2.96	543	465	646	139	950	334	15.1	23.1	1.39	75.3	511	35.4 ± 0.15
GR13	10.1	0.60	133	123	110	40.4	84	2.48	1.71	1.39	0.25	36.6	79	31.4 ± 0.18
GR14	76.5	0.35	355	193	86.2	11.1	133	0.82	0.44	0.99	0.34	93.5	16	
GR15	7.3	0.07	175	156	198	82.6	164	0.38	1.42	0.78	0.29	25.4	184	27.2 ± 0.17
Colloids														
GR1		12.0	55.1	56.2	25.1	24.3	2500	2.2	140	2.0	4.3	0.7	69	16.6 ± 0.15
GR2		7.2	43.3	58.2	20.4	28.2	2350	1.8	132	3.5	4.4	2.4	116	16.4 ± 0.19
GR4		14.8	45.2	63.2	22.7	27.5	4240	8.3	237	1.8	2.7	1.9	99	21.7 ± 0.29
GR5		16.1	47.0	69.6	24.4	29.6	4430	4.8	248	1.9	2.7	1.5	101	20.9 ± 0.15
GR7		47.4	66.8	97.7	39.5	45.1	14000	9.9	782	4.3	6.8	4.2	157	13.2 ± 0.13
GR8		39.9	831	65.3	119	47.8	12300	8.9	692	2.2	6.5	3.1	191	17.9 ± 0.16
GR10		0.3	0.0	607	2710	564	416	7.5	23.3	0.9	20.0	1.8	1920	
GR11		42.1	69.2	266	158	15.5	37000	32.2	2070	29.3	53.5	8.4	64	
GR12		68.1	668	1820	1630	189	352000	328.8	19700	178	373	23.3	734	35.2 ± 0.13
GR13		1.7	150	221	149	47.4	2400	0.4	136	17.3	24.6	4.8	96	30.3 ± 0.09
GR14		2.1	407	332	120	13.0	3370	0.3	189	5.7	22.0	1.6	17	
GR15		0.3	197	272	258	102	953	0.1	53.4	14.0	14.0	0.8	226	29.1 ± 0.19

Appendix B4

Major element and lithium isotope data for solid phases from Greenland rivers (SP = suspended sediment, S = sands and R = bedrock). Amphibolite data is from Wells et al. (1987). [+] All errors are 2σ

Sample	Major cations *(Wt %)*							Minor cations *(ppm)*					Li	δ^7Li
	Si	Al	Na	Ca	Mg	K	Fe	Mn	Ni	Cu	Zn	Sr	*(ppb)*	*(‰)*[+]
GR1-SP		6.95	2.47	3.12	2.07	2.15	5.07	744	69.3	84.6	121	374	35.2	2.95 ± 0.17
GR2-SP		6.86	2.59	3.13	1.69	2.17	4.3	676	52.8	47.2	105	407	29.2	3.58 ± 0.09
GR3-SP		6.53	2.54	3.09	1.79	1.76	4.46	664	62.6	72.8	98.7	378	25.2	3.89 ± 0.09
GR4-SP		6.86	2.66	3.17	1.85	2.05	3.9	611	72.3	51.0	92.1	393	24.9	3.12 ± 0.13
GR5-SP		6.94	2.83	3.24	1.74	1.95	3.68	616	79.1	54.8	96.1	396	21.5	3.62 ± 0.17
GR7-SP		6.77	2.59	3.15	1.92	2.08	4.01	623	90.5	61.6	103	387	26.8	3.63 ± 0.08
GR8-SP		6.9	2.56	3.12	2.12	2.17	4.09	698	61.7	62.7	120	376	29.1	3.11 ± 0.08
GR9-SP		7.21	2.66	3.12	1.97	2.34	4.57	715	77.0	87.1	114	392	35.4	2.73 ± 0.07
GR10-SP		6.7	2.53	3.28	2.07	1.65	4.79	639	67.6	54.2	107	389	30.3	4.00 ± 0.07
GR1-S	32.3	7.36	2.82	2.49	0.99	1.42	3.2	633	24.5	21.4	39.8	388	8.72	5.58 ± 0.10
GR2-S	33.2	7.32	2.87	2.26	0.8	1.38	2.67	544	19.9	12.0	34.5	396	9.27	4.80 ± 0.10
GR3-S	32	7.27	2.7	2.45	1.17	1.11	4.07	806	30.4	24.7	46.9	375	10.3	3.95 ± 0.14
GR4-S	29.9	6.77	2.33	2.53	1.44	1.15	7.09	1170	40.8	18.0	59.7	325	10.8	5.02 ± 0.14
GR5-S	32	7.22	2.74	2.48	1.2	1.33	3.87	746	32.6	14.9	46.3	375	10.3	4.96 ± 0.14
GR7-S	32	7.72	2.96	2.54	1.14	1.52	3.11	596	35.1	20.5	43.4	414	10.2	5.17 ± 0.13
GR8-S	33.7	6.91	2.76	1.86	0.65	1.62	2.25	453	15.8	10.7	29.4	358	9.82	5.60 ± 0.11
GR9-S	30.4	7.12	2.73	2.4	1.18	1.06	4.93	883	29.9	18.6	48.9	412	11.1	6.91 ± 0.13
GR10-S	31.4	7.27	2.77	2.37	1.22	1.59	3.78	733	27.7	18.6	54.3	361	13.5	5.43 ± 0.13
GR11-S	32.4	7.22	2.84	2.21	1.06	1.44	2.73	478	28.6	9.52	42.2	335	13.2	3.94 ± 0.12
GR12-S	30.7	6.41	2.35	2.17	0.94	1.24	5.44	1060	22.2	7.30	46.2	310	9.64	5.64 ± 0.12
GR13-S	33.5	7.07	2.78	2.02	0.83	1.51	2.5	451	21.1	11.7	49.7	362	9.62	4.95 ± 0.14
GR14-S	32.4	6.73	2.5	2.57	1.36	0.74	3.35	601	16.0	10.2	51.2	486	11.1	3.77 ± 0.09
GR15-S	31	7.2	2.73	2.57	1.24	1.36	3.29	637	41.0	20.0	44.6	344	11.1	3.64 ± 0.15
GR1-R	26.1	7.62	1.14	5.66	4.35	0.74	6.64	1130	132	61.2	72.3	155	11.4	9.46 ± 0.13
GR2-R	31.1	7.27	2.6	2.41	1.93	2.13	3.22	743	148	22.6	78.7	434	24.9	5.77 ± 0.17
GR3-R	24.7	6.75	1.77	4.64	3.11	1.28	9.91	1620	67.2	42.0	130	186	15.2	9.59 ± 0.19
GR5-R	23.8	5.05	0.79	4.7	9.16	0.64	8.23	1570	384	25.5	113	88	26.2	10.4 ± 0.17
GR6-R	33	7.83	3.35	1.15	0.71	2.25	1.71	397	19.5	31.4	42.4	413	11.3	7.34 ± 0.17
GR-KISS	23.5	6.75	1.75	5.03	2.9	0.56	12.18	1940	39.3	45.5	187	146	17.7	10.4 ± 0.22
Mean amphibollite*	31.3	8.34	3.53	2.18	0.88	1.79	2.14							

Appendix B5

A table showing the results of a two step leaching procedure on three suspended sediments. The results are presented firstly as a concentration of each element in solution (in ppm). The second figure is a % showing how much of the total element that is present in 0.2g of sediment has been leached by each step. In theory no solution should have more than 100% of the total element that is provided by the suspended sediment. $^{+}$ All errors are 2σ

	Na	Mg	Al	Si	K	Ca	Mn	Fe	Ni	Cu	Zn	Li	δ^7Li (‰)$^{+}$
Acetic blank		0.002	1.97	2.38	0.64	0.548	0.001	0.023	0.0003	0.515	0.0016	0.000	
GR1 Acetic (ppm)		5.30	2193	6.64	24	29.5	0.39	5.06	0.024	0.734	0.028	0.008	13.0 ± 0.16
GR1 Acetic (%)		1.28	158		5.59	4.74	2.63	0.50	1.77	43.4	1.15	1.12	
GR5 Acetic (ppm)		6.21	560	4.01	19.3	30.1	0.40	0.98	0.028	0.613	0.018	0.007	15.4 ± 0.15
GR5 Acetic (%)		1.62	41.3		4.65	4.78	3.27	0.12	1.79	56.0	0.951	1.38	
GR7 Acetic (ppm)		7.39	1413	5.69	21.4	34.9	0.47	2.14	0.038	0.648	0.014	0.011	13.0 ± 0.19
GR7 Acetic (%)		1.75	102		4.92	5.60	3.77	0.26	2.10	52.6	0.671	1.89	
HCl blank	0.828	0	0.984	0.020	0.074	0.186	0.0001	0.010	0.0000	0.0007	-0.0001	0.000	
GR1 HCl (ppm)	95.2			44.0	146	310	10.6	1031	1.28	1.26	1.73	0.463	5.91 ± 0.17
GR1 HCl (%)	19.2				34.1	49.8	71.1	102	92.1	74.3	71.6	65.8	
GR5 HCl (ppm)	96.0			33.9	116	271	7.84	790	1.50	0.89	1.37	0.342	5.12 ± 0.29
GR5 HCl (%)	18.6				27.9	43.0	63.6	98.5	95.1	81.4	71.2	63.7	
GR7 HCl (ppm)	93.7			36.2	124	264	7.77	808	1.67	0.95	1.44	0.388	4.94 ± 0.17
GR7 HCl (%)	18.3				28.6	42.4	62.3	98.9	92.4	77.4	70.3	66.7	

Appendix B6

Saturation indices for a selection of primary and secondary minerals in the ultrafiltered phase of river waters from Greenland. All saturation indices have been calculated using the Wateq4f database within PHREEQC.

	pH	Temp	TDS	$Fe(OH)_3(a)$	Goethite	Haematite	Magnetite	$Al(OH)_3(a)$	Gibbsite	Illite	Kaolinite	Kmica
GR1	8.48	4.2	9.21	-3.74	1.33	4.55	-2.06	-3.13	-0.23	-5.90	-1.22	-0.28
GR2	7.91	4.2	14.4	-3.96	1.10	4.11	-2.17	-2.11	0.79	-1.18	2.46	4.89
GR4	7.27	3.8	9.67	-5.48	-0.48	0.94	-6.26	-1.51	1.40	-2.09	2.77	4.71
GR5	7.18	3	9.77	-6.14	-0.92	0.08	-7.36	-1.54	1.32	-2.91	2.35	3.86
GR7	7.3	8.6	12.7	-5.24	0.03	1.99	-4.82	-2.18	0.67	-3.49	1.33	2.75
GR8	7.2	5.5	10.8	-5.62	-0.48	0.96	-6.21	-1.12	1.76	-1.34	3.17	5.65
GR11	6.8	10	25.1	-0.59	4.74	11.4	9.81	-0.68	2.16	0.18	4.68	7.14
GR12	7.65	19.3	198	1.84	7.53	17.0	17.3	-1.12	1.62	2.66	4.60	9.03
GR13	8.2	14.2	55.3	1.20	6.70	15.4	14.2	-2.14	0.66	-4.73	-0.28	1.64
GR14	8.1	7.5	120	1.82	7.05	16.0	15.5	-1.97	0.89	-1.42	2.14	4.50
GR15	8.25	12.3	106	1.62	7.04	16.0	15.2	-3.01	-0.20	-6.86	-2.23	-0.96

	pH	Temp	TDS	Quartz	Albite	Anorthite	Montmorillonite	Forsterite	Diopside	Phlogopite
GR1	8.48	4.2	9.21	-0.75	-7.68	-9.38	-5.31	-12.4	-7.78	-12.6
GR2	7.91	4.2	14.4	0.08	-4.80	-6.68	-0.08	-13.8	-8.24	-12.8
GR4	7.27	3.8	9.67	-0.38	-6.21	-7.69	-0.55	-16.9	-11.7	-18.0
GR5	7.18	3	9.77	-0.52	-6.83	-8.12	-1.21	-17.4	-12.5	-20.0
GR7	7.3	8.6	12.7	-0.38	-6.67	-8.34	-2.07	-15.8	-10.8	-17.8
GR8	7.2	5.5	10.8	-0.54	-4.85	-6.85	-0.22	-14.9	-10.7	-15.0
GR11	6.8	10	25.1	-0.20	-4.73	-5.50	2.00	-15.8	-11.1	-16.9
GR12	7.65	19.3	198	0.28	-1.84	-2.20	3.14	-8.77	-4.00	-5.41
GR13	8.2	14.2	55.3	-1.19	-7.41	-7.02	-4.52	-10.2	-6.57	-10.1
GR14	8.1	7.5	120	-0.20	-4.10	-5.31	-0.52	-10.8	-5.72	-9.18
GR15	8.25	12.3	106	-1.30	-8.50	-8.97	-6.95	-9.90	-6.48	-10.1

Appendix B7

Magnesium isotope ratios for the dissolved, suspended (SP) and bedload (S) phases in the Greenland rivers.

SAMPLE	[Mg] *ppm*	δ^{26}Mg *(‰)*	Error *(2σ)*	δ^{25}Mg *(‰)*	Error *(2σ)*
GR1	199	**-1.04**	0.04	-0.522	0.03
GR2	264	**-1.07**	0.08	-0.541	0.05
GR3	81	**-1.31**	0.10	-0.670	0.05
GR4	278	**-1.12**	0.06	-0.561	0.03
GR5	274	**-1.17**	0.04	-0.579	0.02
GR7	329	**-1.19**	0.05	-0.640	0.03
GR8	347	**-1.18**	0.05	-0.590	0.03
GR9	233	**-1.06**	0.03	-0.539	0.02
GR11	2071	**-0.66**	0.08	-0.348	0.05
GR12	18622	**-0.58**	0.07	-0.323	0.04
GR13	2794	**-0.65**	0.02	-0.342	0.02
GR15	4853	**-0.62**	0.03	-0.320	0.03
	[Mg] *Wt %*				
GR1-SP	2.07	**-0.41**	0.03	-0.207	0.02
GR3-SP	1.79	**-0.27**	0.04	-0.134	0.03
GR5-SP	1.92	**-0.44**	0.03	-0.234	0.02
GR8-SP	1.97	**-0.46**	0.03	-0.243	0.03
GR1-S	0.99	**-0.53**	0.03	-0.252	0.02
GR3-S	1.17	**-0.39**	0.03	-0.203	0.02
GR5-S	1.20	**-0.43**	0.03	-0.220	0.02
GR8-S	0.65	**-0.44**	0.02	-0.221	0.02
GR11-S	1.06	**-0.10**	0.02	-0.054	0.02
GR12-S	0.94	**-0.31**	0.02	-0.162	0.02
GR15-S	1.24	**-0.34**	0.02	-0.183	0.02

Appendix D

Laterite Data

Appendix D provides supporting data for Chapter 7 and includes:

- *Lithology and mineralogy of the laterite profiles (Appendix D1)*
- *Major and trace element data for the two laterite profiles (Appendices D2 and D3)*
- *Re and Os elemental abundances and isotope ratios for the two laterite profiles (Appendix D4)*

Appendix D1

Lithology and mineralogy of the laterite samples from Bidar and Goa and the Bole samples from Ambenali.

Sample	Depth	Lithology	Mineralogy
Bidar (17°54.87'N, 77°32.39'E)	(m)		
BB9	2	vermiform laterite	Haematite, Goethite, Kaolinite
BB8	5	nodular laterite	Haematite, Goethite, Kaolinite
BB7	6	base of laterite	Haematite, Goethite, Kaolinite
BB6	11	laterite base/top of saprolite	Haematite, Goethite, Kaolinite
BB5	13	saprolized basalt	Haematite, Goethite, Kaolinite, Magnetite
BB4	15	reddened saprolite	Haematite, Goethite, Kaolinite, Magnetite
BB3	26	deeply weathered basalt	Haematite, Goethite, Kaolinite, Magnetite
BB2	35	low alteration basalt	Anorthite, Augite, Illite
BB1	47	unaltered basalt	Anorthite, Augite
Goa (15°28.44'N, 73°52.35'E)			
SQ14	0	indurated laterite	Iron, traces of clay and quartz
SQ13	2.5	indurated laterite	Iron, traces of clay and quartz
SQ12	3.5	indurated laterite	Iron, traces of clay and quartz
SQ11	7.5	massive laterite	Iron 96%, Quartz 2%, Clay 2%
SQ10	8.5	semi-indurated laterite, nodules fusing together	Iron 95%, Quartz 2%, Clay 3%
SQ9	12	increased nodule density and size	Iron 50%, Quartz 45%, Clay 5%
SQ8	13.5	base of nodular laterite, haematite segregations present	Quartz 50%, Iron 45%, Clay 5%
SQ7	14	laterite base/ top of altered greywacke	Quartz 75%, Iron 22%, Biotite 2%, Muscovite 1%
SQ6	15	top of reddened greywacke, soft and well consolidated	Quartz 75%, Biotite 12%, Feldspar 6%, Iron 5%, Muscovite 2%
SQ5	22.5	soft weathered greywacke, base of weathered zone	Quartz 74%, Biotite 20%, Feldspar 2%, Muscovite 2%, Chlorite 1%, Opaques <1%
SQ4	25.5	Softer, white weathered greywacke	Quartz 80%, Biotite 8%, Feldspar 8%, Chlorite/Muscovite 3%, Opaque 1%
SQ3	30	lighter greywacke from start of weathered zone	Quartz 75%, Biotite 12%, Feldspar 8%, Opaque 2%, Other 3%
SQ2	34	unaltered greywacke	Quartz 75%, Biotite 15%, Feldspar 5%, Opaque 2%, Other 3%
Ambenali (17°57.10'N, 73°34.58'E)	(cm)		
MPr2a	10	uniform fine grained ash	
MPr2b	70	Blocky, lithified, reworked ash	
MPr2c	90	Fine-grained ash	
MPr2d	140	Weathered flow top material	

Appendix D2 - Major element abundances for the Bidar and Goa laterite profiles.

Sample	Depth (m)	SiO_2 (Wt%)	TiO_2 (Wt%)	Al_2O_3 (Wt%)	Fe_2O_3 (Wt%)	MnO (Wt%)	MgO (Wt%)	CaO (Wt%)	Na_2O (Wt%)	K_2O (Wt%)	P_2O_5 (Wt%)	(LOI)
Bidar laterite												
BB9	*2*	9.59	2.03	9.85	77.5	0.23	0.16	0.04	0.00	0.03	0.12	7.31
BB8	*5*	31.4	2.33	27.2	38.4	0.07	0.10	0.00	0.00	0.07	0.08	11.1
BB7	*6*	36.7	2.44	31.3	27.7	0.33	0.26	0.05	0.00	0.03	0.07	11.4
BB6	*11*	6.12	1.40	6.97	84.8	0.03	0.14	0.00	0.00	0.00	0.33	11.1
BB5	*13*	30.6	5.76	25.8	37.0	0.06	0.23	0.07	0.00	0.02	0.08	11.1
BB4	*15*	38.8	4.78	32.0	21.6	0.06	0.38	1.91	0.00	0.01	0.03	12.4
BB3	*26*	38.6	5.11	31.5	24.1	0.11	0.40	0.19	0.00	0.02	0.18	11.7
BB2	*35*	50.1	2.29	14.2	12.6	0.22	5.99	11.5	2.78	0.25	0.19	0.72
BB1	*47*	48.9	2.16	13.7	13.4	0.19	6.93	11.0	2.46	0.16	0.16	0.60
Basalt bole												
MPr 2a		57.8	2.19	16.1	16.1	0.10	6.41	2.30	0.04	0.07	0.03	
MPr 2b		57.9	2.08	15.6	15.4	0.11	7.17	2.33	0.08	0.37	0.02	
MPr 2c		57.9	2.07	15.4	15.3	0.14	7.18	2.40	0.05	0.34	0.02	
MPr 2d		50.6	3.41	18.6	21.5	0.31	4.61	2.07	0.06	0.14	0.03	
Goa laterite												
SQ14	*0*	13.6	2.04	34.2	48.5	0.04	0.19	0.06	0.13	0.72	0.70	16.4
SQ13	*2.5*	17.5	1.90	34.6	44.9	0.04	0.18	0.06	0.21	0.74	0.27	15.4
SQ12	*3.5*	19.6	2.28	40.9	36.4	0.06	0.15	0.06	0.12	0.65	0.25	17.2
SQ11	*7.5*	15.2	0.66	13.6	68.3	0.57	0.13	0.05	0.07	0.51	0.93	12.2
SQ10	*8.5*	17.2	1.84	30.5	49.6	0.02	0.10	0.05	0.64	0.28	0.16	12.6
SQ9	*12*	67.9	0.73	18.9	10.8	0.02	0.30	0.04	0.07	1.35	0.06	7.28
SQ8	*13.5*	67.5	0.85	19.6	10.3	0.02	0.32	0.05	0.08	1.43	0.04	7.23
SQ7	*14*	71.2	0.76	18.6	7.64	0.06	0.51	0.05	0.09	1.76	0.08	6.59
SQ6	*15*	75.3	0.43	13.4	3.38	0.05	1.61	0.43	3.50	2.44	0.08	1.80
SQ5	*22.5*	64.2	0.48	16.4	7.63	0.17	4.13	0.43	2.76	3.95	0.05	2.52
SQ4	*25.5*	79.5	0.32	11.4	2.43	0.07	1.29	0.55	3.54	1.63	0.07	1.29
SQ3	*30*	69.7	0.58	13.9	5.58	0.11	2.88	0.65	3.24	3.20	0.11	1.52
SQ2	*34*	67.8	0.56	14.6	6.08	0.13	3.07	0.95	3.31	3.68	0.12	1.34
SQ1	*36*	48.3	1.44	13.9	16.8	0.25	6.61	10.1	2.35	0.59	0.15	0.58
Country rock												
IND108		71.6	0.400	14.4	2.49	0.037	0.64	1.79	3.88	4.43	0.120	0.42
IND114		74.1	0.221	13.9	1.42	0.022	0.29	1.42	3.75	4.54	0.050	0.36
IND120		73.5	0.130	14.3	1.15	0.026	0.47	1.65	4.19	3.72	0.051	0.55
Bhima Lst		16.6	0.341	2.33	1.34	0.061	0.95	42.3	0.38	0.34	0.092	34.6
BIF		55.1	0.016	0.18	44.0	0.011	0.09	0.03	0.01	0.01	0.019	0.72

Appendix D3 - Trace element data for the Bidar and Goa laterite profiles.

Sample	Li (ppm)	Rb (ppm)	Sr (ppm)	Y (ppm)	Zr (ppm)	Nb (ppm)	Ba (ppm)	Pb (ppm)	Th (ppm)	U (ppm)	Sc (ppm)	V (ppm)	Cr (ppm)	Ni (ppm)	Cu (ppm)	Zn (ppm)
Bidar laterite																
BB9	7.65	1.3	9.7	4.2	283	14.8	161.8	36.7	6.9	1.60	190.1	2985.7	691.8	40.3	581.1	35.2
BB8	20.2	3.6	7.1	4.4	211	17.2	17.3	19.7	6.0	1.80	24.4	967.3	736.5	106.1	182.5	70.3
BB7	13.8	1.3	14.9	4.7	184	14.7	430.3	45.1	3.6	1.18	19.6	670.5	257.0	62.7	211.2	56.6
BB6	1.16	0.2	41.0	14.1	76.6	5.3	23.5	6.4	0.9	4.45	153.8	975.0	765.6	242.5	851.6	206.0
BB5	3.68	0.1	3.5	2.6	282	23.4	13.3	9.7	1.4	2.10	14.9	1846.0	249.6	72.4	451.5	62.1
BB4	3.83	0.3	23.4	8.0	246	19.4	10.5	4.2	2.0	1.08	49.3	642.8	212.5	57.7	173.4	86.3
BB3	7.16	1.0	13.4	693	246	19.5	54.9	2.4	1.9	1.00	70.0	687.0	201.3	287.3	394.1	119.9
BB2	5.29	5.6	222	34.6	136	10.7	94.6	1.1	1.1	0.25	36.8	375.1	139.3	137.9	185.0	109.8
BB1	4.69	1.1	210	30.6	128	10.0	52.9	1.0	1.0	0.20	37.7	371.3	148.3	97.9	177.4	106.4
Basalt bole																
MPr 2a		4	69	15.1	119	8.5	44	0	1	1	44	177	131	111	558	99
MPr 2b		24	69	14.8	108	7	44	1	0	0	42	217	180	91	394	80
MPr 2c		22	72	18.8	106	7.5	48	0	0	0	39	191	160	97	179	82
MPr 2d		11	62	30	182	11.7	98	4	2	1	54	351	110	105	168	117
Goa laterite																
SQ14		23.8	38.2	22.8	310	25.8	196.8	37.6	20.4	13.2	79.6	765.2	845.7	42.8	58.6	32.4
SQ13		24.2	34.8	21	296	23.8	176.5	36.2	17.4	5.4	47.2	837.2	1049.8	48.9	55	26.6
SQ12		19.6	38	21.2	339	28.2	186.1	46.8	23.6	9.2	31	625.8	803.8	48.6	38.4	24.8
SQ11		14.8	35.8	25.2	99	10.6	845	32.4	11.2	7	27.6	60.2	196.7	129.1	65.4	92.2
SQ10		7	19.2	15.4	257	20.4	87.1	26.2	21.2	4.2	29.4	779.8	829.9	50.3	37.2	19.2
SQ9		25.8	7.2	8.1	219	15.7	511.2	12.6	21.4	5.8	22.9	157.4	126.7	44.1	29.8	24.3
SQ8		29.8	9.1	10.8	261	17.1	535.5	14.7	22.2	7.2	20.4	151.2	114.6	43.5	33.3	31.9
SQ7		37.3	6.5	11.6	265	14.9	622.7	24.2	25.1	6	16.5	123.5	86.3	69.6	36.2	39.4
SQ6		72.8	109	35.9	134	10.1	556.7	12.3	14.2	4.4	8	65.3	82.5	23.5	42.4	59.6
SQ5		132	80.7	13.9	138	11.9	635.2	12.4	14.2	4.4	10.3	87.7	77.3	38.2	33	137.3
SQ4		43.1	99.6	13.1	91.9	6.6	423.7	13	6.7	2.7	5.3	43.6	63.4	19.1	51	32
SQ3		99.8	108	24.7	228	13.6	609	10.9	18.7	7.5	12.2	97.9	113.5	42.8	30.8	108.4
SQ2		118	114	15.1	194	12.7	701	11.7	15.6	5.7	13.5	92.4	114.2	38.6	40.6	108.9
SQ1		18	239	29.9	67.7	3.2	171.9	3.7	2.8	0	47.2	317.7	118.6	81.6	114.7	111.8
Country rock																
IND108		152	233	42.9	272	14.2	578	20	15	2	4	30	12	5	10	52
IND114		143	220	6.5	141	6.3	646	20	17	1	2	11	7	3	6	28
IND120		94	192	5.5	84	4.5	468	15	10	0	2	14	7	4	3	24
Bhima Lst		16.6	268	14.8	28	3.6	3683	0	4.6	0.1	17.7	13	6.9	2.5	7.4	8.1
BIF		1.4	0.3	1.8	5.1	2.4	5	11	1.6	0	1.1	0	24.5	0	0	21.2

Appendix D4 - Re-Os elemental and isotopic data for the Bidar and Goa laterite profiles

Sample	Os (ppt)	Re (ppt)	$^{187}Os/^{188}Os$	Error	$^{187}Re/^{188}Os$
Bidar laterite					
BB9	863	3410	0.3313	0.0002	19.7
BB9*	887	3540	0.3375	0.0013	20.0
BB8	1410	523	0.4295	0.0002	1.88
BB7	901	10500	0.4634	0.0003	59.4
BB6	87	1390	0.4505	0.0007	81.7
BB5	508	6190	0.4382	0.0036	61.8
BB4	491	5610	0.4695	0.0003	58.1
BB4*	550	5730	0.4725	0.0004	53.0
BB3	83.1	883	0.4964	0.0006	54.2
BB2	4.27	2100	1.1863	0.0028	2286
BB1	4.35	719	0.9805	0.0028	896
BB1*	4.62	736	0.9876	0.0026	863
Basalt bole					
MPr 2a	35.3	273	0.1712	0.0006	37.4
MPr 2b	20.1	97	0.1713	0.0003	23
MPr 2c	43.7	1080	0.1572	0.0004	119
MPr 2d		945			
Goa laterite					
SQ14	224	196	0.4764	0.0004	4.4
SQ13	492	1070	0.5475	0.0003	11.2
SQ13*	502	983	0.5565	0.0006	10.1
SQ12	404	142	0.5630	0.0006	1.8
SQ11	117	393	0.8154	0.0012	17.8
SQ11*	113	428	0.7803	0.0011	20.0
SQ10	324	175	0.5330	0.0004	2.8
SQ9	48.5	1070	1.7602	0.0017	128
SQ8	53.6	610	1.5895	0.0002	65.4
SQ8*	53.6	642	1.6350	0.0022	69.9
SQ7	40.4	155	2.0583	0.0014	23.1
SQ6	39.2	559	4.0769	0.0028	104
SQ5	42.1	801	4.3359	0.0021	142
SQ4	29.6	519	2.5299	0.0021	110
SQ3	44.4	458	5.1031	0.0054	82.0
SQ2	43.4	708	4.5568	0.0067	123
SQ2*	39.4	747	4.0495	0.0030	123
SQ1	46.7	909	68.005	0.0719	889
Country rock					
IND108	4.2		0.7426	0.0011	
IND114	4.5		1.7662	0.0070	
IND120	2.4		1.6692	0.0039	
Bhima Lst	31.0	74	0.1752	0.0008	11.5
BIF	19.6	2830	1.3449	0.0037	786

[1]Errors shown are 2σ mean; $^{187}Os/^{188}Os$ ratios normalised using $^{192}Os/^{188}Os$=3.08271 and corrected using measured $^{18}O/^{16}O$ and $^{17}O/^{16}O$ of 0.002047 and 0.0037 respectively; Given isotope ratios are blank corrected. D.L. samples are below mass spectrometer detection limits.

* Duplicate results for the same laterite powder samples using the high pressure, high temperature microwave method for digestion (HP-HT).